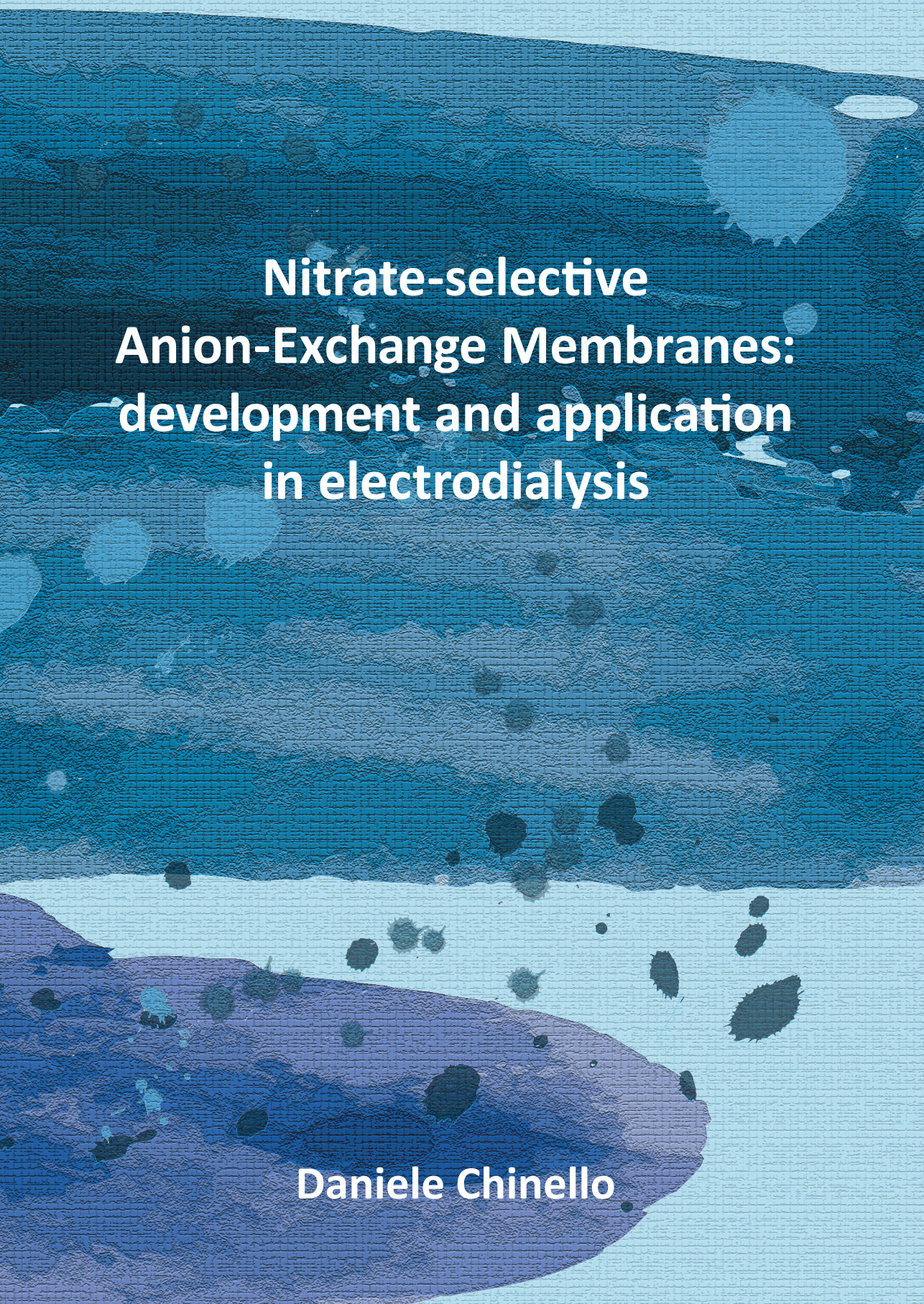
Nitrate-selective
Anion-Exchange Membranes:
development and application
in electrodialysis
Daniele Chinello

Propositions

1. Membrane hydrophobicity is a pivotal parameter for achieving nitrate selectivity. (This thesis).
2. The interplay between membrane selectivity and water consumption is crucial in designing closed-loop processes with nitrate selective membranes. (This thesis).
3. Nuclear energy is currently the most sustainable source of energy available.
4. Establishing standardized experimental methods is essential to facilitate meaningful comparisons of experimental results.
5. The term “healthy food” should also include the health impact of the cooking utensils used, not just the nature of the food itself.
6. Reducing fast fashion would decrease environmental pollution.

Propositions belonging to the thesis, entitled

Nitrate-selective Anion-Exchange Membranes: development and application in electrodialysis

Daniele Chinello
Leeuwarden, 5 December 2024

Nitrate-selective Anion-Exchange Membranes: development and application in electrodialysis

Daniele Chinello

Thesis committee

Promotor
Prof. Dr L.C.P.M. de Smet
Personal Chair at the Laboratory of Organic Chemistry
Wageningen University & Research

Co-promotor
Dr J.W. Post
Program Director
Wetsus, European Centre of Excellence for Sustainable Water Technology, Leeuwarden

Other members
Prof. Dr H.H.M. Rijnaarts, Wageningen University & Research
Dr H. Roth, University of Twente, Enschede
Prof. Dr F. Picchioni, University of Groningen
Prof. Dr E.R. Cornelissen, Ghent University, Belgium

This research was conducted under the auspices of the Graduate School VLAG (Biobased, Biomolecular, Chemical, Food, and Nutrition sciences)

Nitrate-selective Anion-Exchange Membranes: development and application in electrodialysis

Daniele Chinello

Thesis

submitted in fulfilment of the requirements for the degree of doctor
at Wageningen University
by the authority of the Rector Magnificus,
Prof. Dr C. Kroeze,
in the presence of the
Thesis Committee appointed by the Academic Board
to be defended in public
on Thursday 5 December 2024
at 1 p.m. in De Harmonie theater, Leeuwarden.

Daniele Chinello
Nitrate-selective Anion-Exchange Membranes: development and application in electrodialysis,
195 pages.

PhD thesis, Wageningen University, Wageningen, The Netherlands (2024)
With references, with summary in English

DOI: https://doi.org/10.18174/671986

Ten out of ten people die,
so don't take life too seriously

Henry Winkler

TABLE OF CONTENTS

Chapter 1

Introduction

1.1. Nitrogen fertilizer: importance and associated problems

Nitrogen is an indispensable nutrient for agriculture, playing a pivotal role in supporting plant growth and ensuring productivity. As an essential element for the synthesis of amino acids, proteins, and chlorophyll, nitrogen is a key building block for plant structure and function. Its incorporation into plant tissues facilitates the formation of enzymes and other vital cellular components, contributing to overall plant health. Nitrogen is the most abundant element in the atmosphere in the form of N_2 molecules, accounting for 78 %.[1] However, due to the strength of the triple covalent bond between the nitrogen atoms, which requires a significant amount of energy to break, it is chemically inactive, making it difficult to be used by plants and animals. Nevertheless, although inert, it plays a crucial role in the nitrogen cycle. This cycle is a complex biogeochemical process that governs the cycling and availability of nitrogen in various forms within ecosystems.[2] It involves a series of interconnected steps where nitrogen undergoes different chemical transformations. The cycle begins with nitrogen gas in the atmosphere, which is converted into ammonia (NH_3) through a process called nitrogen fixation. This process is energetically demanding and is carried out by nitrogen-fixing bacteria present in the soil. These organisms are equipped with the enzyme nitrogenase, which catalyzes the reduction of N_2 to NH_3. Ammonia can then be further transformed into nitrite (NO_2^-) and nitrate (NO_3^-) through nitrification. This aerobic process occurs in two steps:

I. NH_3 oxidation to nitrite (NO_2^-): carried out by *Nitrosomonas* bacteria by using two different enzymes such as ammonia monooxygenase and hydroxylamine oxidoreductase.[3]
II. NO_2^- oxidation to nitrite (NO_3^-): performed by *Nitrobacter* bacteria species by using the nitrite oxidoreductase multiprotein complex.[4]

At this point, nitrate is assimilated by plants via their roots and converted into organic nitrogen compounds, such as amino acids and proteins. Plants can also absorb nitrogen in the form of ammonium ion (NH_4^+), but due to the nitrate's higher mobility in the soil solution, most plants prefer nitrate over ammonium.[5]

While the nitrogen cycle is crucial for supplying plants with the essential nutrient nitrogen, the need for efficient and large-scale fertilizer production to secure food availability became fundamental as the global population steadily increased in the 19th century. Traditionally, farmers

relied on natural sources of nitrogen, such as animal manure, using legumes in crop rotation,[6] or importing sodium nitrate from Chile (also known as Chile saltpeter),[7] but these methods were not sufficient to meet the demands of a growing population. Therefore, by mid-19th century, a lot of scientific research focused on making fertilizer production possible.[8] Fritz Haber (1868-1934), a German physical chemist, after years of research and also with the theoretical contribution of Walther Nernst (1864-1941), a German physicist and physical chemist,[9] demonstrated the possibility of synthetic nitrogen fixation in the early 20th century. In particular, using an iron metal catalyst and operating at high temperature (400-650 °C) and high pressure (200-400 atm),[10] Haber and his collaborator obtained ammonia by reaction of atmospheric nitrogen with hydrogen:

$$N_2 + 3H_2 \rightarrow 2NH_3$$

In the same year, another German chemist, Carl Bosch (1874-1940), was assigned to develop a commercial scale production plant by the company BASF. The Haber-Bosch process was then born, marking a milestone for modern society development. The use of fertilizers has witnessed a notable surge throughout the 20th century. While in Europe we observe a gradual increase in fertilizer consumption since 1992, countries such as China and India have experienced an even more pronounced upward trend.[11] Overall, with the global population expected to rise to 10 billion by 2060,[12] and given the decline in agricultural production due to climate change,[13] pests,[14] and nutrient deficiencies, the global demand for fertilizers to support crop production is expected to further increase. In particular, nitrate fertilizers stand out as the most effective and dependable nitrogen source currently accessible.[5] Nevertheless, despite its crucial function, the application of nitrogen fertilizers poses challenges and excessive usage can result in environmental problems. Indeed, not all the applied fertilizer is effectively absorbed by crops, with the nitrogen use efficiency (NUE) ranging from around 30 to over 50 %.[15] As a result of rainfall, excess fertilizer drains away from the soil, resulting in water pollution. This leads to issues like surface water eutrophication, which has significant ecological impacts.[16] Additionally, the occurrence of nitrogen oxides like nitrate in drinking water is linked to infant methemoglobinemia, and is associated with an increased risk of cancer and birth defects.[17–19] Furthermore, the energy-intensive production

of fertilizers contributes to 1.5 % of the total global CO_2 emissions,[20] raising concerns about the environmental impact associated with fertilizer production.

1.2. From denitrification to nitrate recovery: potential applications and challenges

As mentioned earlier, the excessive use of nitrate fertilizers contributes to water contamination and, nowadays, denitrification systems are widely employed to reduce nitrate levels in water streams.[21–23] Through such water treatment systems, nitrate is converted to gaseous nitrogen (N_2) which is then released to the atmosphere. Although effective, this process demands considerable energy and produces by-products[24] such as N_2O, a potent greenhouse gas.[25]

Moreover, the conversion to N_2 is irreversible, leading to the removal of biologically accessible nitrogen from the ecosystem and the subsequent need to replenish nitrogen fertilizers. Therefore, considering both economic and sustainability perspectives, an appealing alternative involves recovering nitrate from water streams. One potential application involves retrieving nitrate from the effluent wastewater produced by fertilizer manufacturing plants.[26] Additionally, another area of application relates to greenhouses, as demonstrated by initiatives such as the Greenhouse Horticulture program in The Netherlands.[27] This initiative sets a goal to achieve almost zero emissions of fertilizers and crop protection agents by 2027, highlighting the importance of establishing closed-loop systems for water and nutrient recycling.

A viable technology to achieve nitrate recovery from water is electrodialysis (ED), which makes use of ion-exchange membranes (IEMs). This technology will be discussed in more detail in **Section 1.3**. As an example, Ahdab *et al.*[28] investigated the application of monovalent-selective electrodialysis for greenhouse wastewater in order to obtain a nitrate-rich brine. This brine can then be sent to a denitrification plant, and thus allowing for minimal liquid discharge, but it can also potentially be reused inside the greenhouse loop or to produce fertilizer. However, the presence of other anions can reduce the efficiency of the separation process. In particular, while the monovalent-divalent ion separation has already proved to be effective,[28–30] a more challenging case is represented by the separation of two monovalent ions, such as nitrate/chloride. These two anions share similar physico-chemical characteristics, including hydrated radii[31] and diffusion coefficients,[32] limiting their separation based on differences in size and mobility. However, there

exists a distinction in the ionic radius, leading to implications in dehydration energy. With chloride having an ionic radius of 0.181 nm and nitrate one of 0.264 nm,[31] the latter possesses lower dehydration energy, 71 kcal·mol^{-1} for nitrate and 81 kcal·mol^{-1} for chloride. As will be outlined further in **Section 1.4**, this difference can potentially be exploited to achieve preferential nitrate transportation through a membrane. Next to the above-mentioned applications, achieving such a preference would also be beneficial in addressing nitrate contamination of, *e.g.* groundwater[33,34] and surface water.[35]

1.3. Electrodialysis (ED)

Electrodialysis (ED) is a process that involves the transportation of ions through ion-exchange membranes (IEMs), using an electric field as a driving force. This technology has been applied for the desalination of brackish water sources since the 1950s, and found application in other various industries, including wastewater treatment,[36] and food processing,[37] offering a cost-effective and environmentally friendly solution for ion separation.[38] An electrodialysis (ED) unit (**Figure 1.1**) comprises a series of IEMs, including anion-exchange membranes (AEMs) and cation-exchange membranes (CEMs), which are stacked together in an alternating sequence. IEMs are discussed in more detail in **Section 1.4**. Water streams flow between these membranes, and upon connecting the electrodes to a power source the ions in the water streams are forced to move according to the electric field. Anions migrate towards the positively charged anode, while cations move towards the negatively charged cathode. The inclusion of IEMs acts as a selective barriers; AEMs allow the transportation of anions while impeding the transportation of cations, whereas CEMs selectively transport cations while blocking anions. This process leads to the depletion of salts in the water stream on one side of the membranes and their concentration on the other side, resulting in the formation of two separate streams known as diluate and concentrate, respectively.

The basic unit of an ED system, known as a cell pair, comprises an AEM, a CEM, a dilute stream, and a concentrate stream. An ED stack can consist of a few cell pairs in small-scale units used in laboratories and up to several hundred cell pairs in industrial setups. The unit includes two electrode compartments, where an electrolyte solution is recirculated. If an electrolyte solution

such as Na_2SO_4 is used in these compartments, the reaction taking place at the cathode surface is:

$$2H_2O + 2e^- \rightarrow H_2(g) + 2OH^-$$

while the one at the anode surface is:

$$H_2O \rightarrow 2H^+ + \frac{1}{2}O_2(g) + 2e^-$$

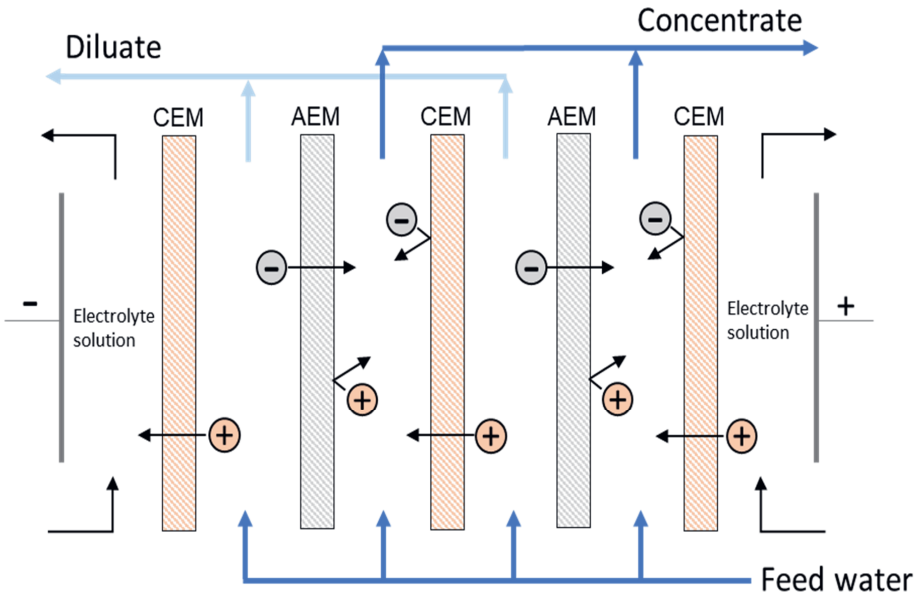

Figure 1.1: Schematic representation of an ED stack and its working principle: anions move through AEMs and cations through CEMs when an electric field is applied. By alternating CEMs and AEMs, diluate and concentrate streams are formed. The stack consists of repeating cell pairs (in this scheme two cell pairs, complemented with an extra shielding CEM between the concentrate and the anode).

1.4. Ion-Exchange Membranes (IEMs)

An ion-exchange membrane consists of a polymeric matrix containing charged groups fixed to the polymeric backbone. Depending on the charge of the fixed groups, IEMs can be categorized in anion-exchange membranes (AEMs), and cation-exchange membranes (CEMs). AEMs possess

positively charged groups such as quaternary ammonium groups,[29,39,40] which allow the transport of anions and rejection of cations. On the other hand, CEMs contain negatively charged groups such as sulfonic acid groups,[29,39,40] which allow the transport of cations and reject anions.

IEMs were originally derived from directly linking cationic or anionic groups to the polymer backbone without the presence of alkyl spacers.[41] However, over time, different polymer architectures have been investigated, including the incorporation of side chains (charged and uncharged),[42–44] and crosslinking within the polymer structure.[45,46] Furthermore, various methods for membrane fabrication, such as blending different types of polymers—whether both charged or only one charged—or incorporating additives, have been explored.[47–49] This approach expands beyond solely modifying the polymer itself, offering additional avenues for controlling membrane properties such as swelling and chemical and mechanical stability. Also, surface modification strategies such as embedding a cross-linked layer or the layer-by-layer (LbL) deposition of polyelectrolytes have been explored extensively.[50–52]

IEMs can also be classified as homogeneous or heterogeneous, in which the charged groups are chemically bonded to or physically mixed with the membrane matrix, respectively.[39] However, it must be realized that, as discussed by Luo *et al*.,[29] at a scale comparable to that of the polymer chain, the composition of an IEM is inherently heterogeneous, with the presence of hydrophilic domains characterized by the ionic groups and predominantly hydrophobic domains such as the polymer chains.

Due to the presence of fixed ionic groups, once in contact with an electrolyte solution, ions possessing the opposite charge of the ionic groups in the membrane (counter-ions) are attracted towards the membrane surface, generating an electrical potential, known as Donnan potential.[29] This potential results in the exclusion of co-ions.[53] At the membrane surface-water interface, an electrical double layer (EDL) forms, described by the Gouy-Chapman-Stern model, with counter-ions distributed according to a concentration profile that decays exponentially moving away from the membrane surface (**Figure 1.2**). In ED, the ion transport through an IEM is realized by applying

a current and involves the partitioning of the ionic species into the membrane and their diffusion through the membrane phase.

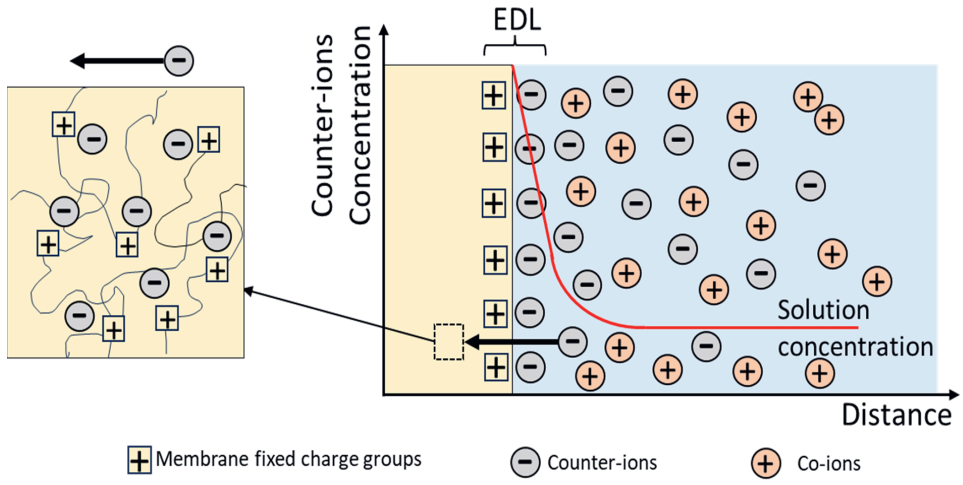

Figure 1.2: Simplified illustration of the ion concentration distribution at the membrane surface-water interface, and the electrical double layer (EDL). On the left, the counter-ions diffusion through the membrane and their interaction with the fixed charge groups.

1.5. Membrane selectivity

The selectivity of a membrane refers to the ability to selectively allow the passage of certain ions while hindering, or ideally even preventing, the transfer of other ions. As discussed in the previous section, the presence of fixed charged groups within the membrane allows the permeation of the counter-ions present in the solution in contact with the membrane. This type of selectivity, counter-ions *vs.* co-ions, is referred to as permselectivity and is measured through membrane potentiometry under zero-current conditions.[54] In this method, the potential across a membrane separating two solutions of the same electrolyte at different concentrations is recorded ($\Delta V_{\text{measured}}$) and used to calculate the membrane permselectivity (a) as a percentage, using the following equation:[55,56]

$$a = 100 \times \frac{\Delta V_{\text{measured}}}{\Delta V_{\text{theoretical}}} \qquad (1.1)$$

where $\Delta V_{theoretical}$ refers to the theoretical Nernst membrane potential for a membrane fully selective towards counter-ions. Typical permselectivity values are around or larger than 90 %, indicating a high membrane selectivity towards counter-ions compared to co-ions. On the other hand, the selectivity between different counter-ions is more challenging, especially for ions having the same valence. In this context, various studies highlight the crucial role of ion dehydration energy.[43,44,52,57–61] Ions in water are surrounded by a water shell (hydrated form), and the strength of this shell depends on the ionic radius. Smaller ions have a higher charge density, leading to stronger hydration and thus higher dehydration energy.[31] Epsztein *et al*.[57] proposed an ion partition mechanism based on partial ion dehydration at the water-membrane interface. Based on this mechanism, ions with a stronger hydration shell – thus higher dehydration energy – experience a higher energy barrier during dehydration compared to ions with weaker hydration, and therefore are less favorably adsorbed onto the membrane. The interaction between the partially dehydrated ion and the membrane fixed charge groups compensates energetically for the removal of water molecules, with ions that can undergo easier dehydration establishing stronger interaction and thus diffusing slowly than ions with stronger hydration shell.

In order to exploit the difference in dehydration energy between counter-ions, several studies focused on increasing the membrane hydrophobicity.[43,47,60,61] Sata *et al*.,[60] designed copolymer anion-exchange membranes functionalized with different tertiary amines such as trimethylamine, triethylamine, tri-*n*-propylamine, tri-*n*-butylamine, and tri-*n*-pentylamine. Their scope was to investigate how the change in the hydrophilic/hydrophobic environment around the anion-exchange groups influenced the membrane preferential ion transport. The results showed that as the surrounding of the charged groups became more hydrophobic, the membrane preferentially transported ions with lower hydration energy.

Following this contribution, Liao *et al.*[43] and Irfan *et al*.[61] applied the approach of Sata *et al.* to manufacture membranes with improved chloride over sulfate selectivity. In particular, Liao *et al*.[43] manufactured poly(arylene ether sulfone) AEMs varying the length of the alkyl side-chain connecting the positive imidazolium quaternary ammonium charge with the polymer backbone, while Irfan *et al*.[61] designed quaternized poly(2,6-dimethyl phenyleneoxide)s AEMs containing alkyl spacers of varied chain length. Both studies are in line with Sata's finding, showing an

increased chloride over sulfate selectivity, which was rationalized by an increased membrane hydrophobicity by increasing the length of the alkyl side chain.

Mubita *et al.*[47] developed heterogeneous anion-exchange membranes for the selective separation of nitrate from chloride, obtained by combining a functionalized polymeric binder and three ion-exchange resins, each containing a different functional group such as trimethyl, triethyl, or tripropyl ammonium moieties. Also in this case, the increased nitrate selectivity was linked to the increased membrane hydrophobicity with increasing the alkyl chain length, with the membrane bearing the most hydrophobic functional group, *i.e.* the tripropyl ammonium, showing the highest nitrate over chloride selectivity.

One approach for evaluating the selectivity of a membrane towards counter-ions involves conducting electrodialysis experiments in batch mode, using a mixed salt solution containing the specific counter-ions under investigation. By monitoring the concentration in the two reservoirs, concentrate and diluate, it is possible to determine the membrane selectivity according to the following equation:[47,62,63]

$$S_{\mathrm{B}}^{\mathrm{A}} = \left(\frac{\Delta C_{\mathrm{A}}}{\Delta C_{B}}\right)_{\mathrm{Concentrate}} \times \left(\frac{C_{\mathrm{A}}}{C_{\mathrm{B}}}\right)_{\mathrm{Diluate}} \tag{1.2}$$

where ΔC_{A} and ΔC_{B} refer to the change of the concentration of the indicated ion in the concentrate reservoir, while C_{A} and C_{B} represent the concentration of the ions in the diluate compartment. In literature, different experimental parameters are used such as current density, time, ion concentration, and membrane configuration, leading to challenges in comparing data.

Another method to get a quick indication of the membrane selectivity is represented by measuring the bi-ionic membrane potential ($\Delta\Psi$) and thus determining the permeability coefficient ratio. The bi-ionic potential is the potential that exists across a membrane, under zero-current conditions, separating two electrolyte solutions containing the same co-ion but different counter-ions, and is the result of the difference in the affinity of the counter-ions for the membrane. This potential can be expressed by using the following equation:[56,64]

$$\Delta\Psi = \frac{RT}{F} \times \ln\frac{P_{\mathrm{A}}}{P_{\mathrm{B}}} \tag{1.3}$$

where R is the universal gas constant (8.314 $J \cdot mol^{-1} \cdot K^{-1}$), T is the temperature (K), F is the Faraday constant (96458 $A \cdot s \cdot mol^{-1}$), and P_A and P_B the permeability coefficients ($m^2 \cdot s^{-1}$) of the counter-ions. By rearranging equation 1.3, it is possible to obtain the permeability coefficient ratio as a function of the potential difference ($\Delta\Psi$):

$$\frac{P_A}{P_B} = e^{\frac{F\Delta\Psi}{RT}} \quad (1.4)$$

1.6. Aim of the thesis

In the previous section, several contributions were reported on increasing the membrane selectivity towards less hydrated ions by increasing the membrane hydrophobicity. Building upon these findings, the aim of this thesis is to develop new anion-exchange membranes (AEMs) for the selective separation of nitrate from chloride by exploring the hydrophobicity of the membranes, investigating their performance in ED, and comparing with the results of one of the most recent studies on nitrate/chloride separation in ED, the one of Mubita *et al.*[63], and several commercial membranes. To identify the separation criteria we first developed a modelling tool to determine the key parameters of a membrane-based purification process for the selective recovery of nitrate from a water stream also containing chloride.

1.7. Outline of the thesis

Below is a visual outline of this thesis, accompanied by pertinent questions addressed in each chapter.

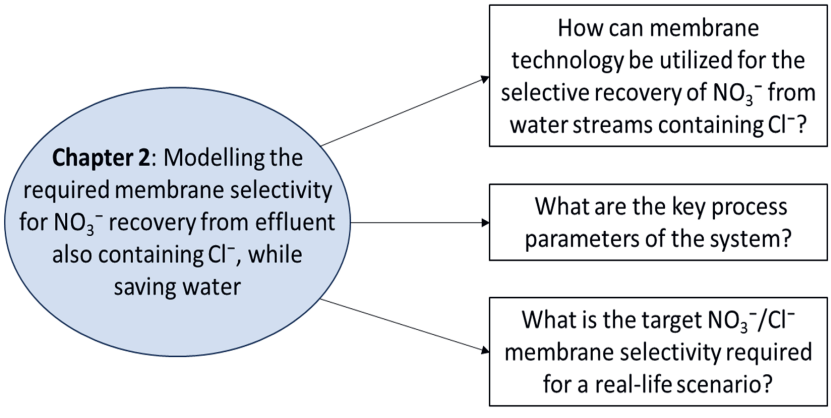

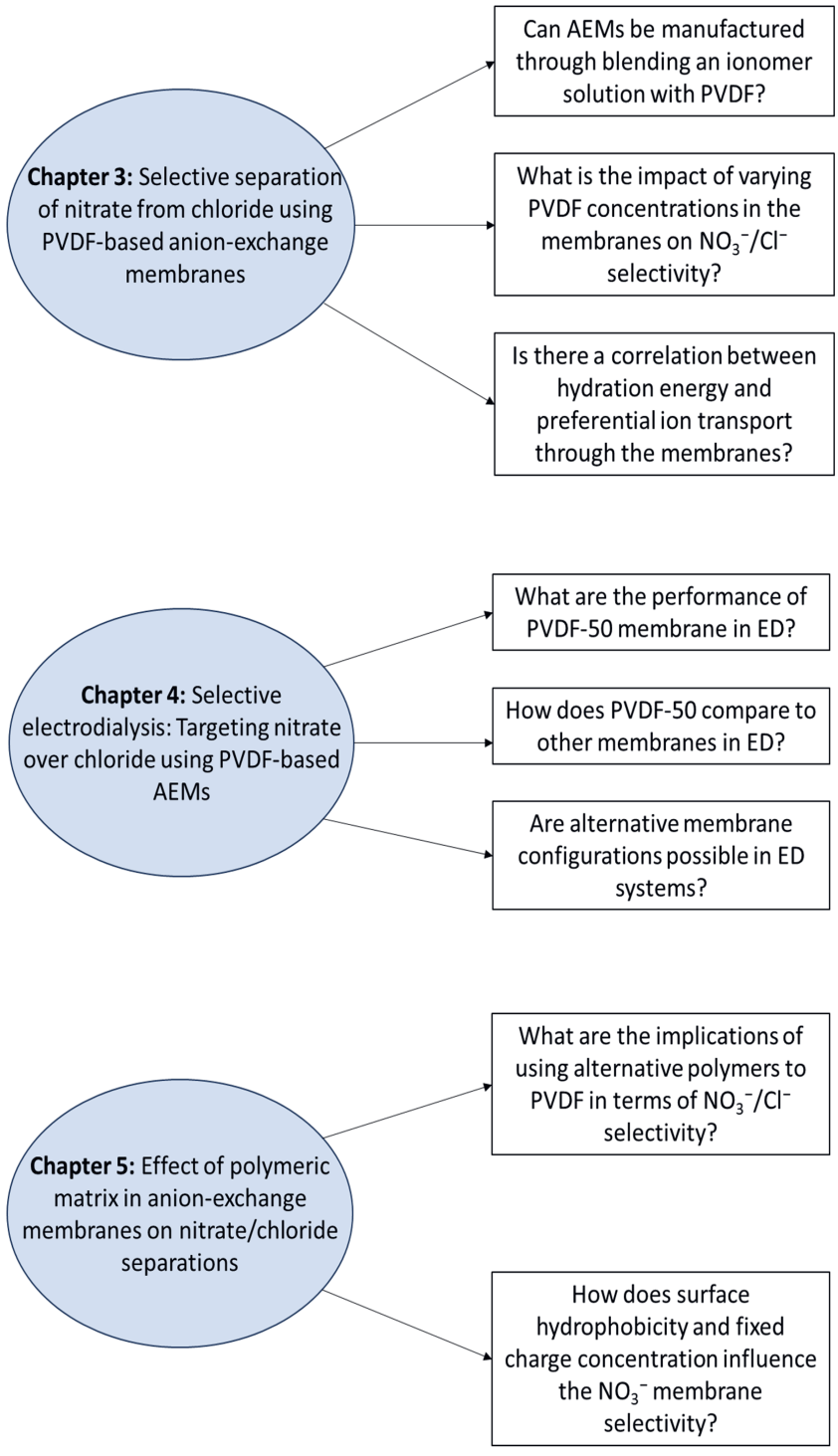
Chapter 3: Selective separation of nitrate from chloride using PVDF-based anion-exchange membranes
Can AEMs be manufactured through blending an ionomer solution with PVDF?
What is the impact of varying PVDF concentrations in the membranes on NO_3^-/Cl^- selectivity?
Is there a correlation between hydration energy and preferential ion transport through the membranes?
Chapter 4: Selective electrodialysis: Targeting nitrate over chloride using PVDF-based AEMs
What are the performance of PVDF-50 membrane in ED?
How does PVDF-50 compare to other membranes in ED?
Are alternative membrane configurations possible in ED systems?
Chapter 5: Effect of polymeric matrix in anion-exchange membranes on nitrate/chloride separations
What are the implications of using alternative polymers to PVDF in terms of NO_3^-/Cl^- selectivity?
How does surface hydrophobicity and fixed charge concentration influence the NO_3^- membrane selectivity?

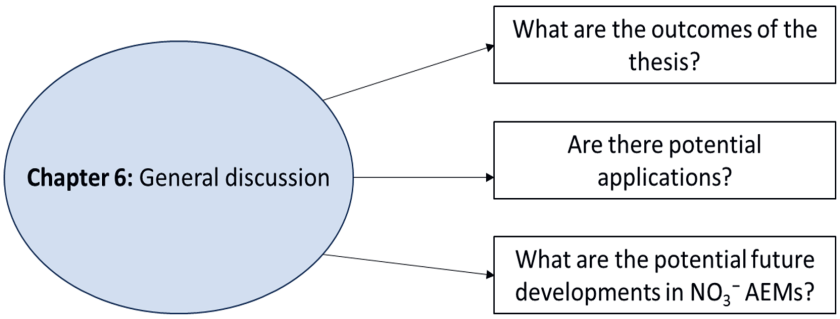

Chapter 2 introduces a membrane-based system for selectively recovering nitrate from wastewater also containing chloride, aiming to enhance water purification efficiency. It discusses key parameters influencing membrane selectivity and applies these to a real-world scenario.

Chapter 3 develops and assesses polyvinylidene fluoride (PVDF) based membranes for nitrate-chloride separation. Membrane with 50 wt% PVDF show optimal nitrate selectivity, and its ion transport properties are studied to understand selectivity mechanisms.

Chapter 4 examines the best PVDF-based membrane obtained in **Chapter 3** in electrodialysis for selective nitrate separation. Membrane properties are compared with commercial ones, and a novel method called nitrate-selectrodialysis (NO_3-SED) is proposed.

Chapter 5 explores alternative polymers like polyvinyl chloride (PVC) and polyacrylonitrile (PAN) for making nitrate-selective membranes. Membrane properties and selectivity are analyzed, comparing results with PVDF and commercial membranes.

Chapter 6 consolidates the insights from the preceding chapters and provides reflections on potential directions for future research.

References

(1) *The Atmosphere: Getting a Handle on Carbon Dioxide*. Climate Change: Vital Signs of the Planet. https://climate.nasa.gov/news/2915/the-atmosphere-getting-a-handle-on-carbon-dioxide (accessed 2024-03-04).

(2) Gruber, N.; Galloway, J. N. An Earth-System Perspective of the Global Nitrogen Cycle. *Nature* **2008**, *451* (7176), 293–296. https://doi.org/10.1038/nature06592.

(3) Ohbayashi, T.; Wang, Y.; Aoyagi, L. N.; Hara, S.; Tago, K.; Hayatsu, M. Diversity of the Hydroxylamine Oxidoreductase (HAO) Gene and Its Enzyme Active Site in Agricultural Field Soils. *Microbes Environ* **2023**, *38* (4), ME23068. https://doi.org/10.1264/jsme2.ME23068.

(4) Chicano, T. M.; Dietrich, L.; de Almeida, N. M.; Akram, M.; Hartmann, E.; Leidreiter, F.; Leopoldus, D.; Mueller, M.; Sánchez, R.; Nuijten, G. H. L.; Reimann, J.; Seifert, K.-A.; Schlichting, I.; van Niftrik, L.; Jetten, M. S. M.; Dietl, A.; Kartal, B.; Parey, K.; Barends, T. R. M. Structural and Functional Characterization of the Intracellular Filament-Forming Nitrite Oxidoreductase Multiprotein Complex. *Nat Microbiol* **2021**, *6* (9), 1129–1139. https://doi.org/10.1038/s41564-021-00934-8.

(5) Nitrate-Based-Fertilizers-Brochure.Pdf. https://www.yara.lt/globalassets/country-websites/campaign-assets/nbs-campaign/sub-pages/profit-page/crop-performance/nitrate-based-fertilizers-brochure.pdf (accessed 2024-03-04).

(6) Chorley, G. P. H. The Agricultural Revolution in Northern Europe, 1750–1880: Nitrogen, Legumes, and Crop Productivity. *The Economic History Review* **1981**, *34* (1), 71–93. https://doi.org/10.1111/j.1468-0289.1981.tb02007.x.

(7) Barnum, D. W. Some History of Nitrates. *J. Chem. Educ.* **2003**, *80* (12), 1393. https://doi.org/10.1021/ed080p1393.

(8) Kissel, D. E. The Historical Development and Significance of the Haber Bosch Process. **2014**, *98* (2).

(9) Johnson, B. *Making Ammonia: Fritz Haber, Walther Nernst, and the Nature of Scientific Discovery*; Springer International Publishing: Cham, 2022. https://doi.org/10.1007/978-3-030-85532-1.

(10) Witschi, H. Fritz Haber: December 9, 1868–January 29, 1934. *Toxicology* **2000**, *149* (1), 3–15. https://doi.org/10.1016/S0300-483X(00)00227-4.

(11) Ritchie, H.; Roser, M.; Rosado, P. Fertilizers. *Our World in Data* **2022**.

(12) World Population Prospects 2019 Highlights.Pdf. https://population.un.org/wpp/publications/files/wpp2019_highlights.pdf (accessed 2022-11-28).

(13) Wang, X.; Zhao, C.; Müller, C.; Wang, C.; Ciais, P.; Janssens, I.; Peñuelas, J.; Asseng, S.; Li, T.; Elliott, J.; Huang, Y.; Li, L.; Piao, S. Emergent Constraint on Crop Yield Response to Warmer Temperature from Field Experiments. *Nature Sustainability* **2020**, *3* (11), 908–916. https://doi.org/10.1038/s41893-020-0569-7.

(14) Skendžić, S.; Zovko, M.; Živković, I. P.; Lešić, V.; Lemić, D. The Impact of Climate Change on Agricultural Insect Pests. *Insects* **2021**, *12* (5). https://doi.org/10.3390/insects12050440.

(15) Anas, M.; Liao, F.; Verma, K. K.; Sarwar, M. A.; Mahmood, A.; Chen, Z.-L.; Li, Q.; Zeng, X.-P.; Liu, Y.; Li, Y.-R. Fate of Nitrogen in Agriculture and Environment: Agronomic, Eco-Physiological and Molecular Approaches to Improve Nitrogen Use Efficiency. *Biol Res* **2020**, *53* (1), 1–20. https://doi.org/10.1186/s40659-020-00312-4.

(16) Liu, L.; Zheng, X.; Wei, X.; Kai, Z.; Xu, Y. Excessive Application of Chemical Fertilizer and Organophosphorus Pesticides Induced Total Phosphorus Loss from Planting Causing Surface Water Eutrophication. *Sci Rep* **2021**, *11* (1), 23015. https://doi.org/10.1038/s41598-021-02521-7.

(17) Picetti, R.; Deeney, M.; Pastorino, S.; Miller, M. R.; Shah, A.; Leon, D. A.; Dangour, A. D.; Green, R. Nitrate and Nitrite Contamination in Drinking Water and Cancer Risk: A Systematic Review with Meta-Analysis. *Environmental Research* **2022**, *210*, 112988. https://doi.org/10.1016/j.envres.2022.112988.

(18) Essien, E. E.; Said Abasse, K.; Côté, A.; Mohamed, K. S.; Baig, M. M. F. A.; Habib, M.; Naveed, M.; Yu, X.; Xie, W.; Jinfang, S.; Abbas, M. Drinking-Water Nitrate and Cancer Risk: A Systematic Review and Meta-Analysis. *Archives of Environmental and Occupational Health* **2022**, *77* (1), 51–67. https://doi.org/10.1080/19338244.2020.1842313.

(19) Fewtrell, L. Drinking-Water Nitrate, Methemoglobinemia, and Global Burden of Disease: A Discussion. *Environmental Health Perspectives* **2004**, *112* (14), 1371–1374. https://doi.org/10.1289/ehp.7216.

(20) Kyriakou, V.; Garagounis, I.; Vourros, A.; Vasileiou, E.; Stoukides, M. An Electrochemical Haber-Bosch Process. *Joule* **2020**, *4* (1), 142–158. https://doi.org/10.1016/j.joule.2019.10.006.

(21) Xu, D.; Li, Y.; Yin, L.; Ji, Y.; Niu, J.; Yu, Y. Electrochemical Removal of Nitrate in Industrial Wastewater. *Front. Environ. Sci. Eng.* **2018**, *12* (1), 9. https://doi.org/10.1007/s11783-018-1033-z.

(22) Singh, V.; Ormeci, B.; Mishra, S.; Hussain, A. Simultaneous Partial Nitrification, ANAMMOX and Denitrification (SNAD) – A Review of Critical Operating Parameters and Reactor Configurations. *Chemical Engineering Journal* **2022**, *433*, 133677. https://doi.org/10.1016/j.cej.2021.133677.

(23) Ni, B. J.; Pan, Y.; Guo, J.; Virdis, B.; Hu, S.; Chen, X.; Yuan, Z. *CHAPTER 16: Denitrification Processes for Wastewater Treatment*; The Royal Society of Chemistry, 2017; Vol. 2017-Janua. https://doi.org/10.1039/9781782623762-00368.

(24) Ye, Y.; Ngo, H. H.; Guo, W.; Liu, Y.; Chang, S. W.; Nguyen, D. D.; Liang, H.; Wang, J. A Critical Review on Ammonium Recovery from Wastewater for Sustainable Wastewater Management. *Bioresource Technology* **2018**, *268* (July), 749–758. https://doi.org/10.1016/j.biortech.2018.07.111.

(25) Thakur, I. S.; Medhi, K. Nitrification and Denitrification Processes for Mitigation of Nitrous Oxide from Waste Water Treatment Plants for Biovalorization: Challenges and Opportunities. *Bioresource Technology* **2019**, *282*, 502–513. https://doi.org/10.1016/j.biortech.2019.03.069.

(26) Chinello, D.; Myrstad, A.; de Smet, L. C. P. M.; Miedema, H. Modelling the Required Membrane Selectivity for $NO3^-$ Recovery from Effluent Also Containing Cl^-, While Saving Water. *Chemical Engineering Research and Design* **2023**, *193*, 409–419. https://doi.org/10.1016/j.cherd.2023.03.038.

(27) van der Salm, C.; Voogt, W.; Beerling, E.; van Ruijven, J.; van Os, E. Minimising Emissions to Water Bodies from NW European Greenhouses; with Focus on Dutch Vegetable Cultivation. *Agricultural Water Management* **2020**, *242*, 106398. https://doi.org/10.1016/j.agwat.2020.106398.

(28) Ahdab, Y. D.; Schücking, G.; Rehman, D.; Lienhard, J. H. Treatment of Greenhouse Wastewater for Reuse or Disposal Using Monovalent Selective Electrodialysis. *Desalination* **2021**, *507*, 115037. https://doi.org/10.1016/j.desal.2021.115037.

(29) Luo, T.; Abdu, S.; Wessling, M. Selectivity of Ion Exchange Membranes: A Review. *Journal of Membrane Science* **2018**, *555* (December 2017), 429–454. https://doi.org/10.1016/j.memsci.2018.03.051.

(30) Ahdab, Y. D.; Rehman, D.; Schücking, G.; Barbosa, M.; Lienhard, J. H. Treating Irrigation Water Using High-Performance Membranes for Monovalent Selective Electrodialysis. *ACS EST Water* **2021**, *1* (1), 117–124. https://doi.org/10.1021/acsestwater.0c00012.

(31) Nightingale, E. R. Phenomenological Theory of Ion Solvation. Effective Radii of Hydrated Ions. *J. Phys. Chem.* **1959**, *63* (9), 1381–1387. https://doi.org/10.1021/j150579a011.

(32) Cussler, E. L. *Diffusion: Mass Transfer in Fluid Systems*; Cambridge University Press, 1997.

(33) Wang, D.; Wu, J.; Li, P.; Li, L.; Yang, J.; Zhang, P.; He, S.; Kou, X.; Wang, Y. Seasonal Nitrate Variations, Risks, and Sources in Groundwater under Different Land Use Types in a Thousand-Year-Cultivated Region, Northwestern China. *Environmental Research* **2024**, 118699. https://doi.org/10.1016/j.envres.2024.118699.

(34) Modi, A.; Kasher, R. Nitrate Removal from Contaminated Groundwater by Micellar-Enhanced Ultrafiltration Using a Polyacrylonitrile Membrane with a Hydrogel-Stabilized ZIF-L Layer. *Water Research* **2024**, *254*, 121384. https://doi.org/10.1016/j.watres.2024.121384.

(35) Zhang, X.; Zhang, Y.; Shi, P.; Bi, Z.; Shan, Z.; Ren, L. The Deep Challenge of Nitrate Pollution in River Water of China. *Science of The Total Environment* **2021**, *770*, 144674. https://doi.org/10.1016/j.scitotenv.2020.144674.

(36) Gurreri, L.; Tamburini, A.; Cipollina, A.; Micale, G. Electrodialysis Applications in Wastewater Treatment for Environmental Protection and Resources Recovery: A Systematic Review on Progress and Perspectives. *Membranes* **2020**, *10* (7), 146. https://doi.org/10.3390/membranes10070146.

(37) Mondor, M.; Ippersiel, D.; Lamarche, F. Electrodialysis in Food Processing. In *Green Technologies in Food Production and Processing*; Boye, J. I., Arcand, Y., Eds.; Springer US: Boston, MA, 2012; pp 295–326. https://doi.org/10.1007/978-1-4614-1587-9_12.

(38) Al-Amshawee, S.; Yunus, M. Y. B. M.; Azoddein, A. A. M.; Hassell, D. G.; Dakhil, I. H.; Hasan, H. A. Electrodialysis Desalination for Water and Wastewater: A Review. *Chemical Engineering Journal* **2020**, *380*, 122231. https://doi.org/10.1016/j.cej.2019.122231.

(39) Xu, T. Ion Exchange Membranes: State of Their Development and Perspective. *Journal of Membrane Science* **2005**, *263* (1–2), 1–29. https://doi.org/10.1016/j.memsci.2005.05.002.

(40) Strathmann, H.; Giorno, L.; Drioli, E. An Introduction to Membrane Science and Technology.

(41) Ran, J.; Wu, L.; He, Y.; Yang, Z.; Wang, Y.; Jiang, C.; Ge, L.; Bakangura, E.; Xu, T. Ion Exchange Membranes: New Developments and Applications. *Journal of Membrane Science* **2017**, *522*, 267–291. https://doi.org/10.1016/j.memsci.2016.09.033.

(42) Sheng, L.; Higashihara, T.; Nakazawa, S.; Ueda, M. Polystyrenes Containing Flexible Alkylsulfonated Side Chains as a Proton Exchange Membrane for Fuel Cell Application. *Polym. Chem.* **2012**, *3* (12), 3289–3295. https://doi.org/10.1039/C2PY20552A.

(43) Liao, J.; Yu, X.; Chen, Q.; Gao, X.; Ruan, H.; Shen, J.; Gao, C. Monovalent Anion Selective Anion-Exchange Membranes with Imidazolium Salt-Terminated Side-Chains: Investigating the Effect of Hydrophobic Alkyl Spacer Length. *Journal of Membrane Science* **2020**, *599*, 117818. https://doi.org/10.1016/j.memsci.2020.117818.

(44) Tekinalp, Ö.; Zimmermann, P.; Holdcroft, S.; Burheim, O. S.; Deng, L. Cation Exchange Membranes and Process Optimizations in Electrodialysis for Selective Metal Separation: A Review. *Membranes* **2023**, *13* (6), 566. https://doi.org/10.3390/membranes13060566.

(45) Mareev, S. A.; Butylskii, D. Yu.; Pismenskaya, N. D.; Larchet, C.; Dammak, L.; Nikonenko, V. V. Geometric Heterogeneity of Homogeneous Ion-Exchange Neosepta Membranes. *Journal of Membrane Science* **2018**, *563*, 768–776. https://doi.org/10.1016/j.memsci.2018.06.018.

(46) Lin, C. X.; Zhuo, Y. Z.; Hu, E. N.; Zhang, Q. G.; Zhu, A. M.; Liu, Q. L. Crosslinked Side-Chain-Type Anion Exchange Membranes with Enhanced Conductivity and Dimensional Stability. *Journal of Membrane Science* **2017**, *539*, 24–33. https://doi.org/10.1016/j.memsci.2017.05.063.

(47) Mubita, T.; Porada, S.; Aerts, P.; van der Wal, A. Heterogeneous Anion Exchange Membranes with Nitrate Selectivity and Low Electrical Resistance. *Journal of Membrane Science* **2020**, *607*, 118000. https://doi.org/10.1016/j.memsci.2020.118000.

(48) Kikhavani, T.; Ashrafizadeh, S. N.; Van Der Bruggen, B. Nitrate Selectivity and Transport Properties of a Novel Anion Exchange Membrane in Electrodialysis. *Electrochimica Acta* **2014**, *144*, 341–351. https://doi.org/10.1016/j.electacta.2014.08.012.

(49) Klaysom, C.; Moon, S.-H.; Ladewig, B. P.; Lu, G. Q. M.; Wang, L. The Influence of Inorganic Filler Particle Size on Composite Ion-Exchange Membranes for Desalination. *J. Phys. Chem. C* **2011**, *115* (31), 15124–15132. https://doi.org/10.1021/jp112157z.

(50) Jonkers, W. A.; de Vos, W. M.; te Brinke, E. Asymmetric Polyelectrolyte Multilayer Membranes: Influence of Bottom Section Polycation on Layer Growth and Retention Mechanisms. *Journal of Membrane Science* **2024**, *698*, 122577. https://doi.org/10.1016/j.memsci.2024.122577.

(51) Krishna B, A.; Zwijnenberg, H. J.; Lindhoud, S.; de Vos, W. M. Sustainable K+/Na+ Monovalent-Selective Membranes with Hot-Pressed PSS-PVA Saloplastics. *Journal of Membrane Science* **2022**, *652*, 120463. https://doi.org/10.1016/j.memsci.2022.120463.

(52) Tekinalp, Ö.; Zimmermann, P.; Burheim, O. S.; Deng, L. Designing Monovalent Selective Anion Exchange Membranes for the Simultaneous Separation of Chloride and Fluoride from Sulfate in an Equimolar Ternary Mixture. *Journal of Membrane Science* **2023**, *666*, 121148. https://doi.org/10.1016/j.memsci.2022.121148.

(53) Aydogan Gokturk, P.; Sujanani, R.; Qian, J.; Wang, Y.; Katz, L. E.; Freeman, B. D.; Crumlin, E. J. The Donnan Potential Revealed. *Nat Commun* **2022**, *13* (1), 5880. https://doi.org/10.1038/s41467-022-33592-3.

(54) Dlugolecki, P.; Nymeijer, K.; Metz, S.; Wessling, M. Current Status of Ion Exchange Membranes for Power Generation from Salinity Gradients. *Journal of Membrane Science* **2008**, *319* (1–2), 214–222. https://doi.org/10.1016/j.memsci.2008.03.037.

(55) Długołęcki, P.; Ogonowski, P.; Metz, S. J.; Saakes, M.; Nijmeijer, K.; Wessling, M. On the Resistances of Membrane, Diffusion Boundary Layer and Double Layer in Ion Exchange Membrane Transport. *Journal of Membrane Science* **2010**, *349* (1–2), 369–379. https://doi.org/10.1016/j.memsci.2009.11.069.

(56) Chinello, D.; Post, J.; de Smet, L. C. P. M. Selective Separation of Nitrate from Chloride Using PVDF-Based Anion-Exchange Membranes. *Desalination* **2023**, 117084. https://doi.org/10.1016/j.desal.2023.117084.

(57) Epsztein, R.; Shaulsky, E.; Qin, M.; Elimelech, M. Activation Behavior for Ion Permeation in Ion-Exchange Membranes: Role of Ion Dehydration in Selective Transport. *Journal of Membrane Science* **2019**, *580* (January), 316–326. https://doi.org/10.1016/j.memsci.2019.02.009.

(58) Zhao, Y.; Mamrol, N.; Tarpeh, W. A.; Yang, X.; Gao, C.; Van der Bruggen, B. Advanced Ion Transfer Materials in Electro-Driven Membrane Processes for Sustainable Ion-Resource Extraction and Recovery. *Progress in Materials Science* **2022**, *128*, 100958. https://doi.org/10.1016/j.pmatsci.2022.100958.

(59) Jiang, C.; Wang, Q.; Li, Y.; Wang, Y.; Xu, T. Water Electro-Transport with Hydrated Cations in Electrodialysis. *Desalination* **2015**, *365*, 204–212. https://doi.org/10.1016/j.desal.2015.03.007.

(60) Sata, T. Studies on Anion Exchange Membranes Having Permselectivity for Specific Anions in Electrodialysis - Effect of Hydrophilicity of Anion Exchange Membranes on Permselectivity of Anions. *Journal of Membrane Science* **2000**, *167* (1), 1–31. https://doi.org/10.1016/S0376-7388(99)00277-X.

(61) Irfan, M.; Ge, L.; Wang, Y.; Yang, Z.; Xu, T. Hydrophobic Side Chains Impart Anion Exchange Membranes with High Monovalent–Divalent Anion Selectivity in Electrodialysis. *ACS Sustainable Chem. Eng.* **2019**, *7* (4), 4429–4442. https://doi.org/10.1021/acssuschemeng.8b06426.

(62) Sata, T.; Yamane, Y.; Matsusaki, K. Relationship of Permselectivity between Two Anions to Water Content of Anion Exchange Membranes with Pyridinium Groups. *Electrochimica Acta* **1997**, *42* (15), 2427–2431. https://doi.org/10.1016/S0013-4686(96)00405-7.

(63) Mubita, T. M.; Porada, S.; Biesheuvel, P. M.; van der Wal, A.; Dykstra, J. E. Strategies to Increase Ion Selectivity in Electrodialysis. *Separation and Purification Technology* **2022**, *292*, 120944. https://doi.org/10.1016/j.seppur.2022.120944.

(64) Qian, Z.; Miedema, H.; Sahin, S.; de Smet, L. C. P. M.; Sudhölter, E. J. R. Separation of Alkali Metal Cations by a Supported Liquid Membrane (SLM) Operating under Electro Dialysis (ED) Conditions. *Desalination* **2020**, *495*. https://doi.org/10.1016/j.desal.2020.114631.

Chapter 2

Modelling the required membrane selectivity for NO_3^- recovery from effluent also containing Cl^-, while saving water

This chapter has been published as:
Chinello, D.; Myrstad, A.; de Smet, L. C. P. M.; Miedema, H. Modelling the required membrane selectivity for NO_3^- recovery from effluent also containing Cl^-, while saving water. *Chemical Engineering Research and Design* **2023**, *193*, 409-419.

Abstract

We present a general outline for the selective recovery of NO_3^- from a (waste) water stream also containing Cl^-. The key element of the technology introduced and simulated here is a membrane unit demonstrating NO_3^- over Cl^- permeation selectivity. The membrane is hypothesized to be hydrophobic and with that exploiting the difference in dehydration energy between NO_3^- and Cl^-. Apart from NO_3^- recovery, the process also aims to reduce water consumption. Based on a generic outline of the process, the key parameters are defined, being the NO_3^-/Cl^- concentration ratio in the (waste) stream, the fraction of NO_3^- and water recovered, and the selectivity of the membrane. The sensitivity of the separation process to these four parameters is evaluated. In the second part of the paper, the same principles are applied to a real-life process, *i.e.*, NO_3^- recovery from the effluent (waste) water of a fertilizer production plant. The aim was to calculate the membrane NO_3^-/Cl^- permeation selectivity required to recover 90 % of NO_3^-, given a threshold value for the Cl^- concentration in the permeate stream and recycle 30 % of the water, starting from two different NO_3^-/Cl^- concentration ratios in the effluent (waste) water. With 51 mM Cl^- in the effluent (waste) water and a Cl^- threshold of 9.9 mM, a membrane selectivity of 3 suffices. The required selectivity increases to 30 when the Cl^- in the effluent (waste) water is 200 mM and the Cl^- threshold is 4.2 mM. Reported NO_3^-/Cl^- membrane selectivities are still modest, with a maximal selectivity found in literature of 3. Strategies to develop membranes of significant higher selectivity are briefly discussed.

2.1. Introduction

Nitrogen is an essential nutrient for agriculture. In 2020 its consumption was estimated to be 10 million tons in the EU alone, 6.9 % above its consumption in 2010[1]. The conversion of N_2 to ammonia, an essential compound for fertilizer production, via the Haber-Bosch process is not only energy intensive but also responsible for no less than 1.5 % of the total worldwide CO_2 emission.[2] With an increasing global population – by 2060, the world population will reach 10 billion[3] – and the decrease in agricultural production due to climate change,[4] pests,[5] and lack of nutrients, the need of using fertilizers to sustain crop production will only increase further. However, not all applied fertilizer is actually taken up by crops. As an example case, in 2015 the nitrogen use efficiency (NUE) of cereal was estimated to be just 35 %.[6] Due to precipitation, excess fertilizer leaches out of the soil, causing eutrophication of surface waters with all its detrimental effects.[7] Furthermore, the presence of nitrogen oxides, such as nitrate (NO_3^-), in drinking water is responsible for infant methemoglobinemia (also known as blue baby syndrome) and increases the risk of cancer[8] and birth defects.[9]

Currently used wastewater treatment technologies remove nitrogen by conversion of N-species to gaseous N_2.[10] However, these nitrification/denitrification processes deal with high costs, high chemical use, and by-product formation such as N_2O and Cl_2.[11] Moreover, the conversion to N_2 is irreversible, resulting in removing biologically directly available nitrogen from the ecosystem. From the point of view of both economics and sustainability, an attractive alternative is the selective recovery of nitrogen. To do so, we here explore the potential and requirements of membrane technology to selectively recover NO_3^-.

Together with phosphorus (P) and potassium (K), nitrogen (N) is the main component of NPK fertilizers; chloride is present as well because potassium chloride (KCl) is the source of potassium. The co-presence of Cl^- makes the recovery of NO_3^- challenging because both ion species have the same valence. However, there is a difference in the (effective) ionic radius and by implication in the dehydration energy. With an ionic radius of 0.181 nm for Cl^- and 0.264 nm for NO_3^-,[12] the latter has a lower dehydration energy.[13]

In membrane technology, differences in dehydration energy can be exploited to separate ion species. As shown in previous studies,[14–20] the transport of ions with low dehydration energy is enhanced by increasing the membrane hydrophobicity. Therefore, in this study, we hypothesize

and introduce a membrane unit possessing a hydrophobic membrane with a permeation preference of NO_3^- over Cl^- because of the lower dehydration energy of the former ion species. Furthermore, it is envisaged that the membrane operates in an electrodialysis setting.

This paper consists of two parts. The first one describes and discusses a rather basic outline of a process for the separation of NO_3^- from Cl^- using membrane technology. The most relevant process parameters are evaluated. In the second part of the paper, we switch to a real-life application, using some of the findings discussed in the first part. Here, we investigate the recovery of NO_3^- from the effluent (waste) water of a fertilizer plant while saving 30 % of fresh water.

2.2. Materials and methods

2.2.1. System Description

Figure 2.1 shows a general outline of a membrane-based process for the selective separation of NO_3^- from Cl^-. The (waste) water stream containing the two ion species, from here on labelled the feed stream, enters the system in the mixer, where fresh and recycled water are added to the extent to keep the volumetric flow constant. The resulting stream (reference point #0) is sent to the membrane unit responsible for the NO_3^- recovery and producing a permeate stream (reference point #1) relatively rich in NO_3^-. Depending on the membrane selectivity, this stream is more or less contaminated with Cl^-. The retentate stream (reference point #2), relatively rich in Cl^-, is split (reference point #3) and, in order to minimize the fresh water consumption, partly recycled and directed towards the mixer.

In the system, four reference points are distinguished:

- point #0: where fresh water, the feed stream, and recycled water are mixed;
- point #1: water stream after filtration by the membrane unit (permeate side);
- point #2: water stream after filtration by the membrane unit (retentate side);
- point #3: water stream after splitting, re-entering the mixer.

The model calculates the NO_3^-/Cl^- concentration ratio (indicated with the letter *R*) at the four reference points at a range of set membrane selectivity values. This way, we can define the NO_3^-

over Cl^- permeation membrane selectivity required to achieve the desired concentration ratio value at reference point #1.

The nomenclature adopted throughout this study is based on the use of two indices, the first representing the reference point and the second the cycle number. For instance, $R_{2;4}$ refers to the NO_3^-/Cl^- concentration ratio at reference point #2 during the fourth cycle:

$$R_{2;4} = \frac{[NO_3^-]_{2;4}}{[Cl^-]_{2;4}}$$

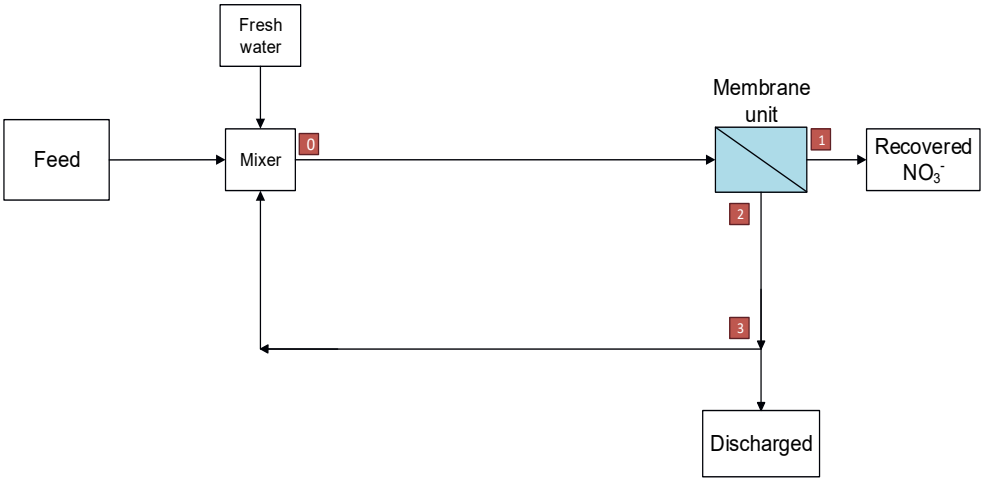

Figure 2.1: General outline of a membrane-based process for the selective recovery of NO_3^- from a water stream also containing Cl^-. Reference points #0-3 are indicated and further explained in the text.

2.2.2. Mass balance

Figure 2.2 shows the basic outline of **Figure 2.1**, complemented with all relevant parameters referred to in this study, which are reported in **Table 2.1**. The volumetric flow leaving point #0 and entering the membrane unit remains constant through the cycles.

For the first cycle, it has been assumed that the composition at point #0 is 50 % feed stream and 50 % fresh water. As remarked, after the first cycle, and in order to limit the fresh water consumption, some of the retentate stream (Φ_v (5), reference point #3) is recycled. This fraction (λ) will be varied in the simulations from 0.5 to 0 to study the influence of the Cl^- build-up in the

system on the required membrane selectivity. Moreover, for all cycles, the fraction of the feed stream entering the mixer has been fixed at 0.5.

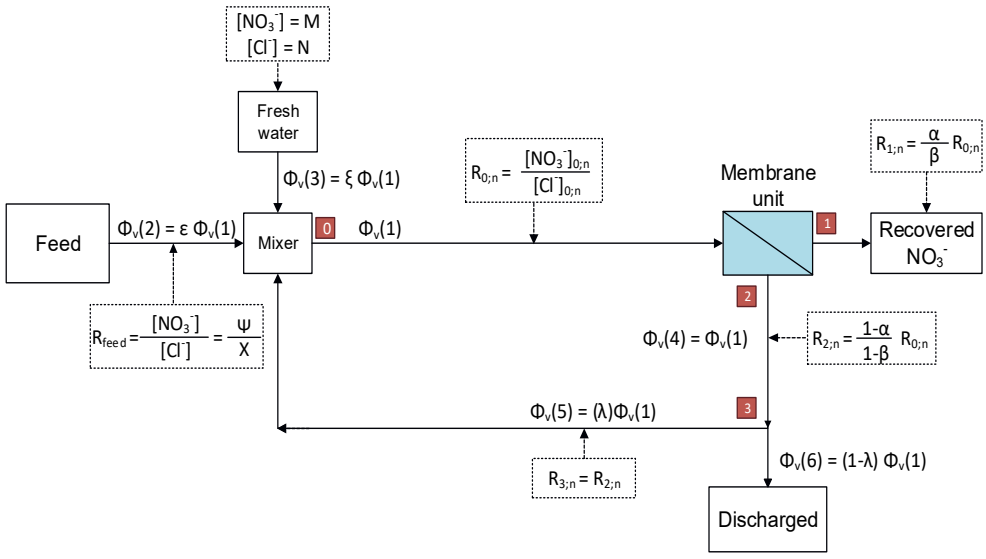

Figure 2.2: Outline of **Figure 2.1**, complemented with volumetric flows Φv(1)-Φv(6) and all relevant process parameters.

Table 2.1: List of the parameters used for this study.

Variable	Description
$\boldsymbol{\Phi_v}$	Volumetric flow
$\boldsymbol{\psi}$	NO_3^- concentration in the feed
$\boldsymbol{X}$	Cl^- concentration in the feed
$\boldsymbol{R_{feed}}$	NO_3^-/ Cl^- concentration ratio in the feed: $\boldsymbol{R_{feed} = \psi / X}$
$\boldsymbol{R_{m,n}}$	NO_3^-/ Cl^- concentration at reference point #*m* in cycle #*n*
$\boldsymbol{M}$	NO_3^- concentration in fresh water
$\boldsymbol{N}$	Cl^- concentration in fresh water

Variable	Description
$\boldsymbol{\varepsilon_1}$	Fraction of feed stream entering at point #0 for the 1st cycle
$\boldsymbol{\varepsilon_n}$	Fraction of feed stream entering at point #0 for cycle number n (n > 1)
$\boldsymbol{\xi_1}$	Fraction of fresh water entering at point #0 for the 1st cycle
$\boldsymbol{\xi_n}$	Fraction of fresh water entering at point #0 for cycles number n (n > 1)
$\boldsymbol{\alpha}$	Fraction of NO_3^- removed by the membrane system
$\boldsymbol{\beta}$	Fraction of Cl^- removed by the membrane system
$\boldsymbol{\gamma}$	NO_3^- over Cl^- permeation selectivity of the membrane system: α/β
$\boldsymbol{\lambda}$	Fraction of water recycled

2.2.2.1. First cycle (n = 1)

2.2.2.1.1. Reference point #0

As mentioned previously, the composition at point #0 is 50 % feed stream ($\varepsilon_1 = 0.5$) and 50 % fresh water ($\xi_1 = 0.5$), resulting in the following volumetric flow:

$$\Phi_v(1) = \Phi_v(2) + \Phi_v(3) = \varepsilon_1 \Phi_v(1) + \xi_1 \Phi_v(1) \tag{2.1}$$

With Ψ and X representing the concentration of NO_3^- and Cl^- in the feed stream, and M and N the concentration of NO_3^- and Cl^- in fresh water, the NO_3^- and Cl^- mass balances read as follows:

$$\Phi_v(1)[NO_3^-]_{0;1} = \varepsilon_1 \Phi_v(1)\Psi + \xi_1 \Phi_v(1)M \tag{2.2}$$

$$[NO_3^-]_{0;1} = \varepsilon_1 \Psi + \xi_1 M \tag{2.3}$$

$$\Phi_v(1)[Cl^-]_{0;1} = \varepsilon_1 \Phi_v(1)X + \xi_1 \Phi_v(1)N \tag{2.4}$$

$$[Cl^-]_{0;1} = \varepsilon_1 X + \xi_1 N \tag{2.5}$$

Therefore, the NO_3^-/Cl^- concentration ratio is defined by:

$$R_{0;1} = \frac{[NO_3^-]_{0;1}}{[Cl^-]_{0;1}} = \frac{\varepsilon_1 \Psi + \xi_1 M}{\varepsilon_1 X + \xi_1 N} \tag{2.6}$$

2.2.2.1.2. Reference point #1

Reference point #1 is positioned at the permeate side of the membrane unit. With α and β representing the fractions of feed NO_3^- and Cl^- that permeate the membrane, the concentration ratio of these two ion species is:

$$R_{1;1} = \frac{[NO_3^-]_{1;1}}{[Cl^-]_{1;1}} = \frac{\alpha}{\beta} R_{0;1} = \gamma R_{0;1} \tag{2.7}$$

where γ represents the membrane permeation selectivity:

$$\gamma = \frac{\alpha}{\beta} \tag{2.8}$$

It can easily be appreciated that γ is indeed a measure of the selectivity of the membrane. Indeed, the ratio of the number of moles of NO_3^- and Cl^- passing the membrane per unit of time, $n_{NO_3^-}$ and n_{Cl^-}, is given by:

$$\frac{n_{NO_3^-}}{n_{Cl^-}} = \frac{\alpha[NO_3^-]_{0;n}}{\beta[Cl^-]_{0;n}} \tag{2.9}$$

To normalize this ratio for the effect of concentration, this number needs to be multiplied by the inverse ratio of their feed concentrations, resulting in:

$$\frac{n_{NO_3^-}}{n_{Cl^-}} \frac{[Cl^-]_{0;n}}{[NO_3^-]_{0;n}} = \frac{\alpha[NO_3^-]_{0;n}}{\beta[Cl^-]_{0;n}} \frac{[Cl^-]_{0;n}}{[NO_3^-]_{0;n}} = \frac{\alpha}{\beta} = \gamma \tag{2.10}$$

2.2.2.1.3. Reference point #2

Reference point #2 is located downstream the membrane unit, as is reference point #1, but at the retentate side instead. Here the concentration ratio is given by:

$$R_{2;1} = \frac{[NO_3^-]_{2;1}}{[Cl^-]_{2;1}} = \frac{(1-\alpha)}{(1-\beta)} R_{0;1} \tag{2.11}$$

Because of the hydrophobic nature of the proposed membrane, any potential water transport over the membrane is neglected, resulting in a volumetric flow balance of:

$$\Phi_v(4) = \Phi_v(1) \tag{2.12}$$

2.2.2.1.4. Reference point #3

At this point, stream $\Phi_v(4)$ is split into two streams. One is discharged and one is recycled and led to the mixer. Given that a fraction (λ) is recycled, the volumetric flow balance reads:

$$\Phi_v(5) = \lambda\Phi_v(1) \tag{2.13}$$

Compared to reference point #2, the NO_3^-/Cl^- concentration ratio at point #3 is the same:

$$R_{3;1} = R_{2;1} = \frac{[NO_3^-]_{3;1}}{[Cl^-]_{3;1}} \tag{2.14}$$

2.2.2.2. Second cycle (n = 2)

2.2.2.2.1. Reference point #0

The calculations for the 2nd cycle, and for that matter for all cycles that follow as well, are essentially the same as those for the first cycle. The main difference with the first cycle regards

the volumetric flow balance at the reference point #0, considering that a fraction (λ) of the retentate stream ($\Phi_v(5)$) has been recycled, resulting in:

$$\Phi_v(1) = \Phi_v(2) + \Phi_v(3) + \Phi_v(5) \quad (2.15)$$

or, expressed slightly differently, in:

$$\Phi_v(1) = \varepsilon_2\Phi_v(1) + \xi_2\Phi_v(1) + \lambda\Phi_v(1) \quad (2.16)$$

The NO_3^- and Cl^- mass balances are:

$$[NO_3^-]_{0;2} = \varepsilon_2\Psi + \xi_2 M + \lambda[NO_3^-]_{3;1} \quad (2.17)$$

$$[Cl^-]_{0;2} = \varepsilon_2 X + \xi_2 N + \lambda[Cl^-]_{3;1} \quad (2.18)$$

where:

$$\varepsilon_2 = \varepsilon_1 = 0.5 \quad (2.19)$$

and

$$\xi_2 = 1 - \varepsilon_2 - \lambda \quad (2.20)$$

Based on equations. 2.17 and 2.18, $R_{0;2}$ is given by:

$$\frac{[NO_3^-]_{0;2}}{[Cl^-]_{0;2}} = R_{0;2} = \frac{\varepsilon_2\Psi+\xi_2 M+\lambda[NO_3^-]_{3;1}}{\varepsilon_2 X+\xi_2 N+\lambda[Cl^-]_{3;1}} \quad (2.21)$$

The expressions regarding reference points #1 to #3 are similar to those for the first cycle, as outlined in the next sections.

2.2.2.2.2. Reference point #1

$$\frac{[NO_3^-]_{1;2}}{[Cl^-]_{1;2}} = R_{1;2} = \frac{\alpha}{\beta} R_{0;2} = \gamma R_{0;2} \quad (2.22)$$

2.2.2.2.3. Reference point #2

$$\frac{[NO_3^-]_{2;2}}{[Cl^-]_{2;2}} = R_{2;2} = \frac{(1-\alpha)}{(1-\beta)} R_{0;2} \quad (2.23)$$

$$\Phi_v(4) = \Phi_v(1) \quad (2.24)$$

2.2.2.2.4. Reference point #3

$$\Phi_v(5) = \lambda\Phi_v(1) \tag{2.25}$$

$$\frac{[NO_3^-]_{3;2}}{[Cl^-]_{3;2}} = R_{3;2} = R_{2;2} \tag{2.26}$$

2.3. Results

As evident from **Section 2.2**, the calculations require input values of a number of parameters. The following four are considered the most important ones:

- The NO_3^-/Cl^- concentration ratio in the feed (R_{feed});
- The fraction of NO_3^- (α) removed at the membrane unit;
- The membrane permeation selectivity (γ) with $\gamma = \alpha/\beta$;
- The fraction of retentate stream that is recycled (λ).

Here we will evaluate the sensitivity of the calculations to the value of each of these key parameters on the (equilibrium) value of $R_{1,n}$, that is the NO_3^-/Cl^- concentration ratio in the permeate stream of the membrane unit. The reason to focus on this parameter, $R_{1;n}$, is that it is a measure of the purity of the recovered NO_3^-. All graphs plot $R_{1;n}$ as a function of γ. The reason to present the data this way is that our prime aim concerns defining the required membrane selectivity in relation to the purity of the recovered NO_3^-.

As stated, the values of $R_{1,n}$ relate to steady-state conditions at which the NO_3^- and Cl^- concentrations at reference point #1 adopt their equilibrium values. The number of cycles needed to reach equilibrium is independent of the NO_3^-/Cl^- concentration ratio in the feed (R_{feed}) due to the assumption that the fraction of recovered NO_3^- is constant, and, in this case, arbitrarily set to 0.9. A model including a limited NO_3^- membrane transport capacity affects the results. **Figure 2.3** shows $R_{1;n}$ as function of the cycle number for R_{feed} = 10 (similar data for R_{feed} = 0.1 and 1 is shown in **Figure S2.1** of the Supporting Information). As shown in **Figure 2.3**, steady-state is reached already from the fourth or fifth cycle on. Note that the decline of $R_{1;n}$ after the first cycle results from Cl^- building up in the system due to the partial recycling of the retentate stream at reference point #3 ($\Phi_v(5)$). From here on, all presented data except those of **Figure 2.6** refer to the equilibrium condition.

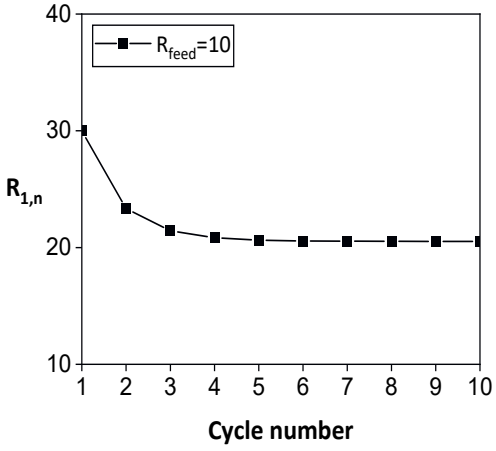

Figure 2.3: NO_3^-/Cl^- concentration ratio in the permeate stream ($R_{1,n}$) in relation to the cycle number for a NO_3^-/Cl^- concentration ratio in the feed of R_{feed} = 10. The numerical values of the other parameters used for the calculations are: α = 0.9, γ = 3, λ = 0.5.

2.3.1. Influence of the NO_3^-/ Cl^- concentration ratio in the feed (R_{feed})

It is expected that the higher the NO_3^-/ Cl^- ratio in the feed (R_{feed}), the lower the membrane selectivity required to achieve a certain purity of the permeate stream at point #1. Calculations confirm this hypothesis. **Figure 2.4** shows $R_{1;n}$ as a function of the membrane selectivity (y) at three different R_{feed} values, 0.1 and 1 (panel A) and 10 (panel B). The value of R_{feed} clearly sets a limit to the maximal value of $R_{1;n}$, that can be obtained, even at high separation ratios. For instance, the combination of R_{feed} = 1 and γ = 10 just results in a modest $R_{1;n}$ of approximately 6. Considering a tenfold excess of NO_3^- in combination with the same membrane selectivity, results in a tenfold increase of $R_{1;n}$.

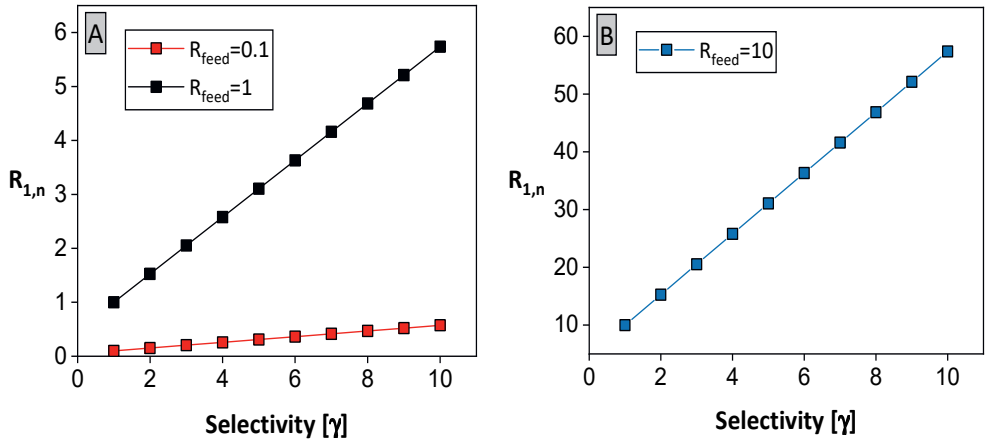

Figure 2.4: NO_3^-/ Cl^- concentration ratio in the permeate stream ($R_{1,n}$) in relation to the membrane selectivity (γ) at NO_3^-/ Cl^- concentration ratios in the feed (R_{feed}) of 0.1 and 1 (panel A) and 10 (panel B). In all cases the value of λ was set at 0.5.

2.3.2. Influence of the fraction of NO_3^- removed by the membrane unit (α)

In addition to the α/β ratio, the absolute value of α also affects $R_{1;n}$. **Figure 2.5** demonstrates this effect for α values ranging from 0.5 to 0.9, at γ values varying from 1 to 10, and for R_{feed} = 10 (similar data for R_{feed} = 0.1 and 1 are shown in **Figure S2.2** of the Supporting Information). At any given value of γ, the higher α, the lower $R_{1;n}$. The explanation for this somehow counterintuitive result is that a higher α implies a lower $R_{0;n}$ at the start of the next cycle because stream $\Phi_v(5)$ contains less NO_3^-. **Figure 2.6** shows this effect. As can be concluded from **Figure 2.4**, $R_{1;n}$ scales linearly with R_{feed}, at any given membrane selectivity. Higher α values thus result in lower values of $R_{1;n}$, as shown in **Figure 2.5** for R_{feed} = 10 (similar data for R_{feed} = 0.1 and 1 is shown in **Figure S2.2** of the Supporting Information).

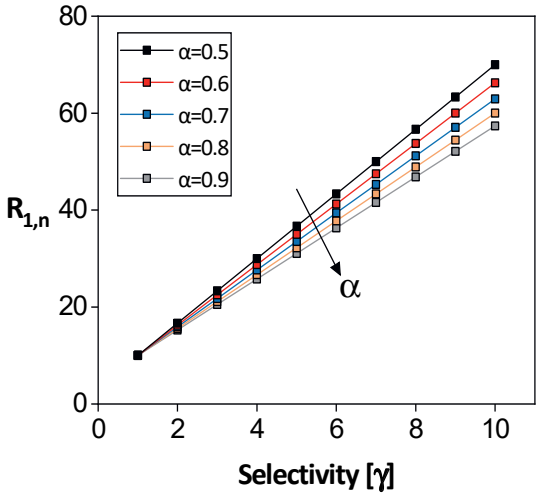

Figure 2.5: NO_3^-/Cl^- concentration ratio in the permeate stream ($R_{1,n}$) in relation to the membrane selectivity (y) and the fraction of NO_3^- removed at the membrane unit (α) for R_{feed} = 10. The value of λ was set at 0.5. The arrow indicates the direction of increasing α.

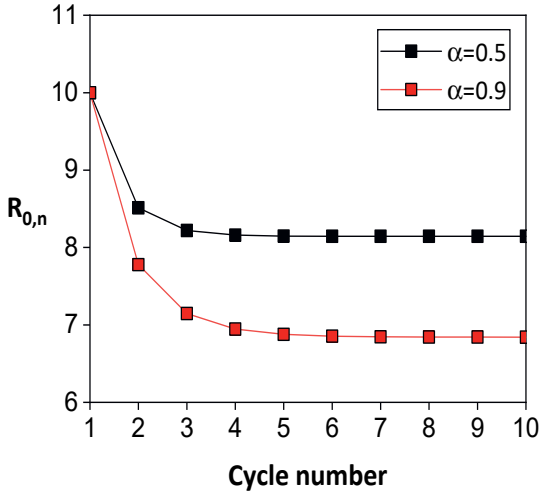

Figure 2.6: NO_3^-/Cl^- concentration at reference point #0 ($R_{0,n}$) in relation to the cycle number and the fraction of NO_3^- removed at the membrane unit (α) for R_{feed} = 10. The α values used are 0.9 and 0.5, and λ was set at 0.5.

2.3.3. Influence of the fraction of water recycled (λ)

Finally, we explore the effect of the fraction of water recycled, λ. From the point of view of reducing fresh water consumption, a high λ is desirable. However, λ clearly influences the concentration of Cl^- and NO_3^- in the system as well, with a higher impact on the Cl^- concentration due to the NO_3^- recovery at the membrane unit. By implication, the membrane selectivity required to achieve a certain NO_3^-/Cl^- concentration ratio in the permeate stream ($R_{1,n}$) is influenced by λ. **Figure 2.7** shows $R_{1;n}$ as function of γ, for λ ranging from 0 to 0.5, and for R_{feed} value of 10, (similar data for R_{feed} = 0.1 and 1 are shown in **Figure S2.3** of the Supporting Information). Suppose we aim for $R_{1;n}$ = 50, according to **Figure 2.7** and without recycling (λ = 0), the required membrane selectivity is around 5. This number doubles when half of the stream at point #3 is recycled, *i.e.* with λ = 0.5.

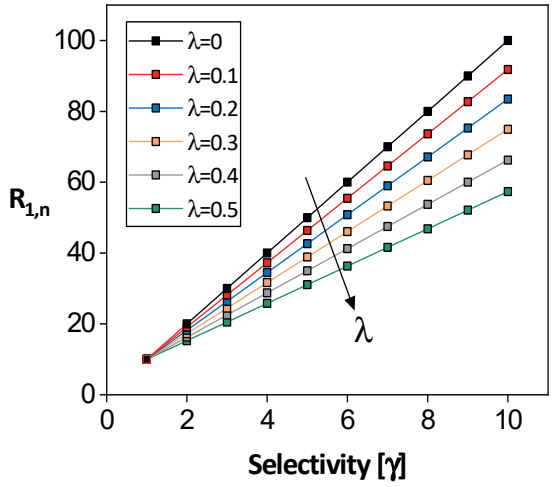

Figure 2.7: NO_3^-/Cl^- concentration ratio in the permeate stream ($R_{1,n}$) in relation to the membrane selectivity (γ) and the fraction of the retentate stream recycled (λ); for R_{feed} = 10; the value of α was set at 0.9. The arrow indicates the direction of increasing λ.

2.3.4. Application: NO_3^- recovery from a fertilizer production plant effluent

The real-life process parameters referred to in this section relate to NPK fertilizer production of Yara in Porsgrunn (Norway). **Figure 2.8** schematically outlines the process of their production plant. Part of the process that is actually involved in the treatment of the effluent water generated

by the fertilizer plant is indicated by the dashed red box (Water Purification System, WPS). After fertilizer production, the plant is cleaned with water and the resulting effluent stream, from now on referred to as feed stream of the WPS, rich in NO_3^- and Cl^-, is sent to a mixer (reference point #0) where recycled water is added. At this stage, also ammonia is added to precipitate the phosphate present as calcium phosphates, which are removed upon settling. After the settler (reference point #1), the stream is divided in two equal streams, with one stream recycled to the fertilizer plant, and the other sent to a scrubber (reference point #2), where gaseous NO_2 and HNO_3 are washed out before being added to the mixer for the next cycle. When the chloride concentration reaches a certain level, all surplus water is discharged (reference point #3).

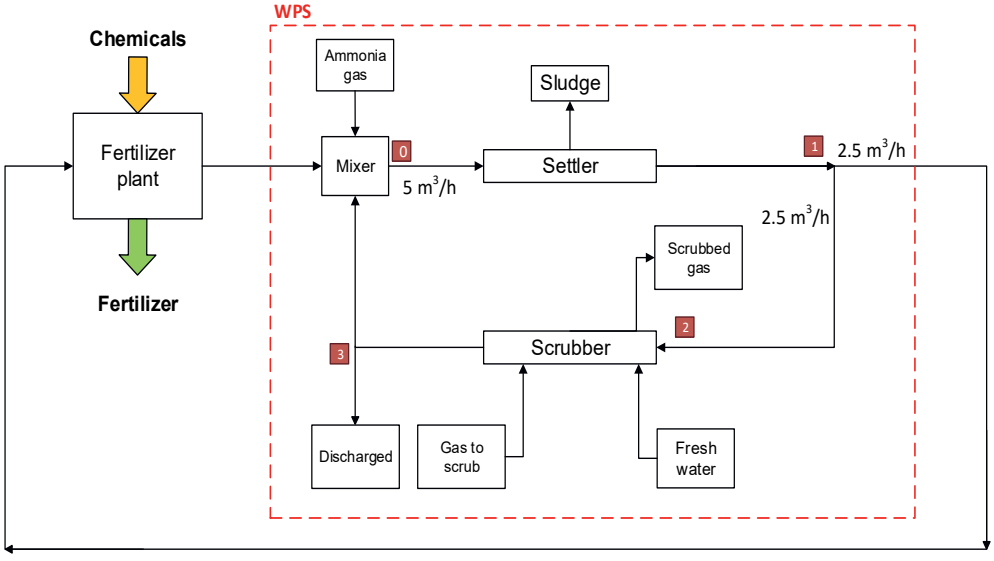

Figure 2.8: Outline of today's Water Purification System (WPS, red dashed box) used in the Porsgrunn NPK fertilizer plant. Reference points #0-3 are further explained in the text.

The amount of $(H)NO_3$ removed by the scrubber is negligible compared to the total amount of NO_3^- present at reference point #0. For that reason, the model does not account for the effect of the scrubber on the NO_3^- concentration. Because of this, the outline of **Figure 2.8** can be simplified into that of **Figure 2.9**. Note that the process now also includes a membrane unit for NO_3^- recovery.

At reference point #0, the feed stream, rich in NO_3^- and Cl^-, is mixed with fresh and recycled water. The volumetric flow of 5 m^3/h leaving the mixer remains constant during all subsequent cycles. After the settler (reference point #1), the stream is sent to a membrane unit responsible for the NO_3^- recovery and producing a permeate stream (reference point #2) that is recycled to the fertilizer plant. Depending on the membrane selectivity, this stream is more or less contaminated with Cl^-. The Cl^- rich retentate stream that results from the membrane unit (reference point #3) is split (reference point #4), with one part, after being scrubbed, recycled to the mixer, and the other part discharged.

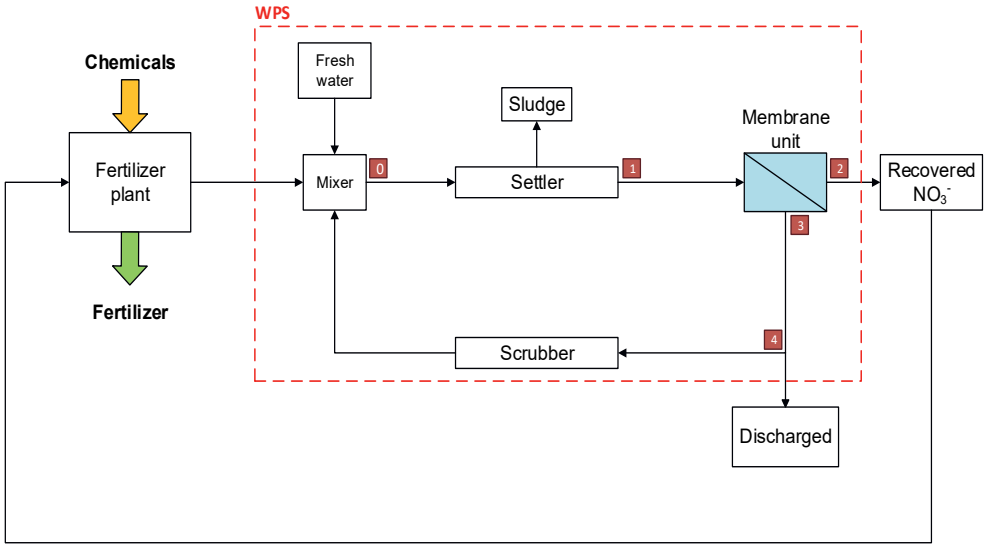

Figure 2.9: Outline of the Water Purification System (WPS, red dashed box) proposed in this study, including a membrane unit for the selective removal of NO_3^-. Reference points #0-4 are further explained in the text.

In the system, five reference points are distinguished:

- point #0: where fresh water, the feed stream, and the recycled water are mixed;
- point #1: stream leaving the settler before it enters the membrane unit;
- point #2: permeate stream after filtration by the membrane unit;
- point #3: retentate stream after filtration by the membrane unit;
- point #4: retentate stream to be recycled after splitting.

Similar to the mass balance model presented in **Section 2.2.2**, the aim is to calculate the NO_3^-/Cl^- concentration ratio at the five indicated reference points and during each cycle. The fertilizer plant in **Figure 2.8**, **Figure 2.9** and **Figure 2.10** is simplified to a unit into which chemicals enter and from which fertilizer is produced. More detailed information regarding this part of the process is beyond the scope of this study. However, one critical parameter is the Cl^- concentration in the permeate stream (reference point #2), recycled to the fertilizer plant; this should not exceed certain levels, depending on the type of fertilizer produced. Given these allowed limit values, the required (minimum) membrane selectivity can be determined. Regulation of the Cl^- level while recovering NO_3^- and reducing the fresh water consumption was the motivation to perform this study.

2.3.4.1. Process parameters

Figure 2.10 shows the basic outline of **Figure 2.9**, now complemented with all relevant process parameters referred to in this study. The parameters are listed in **Table 2.2**, including their numerical values. Whereas the NO_3^- concentration in the feed entering the mixer is fairly constant, 2.1 mol/L, the Cl^- concentration varies, depending on the grade of fertilizer produced. As was the case with the generic model discussed in **Section 2.2.2**, at the start of each cycle, the volumetric flow at reference point #0 remains constant. For the first cycle, it has been assumed that the composition at point #0 is 50 % feed stream and 50 % fresh water. In order to minimize the consumption of fresh water, after the first cycle, some of the retentate stream ($\Phi_v(5)$, reference point #3) is recycled to the mixer. As shown in **Section 2.3.3**, the fraction of water recycled, λ, influences the Cl^- build-up in the system and, with that, the required membrane selectivity (**Figure 2.7**). Decreasing this fraction decreases the required membrane selectivity to achieve the same NO_3^-/Cl^- ratio in the permeate stream at reference point #2. The flip side of the coin is, however, that reducing λ requires adding more fresh water at point #0, in order to maintain the volumetric flow constant. Therefore, a compromise is needed between the water consumption and the required membrane selectivity. For that reason, the value of λ was arbitrarily set at 0.3. Regarding the fraction of NO_3^- recovered at the membrane unit, the value of α was arbitrarily set at 0.9.

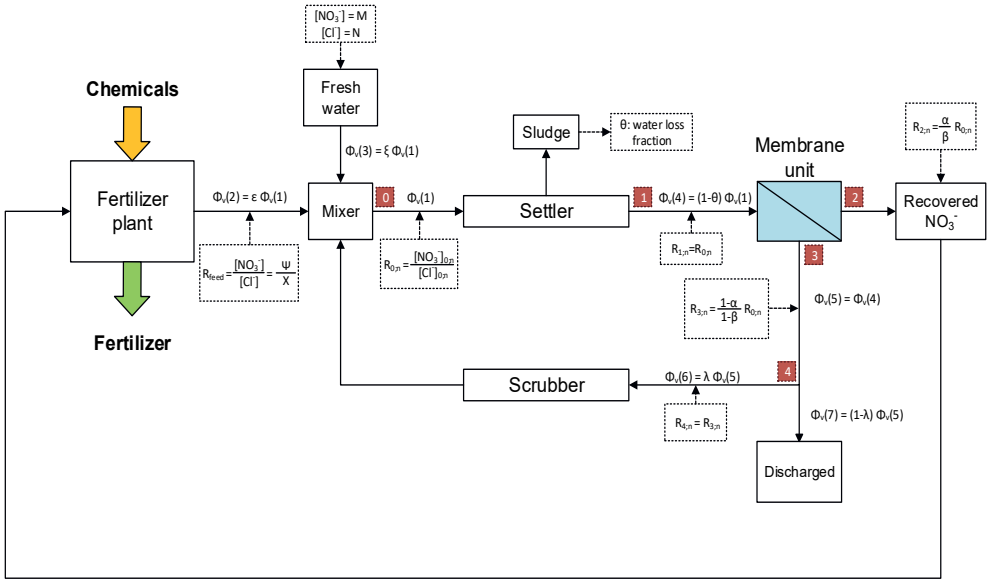

Figure 2.10: Outline of **Figure 2.9**, complemented with the volumetric flows Φv(1)-Φv(7) and the process parameters. Reference points #0-4 are indicated, as well as the relevant (steady-state) volumetric flows.

Table 2.2: List of the parameters used for the application under study.

Variables	Description	Value
$\Phi_v(1)$	Volumetric flow at reference point #0	5 m^3/h
Ψ	NO_3^- concentration in the feed	2.1 mol/L
X	Cl^- concentration in the feed	max 0.2 mol/L min 0.051 mol/L
R_{feed}	NO_3^-/Cl^- concentration ratio in the feed: $R = \Psi / X$	41.2 max 10.5 min
$R_{m,n}$	NO_3^-/Cl^- concentration at reference point #m and cycle n	
M	NO_3^- concentration in fresh water	0.26 mg/L $4.2 \cdot 10^{-6}$ mol/L
N	Cl^- concentration in fresh water	0.76 mg/L $2.1 \cdot 10^{-5}$ mol/L
ε_1	Fraction of feed stream added at point #0 for the 1st cycle	0.5
ε_n	Fraction of feed stream added at point #0 for cycle number n (n > 1)	0.5
ξ_1	Fraction of fresh water for the 1st cycle	0.5
ξ_n	Fraction of fresh water for cycles number n (n > 1) number n (n > 1)	***Equation 2.25***
ϑ	Fraction of $\Phi_v(1)$ lost due to settling	0.0035
α	Fraction of NO_3^- removed by the membrane system	0.9
β	Fraction of Cl^- removed by the membrane system	$\beta = \frac{\alpha}{\gamma}$
γ	NO_3^- over Cl^- permeation selectivity of the membrane system	$\gamma = \frac{\alpha}{\beta}$
λ	Fraction of water recycled	0.3

2.3.4.2. Mass balance

The mass balances follow the ones described in **Section 2.2.2**. The only difference is that due to a slight water loss at the settler (0.35 % of the water stream, $\vartheta = 0.0035$), equation 2.20 is modified into (for n>1):

$$\xi_n = 1 - \varepsilon_1 - \lambda(1 - \theta) \tag{2.27}$$

The volumetric flow at reference point #1 becomes:

$$\Phi_v(4) = (1 - \theta)\Phi_v(1) \tag{2.28}$$

2.3.4.3. Required membrane selectivity

The main purpose of this study is to determine the minimum membrane selectivity (γ_{min}) required to maintain the Cl^- concentration in the permeate stream, recycled to the fertilizer plant, below a certain threshold. As defined by Yara, this limit value is either 4.2 or 9.9 mM, depending on the quality of the fertilizer produced.

As already remarked, whereas the NO_3^- concentration in the feed is fairly constant, the Cl^- concentration varies, ranging from 51 to 200 mM. For that reason, four different combinations of Cl^- in the feed (X) and Cl^- in the permeate at reference point #2 were investigated (case A to D, **Table 2.3**). Combining the mass balance of **Section 2.2.2** with the modification proposed in Section 3.4.2 for the Yara process, and the parameters listed in **Table 2.2,** it is possible to determine the steady-state Cl^- concentrations at reference point #2 (permeate stream). **Figure 2.11** shows these Cl^- concentration values for membrane selectivity values ranging from 1 to 40. Given the Cl^- concentration limits, indicated by dashed lines in **Figure 2.11**, this plot allows the determination of the required minimum membrane selectivity (γ_{min}), which values are reported in **Table 2.3**.

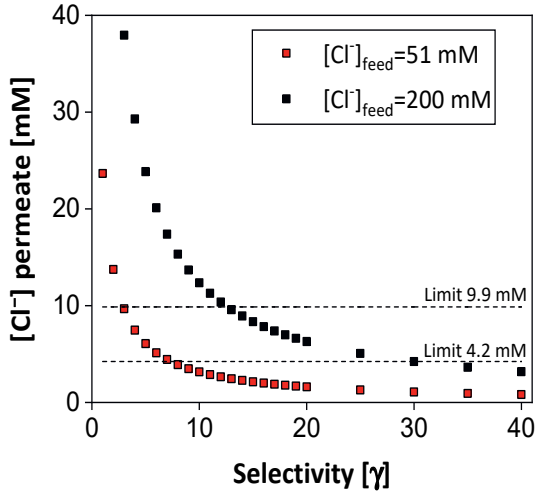

Figure 2.11: Steady-state Cl^- concentration in the permeate stream, $[Cl^-]_{2;n}$, as a function of membrane selectivity, for λ = 0.3 and $[Cl^-]_{feed}$ = 51 mM and 200 mM. Dashed lines indicate the concentration limits of 9.9 mM and 4.2 mM.

Table 2.3: Minimum membrane selectivity, $\gamma_{min,}$ at feed Cl^- concentrations of 51 and 200 mM, required to retain the permeate Cl^- below 4.2 or 9.9 mM. In all cases, the fraction of recycled water (λ) and NO_3^- recovered (α) was set to 0.3 and 0.9, respectively.

Case	$[Cl^-]_{feed}$	$[Cl^-]_{permeate}$ limit	γ_{min}
A	51 mM	9.9 mM	3
B		4.2 mM	8
C	200 mM	9.9 mM	13
D		4.2 mM	30

Lastly, in order to evaluate the influence of water recycling, the selectivity value of 3 reported in **Table 2.3** has been used to calculate the Cl^- concentration in the permeate stream by varying the fraction of water recycled in the WPS, λ. As shown in **Figure 2.12**, a larger water saving is at the expense of Cl^- building up in the system, reflected in a higher Cl^- content in the permeate.

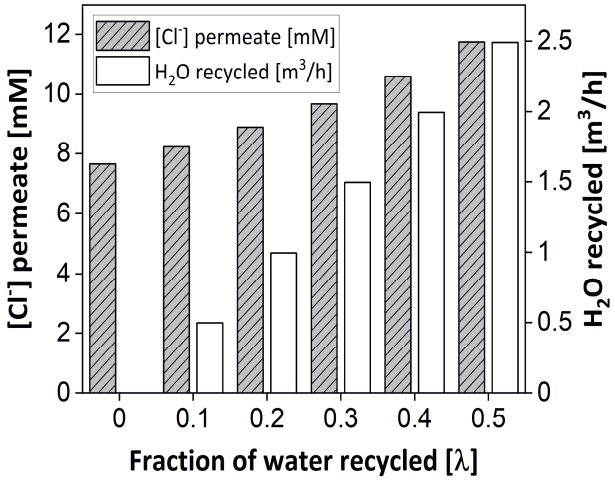

Figure 2.12: Permeate Cl^- content and absolute amount of recycled water in relation to the recycled water fraction, given a total volumetric flow of 5 m^3/h and a (fixed) membrane selectivity of 3.

2.4. Discussion

The current study is primarily focused on the NO_3^-/Cl^- concentration ratio in the permeate (generic model) and the absolute permeate Cl^- concentration of a case study (Yara process). As shown, the values of these two parameters are determined by the interplay of the NO_3^- and Cl^- content in the feed, the permeation properties of the membrane and the fraction of recycled water, to mention the most dominant ones. As our research group[15,16,21–23] and others[19,24–28] work on the development of membranes to discriminate between ion species of the same valence, the prime motivation of this investigation was to explore the actual required membrane selectivity for a real-life process.

Given the calculated selectivity values in **Table 2.3**, ranging from 3-30, and the highest selectivity value reported by Mubita *et al*.[14] of 3, there still is a large margin for improvement. The membranes developed by Mubita *et al*.[14] are heterogeneous anion-exchange membranes with low electrical resistance obtained by combining a functionalized polymeric binder and three ion-exchange resins, each containing a different functional group consisting of either trimethyl, triethyl, or tripropyl ammonium moieties. Within this series, the resin with the most hydrophobic functional group, i.e. the tripropyl ammonium, showed the highest NO_3^- over Cl^- permeation selectivity, a value of 3. However, due to the high water content, around 40-50 %, it seems rather unlikely that the difference in dehydration energy between NO_3^- and Cl^- is the prominent determinant of the selectivity mechanism of these membranes. For this reason, to match the high selectivity values required for cases B, C and D in **Table 2.3**, the development of membranes that fully exploit the difference in dehydration energy between NO_3^- and Cl^-, may be an attractive alternative. Evidently, this approach requires a hydrophobic membrane. Qian *et al*.[15,16] developed Supported Liquid Membranes (SLM) based on a lipophilic, organic phase impregnated with a borate salt. These SLMs showed a K^+ over Na^+ selectivity, which was attributed to the lower dehydration energy of K^+.[13] Whether this approach can be extrapolated to anion selectivity has to be seen. Moreover, apart from the relatively high selectivity, issues still to be addressed are the high electrical resistance of SLMs, mainly due to the limited solubility of the borate salt in the organic phase (NPOE), and leakage of the organic compound into the aqueous phase.

Another interesting alternative approach is the one of membranes onto which polyelectrolyte multilayers (PEMs) are assembled using layer-by-layer technology. For example, Yang *et al*.[29] have

developed a PEMs membrane with a K^+ over Li^+ selectivity of 7 for use in electrodialysis, and Tekinalp *et al*.[30] have demonstrated that this approach can selectively separate Cl^- and F^- from SO_4^{2-}.

In the context of the difference between cation and anion selectivity, it is worth noting that natural anion channels and transporters exhibit relatively low NO_3^- over Cl^- selectivity,[31,32] whereas their cation counterparts can exhibit much higher selectivity values, such as the K^+ over Na^+ selectivity of K^+ channels, which can be as high as 80.[33] In general, to achieve similar selectivity levels as observed in Nature may require design and synthesis at the atomic, angstrom scale as, for instance, in the case of metal-organic frameworks.[34,35]

Finally, a word on the incentive of NO_3^- and water recovery. One may argue that apart from sustainability, it is hard to come up with a solid business case for NO_3^- recovery. Indeed, NO_3^- is not a particular expensive chemical (*e.g.* urea ammonium nitrate price: 687.5 €/Mt on the 28/11/2022),[36] but there is certainly more to say about the economics involved. First, fertilizer production is associated with enormous energy consumption. More than 1 % of the worldwide produced energy is used to fuel the Haber-Bosch process,[37] *i.e.*, the reduction of N_2 to NH_3, a key compound for fertilizer production. Secondly, in order to promote a healthy environment, (European) legislation moves in the direction of zero discharge.[38] Therefore, it is believed that salt discharge will turn out costly in the near future, and investment in water purification systems mandatory. Even more, because nutrient recovery implies water savings as well.

2.5. Conclusion

Here we show the general outline of a membrane-based process aiming to combine NO_3^- recovery from a waste stream also containing Cl^- with water saving. The key process parameters were identified as the NO_3^-/Cl^- ratio in the feed (R), the fraction of feed NO_3^- that is recovered (α), the fraction of recycled water (λ), and the NO_3^- over Cl^- permeation selectivity of the membrane (γ). For instance, increasing the fraction of recovered NO_3^- (α) or the fraction of recycled water (λ) both decrease the purity of the recovered NO_3^-. Process optimization, therefore, asks for prioritizing aims. When applied to a real-life process, four combinations of process parameters were evaluated, resulting in membrane selectivity values ranging from 3 to 30, while assuming that 90 % of the NO_3^- is recovered and 30 % of the water recycled.

Experimentally, the most serious challenge is developing membranes with high selectivity. One of the strategies discussed to achieve such high values is based on exploiting the difference in dehydration energy between NO_3^- and Cl^-, and for this reason, we hypothesized that the membrane used in the process is hydrophobic.

Acknowledgements

The authors thank the Dutch Research Council – Wetsus Partnership Programme on Sustainable Water Technology for funding this project (ALWET.2019.004).This work was performed in the cooperation framework of Wetsus, European Centre of Excellence for Sustainable Water Technology (www.wetsus.nl). Wetsus is co-funded by the Dutch Ministry of Economic Affairs and Ministry of Infrastructure and Environment, the European Union Regional Development Fund, the Province of Fryslan and the Northern Netherlands Provinces. The authors like to thank the participants of the research theme “Desalination” for the fruitful discussions and their financial support. We are especially grateful to Yara (The Netherlands) for all their advice and support. We also would like to thank Dr Porada (Wrocław University of Science and Technology, Poland and Wetsus, The Netherlands) for fruitful discussions and two anonymous reviewers for commenting on earlier versions of this paper.

Supporting Information

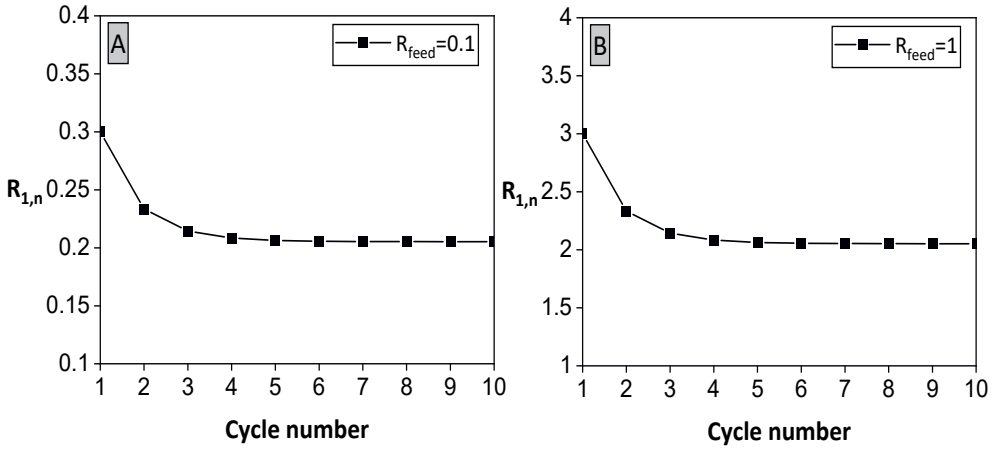

Figure S2.1: NO_3^-/Cl^- concentration ratio in the permeate stream ($R_{1,n}$) in relation to the cycle number for a NO_3^-/Cl^- concentration ratio in the feed of (R_{feed}) of 0.1 (panel A) and 1 (panel B). The numerical values of the other parameters used for the calculations are: α=0.9, γ=3, λ=0.5.

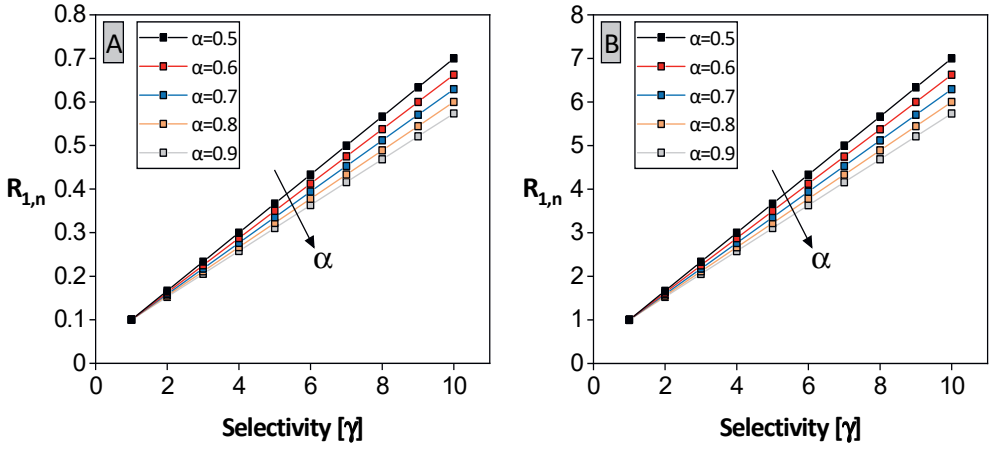

Figure S2.2: NO_3^-/Cl^- concentration ratio in the permeate stream ($R_{1,n}$) in relation to the membrane selectivity (γ) and the fraction of NO_3^- removed at the membrane unit (α) for R_{feed}=0.1 (panel A) and R_{feed}=1 (panel B). The value of λ was set at 0.5. The arrow indicates the direction of increasing α.

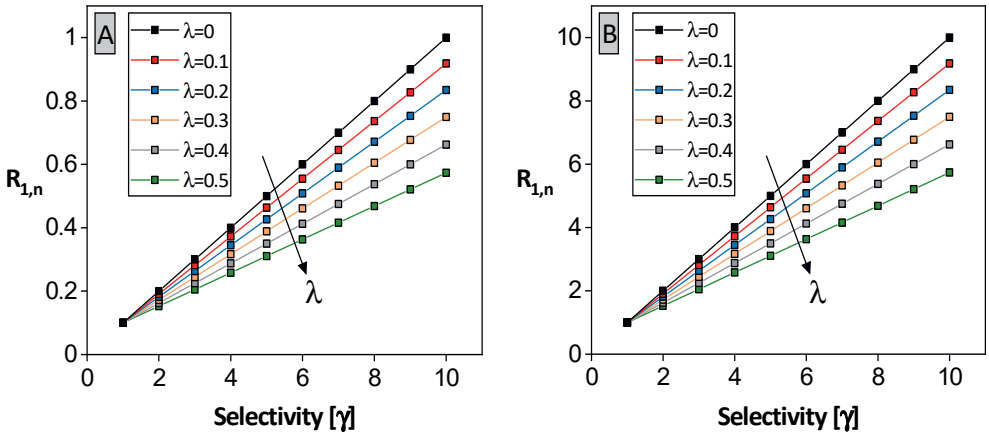

Figure S2.3: NO_3^-/Cl^- concentration ratio in the permeate stream ($R_{1,n}$) in relation to the membrane selectivity (y) and the fraction of the retentate stream recycled (λ) for R_{feed}=0.1 (panel A) and R_{feed}=1 (panel B). The value of α was set at 0.9. The arrow indicates the direction of increasing λ.

References

(1) *Agri-environmental indicator - mineral fertiliser consumption*. https://ec.europa.eu/eurostat/statistics-explained/index.php?title=Agri-environmental_indicator_-_mineral_fertiliser_consumption (accessed 2022-11-28).

(2) Kyriakou, V.; Garagounis, I.; Vourros, A.; Vasileiou, E.; Stoukides, M. An Electrochemical Haber-Bosch Process. *Joule* **2020**, *4* (1), 142–158. https://doi.org/10.1016/j.joule.2019.10.006.

(3) World Population Prospects 2019 Highlights.Pdf. https://population.un.org/wpp/publications/files/wpp2019_highlights.pdf (accessed 2022-11-28).

(4) Wang, X.; Zhao, C.; Müller, C.; Wang, C.; Ciais, P.; Janssens, I.; Peñuelas, J.; Asseng, S.; Li, T.; Elliott, J.; Huang, Y.; Li, L.; Piao, S. Emergent Constraint on Crop Yield Response to Warmer Temperature from Field Experiments. *Nat. Sustain.* **2020**, *3* (11), 908–916. https://doi.org/10.1038/s41893-020-0569-7.

(5) Skendžić, S.; Zovko, M.; Živković, I. P.; Lešić, V.; Lemić, D. The Impact of Climate Change on Agricultural Insect Pests. *Insects* **2021**, *12* (5). https://doi.org/10.3390/insects12050440.

(6) Omara, P.; Aula, L.; Oyebiyi, F.; Raun, W. R. World Cereal Nitrogen Use Efficiency Trends: Review and Current Knowledge. *Agrosystems Geosci. Environ.* **2019**, *2* (1), 1–8. https://doi.org/10.2134/age2018.10.0045.

(7) Dodds, W. K.; Smith, V. H. Nitrogen, Phosphorus, and Eutrophication in Streams. *Inland Waters* **2016**, *6* (2), 155–164. https://doi.org/10.5268/IW-6.2.909.

(8) Essien, E. E.; Said Abasse, K.; Côté, A.; Mohamed, K. S.; Baig, M. M. F. A.; Habib, M.; Naveed, M.; Yu, X.; Xie, W.; Jinfang, S.; Abbas, M. Drinking-Water Nitrate and Cancer Risk: A Systematic Review and Meta-Analysis. *Arch. Environ. Occup. Health* **2022**, *77* (1), 51–67. https://doi.org/10.1080/19338244.2020.1842313.

(9) Ward, M. H.; Jones, R. R.; Brender, J. D.; de Kok, T. M.; Weyer, P. J.; Nolan, B. T.; Villanueva, C. M.; van Breda, S. G. Drinking Water Nitrate and Human Health: An Updated Review. *Int. J. Environ. Res. Public. Health* **2018**, *15* (7), 1–31. https://doi.org/10.3390/ijerph15071557.

(10) Ni, B. J.; Pan, Y.; Guo, J.; Virdis, B.; Hu, S.; Chen, X.; Yuan, Z. *CHAPTER 16: Denitrification Processes for Wastewater Treatment*; The Royal Society of Chemistry, 2017; Vol. 2017-Janua. https://doi.org/10.1039/9781782623762-00368.

(11) Ye, Y.; Ngo, H. H.; Guo, W.; Liu, Y.; Chang, S. W.; Nguyen, D. D.; Liang, H.; Wang, J. A Critical Review on Ammonium Recovery from Wastewater for Sustainable Wastewater Management. *Bioresour. Technol.* **2018**, *268* (July), 749–758. https://doi.org/10.1016/j.biortech.2018.07.111.

(12) Nightingale, E. R. Phenomenological Theory of Ion Solvation. Effective Radii of Hydrated Ions. *J. Phys. Chem.* **1959**, *63* (9), 1381–1387. https://doi.org/10.1021/j150579a011.

(13) Smith, D. W. Ionic Hydration Enthalpies. *J. Chem. Educ.* **1977**, *54* (9), 540. https://doi.org/10.1021/ed054p540.

(14) Mubita, T.; Porada, S.; Aerts, P.; van der Wal, A. Heterogeneous Anion Exchange Membranes with Nitrate Selectivity and Low Electrical Resistance. *J. Membr. Sci.* **2020**, *607*, 118000. https://doi.org/10.1016/j.memsci.2020.118000.

(15) Qian, Z.; Miedema, H.; Sahin, S.; de Smet, L. C. P. M.; Sudhölter, E. J. R. Separation of Alkali Metal Cations by a Supported Liquid Membrane (SLM) Operating under Electro Dialysis (ED) Conditions. *Desalination* **2020**, *495*. https://doi.org/10.1016/j.desal.2020.114631.

(16) Qian, Z.; Miedema, H.; de Smet, L. C. P. M.; Sudhölter, E. J. R. Permeation Selectivity in the Electro-Dialysis of Mono- and Divalent Cations Using Supported Liquid Membranes. *Desalination* **2022**, *521*. https://doi.org/10.1016/j.desal.2021.115398.

(17) Vaselbehagh, M.; Karkhanechi, H.; Takagi, R.; Matsuyama, H. Effect of Polydopamine Coating and Direct Electric Current Application on Anti-Biofouling Properties of Anion Exchange Membranes in Electrodialysis. *J. Membr. Sci.* **2016**, *515*, 98–108. https://doi.org/10.1016/j.memsci.2016.05.049.

(18) Sodaye, S.; Suresh, G.; Pandey, A. K.; Goswami, A. Determination and Theoretical Evaluation of Selectivity Coefficients of Monovalent Anions in Anion-Exchange Polymer Inclusion Membrane. *J. Membr. Sci.* **2007**, *295* (1), 108–113. https://doi.org/10.1016/j.memsci.2007.02.044.

(19) Kikhavani, T.; Ashrafizadeh, S. N.; Van Der Bruggen, B. Nitrate Selectivity and Transport Properties of a Novel Anion Exchange Membrane in Electrodialysis. *Electrochimica Acta* **2014**, *144*, 341–351. https://doi.org/10.1016/j.electacta.2014.08.012.

(20) Sata, T. Studies on Anion Exchange Membranes Having Permselectivity for Specific Anions in Electrodialysis - Effect of Hydrophilicity of Anion Exchange Membranes on Permselectivity of Anions. *J. Membr. Sci.* **2000**, *167* (1), 1–31. https://doi.org/10.1016/S0376-7388(99)00277-X.

(21) Sahin, S.; Zuilhof, H.; Zornitta, R. L.; de Smet, L. C. P. M. Enhanced Monovalent over Divalent Cation Selectivity with Polyelectrolyte Multilayers in Membrane Capacitive Deionization via Optimization of Operational Conditions. *Desalination* **2022**, *522*, 115391. https://doi.org/10.1016/j.desal.2021.115391.

(22) Singh, K.; Sahin, S.; Gamaethiralalage, J. G.; Zornitta, R. L.; de Smet, L. C. P. M. Simultaneous, Monovalent Ion Selectivity with Polyelectrolyte Multilayers and Intercalation Electrodes in Capacitive Deionization. *Chem. Eng. J.* **2022**, *432*, 128329. https://doi.org/10.1016/j.cej.2020.128329.

(23) Paltrinieri, L.; Huerta, E.; Puts, T.; Van Baak, W.; Verver, A. B.; Sudhölter, E. J. R.; De Smet, L. C. P. M. Functionalized Anion-Exchange Membranes Facilitate Electrodialysis of Citrate and Phosphate from Model Dairy Wastewater. *Environ. Sci. Technol.* **2019**, *53* (5), 2396–2404. https://doi.org/10.1021/acs.est.8b05558.

(24) Krishna B, A.; Zwijnenberg, H. J.; Lindhoud, S.; de Vos, W. M. Sustainable K+/Na+ Monovalent-Selective Membranes with Hot-Pressed PSS-PVA Saloplastics. *J. Membr. Sci.* **2022**, *652*, 120463. https://doi.org/10.1016/j.memsci.2022.120463.

(25) Yang, S.; Liu, Y.; Liao, J.; Liu, H.; Jiang, Y.; Van der Bruggen, B.; Shen, J.; Gao, C. Codeposition Modification of Cation Exchange Membranes with Dopamine and Crown Ether To Achieve High K^+ Electrodialysis Selectivity. *ACS Appl. Mater. Interfaces* **2019**, *11* (19), 17730–17741. https://doi.org/10.1021/acsami.8b21031.

(26) Montes-Rojas, A.; Rentería, J. A. Q.; Chávez, N. B. J.; Ávila-Rodríguez, J. G.; Soto, B. Y. Influence of Anion Hydration Status on Selective Properties of a Commercial Anion Exchange Membrane Electrochemically Impregnated with Polyaniline Deposits. *RSC Adv.* **2017**, *7* (41), 25208–25219. https://doi.org/10.1039/C7RA03331A.

(27) Křivčík, J.; Neděla, D.; Hadrava, J.; Brožová, L. Increasing Selectivity of a Heterogeneous Ion-Exchange Membrane. *Desalination Water Treat.* **2015**, *56* (12), 3160–3166. https://doi.org/10.1080/19443994.2014.980970.
(28) Oh, C.-M.; Hwang, C.-W.; Hwang, T.-S. Synthesis of a Quaternarized Poly(Vinylimidazole-Co-Trifluoroethylmethacrylate-Co-Divinylbenzene) Anion-Exchange Membrane for Nitrate Removal. *J. Environ. Chem. Eng.* **2014**, *2* (4), 2162–2169. https://doi.org/10.1016/j.jece.2014.09.014.
(29) Yang, L.; Tang, C.; Ahmad, M.; Yaroshchuk, A.; Bruening, M. L. High Selectivities among Monovalent Cations in Dialysis through Cation-Exchange Membranes Coated with Polyelectrolyte Multilayers. *ACS Appl. Mater. Interfaces* **2018**, *10* (50), 44134–44143. https://doi.org/10.1021/acsami.8b16434.
(30) Tekinalp, Ö.; Zimmermann, P.; Burheim, O. S.; Deng, L. Designing Monovalent Selective Anion Exchange Membranes for the Simultaneous Separation of Chloride and Fluoride from Sulfate in an Equimolar Ternary Mixture. *J. Membr. Sci.* **2023**, *666*, 121148. https://doi.org/10.1016/j.memsci.2022.121148.
(31) Zifarelli, G.; Pusch, M. CLC Transport Proteins in Plants. *FEBS Lett.* **2010**, *584* (10), 2122–2127. https://doi.org/10.1016/j.febslet.2009.12.042.
(32) De Angeli, A.; Monachello, D.; Ephritikhine, G.; Frachisse, J. M.; Thomine, S.; Gambale, F.; Barbier-Brygoo, H. The Nitrate/Proton Antiporter AtCLCa Mediates Nitrate Accumulation in Plant Vacuoles. *Nature* **2006**, *442* (7105), 939–942. https://doi.org/10.1038/nature05013.
(33) Mita, K.; Sumikama, T.; Iwamoto, M.; Matsuki, Y.; Shigemi, K.; Oiki, S. Conductance Selectivity of Na^+ across the K^+ Channel via Na^+ Trapped in a Tortuous Trajectory. *Proc. Natl. Acad. Sci.* **2021**, *118* (12), e2017168118. https://doi.org/10.1073/pnas.2017168118.
(34) Epsztein, R.; DuChanois, R. M.; Ritt, C. L.; Noy, A.; Elimelech, M. Towards Single-Species Selectivity of Membranes with Subnanometre Pores. *Nat. Nanotechnol.* **2020**, *15* (6), 426–436. https://doi.org/10.1038/s41565-020-0713-6.
(35) Li, X.; Jiang, G.; Jian, M.; Zhao, C.; Hou, J.; Thornton, A. W.; Zhang, X.; Liu, J. Z.; Freeman, B. D.; Wang, H.; Jiang, L.; Zhang, H. Construction of Angstrom-Scale Ion Channels with Versatile Pore Configurations and Sizes by Metal-Organic Frameworks. *Nat. Commun.* **2023**, *14* (1), 286. https://doi.org/10.1038/s41467-023-35970-x.
(36) *Urea Ammonium Nitrate - 2022 Data - 2012-2021 Historical - 2023 Forecast - Price*. https://tradingeconomics.com/commodity/urea-ammonium (accessed 2022-11-28).
(37) Capdevila-Cortada, M. Electrifying the Haber–Bosch. *Nat. Catal.* **2019**, *2* (12), 1055–1055. https://doi.org/10.1038/s41929-019-0414-4.
(38) *River basin management - Water - Environment - European Commission*. https://ec.europa.eu/environment/water/water-framework/index_en.html (accessed 2022-11-28).

Chapter 3

Selective separation of nitrate from chloride using PVDF-based anion-exchange membranes

This chapter has been published as:
Chinello, D.; Post, J.; de Smet, L. C. P. M. Selective separation of nitrate from chloride using PVDF-based anion-exchange membranes. *Desalination* **2024**, *572*, 117084.

Abstract

In this study we investigated the selective separation of nitrate from chloride using newly designed PVDF-based anion-exchange membranes. Five membranes were successfully manufactured by casting, each containing a different PVDF concentration (from 0 to 50 wt%). A polyaromatic anion-exchange polymer was used as a binder. Experimental data shows that the binder had no impact on the nitrate selectivity while increasing the PVDF concentration enhanced nitrate transport. The membrane with a 50 wt% PVDF content (PVDF-50), exhibited a nearly double selectivity than a commercial membrane (Neosepta AMX). However, we also found that the membrane electrical resistance increased with the PVDF concentration. As the nitrate selectivity was found to be independent of the membrane thickness, selective boundary layer effects were ruled out, suggesting that the ion selectivity was mainly driven by the increased affinity between the anion and the membrane, with less hydrated ions more favorably transported. To confirm this hypothesis, PVDF-50 was tested using a multi-ion solution, including bromide and fluoride. This equimolar solution experiment indicated a direct correlation between ion selectivity and hydration energy of the ion species. Lastly, we investigated the transport of divalent ions through the hybrid membrane, showing a 10 % transport for sulfate.

3.1. Introduction

The ongoing increase in the world's population[1] is creating an increasing demand for fertilizers[2] to sustain food production and achieve food security. Nitrogen, in the form of nitrate, is one of the main components of fertilizers together with phosphorus and potassium, and it is directly involved in the production of proteins and enzymes in plants.[3] In addition, nitrate is an important component of chlorophyll,[4] which allows plants to carry out photosynthesis. However, excessive use of nitrate-based fertilizers can lead to nitrate pollution of water resources. Indeed, the nitrogen use efficiency (NUE) varies from *ca*. 30 to just over 50 %,[5] where the remaining part can easily leach into groundwater and surface water. When nitrate enters water bodies, it can stimulate the growth of algae and other aquatic plants, leading to eutrophication.[6,7] This can have serious ecological consequences, such as oxygen depletion, loss of biodiversity, altered food availability, and even fish kills. In addition, when nitrate-contaminated water is consumed by humans or animals, nitrate can be converted into nitrite in the body, which in turn can react with hemoglobin in the blood, leading to a condition known as methemoglobinemia, which limits the transport of oxygen.[8,9]

Nowadays, to reduce nitrate contamination, biological denitrification of nitrate to gaseous nitrogen is a common and efficient process.[10–12] Unfortunately, this also leads to the removal of direct biologically available nitrogen from the environment. Therefore, a more attractive alternative resides in selectively separating nitrate from water, meanwhile concentrating it for potential reuse. A potential application is the recovery of nitrate from the effluent (waste) water of a fertilizer production plant, which we described in a previous study.[13] Moreover, another application area relates to greenhouses as becomes clear from, e.g. the Greenhouse Horticulture program of The Netherlands. This program aims to reach (nearly) zero emissions of fertilizers and crop protection agents by 2027,[14] illustrating the importance of the ability to discriminate between nitrate and chloride, in such a way to achieve closed water and nutrient recycling loops.

In the present study, we focus on ion-exchange membranes (IEMs), which can be used in, e.g. electrodialysis (ED). IEMs have become part of well-established separation technology, for example, in desalination,[15,16] with a remarkable ability to discriminate between cations and anions.[17–19] However, IEMs present a limitation in distinguishing between ion species with the

same charge and valence, such as sodium and potassium as well as nitrate and chloride, and no commercial membranes are available for this purpose.

According to previous studies,[20–22] differences in ion hydration energy can be utilized in enhancing the membrane selectivity. Examples thereof include studies that have shown that hydrophobic membranes can enhance the transport of less hydrated ions,[23–25] such as nitrate (**Table 3.1**). This effect has been attributed to the partial loss of the hydration shell water molecules.[26–28] Ions with a lower hydration energy can undergo easier dehydration, resulting in a lower energy barrier for the transport from the solution into the membrane.

In this study we focus on the selective separation of nitrate from chloride by manufacturing polyvinylidene fluoride (PVDF)-based anion-exchange membranes, followed by their investigation under constant current conditions using various electrolyte solutions. PVDF has been selected due to its intrinsic hydrophobic nature and its extensive use in other membrane application processes such as membrane distillation,[29–33] nanofiltration for dye removal from waste water,[34,35] organic pollutants removal,[36] oil-water separation,[37–39] removal of toxic metal from aqueous solutions,[40] and fuel cells.[41–43] A commercially available ionomer solution (Fumion FAS-24, FUMATECH BWT GmbH) was used in combination with PVDF. To the best of our knowledge, the use of PVDF for the realization of membranes for the selective ion separation and in particular the separation of nitrate and chloride has not been reported in the literature before. This approach results in a straightforward membrane fabrication, which makes it a practical choice for potential industrial applications. The ease of membrane preparation not only simplifies the process but also contributes to the potential scalability of our approach.

In particular, we investigated the effect of increasing the PVDF amount within the membrane (0 to 50 wt%) on the nitrate over chloride selectivity. Based on these results, in order to investigate whether the selectivity was based on a boundary layer effect, we manufactured a thinner PVDF-based membrane. Finally, we investigated the relation between hydration energy and preferential ion transport by examining the ionic fluxes of four monovalent anions (NO_3^-, Cl^-, Br^-, and F^-) through a PVDF-based anion-exchange membrane.

Table 3.1: Ionic radius and hydration energy of the anions studied in this work.[44]

Anion	Ionic radius [nm]	Hydration energy [kcal·mol^{-1}]
Nitrate (NO_3^-)	0.264	71
Bromide (Br^-)	0.195	75
Chloride (Cl^-)	0.181	81
Fluoride (F^-)	0.136	111
Sulfate (SO_4^{2-})	0.290	258

3.2. Materials and methods

3.2.1. Chemicals

Polyvinylidene fluoride (PVDF) (average M_w ~ 534,000 by GPC, powder form), sodium chloride (ACS reagent, ≥99.0 %), sodium nitrate (ACS reagent, ≥99.0 %), sodium sulfate (ACS reagent, ≥99.0 %, anhydrous), sodium bromide (ACS reagent, ≥99.0 %), potassium chloride (ACS reagent, ≥99.0-100.5 %), potassium nitrate (ACS reagent, ≥99.0 %), potassium iodate (ACS reagent, ≥99.5 %), were purchased from Sigma Aldrich and used as received. Fumion FAS (24 wt% solution in NMP) was purchased from FUMATECH BWT GmbH. N-methyl-2-pyrrolidone (NMP, HPLC grade 99.5 %) was purchased from Alfa Aesar. The Neosepta AMX, CMX membranes were purchased from Eurodia Industrie SAS, Pertuis, France, the European distributor of the manufacturer ASTOM Corporation, Tokyo, Japan.

3.2.2. Membrane fabrication

The PVDF-based AEMs were manufactured by varying the PVDF:Fumion FAS-24 ratio and labelled accordingly with the weight percentage of PVDF as PVDF-0, PVDF-10, PVDF-30, and PVDF-50. The selected amounts of PVDF and Fumion FAS-24 were dissolved in N-methyl-2-pyrrolidone (NMP) to obtain a 16 wt% solution of polymers in NMP. The resulting mixture was stirred overnight to ensure complete dissolution, before casting it onto a glass plate which was kept at 60 °C for 24 h in a fume hood, to allow the solvent to evaporate. To further ensure the complete solvent removal, the membranes were immersed in 0.5 M NaCl for 2 h. This was repeated five times by

refreshing the solution. The membranes were then cut into discs with a diameter of 67 mm (and hence an area of 35 cm^2) using a punching press, and stored in 0.5 M NaCl solution. At this stage, the membrane thickness was measured using a digital thickness gauge (Mitutoyo Corporation, model no. ID-C112BS).

The electrochemical properties of the manufactured AEMs were compared with a commercial membrane (Neosepta AMX). Finally, in order to investigate the influence of the membrane thickness on the selectivity, a thinner PVDF-50 membrane, named PVDF-50-thin, was manufactured following the fabrication method reported above, halving the quantity of PVDF, Fumion FAS-24, and NMP used for PVDF-50.

3.2.3. Membrane characterization

3.2.3.1. Ion-exchange capacity (IEC)

The IEC of a membrane is an indirect measure of the fixed charges in the membrane, obtained by measuring the concentration of the counter-ion exchanged with a given solution. In particular, after conditioning in 0.5 M NaCl for 48 h, the membrane (35 cm^2) was immersed for several seconds in demineralized water to remove the excess of NaCl solution from the surface. Then, after wiping off the water from the surface with a tissue, the membrane was transferred in 200 mL of 0.5 M $NaNO_3$, the exchange solution. After an exchange period of 24 h, the chloride concentration in the solution was determined by ion chromatography (IC) using a Metrohm Compact IC 761 with conductivity detector and chemical suppression. The IEC was then calculated according to Dlugolecki *et al.*[45] using the following equation:

$$IEC = \frac{n_{eq}}{W_{dry}} \tag{3.1}$$

where n_{eq} refers to the equivalent of exchanged ions (eq) and W_{dry} (g) to the dry mass of the membrane.

3.2.3.2. Water uptake

In order to evaluate the water uptake, the procedure of Mubita *et al.*[23] was followed. Initially, the membranes (35 cm^2) were immersed in demineralized water for 24 hours, and, after removing

the water on the surface with a tissue, the wet membrane mass (W_{wet}, in grams) was recorded. Then, after keeping the membranes at 55 °C for 24 hours to assure complete water evaporation, the dry membrane mass (W_{dry}, in grams) was recorded. The water uptake was determined as a percentage by:

$$Water\ uptake = 100 \times \frac{W_{wet} - W_{dry}}{W_{dry}}\ \% \quad (3.2)$$

3.2.3.3. Electrical resistance

The membrane electrical resistance was assessed according to the method outlined by Galama *et al.*,[46] adapting the configuration of the six-compartment cell reported in **Figure 3.2**, for the measurement of the membranes ion selectivity. In particular, compartment A, B, and C were filled with 0.5 M NaCl, while compartment D was filled with 0.5 M Na_2SO_4. Moreover, the AEM in between compartment B and C was replaced with a cation-exchange membrane (Neosepta CMX). The recirculation flow rate was 170 mL·min^{-1},[23] and all measurements were conducted at room temperature. Before the experiments, the membranes were conditioned for 24 h in 0.5 M NaCl.

The membrane under investigation was placed in a holder, resulting in an active area of 9.6 cm^2, and by applying a step-wise increase of the current density (*I*) from 0 to 2.5 A·m^{-2} using a potentiostat (Autolab AUT72398, Metrohm), the voltage drop across the membrane (*V*) was registered using two Haber–Luggin capillaries (outer diameter 4.0 mm, inner diameter 2.0 mm) situated on the side of the membrane. These capillaries are filled with 0.5 M NaCl and connected to a reservoir where two Ag/AgCl electrodes are placed. The slope resulting from the interpolation of the points of the *I-V* graph represents the membrane's electrical resistance (Ω). The membrane area resistance (Ω·cm^2) was then calculated by subtracting the electrical resistance of the solution (measured without the membrane) from the membrane resistance and multiplying by the active membrane surface area.

3.2.3.4. Membrane morphology

The membrane morphology of the best-performing membrane in terms of nitrate over chloride selectivity (PVDF-50) was investigated using scanning electron microscopy (SEM) with a JEOL JSM-6480LV electron microscope operating at 10 kV acceleration. The membranes were given a gold

coating through the use of a JEOL JFC-1200 Fine Coater sputter prior to analysis. To obtain the clearest cross-sectional image, the membrane was carefully broken after being immersed in liquid nitrogen to minimize any potential distortions caused by shear stress.

3.2.4. Membrane performance

3.2.4.1. Membrane ion selectivity under zero current conditions

3.2.4.1.1. Permselectivity

The permselectivity of an anion-exchange membrane refers to the ability of the membrane to selectively transport anions across the membrane while preventing the passage of cations. This selective transport is achieved through the presence of specific ion-exchange groups within the membrane matrix, such as quaternary ammonium groups.[47] In the present study, we measured the membrane permselectivity through membrane potentiometry, as described by Dlugolecki *et al.*,[45] using a two-compartment cell made of poly(methyl 2-methylpropenoate) (PMMA), with a combined solution volume of 0.2 L, which a schematic representation is reported in **Figure 3.1** (Panel A).

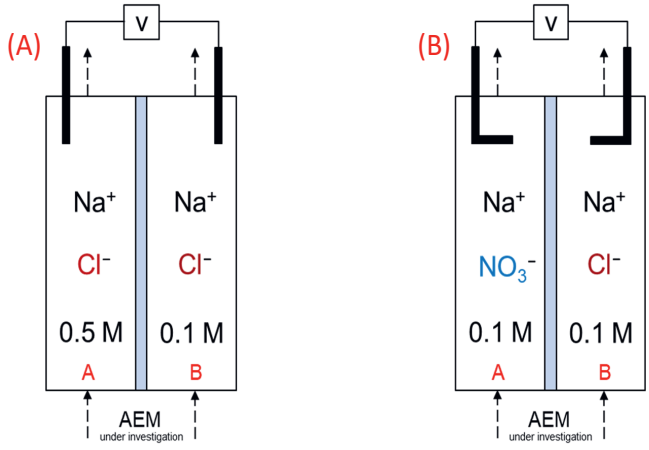

Figure 3.1: Two-compartment cell used to measure the AEM's permselectivity (Panel A) and the permeability coefficient ratio (Panel B).

This method involves measuring the potential difference across the membrane ($\Delta V_{measured}$) in response to an ionic concentration gradient. The AEM under investigation (active surface area of 7 cm^2) separates two solutions having a different concentration: 0.5 M NaCl in compartment A and 0.1 M NaCl in compartment B. The flow rate was maintained at 750 $mL \cdot min^{-1}$ to minimize diffusion boundary effects,[48] and the membrane was conditioned in 0.1 M NaCl for 24 h prior to the experiment. The potential difference was measured at room temperature when the steady state was reached (after 30 min), using two Ag/AgCl electrodes immersed in the solutions and compared to the theoretical one, which was calculated according to the Nernst equation:

$$\Delta V_{theoretical} = \frac{RT}{zF} ln \frac{C_A}{C_B} \quad (3.3)$$

where R is the universal gas constant (8.314 $J\ mol^{-1} \cdot K^{-1}$), T is the temperature (K), z is the valence of the ions, F is the Faraday constant (96,458 $A \cdot s \cdot mol^{-1}$), and C_A and C_B are the ion concentration ($mol \cdot L^{-1}$) in compartment A and B respectively.

The membrane permselectivity (a) is given by the ratio of the potential measured ($\Delta V_{measured}$) over the theoretical one ($\Delta V_{theoretical}$), expressed as a percentage:

$$a = 100 \times \frac{\Delta V_{measured}}{\Delta V_{theoretical}} \% \quad (3.4)$$

3.2.4.1.2. Permeability coefficient ratio

The potential that exists across a membrane separating two electrolyte solutions containing the same co-ion (in our case Na^+) but different counter-ions (in our case Cl^- and NO_3^-) is the result of the difference in the affinity, chemical and physical, of the counter-ions for the membrane. This potential ($\Delta\Psi$) can give a quick indication of the membrane selectivity between the counter-ions[22] and can, according to Ibánez-Mengual *et al*.[49] and Ghosh *et al*.,[50] be related to the counter-ions permeability coefficient ratio by:

$$\Delta\Psi = \frac{RT}{F} ln \frac{P_1}{P_2} \quad (3.5)$$

where F is the Faraday constant (96,458 $A \cdot s \cdot mol^{-1}$), R is the universal gas constant (8.314 $J \cdot mol^{-1} \cdot K^{-1}$), T is the absolute temperature (K), and P_1 and P_2 the permeability coefficients of the counter-ions. The experiments were conducted using the two-compartment cell (**Figure 3.1**), panel B) and

settings of the permselectivity experiments, except for the electrolyte solution composition: 0.1 M $NaNO_3$ in compartment A and 0.1 M NaCl in compartment B. By rearranging equation (3.5), it is possible to obtain the permeability coefficient ratio of nitrate over chloride as function of the potential difference ($\Delta\Psi$):

$$\frac{P_{NO_3^-}}{P_{Cl^-}} = e^{\frac{F\Delta\Psi}{RT}} \qquad (3.6)$$

3.2.4.2. Membrane ion selectivity under constant current conditions

To assess the nitrate over chloride membrane selectivity under constant current conditions, the six-compartment cell represented in **Figure 3.2**, which is described in detail in,[46] was used to determine the transport numbers and ionic fluxes of the two ions across the membrane (active area 9.6 cm^2) placed between compartments A and B. For the other compartments, the cation-exchange membrane (CEM) and anion-exchange membrane (AEM) used were Neosepta CMX and AMX respectively (Eurodia Industrie SAS, Pertuis, France).

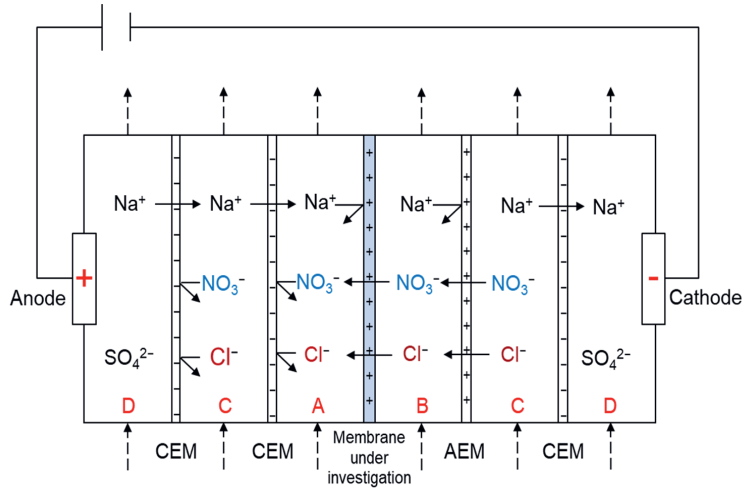

Figure 3.2: Schematic representation of the six-compartment cell used to measure the membranes ion selectivity under constant current conditions. See text for an explanation of the compositions of solutions A, B, C, and D.

The transport number (*t*), which is a measure of the fraction of the total current carried by a specific ion species in an electrolyte solution across a membrane, for a monovalent ion (*i*) is given by:

$$t_i = \frac{FV}{IA}\frac{\Delta C_i}{\Delta t} \quad (3.7)$$

where *F* is the Faraday constant (96,458 A·s·mol^{-1}), *V* is the volume (m^3) of the solution in compartment A, *A* the surface membrane area (m^2), ΔC_i (mol·L^{-1}) is the variation of the ion concentration in compartment A, Δt (s) is the time of the experiments, and *I* is the current density applied (A·m^{-2}). The ionic flux *J* (mol·m^{-2}·s^{-1}) for a monovalent ion (i) is defined by:

$$J_i = \frac{V}{A}\frac{\Delta C_i}{\Delta t} \quad (3.8)$$

and, considering two ions i and j, it can be used to measure the current efficiency (η):

$$\eta = \left(J_i + J_j\right)\frac{F}{I} \quad (3.9)$$

The membrane configuration in the six-compartment cell has been selected according to the contribution of Luo *et al.*[51] and Mubita *et al.*[23] In this way, by placing a CEM between compartments D and C, the eventual oxidation of chloride at the anode is prevented. Moreover, considering that the membrane selectivity is defined by:[52]

$$S_{Cl^-}^{NO_3^-} = \frac{t_{NO_3^-}}{t_{Cl^-}}\left(\frac{C_{Cl^-}}{C_{NO_3^-}}\right)_B \quad (3.10)$$

where $t_{NO_3^-}$ and t_{Cl^-} are the transport numbers for nitrate and chloride across the membrane and $C_{NO_3^-}$ and C_{Cl^-} the concentrations of nitrate and chloride in compartment B, the presence of an AEM between compartments B and C is pivotal to keep the concentration of the ions constant in compartment B, in such a way to avoid any influence of the variation of the concentration on the membrane selectivity. The ionic composition in compartment B, however, is subject to change due to the different selectivities of the membrane under investigation between compartments A and B, and the adjacent membrane between B and C. For this reason, to minimize this effect, compared to the method of Mubita *et al.*,[23] the volume of the electrolyte solution in compartment B was increased to 1 L. Moreover, the concentration of Na_2SO_4 in the solution recirculating in compartment D was decreased from 0.1 M to 0.05 M, in such a way to avoid any

concentration polarization effect (i.e. equal Na^+ concentrations in all compartments). Lastly, it is important to note that the ion selectivity is not only determined by the membrane's properties but also by the experimental conditions.[22] For that reason, we included a commercially available membrane (Neosepta AMX) in our study as a reference.

In this paper, each experiment was conducted for 6 h at a current density of 20 $A \cdot m^{-2}$, with a potentiostat (Autolab AUT72157, Metrohm) used as current supplier. The membrane under investigation was equilibrated overnight in the test solution. Compartments A, B, C, and D were filled with the solutions reported in **Table 3.2** and recirculated at a flow rate 170 $mL \cdot min^{-1}$. Samples were taken every three hours and analysed by ion chromatography (IC) to determine the ion concentrations. After defining the nitrate over chloride membrane selectivity, the best-performing membrane was tested by varying the composition of the electrolyte solution in compartment A, B, and C (**Table 3.2**), in such a way to observe how the membrane performs in the presence of also bromide, fluoride, and sulfate to investigate the role of the hydration energy in the selectivity mechanism.

Table 3.2: Experimental settings for the membrane selectivity under constant current conditions. In all cases sodium salts were used and the current density was 20 $A \cdot m^{-2}$.

Anions investigated	Compartment (volume in L)	$[NO_3^-]$ (M)	$[Cl^-]$ (M)	$[Br^-]$ (M)	$[F^-]$ (M)	$[SO_4^{2-}]$ (M)	Tested membranes
NO_3^- Cl^-	A (0.25)	0.05	0.05	-	-	-	AMX PVDF-0 PVDF-50 PVDF-50-thin
	B,C (1)	0.05	0.05	-	-	-	
	D (1)	-	-	-	-	0.05	
NO_3^- Cl^- Br^- F^-	A (0.25)	0.025	0.025	0.025	0.025	-	PVDF-50
	B,C (1)	0.025	0.025	0.025	0.025	-	
	D (1)	-	-	-	-	0.05	
NO_3^- Cl^- SO_4^{2-}	A (0.25)	0.02	0.02	-	-	0.02	PVDF-50
	B,C (1)	0.02	0.02	-	-	0.02	
	D (1)	-	-	-	-	0.05	

3.3. Results and discussion

3.3.1. Membrane Fabrication

Four different membranes were successfully manufactured by varying the PVDF:Fumion FAS-24 ratio, which are referred to as PVDF-0, PVDF-10, PVDF-30, and PVDF-50, where the number stands for the PVDF wt% in the membrane (**Table 3.3**). We decided not to go into higher PVDF concentrations for two main reasons: higher amounts of PVDF would result in i) a further increased viscosity which would hamper the casting process, and ii) an undesired increase in the electrical resistance. **Table 3.3** also reports the membrane thickness values. Despite the total mass of membrane components used remains constant, the thickness of the resulting membranes decreases with PVDF content. This can be understood by the different charge density of the manufactured membranes: the higher the charge density the thicker the membrane as the degree of swelling increase due higher water uptake.[45,53] This hypothesis is supported by the analysis of water uptake values obtained for the manufactured membranes in **Table 3.3**, which decrease as the PVDF concentration increases. This effect can also be linked to an increased in membrane hydrophobicity.[20,28] Lastly, a thinner PVDF-50 membrane, named PVDF-50-thin, was manufactured by halving the amounts of PVDF, Fumion FAS-24, and NMP compared to the preparation of PVDF-50.

Table 3.3: Composition, thickness and water uptake of the four membranes manufactured and Neosepta AMX.

Membrane	Fumion FAS-24: PVDF wt%	Thickness (µm)	Water Uptake (%)
PVDF-0	100:0	100	22
PVDF-10	90:10	95	15
PVDF-30	70:30	90	10
PVDF-50	50:50	85	7
PVDF-50-thin	50:50	45	6
AMX	-	140	15

3.3.2. Membrane characterization

3.3.2.1. IEC and electrical resistance

In the case of ion-exchange membranes, there is a correlation between the ion exchange capacity (IEC) and electrical resistance.[54] The ion-exchange capacity of a membrane is related to the amount of ion-exchange groups present in the membrane, which can affect its electrical conductivity. As the amount of these ion-exchange groups increases, the membrane's electrical resistance may decrease, allowing for better conductivity.

Figure 3.3 shows that the IEC decreases and the electrical resistance increases upon increasing PVDF concentration. Compared to AMX, the IEC of PVDF-0 and PVDF-10 is found to be similar or higher, while for PVDF≥30 the IEC is evidently lower. The electrical resistance data follows the opposite trend: compared to AMX, these are found to be similar or lower for PVDF-0 and PVDF-10, while for PVDF≥30 the electrical resistance is clearly higher. These trends align well with the findings of Wilhelm *et al.*,[55] who studied cation-exchange membranes produced by blending charged and uncharged polymers, such as sulfonated polyether ether ketone (S-PEEK) and polyether sulfone (PES). Using a binary mixture of a charged (Fumion FAS-24) and uncharged (PVDF) species, one could expect linear trends in **Figure 3.3**, but this is not the case. One possible explanation reported in literature[55] for this could be that the amount of ionic groups becomes less accessible upon increasing PVDF concentration, possibly resulting in phase separation and domain formation. However, from the SEM images obtained at a magnification of 2500× (**Figure S3.1** panel (A), in the Supporting Information), no domains could be observed.

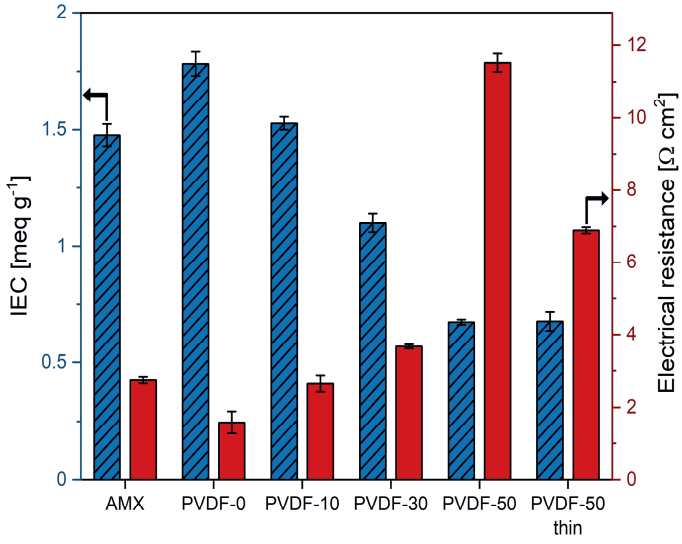

Figure 3.3: Ion Exchange Capacity (IEC) (meq·g^{-1}) and membrane area resistance (Ω·cm^2) of the five manufactured PVDF-based AEM (PVDF-0, PVDF-10, PVDF-30, PVDF-50, and PVDF-50-thin) and a commercial membrane (Neosepta AMX). Experiments have been repeated three times.

3.3.2.2. Membrane morphology

Lastly, the surface and cross-sectional SEM images of the best-performing membrane for nitrate over chloride separation, PVDF-50, display a compact structure with no voids in **Figure S3.1** in the Supporting Information.

3.3.3. Membrane performance

3.3.3.1. Membrane ion selectivity under zero current conditions: permselectivity and permeability coefficient ratio

To study the ability of the AEMs to selectively transport anions, while blocking the movement of cations, the permselectivity values have been obtained for the five manufactured membranes (PVDF-0, PVDF-10, PVDF-30, PVDF-50, and PVDF-50-thin) and the commercial membrane (Neosepta AMX) (**Figure 3.4**). Upon examination of the data, it can be noted that the permselectivity of the manufactured AEMs and the commercial membrane exhibit comparable

values of about 90 %, which is coherent with previous results reported in literature for AMX and also for anion-exchange membrane in general.[45]

Concerning the permeability coefficient ratio, the data of **Figure 3.4** shows that by increasing the PVDF concentration within the membrane, the affinity towards nitrate increases. Moreover, it can also be observed that while the membrane PVDF-0 shows an almost identical value as the commercial membrane AMX, the permeability coefficient ratio of PVDF-0, PVDF-30, and PVDF-50 are respectively 25 %, 50 % and 90 % higher. Also, the permeability ratio values of PVDF-50 and PVDF-50-thin are identical.

As previously stated, the permeability coefficient ratio can give a quick indication of the membrane selectivity. However, although our data consistency demonstrates the method's reproducibility, Qian *et al.*[26] suggest using these values as an indication, given that even a slight shift of a few mV can significantly affect the results.

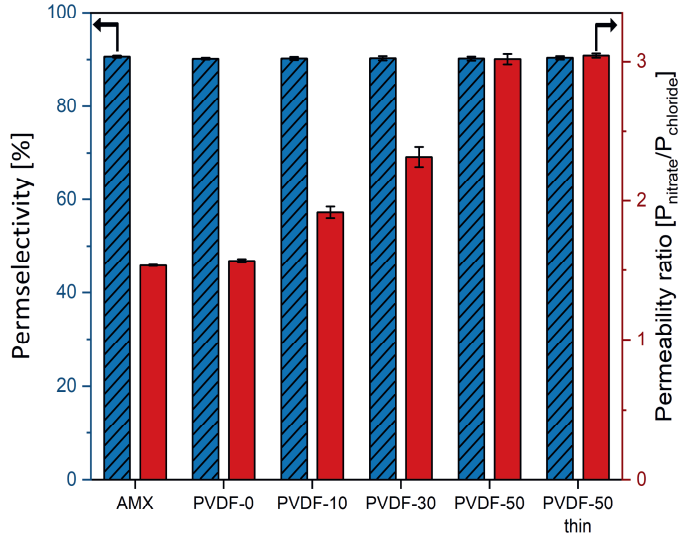

Figure 3.4: Permselectivity and permeability coefficient ratio values, as obtained with the two-compartment cell, of the five manufactured PVDF-based AEMs (PVDF-0, PVDF-10, PVDF-30, PVDF-50, and PVDF-50) and a commercial membrane (Neosepta AMX). Experiments have been repeated three times.

3.3.3.2. Membrane ion selectivity under constant current conditions

3.3.3.2.1. Nitrate over chloride membrane selectivity

Based on the results obtained for the permeability coefficient ratio (**Figure 3.4**), we decided to study the nitrate over chloride selectivity under constant current conditions for the membranes AMX, PVDF-0, and PVDF-50. The AMX membrane was selected again to compare the performance of the proposed manufactured AEMs with a commercial one. PVDF-0 was included to determine whether the binder (Fumion FAS-24) influences the selectivity, while PVDF-50 was selected because of its high permeability coefficient ratio. The nitrate over chloride selectivity of these membranes was tested according to the procedure reported in **Section 3.2.4.2**, repeating the experiment three times for each membrane. As can be observed in **Figure 3.5**, AMX and PVDF-0 present a similar value of the selectivity (~1.3), while PVDF-50 yields a nitrate over chloride selectivity that is nearly twice as high. As PVDF-0, i.e. 100 % Fumion FAS-24, and AMX have a similar selectivity, the increased selectivity for PVDF-50 and PVDF-50-thin can be ascribed to the increased concentration of PVDF and any role of Fumion FAS-24 in this regard can be excluded.

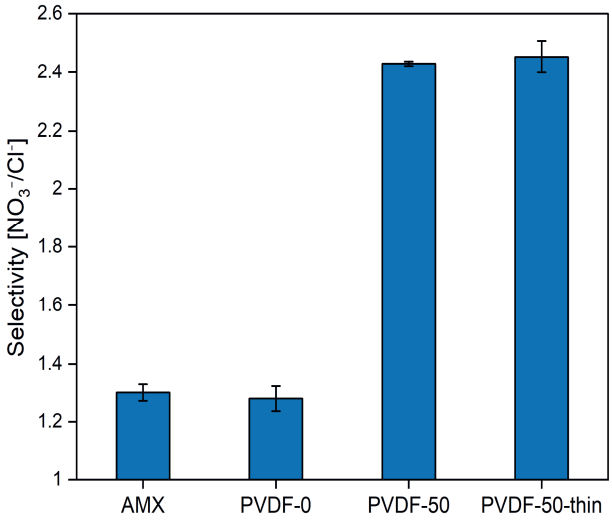

Figure 3.5: Nitrate over chloride selectivity under constant current conditions measured at 20 $A \cdot m^{-2}$, for the manufactured membranes PVDF-0, PVDF-50, and PVDF-50-thin, and a commercial membrane (Neosepta AMX). Selectivity experiments have been repeated three times.

This effect also becomes clear by analyzing the ionic flux of nitrate and chloride (**Figure 3.6**), showing that compared to AMX and PVDF-10, the ionic flux of nitrate increases for PVDF-50, while it decreases for chloride. Lastly, the current efficiency for all experiments was in the range of 88-95 %. When comparing our results with those of the study conducted by Mubita *et al.*,[23] which also employed AMX Neosepta as a reference membrane in determining the selectivity values of heterogeneous AEMs manufactured with ion-exchange resins featuring different quaternary ammonium groups, our findings are consistent with their observations.

Based on the solution-diffusion model, the transportation of ions through a membrane occurs in two distinct stages: firstly, adsorption in the polymer matrix, and secondly, diffusion across the membrane.[56,57] As reported in the introduction, by increasing the hydrophobicity of the membrane, the affinity towards less hydrated ions increases. Along these lines, it can be rationalized that the increased selectivity of PVDF-50 is related to the increased hydrophobicity of the membrane due to the higher PVDF content.

However, in their polyelectrolyte-based membrane work, Krishna *et al.*[58] reported that the selectivity of Cl^- over SO_4^{2-} is influenced by the membrane thickness, with thinner membranes having a higher selectivity compared to thicker ones. This effect was explained by the presence of a boundary layer effect, indicating that the selectivity of thinner membranes is primarily influenced by the difference in concentration between ion species at the surface of the membrane (Donnan equilibrium), rather than the membrane's inherent ability to discriminate between ions (based on differences in solubility and/or speeds of diffusion), with divalent ions being more hindered in approaching the membrane compared to monovalent ones. For this reason, to better understand whether the increased nitrate selectivity of PVDF-50 is due to presence of PVDF or any boundary layer effect, we investigated the nitrate over chloride selectivity for a thinner PVDF-50 membrane, labelled as PVDF-50-thin, with a thickness of 45 µm. The selectivity value obtained for this thinner membrane was found to be similar that the one of PVDF-50 (**Figure 3.5**), showing that no boundary layer effect takes place in the selectivity process. This is an important finding as thinner membranes present a lower electrical resistance,[59] which is an attractive, if not required, property for membrane-based technologies such as electrodialysis. The electrical resistance of PVDF-50-thin was found to be almost half of the one

of PVDF-50 (**Figure 3.3**). Moreover, using thinner membranes also leads to a reduction in the quantity of material required, thereby lowering the overall fabrication costs.

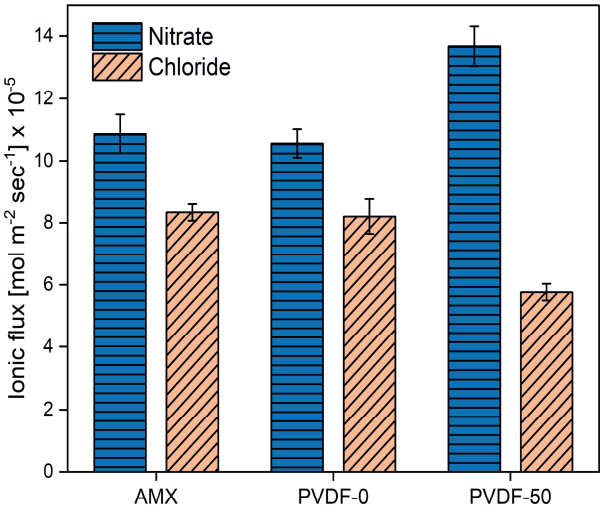

Figure 3.6: Ionic flux of nitrate and chloride through selected membranes: AMX, PVDF-0, and PVDF-50 at 20 $A \cdot m^{-2}$.

3.3.3.2.2. Selectivity of monovalent ions with different hydration energy

In order to confirm whether it is possible to address the ion selectivity based on the hydration energy, we conducted experiments using membrane PVDF-50, with electrolyte solutions containing, next to nitrate and chloride, also bromide and fluoride. The choice of these ions is related to the increased interest in halide anion separation over the last years.[60] The ionic fluxes of the four different monovalent anions are given in **Figure 3.7**, showing a selectivity order of $NO_3^- > Br^- > Cl^- > F^-$. This trend correlates well with the one of the hydration energy of the various ions (**Table 3.1**).

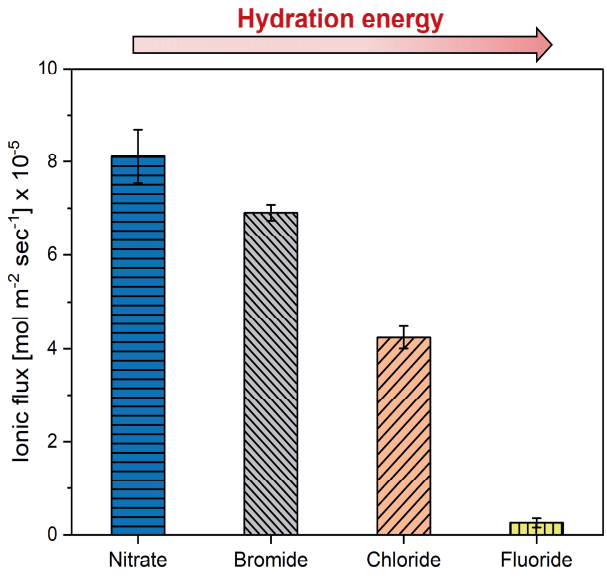

Figure 3.7: Ionic flux of nitrate, bromide, chloride, and fluoride obtained under constant current conditions at 20 $A \cdot m^{-2}$ using PVDF-50. The experiments were repeated three times.

3.3.3.2.3. Monovalent over divalent anion selectivity

In the previous section, we investigated monovalent anion separation, and found a correlation between the anion hydration energy and preferential transport through the membrane. However, also divalent anions such as sulfate are present in drinking water. In electrodialysis, the presence of sulfate in the concentrate compartment would lead to the formation and precipitation of $CaSO_4$ scale, which decreases the process performance.[61,62] Therefore, a low sulfate membrane permeation is desirable. For this reason, following the procedure reported in **Section 3.2.4.2**, we tested the monovalent over divalent selectivity for an electrolyte solution containing equimolar concentration of nitrate, chloride, and sulfate, using membrane PVDF-50. The ionic fluxes of the three ions are reported in **Figure 3.8**. From this data it becomes clear that the two monovalent anions, nitrate and chloride, are preferentially transported over sulfate of which the ionic flux is around 10 % of the total flux. Following the same reasoning as in the previous section when discussing the monovalent data, the limited sulfate transport can be

explained considering the relatively high hydration energy of sulfate compared to those of nitrate and chloride. However, also other effects, such as the steric hindrance and the possibility for the sulfate to create stronger interactions with the ion-exchange sites of the membrane can play a role.[63]

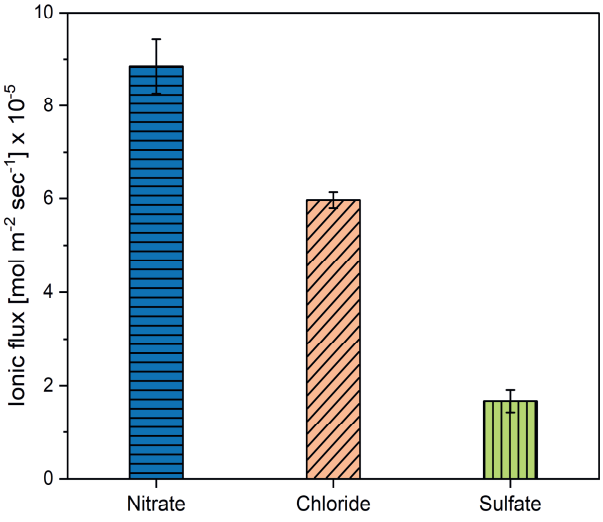

Figure 3.8: Ionic flux of nitrate, chloride, and sulfate obtained under constant current conditions at 20 A·m^{-2} using PVDF-50. The experiments were repeated three times.

Upon examination of **Figure 3.7** and **Figure 3.8**, it can be observed how the presence of other ions in the solution affect the ionic flux of nitrate and chloride. In the case of the experiments conducted including bromide and fluoride as well, our hypothesis is that the presence of bromide, which presents a similar value for the hydration energy to that of nitrate and chloride, competes with these two ions and in particular with nitrate, given the smaller difference in hydration energy. Indeed, in comparison to **Figure 3.6**, the decrease in the ionic flux of nitrate is more pronounced than the one of chloride. In the case reported in **Figure 3.8**, we observe that the presence of sulfate, which has a much higher hydration energy compared to both nitrate and chloride, has a more pronounced impact on the transport of nitrate than on chloride, again by comparing the ionic fluxes to those reported in **Figure 3.6**. This phenomenon has also been noted

in literature,[23] although no explanation was provided. Possibly, also other factors than the hydration energy should be taken into consideration to explain the transport mechanism and competition when divalent ions are present, such as the size and valence of the ion.

3.4. Conclusion

Newly developed AEMs were fabricated via a casting process using PVDF and a polymeric binder. We investigated the impact of increasing the PVDF concentration in the membrane on the separation of nitrate from chloride. Our findings show an improved nitrate transport upon increasing the PVDF concentration, with the membranes composed of 50 wt% PVDF exhibiting nitrate selectivity that is nearly twice as high than those of the PVDF-free equivalent and a commercial membrane (AMX). This selectivity enhancement was attributed to the membrane's increased hydrophobicity, boosting the affinity for ions with lower hydration energy. Decreasing the membrane thickness showed no effect on the nitrate selectivity, supporting the use of a thinner membrane, which in turn presents a lower electrical resistance and requires less material for its fabrication. This study provides valuable insight into the role of ion hydration energy in the selectivity process, confirming its importance in driving the separation process. These findings hold significant potential for the development of high-performance, ion-exchange membranes for a wide range of applications, including water treatment and desalination.

Acknowledgments

The authors thank the Dutch Research Council – Wetsus Partnership Programme on Sustainable Water Technology for funding this project (ALWET.2019.004). This work was performed in the cooperation framework of Wetsus, European Centre of Excellence for Sustainable Water Technology (www.wetsus.nl). Wetsus is co-funded by the Dutch Ministry of Economic Affairs and Ministry of Infrastructure and Environment, the European Union Regional Development Fund, the Province of Fryslân and the Northern Netherlands Provinces. The authors like to thank the participants of the research theme “Desalination” for the fruitful discussions and their financial support. We also would like to thank Dr. Slawomir Porada (Wrocław University of Science and Technology, Poland and Wetsus, The Netherlands) and Prof. Wiebe de Vos (University of Twente,

The Netherlands) for fruitful discussions, and Jean Wavelet, Idoia Urteaga Contín and Eirini Aikaterini Gkougkousi for their precious contributions to the experimental work.

Supporting Information

Table S3.1: Physicochemical properties of Fumion FAS-24.

	Matrix	Functional group	Counter-ion	IEC [meq/g]
Fumion FAS-24	Polyaromatic polymer	Quaternary ammonium	Bromide	1.7-1.9

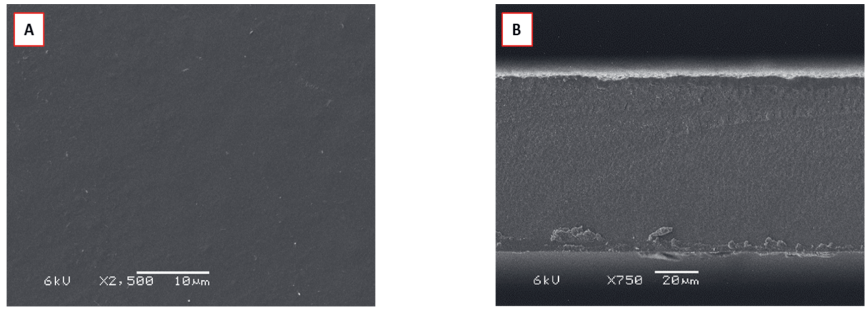

Figure S3.1: SEM images of surface (A) and cross-section (B) of PVDF-50.

References

(1) *World Population Prospects - Population Division - United Nations*. https://population.un.org/wpp/ (accessed 2023-08-10).

(2) *Fertilizer consumption*. Our World in Data. https://ourworldindata.org/grapher/fertilizer-consumption-usda (accessed 2023-08-10).

(3) Lamig, L.; Moreno, S.; Álvarez, J. M.; Gutiérrez, R. A. Molecular Mechanisms Underlying Nitrate Responses in Plants. *Curr. Biol.* **2022**, *32* (9), R433–R439. https://doi.org/10.1016/j.cub.2022.03.022.

(4) Wen, B.; Li, C.; Fu, X.; Li, D.; Li, L.; Chen, X.; Wu, H.; Cui, X.; Zhang, X.; Shen, H.; Zhang, W.; Xiao, W.; Gao, D. Effects of Nitrate Deficiency on Nitrate Assimilation and Chlorophyll Synthesis of Detached Apple Leaves. *Plant Physiol. Biochem.* **2019**, *142*, 363–371. https://doi.org/10.1016/j.plaphy.2019.07.007.

(5) Anas, M.; Liao, F.; Verma, K. K.; Sarwar, M. A.; Mahmood, A.; Chen, Z.-L.; Li, Q.; Zeng, X.-P.; Liu, Y.; Li, Y.-R. Fate of Nitrogen in Agriculture and Environment: Agronomic, Eco-Physiological and Molecular Approaches to Improve Nitrogen Use Efficiency. *Biol. Res.* **2020**, *53* (1), 1–20. https://doi.org/10.1186/s40659-020-00312-4.

(6) Domingues, R. B.; Barbosa, A. B.; Sommer, U.; Galvão, H. M. Ammonium, Nitrate and Phytoplankton Interactions in a Freshwater Tidal Estuarine Zone: Potential Effects of Cultural Eutrophication. *Aquat. Sci.* **2011**, *73* (3), 331–343. https://doi.org/10.1007/s00027-011-0180-0.

(7) Akinnawo, S. O. Eutrophication: Causes, Consequences, Physical, Chemical and Biological Techniques for Mitigation Strategies. *Environ. Chall.* **2023**, *12*, 100733. https://doi.org/10.1016/j.envc.2023.100733.

(8) Fewtrell, L. Drinking-Water Nitrate, Methemoglobinemia, and Global Burden of Disease: A Discussion. *Environ. Health Perspect.* **2004**, *112* (14), 1371–1374. https://doi.org/10.1289/ehp.7216.

(9) Shuval, H. I.; Gruener, N. INFANT METHEMOGLOBINEMIA AND OTHER HEALTH EFFECTS OF NITRATES IN DRINKING WATER. In *Proceedings of the Conference on Nitrogen As a Water Pollutant*; Jenkins, S. H., Ed.; Pergamon, 2013; pp 183–193. https://doi.org/10.1016/B978-1-4832-1344-6.50017-4.

(10) Xu, D.; Li, Y.; Yin, L.; Ji, Y.; Niu, J.; Yu, Y. Electrochemical Removal of Nitrate in Industrial Wastewater. *Front. Environ. Sci. Eng.* **2018**, *12* (1), 9. https://doi.org/10.1007/s11783-018-1033-z.

(11) Singh, V.; Ormeci, B.; Mishra, S.; Hussain, A. Simultaneous Partial Nitrification, ANAMMOX and Denitrification (SNAD) – A Review of Critical Operating Parameters and Reactor Configurations. *Chem. Eng. J.* **2022**, *433*, 133677. https://doi.org/10.1016/j.cej.2021.133677.

(12) Ni, B. J.; Pan, Y.; Guo, J.; Virdis, B.; Hu, S.; Chen, X.; Yuan, Z. *CHAPTER 16: Denitrification Processes for Wastewater Treatment*; The Royal Society of Chemistry, 2017; Vol. 2017-Janua. https://doi.org/10.1039/9781782623762-00368.

(13) Chinello, D.; Myrstad, A.; de Smet, L. C. P. M.; Miedema, H. Modelling the Required Membrane Selectivity for $NO3^-$ Recovery from Effluent Also Containing Cl^-, While Saving Water. *Chem. Eng. Res. Des.* **2023**, *193*, 409–419. https://doi.org/10.1016/j.cherd.2023.03.038.
(14) van der Salm, C.; Voogt, W.; Beerling, E.; van Ruijven, J.; van Os, E. Minimising Emissions to Water Bodies from NW European Greenhouses; with Focus on Dutch Vegetable Cultivation. *Agric. Water Manag.* **2020**, *242*, 106398. https://doi.org/10.1016/j.agwat.2020.106398.
(15) Campione, A.; Gurreri, L.; Ciofalo, M.; Micale, G.; Tamburini, A.; Cipollina, A. Electrodialysis for Water Desalination: A Critical Assessment of Recent Developments on Process Fundamentals, Models and Applications. *Desalination* **2018**, *434*, 121–160. https://doi.org/10.1016/j.desal.2017.12.044.
(16) Al-Amshawee, S.; Yunus, M. Y. B. M.; Azoddein, A. A. M.; Hassell, D. G.; Dakhil, I. H.; Hasan, H. A. Electrodialysis Desalination for Water and Wastewater: A Review. *Chem. Eng. J.* **2020**, *380*, 122231. https://doi.org/10.1016/j.cej.2019.122231.
(17) Xu, T. Ion Exchange Membranes: State of Their Development and Perspective. *J. Membr. Sci.* **2005**, *263* (1–2), 1–29. https://doi.org/10.1016/j.memsci.2005.05.002.
(18) *Ion Exchange Technology I: Theory and Materials*; Dr., I., Luqman, M., Eds.; Springer Netherlands: Dordrecht, 2012. https://doi.org/10.1007/978-94-007-1700-8.
(19) Ran, J.; Wu, L.; He, Y.; Yang, Z.; Wang, Y.; Jiang, C.; Ge, L.; Bakangura, E.; Xu, T. Ion Exchange Membranes: New Developments and Applications. *J. Membr. Sci.* **2017**, *522*, 267–291. https://doi.org/10.1016/j.memsci.2016.09.033.
(20) Sata, T.; Yamane, Y.; Matsusaki, K. Relationship of Permselectivity between Two Anions to Water Content of Anion Exchange Membranes with Pyridinium Groups. *Electrochimica Acta* **1997**, *42* (15), 2427–2431. https://doi.org/10.1016/S0013-4686(96)00405-7.
(21) Epsztein, R.; Shaulsky, E.; Qin, M.; Elimelech, M. Activation Behavior for Ion Permeation in Ion-Exchange Membranes: Role of Ion Dehydration in Selective Transport. *J. Membr. Sci.* **2019**, *580* (January), 316–326. https://doi.org/10.1016/j.memsci.2019.02.009.
(22) Luo, T.; Roghmans, F.; Wessling, M. Ion Mobility and Partition Determine the Counter-Ion Selectivity of Ion Exchange Membranes. *J. Membr. Sci.* **2020**, *597*, 117645. https://doi.org/10.1016/j.memsci.2019.117645.
(23) Mubita, T.; Porada, S.; Aerts, P.; van der Wal, A. Heterogeneous Anion Exchange Membranes with Nitrate Selectivity and Low Electrical Resistance. *J. Membr. Sci.* **2020**, *607*, 118000. https://doi.org/10.1016/j.memsci.2020.118000.
(24) Kikhavani, T.; Ashrafizadeh, S. N.; Van Der Bruggen, B. Nitrate Selectivity and Transport Properties of a Novel Anion Exchange Membrane in Electrodialysis. *Electrochimica Acta* **2014**, *144*, 341–351. https://doi.org/10.1016/j.electacta.2014.08.012.
(25) Oh, C.-M.; Hwang, C.-W.; Hwang, T.-S. Synthesis of a Quaternarized Poly(Vinylimidazole-Co-Trifluoroethylmethacrylate-Co-Divinylbenzene) Anion-Exchange Membrane for Nitrate Removal. *J. Environ. Chem. Eng.* **2014**, *2* (4), 2162–2169. https://doi.org/10.1016/j.jece.2014.09.014.
(26) Qian, Z.; Miedema, H.; Sahin, S.; de Smet, L. C. P. M.; Sudhölter, E. J. R. Separation of Alkali Metal Cations by a Supported Liquid Membrane (SLM) Operating under Electro Dialysis (ED) Conditions. *Desalination* **2020**, *495*. https://doi.org/10.1016/j.desal.2020.114631.

(27) Qian, Z.; Miedema, H.; de Smet, L. C. P. M.; Sudhölter, E. J. R. Permeation Selectivity in the Electro-Dialysis of Mono- and Divalent Cations Using Supported Liquid Membranes. *Desalination* **2022**, *521*. https://doi.org/10.1016/j.desal.2021.115398.
(28) Mubita, T. M.; Porada, S.; Biesheuvel, P. M.; van der Wal, A.; Dykstra, J. E. Strategies to Increase Ion Selectivity in Electrodialysis. *Sep. Purif. Technol.* **2022**, *292*, 120944. https://doi.org/10.1016/j.seppur.2022.120944.
(29) Zou, D.; Xia, L.; Luo, P.; Guan, K.; Matsuyama, H.; Zhong, Z. Fabrication of Hydrophobic Bi-Layer Fiber-Aligned PVDF/PVDF-PSF Membranes Using Green Solvent for Membrane Distillation. *Desalination* **2023**, *565*, 116810. https://doi.org/10.1016/j.desal.2023.116810.
(30) Teoh, G. H.; Jawad, Z. A.; Chan, D. J. C.; Low, S. C. Surface Regeneration of Templated PVDF Membrane for Efficient Microalgae-Rich High Saline Aquaculture Wastewater Treatment in Membrane Distillation. *Desalination* **2023**, *565*, 116858. https://doi.org/10.1016/j.desal.2023.116858.
(31) Li, B.; Tian, T.; Zhang, X.; Han, C.; Yun, Y.; Zhu, X.; Wu, J. Mussels-Inspired Design a Multi-Level Micro/Nano Re-Entrant Structure Amphiphobic PVDF Membrane with Robust Anti-Fouling for Direct Contact Membrane Distillation. *Desalination* **2023**, *565*, 116857. https://doi.org/10.1016/j.desal.2023.116857.
(32) Zheng, L.; Wang, K.; Hou, D.; Jia, X.; Zhao, Z. Hierarchically-Structured Superhydrophobic POSS/PVDF Composite Membrane for Anti-Fouling and Anti-Wetting Membrane Distillation. *Desalination* **2022**, *526*, 115512. https://doi.org/10.1016/j.desal.2021.115512.
(33) Kujawa, J.; Zięba, M.; Zięba, W.; Al-Gharabli, S.; Kujawski, W.; Terzyk, A. P. Carbon Nanohorn Improved Durable PVDF Membranes - The Future of Membrane Distillation and Desalination. *Desalination* **2021**, *511*, 115117. https://doi.org/10.1016/j.desal.2021.115117.
(34) Zhang, P.; Rajabzadeh, S.; Song, Q.; Gonzales, R. R.; Jia, Y.; Xiang, S.; Li, Z.; Matsuyama, H. Development of Loose Nanofiltration PVDF Hollow Fiber Membrane for Dye/Salt Separation. *Desalination* **2023**, *549*, 116315. https://doi.org/10.1016/j.desal.2022.116315.
(35) Wang, C.; Chen, Y.; Hu, X.; Feng, X. In-Situ Synthesis of PA/PVDF Composite Hollow Fiber Membranes with an Outer Selective Structure for Efficient Fractionation of Low-Molecular-Weight Dyes-Salts. *Desalination* **2021**, *503*, 114957. https://doi.org/10.1016/j.desal.2021.114957.
(36) Shi, Y.; Chen, X.; Wu, Q.; Zhen, H.; Wang, S.; Dong, H.; Wang, J.; Li, Y. Enhance Organic Pollutants Removal of Wastewater by a PVDF/PDA-TiO2 Composite Membrane with Photocatalytic Property. *J. Environ. Chem. Eng.* **2023**, *11* (5), 110389. https://doi.org/10.1016/j.jece.2023.110389.
(37) Tinh, V. D. C.; Bhandari, S. C.; Bose, A. A Sulfonated Polydopamine Coated-PVDF Membrane Development for Oil/Water Separation via Eco-Friendly Methodology. *J. Environ. Chem. Eng.* **2023**, *11* (5), 110560. https://doi.org/10.1016/j.jece.2023.110560.
(38) Baig, N.; Alowaid, A. M.; Abdulazeez, I.; Salhi, B.; Sajid, M.; Kammakakam, I. Designing of Nanotextured Inorganic-Organic Hybrid PVDF Membrane for Efficient Separation of the Oil-in-Water Emulsions. *Chemosphere* **2022**, *308*, 136531. https://doi.org/10.1016/j.chemosphere.2022.136531.

(39) Zhao, Y.; Guo, J.; Li, Y.; Zhang, X.; An, A. K.; Wang, Z. Superhydrophobic and Superoleophilic PH-CNT Membrane for Emulsified Oil-Water Separation. *Desalination* **2022**, *526*, 115536. https://doi.org/10.1016/j.desal.2021.115536.

(40) Ibrahim, Y.; Naddeo, V.; Banat, F.; Hasan, S. W. Preparation of Novel Polyvinylidene Fluoride (PVDF)-Tin(IV) Oxide (SnO2) Ion Exchange Mixed Matrix Membranes for the Removal of Heavy Metals from Aqueous Solutions. *Sep. Purif. Technol.* **2020**, *250*, 117250. https://doi.org/10.1016/j.seppur.2020.117250.

(41) Pal, S.; Mondal, R.; Chatterjee, U. Sulfonated Polyvinylidene Fluoride and Functional Copolymer Based Blend Proton Exchange Membrane for Fuel Cell Application and Studies on Methanol Crossover. *Renew. Energy* **2021**, *170*, 974–984. https://doi.org/10.1016/j.renene.2021.02.046.

(42) Çalı, A.; Şahin, A.; Ar, İ. Experimental Investigation of Boron Phosphate Incorporated Speek/Pvdf Blend Membrane for Proton Exchange Membrane Fuel Cells. *Int. J. Hydrog. Energy* **2022**, *47* (95), 40476–40490. https://doi.org/10.1016/j.ijhydene.2022.05.171.

(43) Nayak, J. K.; Shankar, U.; Samal, K. Fabrication and Development of SPEEK/PVdF-HFP/SiO2 Proton Exchange Membrane for Microbial Fuel Cell Application. *Chem. Eng. J. Adv.* **2023**, *14*, 100459. https://doi.org/10.1016/j.ceja.2023.100459.

(44) Nightingale, E. R. Phenomenological Theory of Ion Solvation. Effective Radii of Hydrated Ions. *J. Phys. Chem.* **1959**, *63* (9), 1381–1387. https://doi.org/10.1021/j150579a011.

(45) Dlugolecki, P.; Nymeijer, K.; Metz, S.; Wessling, M. Current Status of Ion Exchange Membranes for Power Generation from Salinity Gradients. *J. Membr. Sci.* **2008**, *319* (1–2), 214–222. https://doi.org/10.1016/j.memsci.2008.03.037.

(46) Galama, A. H.; Hoog, N. A.; Yntema, D. R. Method for Determining Ion Exchange Membrane Resistance for Electrodialysis Systems. *Desalination* **2016**, *380*, 1–11. https://doi.org/10.1016/j.desal.2015.11.018.

(47) Hagesteijn, K. F. L.; Jiang, S.; Ladewig, B. P. A Review of the Synthesis and Characterization of Anion Exchange Membranes. *J. Mater. Sci.* **2018**, *53* (16), 11131–11150. https://doi.org/10.1007/s10853-018-2409-y.

(48) Sata, T.; Jones, G. N.; Sata, T. *Ion Exchange Membranes: Preparation, Characterization, Modification and Application*; 2004. https://doi.org/10.1039/9781847551177.

(49) Ibáñez-Mengual, J. A.; García-Gamuz, J. A.; Valerdi-Pérez, R. P. Bi-Ionic Potential: Experimental Measurements and Diffusion Coefficients Determinations. *Desalination Water Treat.* **2011**, *36* (1–3), 81–88. https://doi.org/10.5004/dwt.2011.2072.

(50) Ghosh, M.; Madauß, L.; Schleberger, M.; Lebius, H.; Benyagoub, A.; Wood, J. A.; Lammertink, R. G. H. Understanding Mono- and Bivalent Ion Selectivities of Nanoporous Graphene Using Ionic and Bi-Ionic Potentials. *Langmuir* **2020**, *36* (26), 7400–7407. https://doi.org/10.1021/acs.langmuir.0c00924.

(51) Luo, T.; Abdu, S.; Wessling, M. Selectivity of Ion Exchange Membranes: A Review. *J. Membr. Sci.* **2018**, *555*, 429–454. https://doi.org/10.1016/j.memsci.2018.03.051.

(52) Sata, T. Studies on Anion Exchange Membranes Having Permselectivity for Specific Anions in Electrodialysis — Effect of Hydrophilicity of Anion Exchange Membranes on Permselectivity of Anions. *J. Membr. Sci.* **2000**, *167* (1), 1–31. https://doi.org/10.1016/S0376-7388(99)00277-X.

(53) Guler, E.; Zhang, Y.; Saakes, M.; Nijmeijer, K. Tailor-Made Anion-Exchange Membranes for Salinity Gradient Power Generation Using Reverse Electrodialysis. *ChemSusChem* **2012**, *5* (11), 2262–2270. https://doi.org/10.1002/cssc.201200298.
(54) Giorno, L.; Drioli, E.; Strathmann, H. Ion-Exchange Membrane Characterization. In *Encyclopedia of Membranes*; Drioli, E., Giorno, L., Eds.; Springer: Berlin, Heidelberg, 2016; pp 1052–1056. https://doi.org/10.1007/978-3-662-44324-8_994.
(55) Wilhelm, F. G.; Pünt, I. G. M.; van der Vegt, N. F. A.; Strathmann, H.; Wessling, M. Cation Permeable Membranes from Blends of Sulfonated Poly(Ether Ether Ketone) and Poly(Ether Sulfone). *J. Membr. Sci.* **2002**, *199* (1), 167–176. https://doi.org/10.1016/S0376-7388(01)00695-0.
(56) Geise, G. M.; Paul, D. R.; Freeman, B. D. Fundamental Water and Salt Transport Properties of Polymeric Materials. *Prog. Polym. Sci.* **2014**, *39* (1), 1–42. https://doi.org/10.1016/j.progpolymsci.2013.07.001.
(57) Wijmans, J. G.; Baker, R. W. The Solution-Diffusion Model: A Review. *J. Membr. Sci.* **1995**, *107* (1), 1–21. https://doi.org/10.1016/0376-7388(95)00102-I.
(58) Krishna B, A.; Lindhoud, S.; de Vos, W. M. Hot-Pressed Polyelectrolyte Complexes as Novel Alkaline Stable Monovalent-Ion Selective Anion Exchange Membranes. *J. Colloid Interface Sci.* **2021**, *593*, 11–20. https://doi.org/10.1016/j.jcis.2021.02.077.
(59) Krishna B, A.; Zwijnenberg, H. J.; Lindhoud, S.; de Vos, W. M. Sustainable K+/Na+ Monovalent-Selective Membranes with Hot-Pressed PSS-PVA Saloplastics. *J. Membr. Sci.* **2022**, *652*, 120463. https://doi.org/10.1016/j.memsci.2022.120463.
(60) Tekinalp, Ö.; Zimmermann, P.; Burheim, O. S.; Deng, L. Designing Monovalent Selective Anion Exchange Membranes for the Simultaneous Separation of Chloride and Fluoride from Sulfate in an Equimolar Ternary Mixture. *J. Membr. Sci.* **2023**, *666*, 121148. https://doi.org/10.1016/j.memsci.2022.121148.
(61) Mulyati, S.; Takagi, R.; Fujii, A.; Ohmukai, Y.; Matsuyama, H. Simultaneous Improvement of the Monovalent Anion Selectivity and Antifouling Properties of an Anion Exchange Membrane in an Electrodialysis Process, Using Polyelectrolyte Multilayer Deposition. *J. Membr. Sci.* **2013**, *431*, 113–120. https://doi.org/10.1016/j.memsci.2012.12.022.
(62) Vaselbehagh, M.; Karkhanechi, H.; Takagi, R.; Matsuyama, H. Surface Modification of an Anion Exchange Membrane to Improve the Selectivity for Monovalent Anions in Electrodialysis – Experimental Verification of Theoretical Predictions. *J. Membr. Sci.* **2015**, *490*, 301–310. https://doi.org/10.1016/j.memsci.2015.04.014.
(63) Van der Bruggen, B.; Koninckx, A.; Vandecasteele, C. Separation of Monovalent and Divalent Ions from Aqueous Solution by Electrodialysis and Nanofiltration. *Water Res.* **2004**, *38* (5), 1347–1353. https://doi.org/10.1016/j.watres.2003.11.008.

Chapter 4

Selective electrodialysis: targeting nitrate over chloride using PVDF-based AEMs

This chapter has been published as:
Chinello, D.; de Smet, L. C. P. M.; Post, J. Selective electrodialysis: targeting nitrate over chloride using PVDF-based AEMs. *Separation and Purification Technology* **2024**, *342*, 126885

Abstract

The depletion of natural resources and the escalating environmental concerns associated with pollution necessitate innovative approaches for sustainable resource management. In this study, we investigated the selective separation of nitrate from chloride in electrodialysis (ED) using a recently introduced PVDF-based anion-exchange membrane (PVDF-50) and two commercially available membranes (ACS and AMX from Neosepta). Experimental ED data show that the membrane PVDF-50 presents a higher value of nitrate over chloride selectivity compared with the two commercial membranes, the highest reported in literature.

However, recognizing that completely preventing the permeation of chloride ions into the concentrate stream was not feasible, we explored the potential of a system in which anion-exchange membranes presenting different monovalent selectivity were alternated. In this approach, referred to as nitrate-selectrodialysis (NO_3-SED), the different selectivity of PVDF-50 and AMX membranes was leveraged to demonstrate the possibility of increasing nitrate concentration, while simultaneously reducing chloride levels in a stream. This approach proves highly advantageous in applications where mitigating chloride contamination is a significant concern while recovering nitrate.

4.1. Introduction

Nitrate, a key source of nitrogen for plants, plays a crucial role in promoting agricultural productivity and ensuring adequate food production to sustain a growing global population.[1] It is a fundamental component of fertilizers, facilitating the enhanced growth of crops and bolstering agricultural yield.[2,3] However, excessive use of nitrogen-based fertilizers has led to a range of environmental issues, notably eutrophication. Eutrophication occurs when excess nitrogen enters water bodies, stimulating excessive growth of algae and other aquatic plants, ultimately degrading water quality and disrupting ecosystems.[4] To mitigate this, denitrification systems are employed to reduce nitrogen levels in wastewater and prevent its adverse impact on the environment. Denitrification involves converting nitrate into nitrogen gas,[5,6] which can be released harmlessly into the atmosphere. While effective, this approach may not be the most efficient, as it leads to the loss of valuable nitrogen and necessitates the subsequent replenishment of nitrogen-based fertilizers. On the other hand, selective separation of nitrate offers a more convenient solution by allowing for the recycling of nitrate and can have potential application such as in industry[7] or greenhouses.[8]

Electrodialysis can effectively remove nitrate ions by utilizing ion-exchange membranes. However, a challenge remains when also other monovalent ions are present in the water, such as chloride, because of their similar physicochemical properties (**Table 4.1**). Therefore, the need for advancements in membrane technology to develop selective nitrate membranes is pivotal to achieve responsible nitrate management while enabling the recycling of this important nutrient.

A strategy to increase the membranes selectivity towards ions possessing the same valence is based on exploiting the difference in dehydration energy of the ions.[9–12] Several studies[13–15] have demonstrated that increasing the membranes' hydrophobicity can promote the selective transport of ions with lower hydration energy, such as nitrate (**Table 4.1**). This approach has also been explored for the selective separation of monovalent cations like sodium and potassium.[16–18] Ions with a reduced hydration energy undergo easier dehydration, thereby reducing the energy barrier for their transport from the solution into the membrane.[19,20] Moreover, less hydrated ions can interact easily with the fixed charged group in the membrane,[19,21] further lowering the energy barrier. At the same time, the hydrophobicity of the fixed charged groups can be increased, further enhancing selectivity.[22–26]

However, the precise ion-transport mechanism within a membrane is intricate, and most likely, the membrane's selective behavior results from multiple mechanisms operating simultaneously. Indeed, other studies suggest that increasing the membrane's hydrophobicity also influence the ion sieving properties of the membrane, thereby leading to a selective behavior.[18,27–30] Specifically, more hydrophobic membranes exhibit lower water uptake and degree of swelling, which in turn influence the size of the nanochannels in the membranes. Consequently, when the hydrated radii of the ions are comparable to the pores size of the nanochannels, dehydration is required for the transport of ions through the membrane and hence ions presenting lower hydration energy permeate easily.[28,31,32]

Also, the hydrophobic/hydrophilic nature of the membranes may influence the characteristics of the ionic pathway, affecting the ions mobility within the membrane and thus the selectivity.[13,20] In our previous research (**Chapter 3**),[33] we studied the transport of nitrate and chloride using newly developed PVDF-based anion-exchange membranes. Specifically, we explored the impact of varying the PVDF content within the membranes (ranging from 0 to 50 wt%), using a ionomer solution (Fumion FAS-24, FUMATECH BWT GmbH) in combination with PVDF. Our results indicated an enhanced nitrate transport upon increasing PVDF concentration, with the membrane containing 50 wt% PVDF exhibiting the highest nitrate transport. Building on these findings, we decided to investigate the performance of this membrane in comparison to two commercially available membranes (ACS, a monovalent selective membrane, and AMX, a standard grade membrane, from Neosepta) in an electrodialysis (ED) system, presenting the results in this current study. Additionally, we also investigated the potential of a proposed approach called nitrate-selectrodialysis (NO_3-SED), leveraging the differences in nitrate over chloride selectivity of various membranes to achieve concurrent nitrate concentration and chloride depletion in a stream. The approach of alternating a series of cation or anion-exchange membrane in a stack has been explore in literature for various applications such as the separation of divalent from monovalent ions,[34–36] selective production of carboxylic acids,[37] and recovery of L-lysine from L-lysine monohydrochloride.[38] Nevertheless, to the best of our knowledge, this study introduces a novel application of this system, specifically targeting the challenging separation of two monovalent ions.

Table 4.1: Ionic radii, hydrated radii and hydration energies of nitrate and chloride.[39]

Anion	Ionic radius [nm]	Hydrated radius [nm]	Hydration energy [kcal·mol^{-1}]
Nitrate (NO_3^-)	0.264	0.335	71
Chloride (Cl^-)	0.181	0.332	81

4.2. Materials and methods

4.2.1. Chemicals

Polyvinylidene fluoride (PVDF) (average M_w~534,000 by GPC, powder form), sodium chloride (ACS reagent, ≥99.0 %), sodium nitrate (ACS reagent, ≥99.0 %), sodium sulphate (ACS reagent, ≥99.0 %, anhydrous), were purchased from Sigma Aldrich and used without any further treatment. N-methyl-2-pyrrolidone (NMP, HPLC grade 99.5 %) was purchased from Alfa Aesar. Fumion FAS (24 wt% solution in NMP), which physicochemical properties are reported in **Table S4.1** of the supporting information, was purchased from FUMATECH BWT GmbH, Bietigheim-Bissingen, Germany. The Neosepta AMX, ACS, and CMX membranes were purchased from ASTOM Corporation, Tokyo, Japan. The chemical composition and physical properties of Neosepta AMX and ACS are reported in **Table 4.2**.

4.2.2. PVDF-based AEM fabrication

The PVDF-based AEM was manufactured by mixing in NMP PVDF and Fumion FAS-24 in a weight ratio of 50:50. The resulting mixture, with a concentration of polymers of 16 wt%, was stirred overnight to achieve complete dissolution prior casting it onto a glass plate kept at 60 °C for 24 hours, in order to remove the solvent by evaporation. To additionally guarantee thorough solvent elimination, the membranes were immersed in a 0.5 M NaCl solution for a duration of 2 hours. This process was reiterated five times, with each repetition involving the replacement of the solution. The wet membrane thickness was then measured using a digital thickness gauge (Mitutoyo Corporation, model no. ID-C112BS) and stored in a 0.5 M NaCl solution. The membrane was labelled PVDF-50, in order to indicate the percentage of PVDF, and selected characteristics,

together with those of the commercial anion-exchange membranes used in this study, are reported in **Table 4.2**.

4.2.3. Membrane characterization

4.2.3.1. Ion-exchange capacity (IEC)

The ion-exchange capacity (IEC) of an ion-exchange membrane refers to the amount of ions, expressed in milliequivalents per gram (meq·g^{-1}) that the membrane can exchange, and it is an indirect measure of the membrane's fixed charge density. The procedure to measure the IEC involves conditioning the membrane in 0.5 M NaCl for 48 hours and then transferring it in 0.5 M $NaNO_3$, the exchange solution. After 24 hours, the chloride concentration was evaluated using ion chromatography and then the IEC was calculated using the following equation:[40]

$$IEC = \frac{n_{\mathrm{eq}}}{W_{\mathrm{dry}}} \tag{4.1}$$

where n_{eq} refers to the equivalent of exchanged ions (eq) and W_{dry} (g) to the membrane's dry mass.

4.2.3.2. Water uptake

The water uptake of the membranes was measured as follows. The membranes were immersed in demineralized water for 24 hours, and then weighted after removing the water from the surface with a tissue. After recording the wet membrane mass (W_{wet}, in grams), the membranes were placed in an oven at 55 °C for 24 hours in order to achieve complete water evaporation. The water uptake was then calculated after measuring the dry membrane mass (W_{dry}, in grams), using the following equation:

$$Water\ uptake = 100 \times \frac{W_{\mathrm{wet}} - W_{\mathrm{dry}}}{W_{\mathrm{dry}}}\ \% \tag{4.2}$$

4.2.3.3. Contact angle

The hydrophobicity of the membranes under investigation was evaluated by measuring the contact angle through the captive bubble method. This technique involves measuring the contact

angle formed between an air bubble (1 µL) and the surface of the membrane immerse in water. This angle is indicative for the hydrophobicity of the surface. A higher contact angle indicates a higher hydrophobicity, meaning the material is less likely to interact with or be wetted by water. Conversely, a lower contact angle indicates a more hydrophilic surface, indicating a higher affinity for water. Contact angles were determined using a contour analysis system (OCA35, DataPhysics Instruments, Germany), and six measurements were taken for each membrane, varying the position of each measurement.

4.2.3.4. Permselectivity

The permselectivity of an ion-exchange membrane refers to its ability to selectively allow the passage of counter-ions, ions with the opposite charge of the fixed group within the membranes, while blocking the co-ions, ions with the same charge. The permselectivity was determined following previous contribution in literature[40,16,33] by recording the potential across the membrane separating two electrolyte solution such as NaCl 0.1 M and NaCl 0.5 M, which are recirculated in the system at a flow of 750 mL·min^{-1}. Two Ag/AgCl electrodes immersed in the solutions where used to record the potential after reaching the steady state. The membrane permselectivity expressed as a percentage is then calculated by the following equation:

$$a = 100 \times \frac{\Delta V_{\text{measured}}}{\Delta V_{\text{theoretical}}} \% \quad (4.3)$$

where $\Delta V_{\text{theoretical}}$ represents the theoretical membrane potential calculated according to the Nernst equation for a membrane 100 % selective towards counter-ions.

4.2.3.5. Permeability coefficients ratio

The permeability coefficients ratio of ion-exchange membranes is a parameter that characterizes the affinity between the membranes and the counter-ions present in a solution. It can be determined by measuring the zero-current potential existing across a membrane separating two electrolyte solutions containing the same co-ion but different counter-ion (in our case Na^+, and NO_3^- and Cl^-, respectively). It can be used to get a quick indication of the selective behavior of the membranes toward target ions, *e.g.* nitrate *vs.* chloride. The permeability coefficients ratio was determined according to a procedure we published earlier (**Chapter 3**).[33] The potential across the

membrane ($\Delta\Psi$) separating two electrolyte solutions such as 0.1 M NaCl and 0.1 M $NaNO_3$ recirculating at a flow rate of 750 mL min^{-1}, was recorded using two Ag/AgCl electrodes immersed in the solutions for a period of 40 min. The potential used for the calculations is the average of the values recorded once the steady state was reached, after *ca.* 10 min, and it is related to the permeability coefficients of the counter-ions by the Nernst equation:

$$\Delta\Psi = \frac{RT}{F} ln \frac{P_{NO_3^-}[NO_3^-]}{P_{Cl-}[Cl^-]} \quad (4.4)$$

where *F* is the Faraday constant (96,458 A·s·mol^{-1}), *R* is the universal gas constant (8.314 J·mol^{-1}·K^{-1}), *T* is the absolute temperature (K), $P_{NO_3^-}$ and P_{Cl-} are the permeability coefficients of the counter-ions, and $[NO_3^-]$ and $[Cl^-]$ are the concentrations of the ions in each compartment. Considering that the concentration of nitrate and chloride is the same, rearranging equation 4.4 enables the determination of the permeability ratio using the following equation:

$$\frac{P_{NO_3^-}}{P_{Cl-}} = e^{\frac{F\Delta\Psi}{RT}} \quad (4.5)$$

4.2.4. Membrane Performance

4.2.4.1. Electrodialysis experiments

The electrodialysis (ED) setup used in this study to determine the nitrate over chloride selectivity of the anion-exchange membranes under investigation (PVDF-50, ACS, and AMX), is schematically represented in **Figure 4.1**. The configuration consists in a sequence of five ion-exchange membranes arranged as follows: three cation-exchange membranes (CMX from Neosepta) alternated with two anion-exchange membranes. This configuration results in a total of two cell pairs, each consisting of a cation and an anion-exchange membrane, separating a diluate and concentrate stream. The IEM area available for the ion transport is 20 cm^2, and each membrane is separated from the other by a spacer-integrated gasket with a thickness of 0.5 mm. The setup is equipped with platinum-coated titanium mesh electrodes, and the compartments are separated from each other by a cation-exchange membrane (CMX), in order to prevent the migration of chloride ions towards the anode, thereby avoiding chlorine formation. The electrode

compartments maintain a recirculating solution of 0.05 M Na_2SO_4; in the outlets of these compartments two Ag/AgCl electrodes connected to the potentiostat are placed to measure the potential across the five membranes.

The experiments are conducted in batch-mode at a current density of 20 $A{\cdot}m^{-2}$, with a potentiostat (Autolab AUT72157, Metrohm) used as current supplier. The solutions recirculating in the concentrate and dilute compartments are equimolar solutions of NaCl and $NaNO_3$ with a total concentration of anion of 0.1 M and a volume of 0.1 L each. The duration of each experiment is 3 hours, which results in a theoretical total anion removal from the diluate stream of 90 %. For each membrane, experiments were repeated three times to assess reproducibility.

In order to evaluate the nitrate over chloride selectivity over time, samples were taken every 30 min and analyzed by ion chromatography (IC) to determine the ion concentrations. The concentrations obtained were first used to calculate the transport number (*t*), which refers to the fraction of current transported by a specific ion, and for a monovalent ion (*i*) is calculated using the following equation:

$$t_{\mathrm{i}} = \frac{FV}{iAN} \cdot \frac{\Delta C_{\mathrm{i}}}{\Delta t} \tag{4.6}$$

where *F* is the Faraday constant (96,458 $A{\cdot}s{\cdot}mol^{-1}$), *V* (m^3) and ΔC_i ($mol{\cdot}L^{-1}$) are respectively the volume and the variation of the ion concentration in the concentrate stream, *A* (m^2) the surface membrane area, *N* the number of cell pairs, Δt (s) is the time of the experiments, and *i* is the current density applied ($A{\cdot}m^{-2}$). The current efficiency of the experiments is defined by the equation:

$$\eta = \left(J_{\mathrm{i}} + J_{\mathrm{j}}\right)\frac{F}{i} \tag{4.7}$$

where J_i and J_j are the ionic fluxes across the membrane expressed in $mol{\cdot}m^{-2}{\cdot}s^{-1}$ of the ions under consideration, which are calculated using the equation:

$$J_{\mathrm{i}} = \frac{V}{AN} \cdot \frac{\Delta C_{\mathrm{i}}}{\Delta t} \tag{4.8}$$

In order to compare our results with other studies, the nitrate over chloride selectivity over time of the membranes under investigation was calculated according to the following equation reported by Mubita *et al.*:[41]

$$S_{Cl^-}^{NO_3^-} = \left(\frac{\Delta C_{NO_3^-}}{\Delta C_{Cl^-}}\right)_{Concentrate} \cdot \left(\frac{C_{Cl^-}}{C_{NO_3^-}}\right)_{Diluate} \quad (4.9)$$

where $\Delta C_{NO_3^-}$ and ΔC_{Cl^-} refer to the variation of the concentration of nitrate and chloride in the concentrate reservoir between two samples and $C_{NO_3^-}$ and C_{Cl^-} refer to the concentration of the ions in the diluate compartment.

From an application point of view, the recovery ratio is another parameter of interest, which for an ion (*i*) is defined by Chen *et al.* [42] as:

$$R_i = \frac{V_{ct}(C_{ct} - C_{c0})}{V_{d0}C_{d0}} \times 100 \quad (4.10)$$

where C_{ct}, C_{c0} and C_{d0} are the concentrations of the ion at time t and 0 respectively in the concentrate and diluate stream, and V_{ct} and V_{d0} are the volume in the concentrate and dilute at time *t* and zero, respectively.

The energy consumption (*E*) was evaluated as kilojoules per gram of nitrate recovered following the equation:

$$E = \frac{\Delta V_{stack} \cdot i \cdot A \cdot \Delta t}{\Delta n_{NO_3^-} \cdot MW_{NO_3^-}} \quad (4.11)$$

where ΔV_{stack} is the average stack potential (V), i is the current density applied ($A \cdot m^{-2}$), *A* the surface membrane area (m^2), Δt is the time of the experiments (s), $\Delta n_{NO_3^-}$ is the variation in moles of the nitrate in the concentrate stream, and $MW_{NO_3^-}$ the nitrate's molecular weight ($g \cdot mol^{-1}$).

Lastly, in order to assess any dependency of the current applied on its performance, membrane PVDF-50 has also been tested at an increased current density of 40 $A \cdot m^{-2}$.

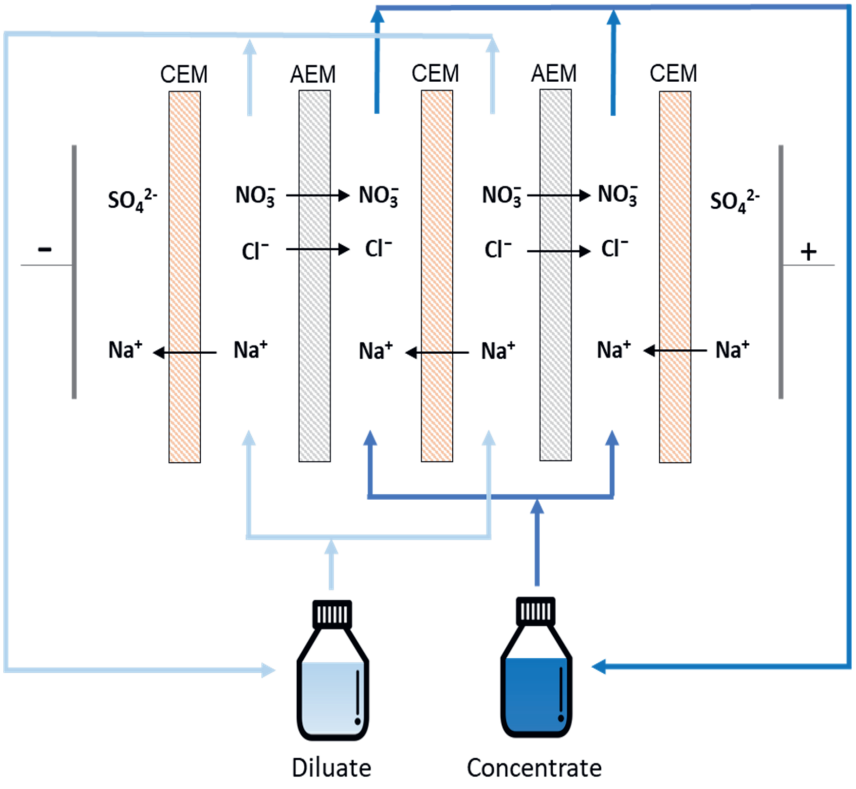

Figure 4.1: Schematic representation of the ED setup used to assess the nitrate over chloride selectivity of the anion-exchange membranes PVDF-50, ACS, and AMX. The system is composed of five membranes in total, three Cation-Exchange Membranes (CEMs) and two Anion-Exchange Membranes (AEMs). The experiments are performed in batch-mode, with the concentrate and diluate streams pumped from the reservoirs. The electrodes are from platinum-coated titanium and a Na_2SO_4 solution was recirculated in the electrode compartments.

4.2.5. Nitrate-selectrodialysis (mSED) experiments

Based on the conventional electrodialysis approach, chloride ions also permeate into the concentrate stream, and in applications[7] where the nitrate recycling should be paired with the simultaneous chloride removal, other membranes configurations might be more beneficial. For this reason, we investigated the potential of a system referred to as nitrate-selectrodialysis (NO_3-SED), which schematic configuration is reported in **Figure 4.2**.

This system capitalizes on the different nitrate over chloride selectivity of two distinct anion-exchange membranes (PVDF-50 and AMX). By strategically alternating between these membranes, we exploit the superior permeability of nitrate ions through PVDF-50 compared to AMX and, conversely, the higher permeability of chloride ions through AMX. Consequently, over time, in Feed 2, the nitrate concentration increases and chloride concentration decreases, while in Feed 1, chloride concentration increases and nitrate concentration decreases.

The experimental settings are similar to those of ED experiments: two platinum-coated titanium mesh electrodes, separated from the AEMs by two CMX membranes, are present with a recirculating solution of 0.05 M Na_2SO_4. The composition of Feed 1 and Feed 2 is 0.05 M NaCl + 0.05 M $NaNO_3$ with a volume of 0.1 L per each feed. A spacer-integrated gasket with a thickness of 0.5 mm was used to separate the membranes and each experiment was conducted in batch-mode lasting for 3 hours. Regarding the current density applied, we decided to investigate the performance of the system at two different values: 20 $A \cdot m^{-2}$, and 40 $A \cdot m^{-2}$. The variation of the concentration in the reservoirs of Feed 1 and Feed 2 is monitored over time by taking samples every 30 minutes and analyzing them using ion chromatography. The energy consumption of each experiment have been calculated using the equation:

$$E = \Delta V_{stack} \cdot i \cdot A \cdot \Delta t \tag{4.12}$$

where ΔV_{stack} is the average stack potential (V), i is the current density applied ($A \cdot m^{-2}$), A the surface membrane area (m^2), Δt is the time of the experiments.

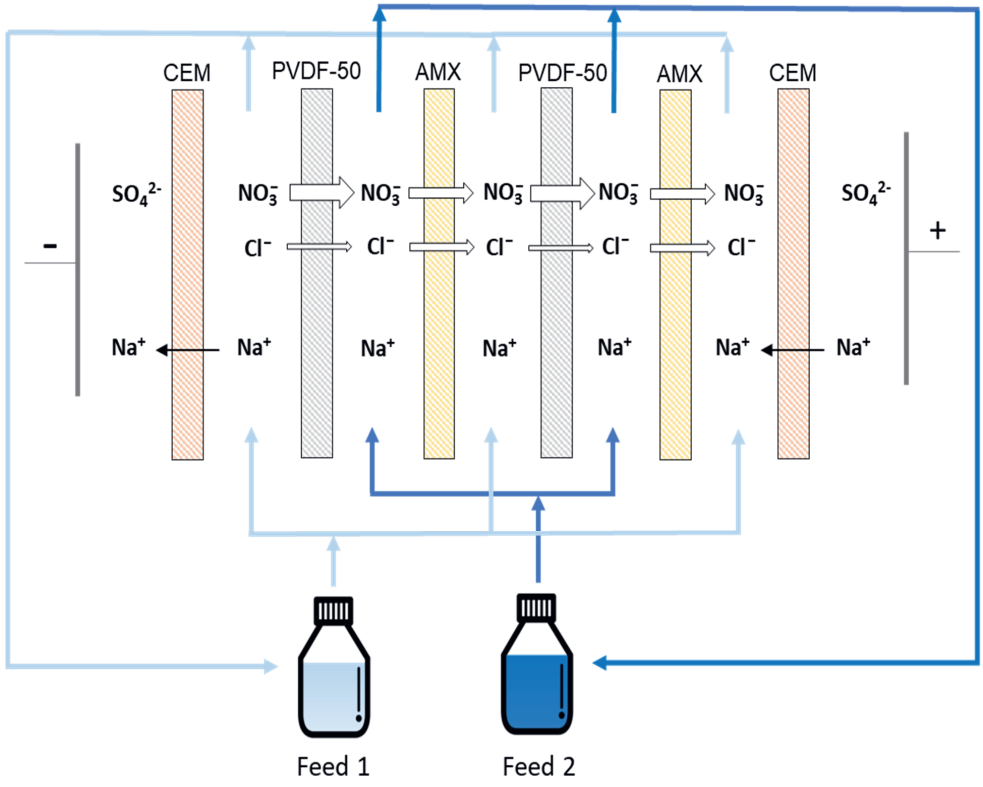

Figure 4.2: Schematic representation of the nitrate-selectrodialysis (NO_3-SED) setup used in this study. The system is composed of six membranes in total, two Cation-Exchange Membranes (CEMs) near the electrodes and four Anion-Exchange Membranes (AEMs) in between, featuring an alternating arrangement of two PVDF-50 membranes and two AMX membranes. The experiments are performed in batch-mode, with the Feed 1 and 2 streams pumped from the reservoirs. The electrodes are from platinum-coated titanium and a Na_2SO_4 solution was recirculated in the electrode compartments.

4.3. Results and discussion

4.3.1. Membrane characterization

4.3.1.1. IEC and water uptake

Table 4.2 presents the IEC and water uptake values for the three membranes, which were determined following the procedures described in **Sections 4.2.3.1** and **4.2.3.2**. Notably, the IEC values exhibit the following order: AMX > ACS > PVDF-50. Conversely, the water uptake values follow a different trend: ACS > AMX > PVDF-50. It is worth noting that while we expected a similar

trend between IEC and water uptake, the water uptake values of AMX and ACS align with previous findings in the literature.[43]

Indeed, the water uptake of a membrane is directly correlated with the proportion of charged groups within the membrane. Elevated quantities of charged groups, resulting in high values of the IEC, result in a higher osmotic pressure and thus a higher water uptake of the membrane.[23,44] However, the water content is also influenced by other parameters, such as the affinity between the polymer matrix of the membrane and water,[23] and the presence of reinforcing materials.[45] Typically, the membrane's water absorption capacity depends on the number of hydrophilic groups it contains. When there is low water uptake, it suggests that hydrophobic membrane groups are more prevalent than their hydrophilic counterparts.[46]

Table 4.2: Chemical and physical properties of the membranes used in this study: PVDF-50, AMX, ACS, and CMX.

Membrane	Composition	Thickness (µm)	IEC ($meq \cdot g^{-1}$)	Water Uptake (%)
PVDF-50	PVDF:Fumion FAS-24 = 50:50	80-85	0.7	7
AMX	Styrene-divinyl benzene reinforced with PVC[47]	140	2.1	22
ACS	Styrene-divinyl benzene reinforced with PVC, with highly cross-linked layer on both of the membrane surfaces[47]	120	1.9	26
CMX	Cross-linked sulfonated styrene-divinylbenzene copolymer (45–65%) and polyvinylchloride (45–55%)[48]	150	2.5	30

4.3.1.2. Contact angle analysis

In an attempt to obtain more insight in the hydrophobic properties of the membranes, drops of water were placed on each membrane. However, quantification of the contact angles turned out to be very difficult as the membranes curled up. Instead, the captive bubble method, a configuration that allows the membranes to be wetted, turned out to be a suitable alternative. **Figure 4.3** displays the contact angle values measured using this method for the three membranesunder investigation in the study: AMX, ACS, and PVDF-50.

As becomes clear from these data, the contact angle, and with that the hydrophobicity, increases in the order of PVDF-50 > ACS > AMX.

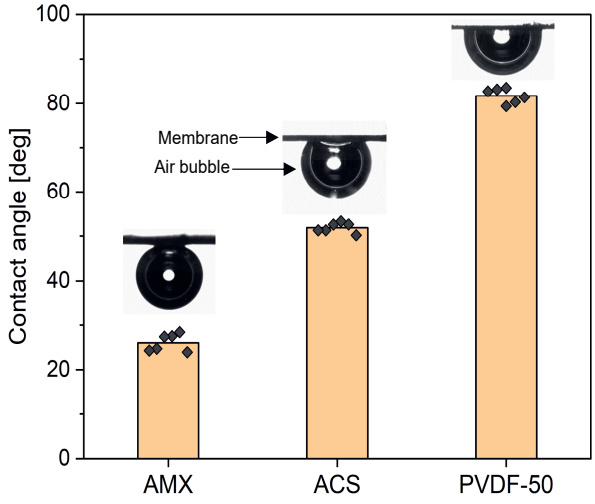

Figure 4.3: Contact angle measured by the captive bubble method for the three membranes investigated in this study: AMX, ACS, and PVDF-50. Optical images of the membranes and the air bubble are provided for enhanced clarity.

4.3.1.3. Permselectivity and permeability coefficients ratio

From the results presented in **Figure 4.4**, it is evident that, across all three membranes, the permselectivity values are consistently around 90%, aligning with previous findings in the literature.[49] When it comes to the permeability coefficients ratio, a key indicator of a membrane's affinity for nitrate or chloride, we observe that the ratio is consistently larger than 1 for all membranes. This means that all three membranes exhibit a preference for nitrate over chloride ions. The values of the permeability coefficients ratio follow the trend of PVDF-50 > ACS > AMX, indicating that PVDF-50 exhibits the highest selectivity for nitrate over chloride, while AMX is the least selective among the three membranes. Comparison of the permselectivity and permeability coefficients ratio results of the AMX and PVDF-50 membranes with those obtained in our precedent study (**Chapter 3**),[33] affirms the high reproducibility of the proposed methods for determining these parameters.

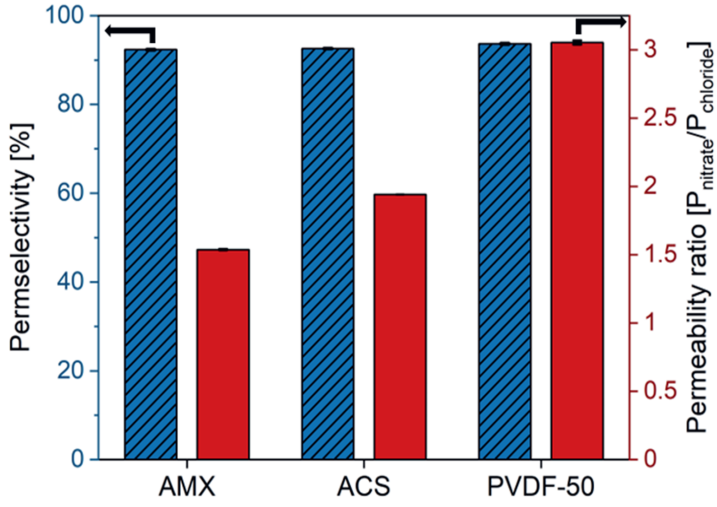

Figure 4.4: Permselectivity and permeability coefficient ratio values of the investigated membranes: AMX, ACS, and PVDF-50. Experiments have been repeated three times.

4.3.2. Membrane performance

4.3.2.1. Selective separation in batch-mode electrodialysis

In accordance with the experiment details outlined in **Section 4.2.4.1**, we present the experimental results of the transport of nitrate and chloride through the three membranes under investigation, PVDF-50, ACS, and AMX, obtained in batch-mode electrodialysis. The concentrations of nitrate and chloride in the two reservoirs were monitored over time (**Figure 4.5**) for the PVDF-50 membrane (for the other membranes, see Supporting Information **Figure S4.1**), and, as expected, they increased in the concentrate reservoir while decreasing in the diluate one. Additionally, we observed that in the concentrate reservoir, the concentration of nitrate increased more rapidly over time compared to chloride for all membranes under examination. However, upon analyzing the average ionic flux of nitrate and chloride for the three membranes (**Figure 4.6**), it became evident that PVDF-50 transports more nitrate and less chloride compared to ACS and AMX, indicating a higher selectivity for nitrate. The current efficiency for all experiments was in the range of 91–94 %.

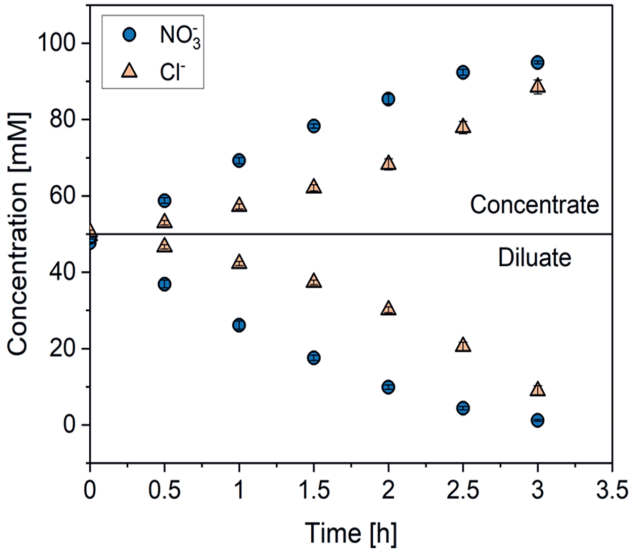

Figure 4.5: Evolution of the nitrate and chloride concentration in the concentrate (top) and diluate (bottom) reservoir by ED with a CMX | PVDF-50 | CMX | PVDF-50 | CMX membrane stack. Experiments were conducted in triplicate.

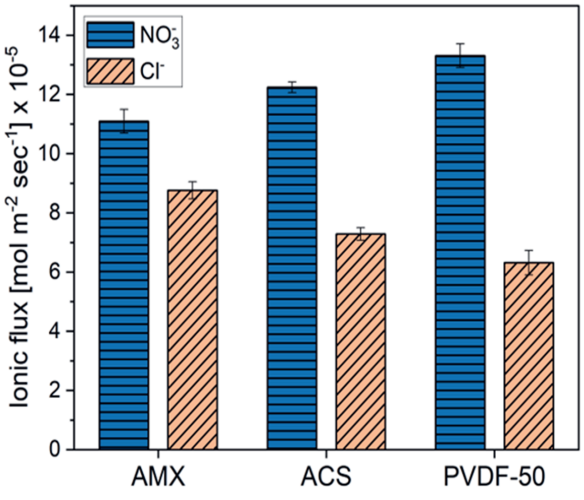

Figure 4.6: Average ionic flux of nitrate and chloride obtained by ED using a membrane stack configuration of CMX | AEM | CMX | AEM | CMX, for the three selected AEMs: AMX, ACS, and PVDF-50. The measurements were conducted at a current density of 20 $A \cdot m^{-2}$.

We further assessed the nitrate over chloride selectivity of the three membranes over time using equation 4.7 (**Figure 4.7**). The data clearly shows that PVDF-50 presents higher selectivity values compared to ACS, which in turn presents higher values than AMX. Moreover, the selectivity was found to change in time due to changes in the actual concentration ratio in the diluate stream, a trend that has also been reported by Mubita *et al*.[41] Their work involved both theoretical and experimental investigations into the nitrate over chloride selectivity of three anion-exchange membranes, two commercial, AMX from Neosepta and Ralex AMH-PES from Mega a.s. (Czech Republic), and one heterogeneous AEMs manufactured with a ion-exchange resin featuring quaternary ammonium groups with propyl substituents. The theoretical analysis revealed a significant time dependency of the selectivity, while the reported experimental results showed a less pronounced decrease. Notably, the experimental outcomes for the AMX membrane exhibited a similar trend to our data. Conversely, in the reported case of the Ralex AMH-PES membrane, the selectivity demonstrated an increase over time. Furthermore, the examination of their manufactured anion-exchange membrane with a thickness of 70 µm disclosed a pronounced decrease in selectivity over time, aligning with the theoretical trend. However, the study does not provide an explanation for the observed trends.

Our analysis is based on the equation used to calculate the selectivity (equation 4.9), widely employed in literature[9,13,22,27,41,47,50,51], which might present limitations. Specifically, the second term of the equation refers to the concentration of chloride and nitrate at the membrane surface on the diluate stream, typically approximated to the concentration in the bulk solution.[9] We hypothesize that phenomena such as concentration polarization may occur, leading to an inaccurate definition of the concentration at the membrane surface on the desalting side and thus selectivity. This effect becomes more pronounced for higher degrees of desalination.[52] However, given the significance of comparing our results with existing literature, we decided to adopt the selectivity definition provided by Mubita *et al.* in their study.

By analyzing our data is possible to observe that for the membranes ACS and AMX, the selectivity decreases nearly linearly with time, while for PVDF-50 is steadily declining. Two different regimes can be distinguished. The first one spans from 0 hours to 2 hours, during which the selectivity remains relatively constant within the range of 3.7-4. The second regime ($t > 2$ h)

exhibits a more pronounced reduction. The observed decrease after two hours of the experiments can be attributed to the substantial removal of nitrate from the diluate stream and, consequently, the potential emergence of concentration polarization phenomena. PVDF-50, therefore, presents a superior behavior compared to the other two membranes, which is also evident by analyzing the trends of the recovery ratio of nitrate and chloride reported in **Figure 4.8**, with PVDF-50 presenting a higher recovery for nitrate compared to those of ACS and AMX.

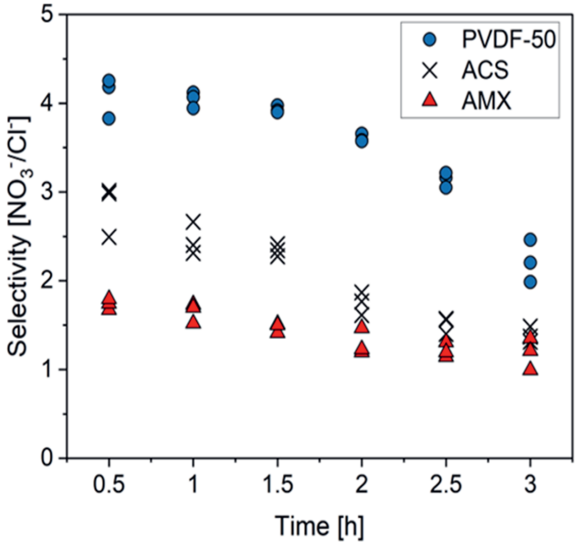

Figure 4.7: Evolution of the nitrate over chloride selectivity by ED with a CMX|AEM|CMX|AEM|CMX membrane stack for three selected AEMs: AMX, ACS, and PVDF-50 at 20 $A \cdot m^{-2}$. For each membrane, the experiments were repeated three times.

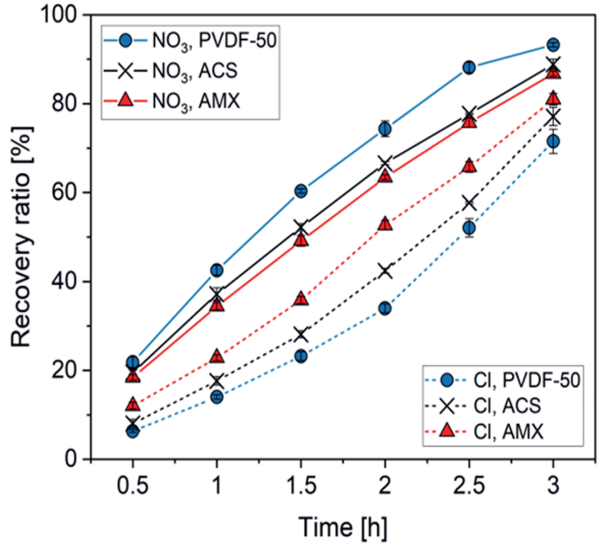

Figure 4.8: Evolution of the recovery ratio of nitrate (solid lines) and chloride (dashed lines) by ED with a CMX | AEM | CMX | AEM | CMX membrane stack for three selected AEMs: AMX, ACS, and PVDF-50 at 20 $A \cdot m^{-2}$. For each membrane, the experiments were repeated three times.

When comparing the energy consumption values, PVDF-50 exhibits a slightly higher value than ACS and AMX, as indicated in **Table 4.3**.

Table 4.3: Energy consumption obtained for the batch-mode ED experiments at 20 $A \cdot m^{-2}$ for the membranes PVDF-50, ACS, and AMX.

	PVDF-50	**ACS**	**AMX**
E ($kJ \cdot g^{-1}\ NO_3^-$)	0.57	0.48	0.45
E ($kWh \cdot m^{-3}$)	0.92	0.75	0.68

Nevertheless, this slight increase in energy consumption is a reasonable trade-off considering the membrane's superior nitrate selectivity. The enhanced selectivity for nitrate can be attributed to the increased hydrophobic nature of the membrane, as highlighted by the measurements of contact angles through captive bubble method, compared to the two commercial membranes. This characteristic promotes the permeation of less hydrated ions, such as nitrate, by requiring

less energy to enter the membrane due to easier dehydration. Moreover, the increased hydrophobic environment within the membrane can also affect the mobility of ions with higher hydration energy, such as chloride, which are impeded by the hydrophobic structure.[13]

Studies on the ACS membrane reported that the highly cross-linked surface layer on the membrane was responsible for the steric sieving of monovalent over divalent ions due to their different hydrated radii.[27,29] Despite the minimal difference in the hydrated radii of nitrate and chloride,[39] (**Table 4.1**) we do find that ACS presents a higher selectivity than AMX, an AEM that does not possess a cross-linked surface layer. Furthermore, Hawks *et al*.,[53] proposed that the solvation structure of ions is another crucial parameter influencing the steric sieving mechanism. Indeed, while investigating the adsorption mechanisms of nitrate and chloride in ultramicroporous carbon during capacitive deionization, they ascribed the preference for nitrate adsorption to differences in the solvation structure and hydration energy of the two ions. Indeed, despite the similarity in their hydrated radii, nitrate's trigonal planar molecular geometry results in its preferential solvation around the edges, rather than on the planar faces, while chloride maintains symmetry across all three spatial dimensions. These structural characteristics, combined with the ~12 % lower hydration energy of nitrate – increasing the ability to alter its solvation structure when entering narrow pores – was reported to be the driving force behind the preferential adsorption of nitrate, and can be used to explain the higher nitrate selectivity of the ACS membrane compare to the AMX.

The most recent study examining nitrate and chloride transport in an electrodialysis (ED) setup was conducted by Mubita *et al*.[41] In the present study, we maintained identical conditions regarding ion concentration in the solution, current density, and experiment duration, enabling a direct comparison of results. The membrane selectivity value reported by Mubita *et al*. for a heterogeneous anion-exchange membrane made with ion-exchange resins featuring quaternary ammonium groups with propyl substituents, ranged from 2.5 to 3. This range is lower than the selectivity values reported in our current study.

In order to assess whether the current density influences the performance of PVDF-50, batch-mode ED experiments were conducted at double the current density. In **Figure 4.9**, the recovery ratio of nitrate and chloride for the two sets of experiments, 20 $A \cdot m^{-2}$ and 40 $A \cdot m^{-2}$, are reported

over the amount of charge passing through the membrane at the time of the sampling. Indeed, with the current doubled, the experiment's duration is halved, allowing correlation between the two trends using the transferred charge quantity. As can be observed from **Figure 4.9**, the trends for nitrate and chloride for the two current densities are quite similar.

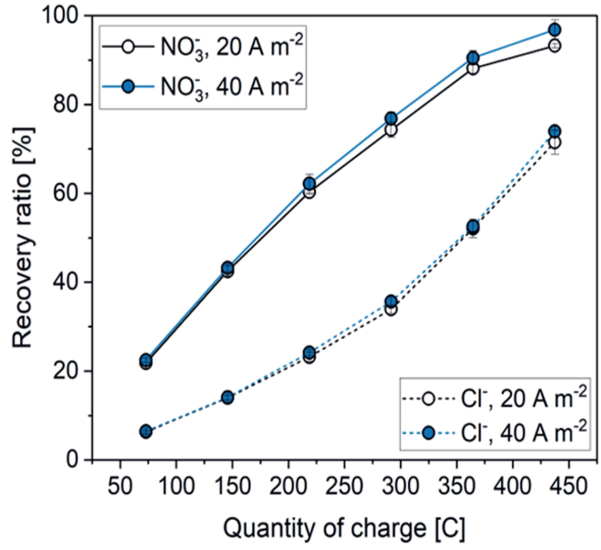

Figure 4.9: Nitrate and chloride recovery ratio for the ED experiments at 20 and 40 A·m^{-2} as function of the amount of charge passing through the membrane. Experiments were conducted in triplicate.

4.3.2.2. Nitrate-selectrodialysis (NO_3-SED)

In this section, we present the experimental results and performance of the nitrate-selectrodialysis (NO_3-SED) system, which is schematically represented in **Figure 4.2**. As described in **Section 4.2.5**, the system exploits the difference in the nitrate over chloride selectivity of two different membranes, *i.e.* PVDF-50 and AMX. The membrane choices were made based on the insights obtained from the batch-mode electrodialysis (**Section 4.3.2.1**), with PVDF-50 exhibiting superior nitrate selectivity and AMX having the lowest.

The experiments were conducted three times and **Figure 4.10** illustrates the concentrations of nitrate and chloride in the two reservoirs, Feed 1 (Panel **A**) and Feed 2 (Panel **B**), over time. As anticipated, alternating between PVDF-50 and AMX membranes enables us to increase the nitrate concentration in Feed 2 while decreasing chloride concentration, whereas the opposite occurs in

Feed 1. For experiments conducted at 20 $A \cdot m^{-2}$, we observed an approximately 6-7 % increase/decrease in anion concentration in the two streams, as shown in **Figure 4.10**.

Doubling the current density results in an increase of the nitrate concentration in Feed 2 of approximately 10 %, accompanied by a subsequent decrease in chloride levels. Although these changes may be evaluated as modest, it is important to realize that with advancements in membrane technology, there is potential for further improvements and achieving higher values in system performance. Additionally, to further explore the potential of this system, it may be worthwhile to explore alternative configurations, including the use of multiple reservoirs.

Finally, this strategy can be extended to other scenarios such as the selective separation of potassium from sodium,[16,54] by alternating cation-exchange membranes, each with a different selectivity towards one of the two ions. When comparing the energy consumption of the experiments, it is possible to observe from **Table 4.4** that the experiments conducted at 40 $A \cdot m^{-2}$ require more than four times the energy of those at a lower current density.

Table 4.4: Energy consumption obtained for the batch-mode nitrate-selectrodialysis (NO_3-SED) experiments at 20 and 40 $A \cdot m^{-2}$.

	20 $A \cdot m^{-2}$	40 $A \cdot m^{-2}$
E ($kJ \cdot g^{-1}\, NO_3^-$)	3.6	9.4

Exploiting the difference in the hydration energy of ions appears to be an interesting approach, and designing membranes that promote this effect have the potential to control and yield high ion selectivity. Various strategies can be pursued and eventually combined to further magnify the impact. For example, Mubita *et al.*[15] report on enhancing nitrate transport upon increasing the hydrophobicity of the membrane, by using resins containing different quaternary ammonium groups with alkyl chain length. Similarly, in our previous work (**Chapter 3**),[33] we report on a comparable effect by increasing the concentration of PVDF within the membrane. Additionally, the higher selectivity of the ACS membrane compared to the one of AMX observed in this study suggests that the presence of a crosslinked layer on the surface of the membranes promote the

permeation of nitrate over chloride. We therefore believe that future membranes incorporating all these effects are key to achieving high separation values.

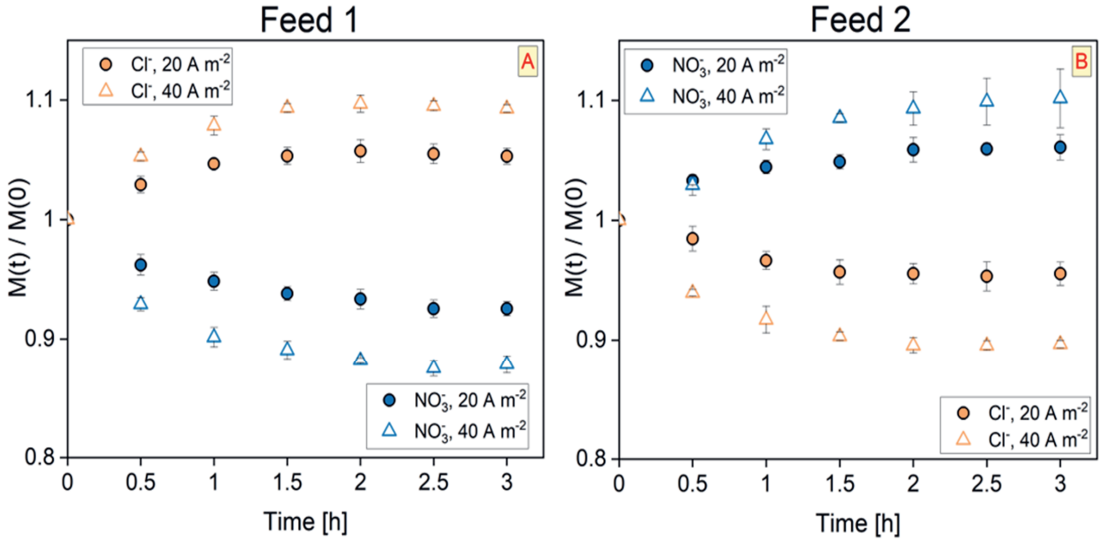

Figure 4.10: Nitrate and chloride concentration variation in Feed 1 (A) and Feed 2 (B) for the selectrodialysis experiments conducted at the current density of 20 and 40 A·m^{-2}.

4.4. Conclusion

In terms of the selective separation of nitrate from chloride the performance of a recently introduced PVDF-based anion exchange membrane, PVDF-50, was tested for the first time in an electrodialysis setup, operating in batch mode. Our results demonstrate that this membrane exhibits higher and more stable nitrate over chloride selectivity values compared to two commercial membranes, surpassing the highest reported values in the literature. Additionally, we found that the current density does not significantly influence the performance of PVDF-50, enabling a reduction in operational time or installed membrane area.

However, it is important to note that this system cannot entirely prevent the transport of chloride to the concentrate stream. To mitigate this limitation, and selectively separate nitrate from chloride, we investigate the approach of alternating a series of AEMs with different nitrate selectivity (PVDF-50 and AMX), which we referred to as nitrate-selectrodialysis (NO_3-SED). Our

findings indicate that with this system, it is possible to increase the concentration of nitrate while concurrently decreasing the concentration of chloride by approximately 10-11 % when operating at 40 $A \cdot m^{-2}$.

We believe that fine-tuning the chemical properties of membranes will become increasingly important for advancements in membrane technology, enabling further enhancement of selectivity. Such developments are not only relevant for the field of nitrate recovery but also for applications where the reduction of chloride concentration is of significant importance.

Acknowledgments

The authors thank the Dutch Research Council – Wetsus Partnership Programme on Sustainable Water Technology for funding this project (ALWET.2019.004). This work was performed in the cooperation framework of Wetsus, European Centre of Excellence for Sustainable Water Technology (www.wetsus.nl). Wetsus is co-funded by the Dutch Ministry of Economic Affairs and Ministry of Infrastructure and Environment, the European Union Regional Development Fund, the Province of Fryslan and the Northern Netherlands Provinces. The authors like to thank the participants of the research theme “Desalination & Concentrates” for the fruitful discussions and their financial support. We also would like to thank Eirini Aikaterini Gkougkousi and Tesse van der Wal for their precious contributions to the experimental work and Rodrigo Nobre for his invaluable support in the measurement of contact angles.

Supporting Information

Table S4.1: Physicochemical properties of Fumion FAS-24.

	Matrix	Functional group	Counter-ion	IEC (meq/g)
Fumion FAS-24	Polyaromatic polymer	Quaternary ammonium	Bromide	1.7-1.9

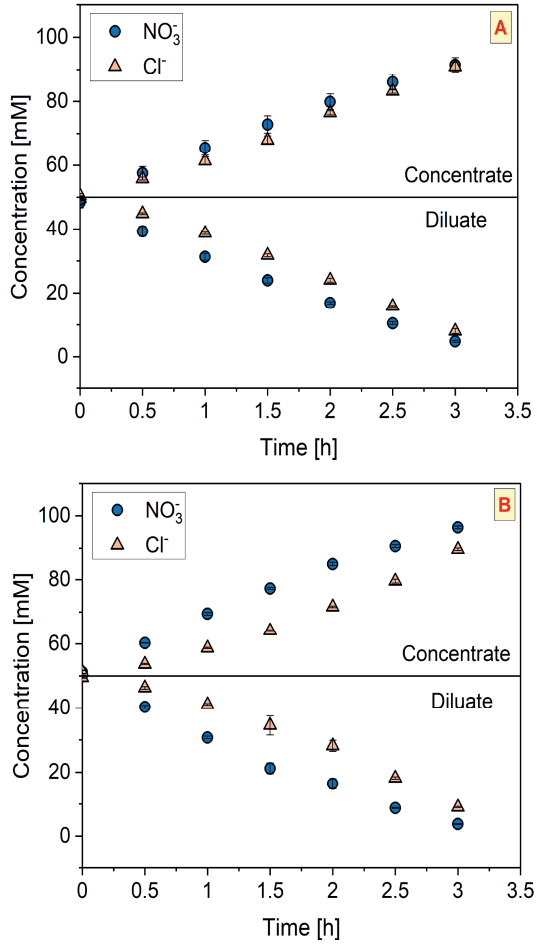

Figure S4.1: Concentration of the nitrate and chloride in the concentrate and diluate reservoir over time for AMX (A) and ACS (B). Experiments were conducted in triplicate.

References

(1) *World Population Prospects - Population Division - United Nations*. https://population.un.org/wpp/ (accessed 2023-08-10).

(2) Cui, H.; Luo, Y.; Li, C.; Chang, Y.; Jin, M.; Li, Y.; Wang, Z. Effects of Nitrogen Forms on Nitrogen Utilization, Yield, and Quality of Two Wheat Varieties with Different Gluten Characteristics. *European Journal of Agronomy* **2023**, *149*, 126919. https://doi.org/10.1016/j.eja.2023.126919.

(3) Carillo, P.; Rouphael, Y. Nitrate Uptake and Use Efficiency: Pros and Cons of Chloride Interference in the Vegetable Crops. *Front. Plant Sci.* **2022**, *13*, 899522. https://doi.org/10.3389/fpls.2022.899522.

(4) Kornijów, R. Eutrophication and Derivative Concepts. Origins, Compatibility and Unresolved Issues. *Ecohydrology & Hydrobiology* **2023**. https://doi.org/10.1016/j.ecohyd.2023.07.001.

(5) Liu, E.; Fan, C.; Zhao, M.; Jiang, S.; Wang, Z.; Jin, Z.; Bei, K.; Zheng, X.; Wu, S.; Zeng, Q. Effects of Heavy Metals on Denitrification Processes in Water Treatment: A Review. *Separation and Purification Technology* **2022**, *299*, 121793. https://doi.org/10.1016/j.seppur.2022.121793.

(6) Zhang, L.; Cui, B.; Yuan, B.; Zhang, A.; Feng, J.; Zhang, J.; Han, X.; Pan, L.; Li, L. Denitrification Mechanism and Artificial Neural Networks Modeling for Low-Pollution Water Purification Using a Denitrification Biological Filter Process. *Separation and Purification Technology* **2021**, *257*, 117918. https://doi.org/10.1016/j.seppur.2020.117918.

(7) Chinello, D.; Myrstad, A.; de Smet, L. C. P. M.; Miedema, H. Modelling the Required Membrane Selectivity for $NO3^-$ Recovery from Effluent Also Containing Cl^-, While Saving Water. *Chemical Engineering Research and Design* **2023**, *193*, 409–419. https://doi.org/10.1016/j.cherd.2023.03.038.

(8) van der Salm, C.; Voogt, W.; Beerling, E.; van Ruijven, J.; van Os, E. Minimising Emissions to Water Bodies from NW European Greenhouses; with Focus on Dutch Vegetable Cultivation. *Agricultural Water Management* **2020**, *242*, 106398. https://doi.org/10.1016/j.agwat.2020.106398.

(9) Luo, T.; Roghmans, F.; Wessling, M. Ion Mobility and Partition Determine the Counter-Ion Selectivity of Ion Exchange Membranes. *Journal of Membrane Science* **2020**, *597*, 117645. https://doi.org/10.1016/j.memsci.2019.117645.

(10) Pang, X.; Yu, X.; He, Y.; Dong, S.; Zhao, X.; Pan, J.; Zhang, R.; Liu, L. Preparation of Monovalent Cation Perm-Selective Membranes by Controlling Surface Hydration Energy Barrier. *Separation and Purification Technology* **2021**, *270*, 118768. https://doi.org/10.1016/j.seppur.2021.118768.

(11) Wang, W.; Zhang, Y.; Tan, M.; Xue, C.; Zhou, W.; Bao, H.; Hon Lau, C.; Yang, X.; Ma, J.; Shao, L. Recent Advances in Monovalent Ion Selective Membranes towards Environmental Remediation and Energy Harvesting. *Separation and Purification Technology* **2022**, *297*, 121520. https://doi.org/10.1016/j.seppur.2022.121520.

(12) Zhang, N.; Yu, H.; Zhang, J.; Jiang, X.; Yin, S.; Zhou, G.; Zhang, X.; Bao, J.; He, G. Pressure-Driven Li+/Mg2+ Selective Permeation through Size-Sieving Nanochannels: The Role of the Second Hydration Shell. *Separation and Purification Technology* **2023**, *327*, 124818. https://doi.org/10.1016/j.seppur.2023.124818.

(13) Tekinalp, Ö.; Zimmermann, P.; Burheim, O. S.; Deng, L. Designing Monovalent Selective Anion Exchange Membranes for the Simultaneous Separation of Chloride and Fluoride from Sulfate in an Equimolar Ternary Mixture. *Journal of Membrane Science* **2023**, *666*, 121148. https://doi.org/10.1016/j.memsci.2022.121148.

(14) Kikhavani, T.; Ashrafizadeh, S. N.; Van Der Bruggen, B. Nitrate Selectivity and Transport Properties of a Novel Anion Exchange Membrane in Electrodialysis. *Electrochimica Acta* **2014**, *144*, 341–351. https://doi.org/10.1016/j.electacta.2014.08.012.

(15) Mubita, T.; Porada, S.; Aerts, P.; van der Wal, A. Heterogeneous Anion Exchange Membranes with Nitrate Selectivity and Low Electrical Resistance. *Journal of Membrane Science* **2020**, *607*, 118000. https://doi.org/10.1016/j.memsci.2020.118000.

(16) Qian, Z.; Miedema, H.; Sahin, S.; de Smet, L. C. P. M.; Sudhölter, E. J. R. Separation of Alkali Metal Cations by a Supported Liquid Membrane (SLM) Operating under Electro Dialysis (ED) Conditions. *Desalination* **2020**, *495*. https://doi.org/10.1016/j.desal.2020.114631.

(17) Qian, Z.; Miedema, H.; de Smet, L. C. P. M.; Sudhölter, E. J. R. Permeation Selectivity in the Electro-Dialysis of Mono- and Divalent Cations Using Supported Liquid Membranes. *Desalination* **2022**, *521*. https://doi.org/10.1016/j.desal.2021.115398.

(18) Wang, Y.; Zhang, W.; Zeng, X.; Deng, T.; Wang, J. Membranes for Separation of Alkali/Alkaline Earth Metal Ions: A Review. *Separation and Purification Technology* **2021**, *278*, 119640. https://doi.org/10.1016/j.seppur.2021.119640.

(19) Epsztein, R.; Shaulsky, E.; Qin, M.; Elimelech, M. Activation Behavior for Ion Permeation in Ion-Exchange Membranes: Role of Ion Dehydration in Selective Transport. *Journal of Membrane Science* **2019**, *580* (January), 316–326. https://doi.org/10.1016/j.memsci.2019.02.009.

(20) Tekinalp, Ö.; Zimmermann, P.; Holdcroft, S.; Burheim, O. S.; Deng, L. Cation Exchange Membranes and Process Optimizations in Electrodialysis for Selective Metal Separation: A Review. *Membranes* **2023**, *13* (6), 566. https://doi.org/10.3390/membranes13060566.

(21) Cheng, Y.; Dong, Y.; Huang, Q.; Huang, K.; Lyu, S.; Chen, Y.; Duan, J.; Mo, D.; Sun, Y.; Liu, J.; Peng, Y.; Yao, H. Ionic Transport and Sieving Properties of Sub-Nanoporous Polymer Membranes with Tunable Channel Size. *ACS Appl. Mater. Interfaces* **2021**, *13* (7), 9015–9026. https://doi.org/10.1021/acsami.0c22689.

(22) Sata, T. Studies on Anion Exchange Membranes Having Permselectivity for Specific Anions in Electrodialysis - Effect of Hydrophilicity of Anion Exchange Membranes on Permselectivity of Anions. *Journal of Membrane Science* **2000**, *167* (1), 1–31. https://doi.org/10.1016/S0376-7388(99)00277-X.

(23) Higa, M.; Tanaka, N.; Nagase, M.; Yutani, K.; Kameyama, T.; Takamura, K.; Kakihana, Y. Electrodialytic Properties of Aromatic and Aliphatic Type Hydrocarbon-Based Anion-Exchange Membranes with Various Anion-Exchange Groups. *Polymer* **2014**, *55* (16), 3951–3960. https://doi.org/10.1016/j.polymer.2014.06.072.

(24) Lin, C. X.; Huang, X. L.; Guo, D.; Zhang, Q. G.; Zhu, A. M.; Ye, M. L.; Liu, Q. L. Side-Chain-Type Anion Exchange Membranes Bearing Pendant Quaternary Ammonium Groups via Flexible Spacers for Fuel Cells. *J. Mater. Chem. A* **2016**, *4* (36), 13938–13948. https://doi.org/10.1039/C6TA05090E.

(25) Chang, K.; Xue, T.; Geise, G. M. Increasing Salt Size Selectivity in Low Water Content Polymers via Polymer Backbone Dynamics. *Journal of Membrane Science* **2018**, *552*, 43–50. https://doi.org/10.1016/j.memsci.2018.01.057.

(26) Irfan, M.; Ge, L.; Wang, Y.; Yang, Z.; Xu, T. Hydrophobic Side Chains Impart Anion Exchange Membranes with High Monovalent–Divalent Anion Selectivity in Electrodialysis. *ACS Sustainable Chem. Eng.* **2019**, *7* (4), 4429–4442. https://doi.org/10.1021/acssuschemeng.8b06426.

(27) Luo, T.; Abdu, S.; Wessling, M. Selectivity of Ion Exchange Membranes: A Review. *Journal of Membrane Science* **2018**, *555* (December 2017), 429–454. https://doi.org/10.1016/j.memsci.2018.03.051.

(28) Zhang, D.; Jiang, C.; Li, Y.; Shehzad, M. A.; Wang, X.; Wang, Y.; Xu, T. Electro-Driven in Situ Construction of Functional Layer Using Amphoteric Molecule: The Role of Tryptophan in Ion Sieving. *ACS Appl. Mater. Interfaces* **2019**, *11* (40), 36626–36637. https://doi.org/10.1021/acsami.9b11163.

(29) Sarkar, S.; Patnaik, P.; Mondal, R.; Chatterjee, U. Cross-Linked, Monovalent Selective Anion Exchange Membrane: Effect of Prealkylation and Co-Ions on Selectivity. *ACS Appl. Polym. Mater.* **2023**, *5* (3), 1977–1988. https://doi.org/10.1021/acsapm.2c02045.

(30) Zhao, Y.; Zhu, J.; Li, J.; Zhao, Z.; Charchalac Ochoa, S. I.; Shen, J.; Gao, C.; Van der Bruggen, B. Robust Multilayer Graphene–Organic Frameworks for Selective Separation of Monovalent Anions. *ACS Appl. Mater. Interfaces* **2018**, *10* (21), 18426–18433. https://doi.org/10.1021/acsami.8b03839.

(31) Zhao, Y.; Mamrol, N.; Tarpeh, W. A.; Yang, X.; Gao, C.; Van der Bruggen, B. Advanced Ion Transfer Materials in Electro-Driven Membrane Processes for Sustainable Ion-Resource Extraction and Recovery. *Progress in Materials Science* **2022**, *128*, 100958. https://doi.org/10.1016/j.pmatsci.2022.100958.

(32) Xiao, X.; Shehzad, M. A.; Yasmin, A.; Ge, Z.; Liang, X.; Sheng, F.; Ji, W.; Ge, X.; Wu, L.; Xu, T. Anion Permselective Membranes with Chemically-Bound Carboxylic Polymer Layer for Fast Anion Separation. *Journal of Membrane Science* **2020**, *614*, 118553. https://doi.org/10.1016/j.memsci.2020.118553.

(33) Chinello, D.; Post, J.; de Smet, L. C. P. M. Selective Separation of Nitrate from Chloride Using PVDF-Based Anion-Exchange Membranes. *Desalination* **2024**, *572*, 117084. https://doi.org/10.1016/j.desal.2023.117084.

(34) Zhang, Y.; Paepen, S.; Pinoy, L.; Meesschaert, B.; Van der Bruggen, B. Selectrodialysis: Fractionation of Divalent Ions from Monovalent Ions in a Novel Electrodialysis Stack. *Separation and Purification Technology* **2012**, *88*, 191–201. https://doi.org/10.1016/j.seppur.2011.12.017.

(35) Galama, A. H.; Daubaras, G.; Burheim, O. S.; Rijnaarts, H. H. M.; Post, J. W. Fractioning Electrodialysis: A Current Induced Ion Exchange Process. *Electrochimica Acta* **2014**, *136*, 257–265. https://doi.org/10.1016/j.electacta.2014.05.104.

(36) Jiang, C.; Chen, B.; Xu, Z.; Li, X.; Wang, Y.; Ge, L.; Xu, T. Ion-"Distillation" for Isolating Lithium from Lake Brine. *AIChE Journal* **2022**, *68* (6), e17710. https://doi.org/10.1002/aic.17710.

(37) Zhao, W.; Yan, B.; Ren, Z. J.; Wang, S.; Zhang, Y.; Jiang, H. Highly Selective Butyric Acid Production by Coupled Acidogenesis and Ion Substitution Electrodialysis. *Water Research* **2022**, *226*, 119228. https://doi.org/10.1016/j.watres.2022.119228.

(38) Zhang, Y.; Chen, Y.; Yue, M.; Ji, W. Recovery of L-Lysine from L-Lysine Monohydrochloride by Ion Substitution Using Ion-Exchange Membrane. *Desalination* **2011**, *271* (1), 163–168. https://doi.org/10.1016/j.desal.2010.12.016.

(39) Nightingale, E. R. Phenomenological Theory of Ion Solvation. Effective Radii of Hydrated Ions. *J. Phys. Chem.* **1959**, *63* (9), 1381–1387. https://doi.org/10.1021/j150579a011.

(40) Dlugolecki, P.; Nymeijer, K.; Metz, S.; Wessling, M. Current Status of Ion Exchange Membranes for Power Generation from Salinity Gradients. *Journal of Membrane Science* **2008**, *319* (1–2), 214–222. https://doi.org/10.1016/j.memsci.2008.03.037.

(41) Mubita, T. M.; Porada, S.; Biesheuvel, P. M.; van der Wal, A.; Dykstra, J. E. Strategies to Increase Ion Selectivity in Electrodialysis. *Separation and Purification Technology* **2022**, *292*, 120944. https://doi.org/10.1016/j.seppur.2022.120944.

(42) Chen, Q.-B.; Ji, Z.-Y.; Liu, J.; Zhao, Y.-Y.; Wang, S.-Z.; Yuan, J.-S. Development of Recovering Lithium from Brines by Selective-Electrodialysis: Effect of Coexisting Cations on the Migration of Lithium. *Journal of Membrane Science* **2018**, *548*, 408–420. https://doi.org/10.1016/j.memsci.2017.11.040.

(43) Pintossi, D.; Chen, C.-L.; Saakes, M.; Nijmeijer, K.; Borneman, Z. Influence of Sulfate on Anion Exchange Membranes in Reverse Electrodialysis. *npj Clean Water* **2020**, *3* (1), 29. https://doi.org/10.1038/s41545-020-0073-7.

(44) Sosa-Fernández, P. A.; Post, J. W.; Nabaala, H. L.; Bruning, H.; Rijnaarts, H. Experimental Evaluation of Anion Exchange Membranes for the Desalination of (Waste) Water Produced after Polymer-Flooding. *Membranes* **2020**, *10* (11), 352. https://doi.org/10.3390/membranes10110352.

(45) Kingsbury, R. S.; Bruning, K.; Zhu, S.; Flotron, S.; Miller, C. T.; Coronell, O. Influence of Water Uptake, Charge, Manning Parameter, and Contact Angle on Water and Salt Transport in Commercial Ion Exchange Membranes. *Ind. Eng. Chem. Res.* **2019**, *58* (40), 18663–18674. https://doi.org/10.1021/acs.iecr.9b04113.

(46) Sriram, G.; Dhanabalan, K.; Ajeya, K. V.; Aruchamy, K.; Ching, Y. C.; Oh, T. H.; Jung, H.-Y.; Kurkuri, M. Recent Progress in Anion Exchange Membranes (AEMs) in Water Electrolysis: Synthesis, Physio-Chemical Analysis, Properties, and Applications. *J. Mater. Chem. A* **2023**, *11* (39), 20886–21008. https://doi.org/10.1039/D3TA04298G.

(47) Güler, E.; Van Baak, W.; Saakes, M.; Nijmeijer, K. Monovalent-Ion-Selective Membranes for Reverse Electrodialysis. *Journal of Membrane Science* **2014**, *455*, 254–270. https://doi.org/10.1016/j.memsci.2013.12.054.

(48) Mareev, S. A.; Butylskii, D. Yu.; Pismenskaya, N. D.; Larchet, C.; Dammak, L.; Nikonenko, V. V. Geometric Heterogeneity of Homogeneous Ion-Exchange Neosepta Membranes. *Journal of Membrane Science* **2018**, *563*, 768–776. https://doi.org/10.1016/j.memsci.2018.06.018.

(49) Długołęcki, P.; Ogonowski, P.; Metz, S. J.; Saakes, M.; Nijmeijer, K.; Wessling, M. On the Resistances of Membrane, Diffusion Boundary Layer and Double Layer in Ion Exchange Membrane Transport. *Journal of Membrane Science* **2010**, *349* (1–2), 369–379. https://doi.org/10.1016/j.memsci.2009.11.069.

(50) Wang, W.; Liu, R.; Tan, M.; Sun, H.; Niu, Q. J.; Xu, T.; Nikonenko, V.; Zhang, Y. Evaluation of the Ideal Selectivity and the Performance of Selectrodialysis by Using TFC Ion Exchange Membranes. *Journal of Membrane Science* **2019**, *582*, 236–245. https://doi.org/10.1016/j.memsci.2019.04.007.

(51) Luo, H.; Agata, W.-A. S.; Geise, G. M. Connecting the Ion Separation Factor to the Sorption and Diffusion Selectivity of Ion Exchange Membranes. *Ind. Eng. Chem. Res.* **2020**, *59* (32), 14189–14206. https://doi.org/10.1021/acs.iecr.0c02457.

(52) Biesheuvel, P. M.; Porada, S.; Elimelech, M.; Dykstra, J. E. Tutorial Review of Reverse Osmosis and Electrodialysis. *Journal of Membrane Science* **2022**, *647*, 120221. https://doi.org/10.1016/j.memsci.2021.120221.

(53) Hawks, S. A.; Cerón, M. R.; Oyarzun, D. I.; Pham, T. A.; Zhan, C.; Loeb, C. K.; Mew, D.; Deinhart, A.; Wood, B. C.; Santiago, J. G.; Stadermann, M.; Campbell, P. G. Using Ultramicroporous Carbon for the Selective Removal of Nitrate with Capacitive Deionization. *Environmental Science & Technology* **2019**. https://doi.org/10.1021/acs.est.9b01374.

(54) Qian, Z.; Miedema, H.; de Smet, L. C. P. M.; Sudhölter, E. J. R. Modelling the Selective Removal of Sodium Ions from Greenhouse Irrigation Water Using Membrane Technology. *Chemical Engineering Research and Design* **2018**, *134*, 154–161. https://doi.org/10.1016/j.cherd.2018.03.040.

Chapter 5

Effect of polymeric matrix in anion-exchange membranes on nitrate/chloride separation

This chapter has been published as:
Chinello, D.; Post, J.; de Smet, L. C. P. M. Effect of polymeric matrix in anion-exchange membranes on nitrate-chloride separations. *Separation and Purification Technology* **2025**, *355*, 129440

Abstract

Selective separation of monovalent ions such as nitrate from chloride using Anion-Exchange Membranes (AEMs) is challenging. Previously, we showed that an increased polyvinylidene fluoride (PVDF) concentration in AEMs manufactured with an anion-exchange ionomer solution (Fumion FAS-24) increased nitrate over chloride selectivity. The membrane containing 50 wt% of PVDF showed higher selectivity compared to two commercial membranes (AMX and ACS from Neosepta) when tested in electrodialysis. This improved selectivity was associated with increased hydrophobicity of the membrane, facilitating the permeation of less hydrated ions such as nitrate.

However, due to concerns regarding per- and polyfluoroalkyl substances (PFAS), there is a quest for substitutes for fluoropolymers. In this study, we investigated whether using alternative polymers to PVDF influences nitrate/chloride separation performance. Polyvinyl chloride (PVC) and polyacrylonitrile (PAN) were blended with Fumion FAS-24 to manufacture new AEMs. The nitrate/chloride selective separation performance of these membranes was tested in electrodialysis and compared with the recently introduced PVDF-based AEM.

Results show that although the PVDF-based membrane presents higher hydrophobicity, the PAN-based membrane possesses slightly lower selectivity, while the PVC-based membrane exhibits higher nitrate selectivity. This study proves that increasing the membrane hydrophobicity is a valid strategy to increase selectivity toward nitrate. However, it also suggests that other parameters, such as fixed charge concentration, can play a role. Therefore, balancing properties such as hydrophobicity and fixed charge concentration is imperative to achieving optimal selectivity and performance when developing ion-selective membranes.

5.1. Introduction

Ion-exchange membranes (IEMs) have considerable importance in membrane-based technology such as electrodialysis (ED),[1–3] capacitive deionization,[4–6] and fuel cells.[7,8] These membranes are made from polymer materials and contain charged moieties. Depending on the type of charge of these groups, IEMs can be categorized into two main types: Anion-Exchange Membranes (AEMs) and Cation-Exchange Membranes (CEMs). AEMs feature fixed cations such as quaternary ammonium groups, and allow the permeance of anions while impeding cations. In contrast, CEMs possess anionic moieties like sulfonic groups, allowing the permeation of cations while hindering anions.

IEMs find extensive use in various separation technologies, such as desalination,[9–11] and in this study we focus on AEMs for the application of electrodialysis (ED). AEMs have already proved to be effective in the separation of monovalent from divalent ions.[12] However, the separation of two monovalent ions poses a larger challenge, especially if these ions present similar hydrated radius and hydration energy, such as nitrate and chloride (**Table 5.1**). Developing membranes possessing high monovalent/monovalent selectivity is crucial in applications such as the recovery and recycling of important resources like nitrate from, *e.g.*, waste/process water streams in fertilizer plants[13] and horticulture,[14] with the overarching aim of achieving a circular economy.

In order to increase the membrane's ability to discriminate between ions bearing the same valence, previous studies[15–18] focused on leveraging the difference in the ion dehydration. Ions with lower dehydration energy, such as nitrate (**Table 5.1**), are more favourable transported through the AEMs due to an easier (partial) dehydration at the membrane surface.[19–22] In particular, these mostly e-driven separation studies indicate that an increased membrane hydrophobicity triggers the dehydration of ions with lower dehydration energy, while more hydrated ions are hindered by the hydrophobic structure.

Furthermore, the strength of the interaction between the dehydrated ion and the charged groups within the membrane is a determining factor in the dehydration process. A stronger interaction has been observed to reduce the associated energy barrier, since it leads to an energetically more favorable state of the ion.[23,24] However, this electrostatic interaction also influences the ion's mobility. Specifically, the stronger the interaction, the slower the transportation.[23,24]

Building further on these findings, we studied, in previous research,[25] the transport of nitrate and chloride using newly developed PVDF-based AEMs, manufactured in combination with an anion-exchange ionomer solution (Fumion FAS-24, FUMATECH BWT GmbH). PVDF was chosen for its intrinsic hydrophobic nature and its wide application in membrane technology such as membrane distillation,[26–32] dye removal from water streams using nanofiltration,[33–35] oil-water separation,[36,37] organic pollutant removal,[38,39] selective ion separation,[40–46] and removal of toxic metal ions from aqueous streams.[47,48] PVDF has also been used in selective ion-separation applications, such as fabricating electrodes for capacitive deionization (CDI) to separate divalent from monovalent cations.[40–42] Additionally, it has also been used in manufacturing AEM sfor example in combination with cross-linked quaternized polyepichlorohydrin for selective hydroxide ion transport in fuel cells,[49] and with styrene-co-vinylbenzyl chloride for water desalination in ED.[50] Furthermore, PVDF has been combined with morpholine-functionalized vinyl benzyl chloride for acid recovery by diffusion dialysis[51] and with polyaniline for desalination in ED and CDI. However, the use of PVDF for manufacturing membranes specifically designed for the selective separation of monovalent ions like nitrate and chloride has not been documented in the literature, except in our previous studies (**Chapters 3** and **4**).[25,52]

In those studies, our focus was on investigating the influence of different PVDF content levels in the membranes, ranging from 0 to 50 wt%. The outcomes of that work revealed an improved nitrate affinity with increasing PVDF concentration, and thus membrane hydrophobicity, with the membrane containing 50 wt% PVDF reporting the highest nitrate permeability (**Chapter 3**).[25] However, by increasing the PVDF content, we also noted an increase in the membrane's electrical resistance, and for this reason, we decided not to exceed 50 wt% of PVDF.

The performance of this membrane was then investigated in ED (**Chapter 4**).[52] Experimental data showed higher values of the nitrate over chloride selectivity compared with two commercial membranes (AMX and ACS from Neosepta), the highest reported in literature.

However, considering that Per- and polyFluoroAlkyl Substances (PFAS) pose a significant environmental and health concern due to their persistent nature and widespread contamination,[53–55] alternatives for fluoropolymers become imperative to mitigate the adverse

effects of PFAS exposure, safeguard human health,[56,57] and reduce the long-term environmental impact associated with these persistent chemicals.

For this reason, we decided to now investigate the impact of the type of the polymer used in combination with the ionomer solution Fumion FAS-24 to manufacture new AEMs. Specifically, we opted for polyvinyl chloride (PVC) and polyacrylonitrile (PAN) as alternatives to PVDF. PVC was selected for its presence in commercial membranes as reinforcement material, solubility in N-methyl-2-pyrrolidone (NMP), the solvent of the ionomer solution, and cost-effectiveness,[58,59] making it an attractive alternative for large-scale applications where cost efficiency is crucial. PVC has already been used in the manufacturing of membranes,[60] including AEMs.[61] For example, Nemati *et al.*[62] modified the properties of PVC-AEMs by incorporating TiO_2 nanoparticles (0-4 wt%) to improve the anion permeation efficiency and tested them in ED. The study reported improved permeation of chloride and sulfate in the TiO_2 concentration interval of 0.5-2 wt%. Liu *et al.*[63] used PVC to manufacture films by casting, which were then modified by immersing these films in a solution of triethylenetetramine, obtaining AEMs. These AEMs showed good stability and antifouling potential. Moreover, when applied in ED, the optimized PVC-AEM demonstrated a NaCl removal ratio of 90%, outperforming a commercial membrane (JAM-II-5 AEM). Recently, Zafari *et al.*[64] prepared heterogeneous AEMs by combining PVC and an anion-exchange resin (Amberlite IRA-410). The surface of these membranes was subsequently modified through a three-step process, including plasma treatment and coupling with polyethylenimine and glutaraldehyde. By changing the surface hydrophilicity of the membranes, they increased the membrane selectivity towards formate ($CHOO^-$) over oxalate ($C_2O_4^{2-}$) — exploiting the lower hydration energy of the former — reaching a selectivity value of 4.3 in ED.

PAN was also chosen for its solubility in NMP, and for its potential for further modification of the nitrile groups.[65–67] The characteristics of these new membranes together with the nitrate/chloride separation performance in ED are evaluated in this study and compared with the previously introduced PVDF-membrane.

Table 5.1: Ionic radii, hydrated radii and hydration energies of nitrate, and chloride.[68]

Anion	Ionic radius [nm]	Hydrated radius [nm]	Hydration energy [kcal·mol^{-1}]
Nitrate (NO_3^-)	0.264	0.335	71
Chloride (Cl^-)	0.181	0.332	81

5.2. Materials and methods

5.2.1. Chemicals

Polyvinyl chloride (average M_w~233,000 by GPC, powder form) (PVC), polyacrylonitrile (PAN) (average M_w~150,000 by GPC, powder form), sodium chloride (ACS reagent, ≥99.0%), sodium nitrate (ACS reagent, ≥99.0%), sodium sulphate (ACS reagent, ≥99.0%, anhydrous), were purchased from Sigma Aldrich and used as received. N-methyl-2-pyrrolidone (NMP, HPLC grade 99.5%) was purchased from Alfa Aesar. Fumion FAS (24 wt% solution in NMP), which physicochemical properties are reported in **Table S5.1** of the Supporting Information, was purchased from FUMATECH BWT GmbH, Bietigheim-Bissingen, Germany. The Neosepta AMX, ACS and CMX membranes were purchased from ASTOM Corporation, Tokyo, Japan. The physicochemical properties of these commercial membranes are reported in **Table S5.2** of the Supporting Information.

5.2.2. Membrane fabrication

The AEMs were manufactured following the procedure reported in our previous study.[25] Each membrane is composed of 50 wt% of ionomer (Fumion FAS-24) and 50 wt% of the selected polymer (PVC or PAN). This ratio was selected in order to enable direct comparison with the PVDF-based membrane composed of 50 wt% of ionomer and 50 wt% of PVDF, labelled as PVDF-50, investigated in our previous studies (**Chapters 3** and **4**).[25,52] Specifically, 0.75 g of ionomer were mixed with 0.75 g of PVC or PAN. NMP was used as solvent to dissolve the polymers, obtaining solutions with a concentration of 16 wt%. The solvent was removed by casting the solutions onto

a glass plate kept at 60 °C for 24 hours. To completely remove the solvent, the obtained membranes were immersed in 0.5 M NaCl, refreshing the solution every 2 hours (5 ×). During this phase, the thickness of the wet membranes was measured using a digital thickness gauge (Mitutoyo Corporation, model no. ID-C112BS). The membranes were stored in 0.5 M NaCl and labelled as PVC-50 and PAN-50, where the number indicates the weight percentage of polymer, PVC or PAN, present in the membrane. Selected characteristics, together with those of the previously introduced PVDF-membrane, labelled PVDF-50, are reported in **Table 5.2**.

5.3. Membrane characterization

5.3.1. Water uptake (*WU*)

To assess water uptake (*WU*), we followed the methodology outlined in our previous work.[25] After immersing the membrane in demineralized water for 24 hours, the mass of the wet membrane was recorded after removing any surface water with a tissue. Subsequently, the membrane was dried in an oven maintained at 55 °C for 24 hours. The mass of the resulting dry membrane (W_{dry}, in grams) was then recorded. The water uptake (*WU*) was calculated as a percentage by:

$$WU = 100 \times \frac{W_{wet} - W_{dry}}{W_{dry}} \ \% \qquad (5.1)$$

5.3.2. Ion-exchange capacity (IEC)

The quantity of fixed charged groups within an AEMs can be determined indirectly by measuring the concentration of counter-ions exchanged with a specific solution. In particular, following a 48 hours conditioning period in 0.5 M NaCl, the selected membrane was immersed in the exchange solution (200 mL of 0.5 M $NaNO_3$) after a rapid immersion in demineralized water to eliminate the excess of NaCl solution. After a 24-hour exchange duration, the chloride concentration in the solution was assessed through ion chromatography (IC), using a Metrohm Compact IC 761 equipped with a conductivity detector and chemical suppression.

The ion-exchange capacity (*IEC*) of the membrane, expressed in milliequivalents per gram ($meq \cdot g^{-1}$), was then calculated according to the following equation:[69]

$$IEC = \frac{n_{\mathrm{eq}}}{W_{\mathrm{dry}}} \tag{5.2}$$

where n_{eq} denotes the equivalent of exchanged ions in equivalents (eq), and W_{dry} (g) represents the dry mass of the membrane.

5.3.3. Fixed charge concentration (*FCC*)

By using the values of the *IEC* and *WU*, it is possible to calculate the fixed charge concentration (*FCC*) of the hydrated membranes, which refers to the density of charged groups expressed in terms of moles per volume of adsorbed water (mol·L^{-1}). The *FCC* was calculated according to the following equation:[70]

$$FCC = \frac{IEC}{WU/100} \times \rho_W \tag{5.3}$$

where ρ_w is the density of the water in the membrane, typically assumed to be equivalent to the density of pure water.[70]

5.3.4. Electrical resistance

The electrical resistance of the manufactured IEMs was evaluated according to the protocol established by Galama *et al*.,[71] by using a six-compartment cell as schematically outlined in **Figure S5.1** in the Supporting Information. The membrane configuration in the setup consists of four CEMs, specifically CMX from Neosepta, while the AEM under investigation separates compartments A and B. An electrolyte solution such as 0.5 M NaCl was recirculated in compartments A, B, and C at 170 mL·min^{-1}, while in compartment D, 0.5 M Na_2SO_4 was used. A potentiostat (Autolab AUT72398, Metrohm) with a four-electrode configuration was used to apply a current between the two Pt/Ir electrodes situated in compartments D. The potential across the membrane was recorded by using two Haber–Luggin capillaries (outer diameter 4.0 mm, inner diameter 2.0 mm) placed on the side of the membrane under investigation and connected to Ag/AgCl electrodes.

Specifically, the current (*I*) is increased gradually from 1 to 25 mA. For each value, the current is applied for 2 minutes to equilibrate the system, with the potential (*V*) recorded during the final 8 seconds. Iterating this process across all current values results in a potential/current graph. The

angular coefficient of the extrapolated equation obtained from the data interpolation in the graph represents the electrical resistance (R) of the membrane (Ω) according to Ohm's law:

$$V = R \times I \tag{5.4}$$

However, this value also includes the electrical resistance generated by the 0.5 M NaCl electrolyte solution. Therefore, by removing the membrane under investigation between compartments A and B, it is possible to determine this contribution (R_s), which is then subtracted from the one obtained in the experiment involving the membrane. This process yields the specific electrical resistance of the membrane (R_m):

$$R_m = R - R_s \tag{5.5}$$

This value was then multiplied for the membrane's active area to obtain the membrane area resistance ($\Omega \cdot cm^2$).

5.3.5. Contact angle

In order to evaluate the surface hydrophobicity, contact angles were measured through the captive bubble method. In this method, an air bubble (1 µL) is introduced beneath the membrane surface immersed in water, using a needle with a hook-like shape. The contact angles were then determined by analyzing the shape of the bubble at the membrane surface interface, using a contour analysis system (OCA35, DataPhysics Instruments, Germany). For each membrane, six drops at different locations were analyzed.

5.3.6. SEM-EDX

The surface morphology of the three membranes was examined through scanning electron microscopy (SEM) employing a JEOL JSM-6480LV electron microscope at 10 kV acceleration. Additionally, to evaluate the polymer distribution within the membranes, the elemental distribution of fluorine, chlorine, and nitrogen, was examined respectively for the PVDF-50, PVC-50, and PAN-50 membranes using an energy-dispersive X-ray spectrometer (EDX).

5.4. Membrane performance

5.4.1. Permselectivity

The permselectivity refers to the ability of a membrane to selectively allow counter-ion while hindering co-ions. Following the procedure of Duglokecki *et al.,*[69] the permselectivity of the manufacture AEMs was assessed in a two-compartment cell made of poly(methyl 2-methylpropenoate) (PMMA), with a total solution volume of 0.2 L. Specifically, the potential across the membrane separating two electrolyte solutions (0.1 M and 0.5 M NaCl respectively) recirculating at a flow rate of 750 mL·min^{-1} was recorded using Ag/AgCl electrodes immersed in the solution. Subsequently, the membrane permselectivity (α), expressed as a percentage, was calculated using the following equation:

$$a = 100 \times \frac{\Delta V_{\text{measured}}}{\Delta V_{\text{theoretical}}} \quad (5.6)$$

where $\Delta V_{\text{theoretical}}$ is the theoretical Nernst membrane potential for a membrane 100% selective towards counter-ions.

5.4.2. Permeability coefficients ratio

The permeability coefficients ratio serves as a measure of the affinity between a membrane and two distinct counter-ions, providing a quick indication of the membrane selectivity. The experimental setup employed to determine this parameter mirrors that used for the permselectivity experiments. However, while on one side of the membrane a 0.1 M NaCl solution is still used, on the other side a 0.1 M $NaNO_3$ solution is present now. The potential across the membrane was continuously monitored for a duration of 40 minutes using a Ag/AgCl electrodes. For the calculation, the averaged potential ($\Delta\Psi$) obtained after reaching steady-state conditions, approximately 10 minutes into the experiment, was utilized. The permeability coefficient ratio was determined using the following equation:[25,72]

$$\frac{P_{\text{NO}_3^-}}{P_{\text{Cl}^-}} = e^{\frac{F\Delta\Psi}{RT}} \quad (5.7)$$

where *F* is the Faraday constant (96,458 A·s·mol^{-1}), *R* is the universal gas constant (8.314 J·mol^{-1}·K^{-1}), *T* is the absolute temperature (K), and $P_{NO_3^-}$ and P_{Cl^-} are the permeability coefficients of the counterions.

5.4.3. Electrodialysis experiments

In order to assess the performance of the manufactured AEMs in electrodialysis (ED) and thus determine the nitrate over chloride selectivity, the experimental setup and procedure reported in our previous work were used.[52] The membrane configuration of the ED setup is reported in **Figure 5.1**, and consists of a total of five IEMs; three cation-exchange membranes (CMX from Neosepta) are alternated with two of the manufactured AEMs (PVC-50, or PAN-50), resulting in two cell pairs. Each membrane is separated from the adjacent one by a gasket with an integrated spacer, which has a thickness of 0.5 mm, and the available membrane area for ion transport is 20 cm^2.

Two platinum-coated titanium mesh electrodes are present in the setup, with a solution of 1 L of 0.1 M Na_2SO_4 recirculating in these compartments. In the outlets of the electrode compartments, two Ag/AgCl electrodes are placed to measure the potential across the five membranes.

The experiments are carried out in batch mode with a current density set at 20 A·m^{-2}, employing a potentiostat (Autolab AUT72157, Metrohm) as the current source. Experiments were conducted in triplicate for each membrane, with a duration of 3 hours, corresponding to a theoretical anion removal of 90 %. The initial composition of the electrolyte solutions in the two reservoirs is 0.1 L of 0.05 M $NaNO_3$ and 0.05 M of NaCl.

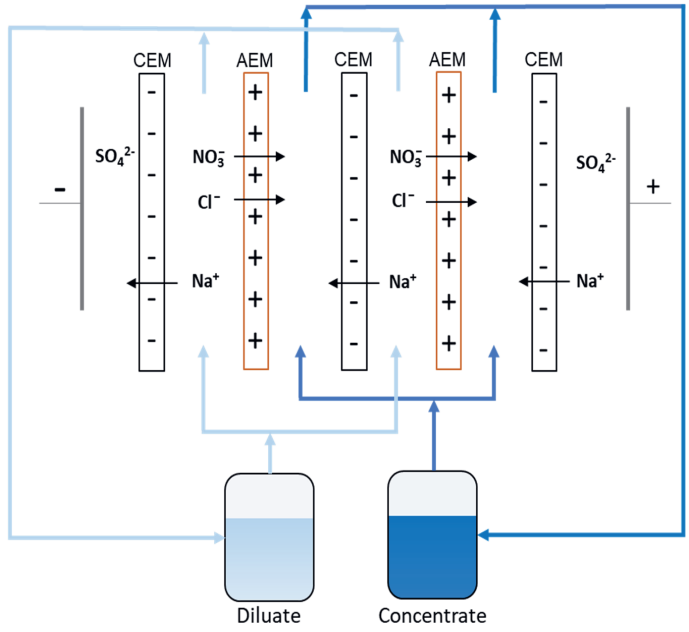

Figure 5.1: Schematic representation of the ED setup used to determine the nitrate over chloride selectivity of the manufactured PVC-50 and PAN-50 AEMs. See **Section 5.4.3** for a detailed explanation of the system. Light and dark blue stand for diluate and concentrate stream, respectively.

Samples from the diluate and the concentrate reservoirs were taken at intervals of 30 min and analysed by ion chromatography (IC) to determine the ion concentrations. The values obtained were used to assess the nitrate over chloride selectivity ($S_{Cl^-}^{NO_3^-}$) over time, employing the equation reported in a previous contribution in literature:[16,25,52]

$$S_{Cl^-}^{NO_3^-} = \left(\frac{\Delta C_{NO_3^-}}{\Delta C_{Cl^-}}\right)_{Concentrate} \times \left(\frac{C_{Cl^-}}{C_{NO_3^-}}\right)_{Diluate} \quad (5.8)$$

where $\Delta C_{NO_3^-}$ and ΔC_{Cl^-} refer to the change of the concentration of the indicated ion in the concentrate reservoir between two samples, while $C_{NO_3^-}$ and C_{Cl^-} represent the concentration of the ions in the diluate compartment. Theoretically, the concentration of nitrate and chloride in the diluate compartment to be used should ideally be the one at the membrane surface[21]. However, it is commonly accepted in literature to approximate these concentrations to the concentration in the bulk solution.[73,74] Therefore, at high degree of desalination this equation

might present limitations due to the presence of the concentration polarization effect.[75] However, in order to allow a direct comparison of our results with those reported in literature, concentration polarization effects are neglected and the concentrations of the ions are approximated to those in the bulk throughout the entire ED process.

Another relevant parameter from an application point of view is the recovery ratio (R_i), which for an ion (i) is calculated according to the equation reported by Chen *et al.*:[76]

$$R_i = \frac{V_{ct}(C_{ct} - C_{c0})}{V_{d0}C_{d0}} \times 100 \quad (5.9)$$

Here, C_{ct}, C_{c0} and C_{d0} represent the concentrations of the ion at time t and 0, respectively, in the concentrate and dilute streams. Similarly, V_{ct} and V_{d0} denote the volumes in the concentrate and dilute at time t and 0, respectively.

The coulombic efficiency (η) of the experiments was calculated according to the equation:

$$\eta = (J_i + J_j)\frac{F}{i} \quad (5.10)$$

where F is the Faraday constant (96,458 A·s·mol^{-1}), i is the current density applied (A·m^{-2}), and J_i and J_j are the ionic fluxes, expressed in mol·m^{-2}·s^{-1}, across the membranes for the two counter-ions, which, for a monovalent ion (i), is defined by the following equation:

$$J_i = \frac{V}{A} \times \frac{\Delta C_i}{\Delta t} \quad (5.11)$$

where V (m^3) and ΔC_i (mol·L^{-1}) are respectively the volume and the variation of the ion concentration in the concentrate stream, A (m^2) is the surface membrane area, and Δt (s) is the time of the experiments.

Lastly, the energy consumption (E) was measured according to our previous work[52] in kilojoules per gram of nitrate recovered, using the following equation

$$E = \frac{\Delta V_{stack} \cdot i \cdot A \cdot \Delta t}{\Delta n_{NO_3^-} \cdot MW_{NO_3^-}} \quad (5.12)$$

where ΔV_{stack} represents the average stack potential (V), i is the applied current density (A·m^{-2}), A is the membrane surface area (m²), Δt denotes the duration of the experiments (s), $\Delta n_{NO_3^-}$ is

the change in moles of nitrate in the concentrate stream, and $MW_{NO_3^-}$ is the molecular weight of nitrate (g·mol^{-1}).

5.5. Results and discussion

5.5.1. Membrane characterization

5.5.1.1. Membrane preparation

Two membranes were successfully manufactured via casting by mixing the selected polymer (PVC or PAN), with the ionomer solution (Fumion FAS-24) in a ratio 50:50. This ratio was selected accordingly to our previous studies on PVDF-based membrane,[25,52] in such a way to compare membranes with the same amount of ionomer, and therefore focusing on the influence of the non-charged polymer added (PVDF, PVC, or PAN). The two membranes manufactured in this study are labelled as PVC-50 and PAN-50, and **Table 5.2** reports some of the chemical and physical properties of the PVC-50 and PAN-50 membranes investigated in this study, along with those of the PVDF-50 membrane obtained in our previous work.[52]

5.5.1.2. IEC, WU, and FCC

As reported in **Table 5.2**, the IEC values for the three membranes are reasonably similar. This aligns with our expectations, considering that the same amount of ionomer solution (Fumion FAS-24) and polymers (PVC, PAN, and PVDF) were used for all membranes. Considering that the IEC influences the *WU* — typically membranes with high IEC present high values of the *WU*[77–81] — in the case of the membranes under investigation, the variation of the *WU* among the membranes can be attributed to the different nature of the polymers used. Indeed, as expected, the PVDF-50 membrane exhibits the lowest water sorption due to the inherently higher hydrophobic nature of the polymer PVDF.[82–85] Moreover, we can also observe that the water uptake trend aligns with that of the wet membrane thickness, *i.e.* PAN-50 > PVC-50 > PVDF-50, where membranes with higher water uptake present higher thickness. Additionally, combining the IEC and *WU* allows one to calculate the fixed charge concentration (FCC) of the membranes. As evident from **Table 5.2**, with the IEC being constant, the trend of FCC aligns inversely with that of *WU*, following the order PAN-50 < PVC-50 < PVDF-50. Therefore, since the distance-dependent electrostatic interaction

between the mobile counterions and the fixed charged groups in the membrane follows Coulomb's law,[23,86] within the PVDF-50 membrane, the counterions can experience a larger electrostatic interaction due to the higher FCC.

5.5.1.3. Electrical resistance

The membrane electrical resistance values reported in **Table 5.2** show the following trend: PVDF-50 > PVC-50 > PAN-50. Given the similar IEC values for the various membranes, and considering that a correlation exists between the IEC and the electrical resistance[87] – membranes with higher IEC values exhibit lower electrical resistance – this result indicates that the electrical resistance is influenced by the nature of the polymer. In this context, it is worth comparing the manufactured membranes with two commercial membranes such as AMX and ACS from Neosepta. These commercial membranes possess IEC values of 2.1 and 1.9 $mmol \cdot g^{-1}$, respectively, which is almost three times higher than those of the PAN-50, PVC-50, and PVDF-50 membranes. Consequently, their electrical resistance values are 3.1 and 3.9 $\Omega \cdot cm^2$, respectively, which are three to four times lower than those observed for the membranes investigated in this study. This can limit the application of the manufactured membranes at high current density since a higher electrical resistance results in a higher energy consumption.[52]

Table 5.2: Chemical and physical properties of the PVC-50 and PAN-50 membranes investigated in this study, along with those of PVDF-50. (**Chapter 4**)[52]

Membrane	Composition (wt%:wt%)	Polymer structure	Thickness (μm)	IEC ($meq \cdot g^{-1}$)	WU (%)	FCC ($mol \cdot L^{-1}$)	Electrical Resistance ($\Omega\ cm^2$)
PAN-50	PAN:Fumion FAS-24 = 50:50	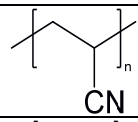	100-105	0.75 ± 0.01	15.0 ± 0.4	5.0 ± 0.2	8.8 ± 0.1
PVC-50	PVC:Fumion FAS-24 = 50:50	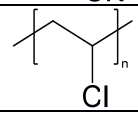	95-100	0.72 ± 0.01	9.5 ± 0.4	7.7 ± 0.3	9.4 ± 0.1
PVDF-50	PVDF:Fumion FAS-24 = 50:50	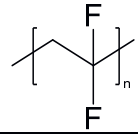	80-85	0.74 ± 0.02	6.5 ± 0.8	11.0 ± 0.8	11.5 ± 0.3

5.5.1.4. Contact angle analysis

The hydrophobic nature of the PAN-50 and PVC-50 membranes was investigated by determining their contact angles, measured through the captive bubble method. In **Figure 5.2**, the obtained values are reported and compared with those of the PVDF-50 membrane described in our previous work (**Chapter 4**)[52]. The observed contact angle trend PVDF-50 > PVC-50 > PAN-50 can be attributed to the different nature of the polymers employed, where the use of more hydrophobic polymers imparts a larger hydrophobicity to the membrane.

The contact angle values displayed in **Figure 5.2** for the three membranes are considerably higher than those of the two commercial AMX and ACS membranes, which were reported to be 26° and 52° respectively (**Chapter 4**).[52] Generally, by increasing the IEC, a membrane becomes more hydrophilic due to the increased amount of charged moieties.[81,77] As a result, membranes with higher IEC values tend to have typically higher water content,[77–81,88] as we also observed in our previous study (**Chapter 3**).[25] As previously discussed, the IEC values of the AMX and ACS membranes are higher than those of PAN-50, PVC-50, and PVDF-50. This indicates that a strategy to increase the hydrophobicity of a membrane is decreasing its IEC. Along these lines, Tekinalp *et al.*[22] modified poly(2,6-dimethyl-1,4-phenylene oxide) by introducing quaternary ammonium

groups using trimethylamine to produce AEMs. Specifically, increasing the functionalization reaction temperature enabled them to increase the incorporation of quaternary ammonium groups into the polymeric backbone, thereby increasing the IEC. Their examination of water contact angles and *WU* revealed a reduction in membrane hydrophobicity.

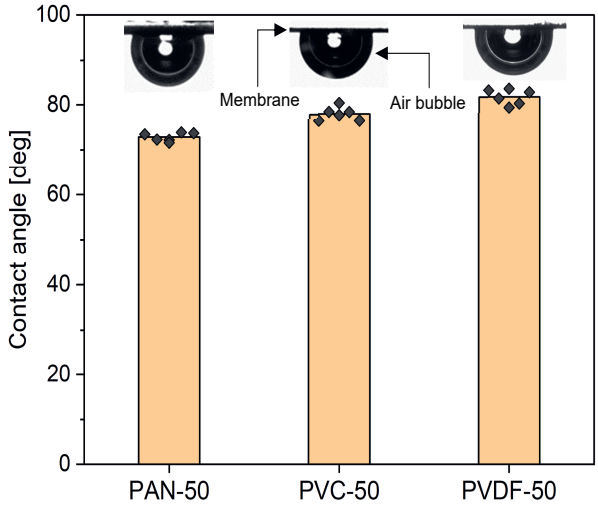

Figure 5.2: Contact angle values obtained through captive bubble method for the PAN-50, PVC-50, and PVDF-50 membranes; optical images of the membranes and air bubbles are provided on top of each bar.

5.5.1.5. SEM-EDX analysis

The SEM images of the PVDF-50, PVC-50, and PAN-50 membranes, obtained with a magnification of ×1,000, along with their respective EDX analyses, are presented in **Figure 5.3**. Additional SEM images at ×500 and ×1,500 magnifications are provided in **Figure S5.2** of the Supporting Information. All membranes present a compact structure without visible voids. The EDX analysis focused on the distribution of fluorine (F), chlorine (Cl), and nitrogen (N) respectively in the PVDF-50 (**Figure 5.3 a_1)**), PVC-50 (**Figure 5.3 b_1)**), and PAN-50 (**Figure 5.3 c_1)**) membranes. The images confirm a similar and even distribution of the three polymers within the membranes. The presence of oxygen (O) and bromine (Br) in the EDX analysis can be attributed to the ionomer (Fumion FAS-24), which also turns out to be evenly distributed. The assignment that goes along

with this elemental mapping is supported by the analysis of a polymer-free membrane containing this component exclusively, as illustrated in **Figure S5.3** of the Supporting Information.

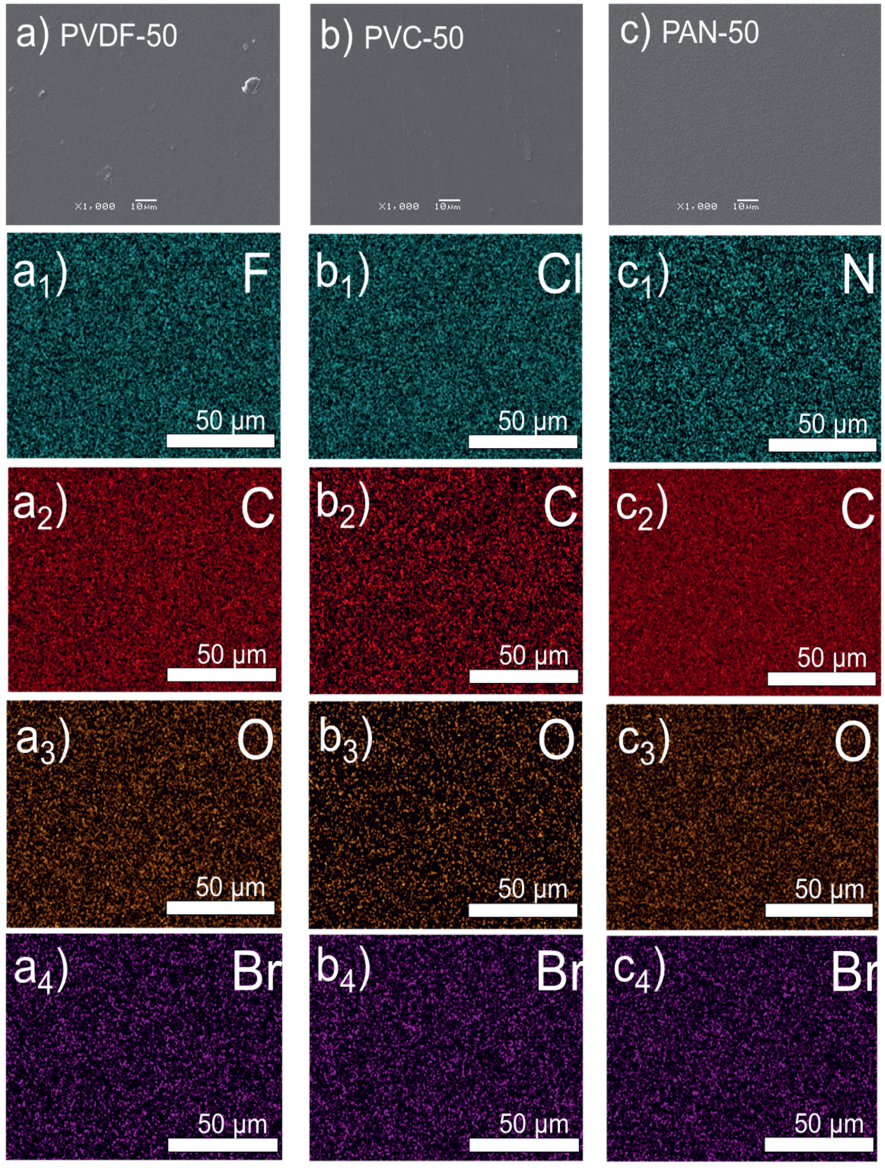

Figure 5.3: SEM images obtained with a magnification of ×1,000 for **a)** PVDF-50, **b)** PVC-50, and **c)** PAN-50. Images of the EDX analysis for each membrane are placed below the SEM images. The images with subscript 2, 3, and 4, indicate the element carbon (C), oxygen (O), and bromine (Br) for all membranes, while with subscript 1 we refer to fluorine (F) for the PVDF-50 membrane, to chlorine (Cl) for the PVC-50 membrane, to nitrogen (N) for the PAN-50 membrane.

5.5.2. Membrane performance

5.5.2.1. Permselectivity and permeability coefficient ratio

Figure 5.4 displays the measured values of permselectivity and permeability coefficient ratio for the three membranes. Notably, all membranes exhibit a permselectivity value exceeding 90%, a result that is consistent with existing literature.[69]

While the permeability coefficient ratio of the PVDF-50 and PVC-50 membranes are as high as 3 and similar, the one of PAN-50 was found to be lower (**Figure 5.4**). Despite this difference, all membranes possess a higher permeability value compared to those of the two commercial membranes AMX and ACS (1.5 and 1.9, respectively) (**Chapter 4**)[52]. The reduced value for PAN-50 can be attributed to its lower surface hydrophobicity, leading to a decreased affinity between nitrate and the membrane. On the other hand, given the observed differences in hydrophobicity for PVDF-50 and PVC-50, one might have expected a higher value for the former than the latter. Therefore, while this method serves as a quick indicator of a membrane's selective behavior,[73] we proceed conducting electrodialysis experiments for a more precise determination of selectivity.

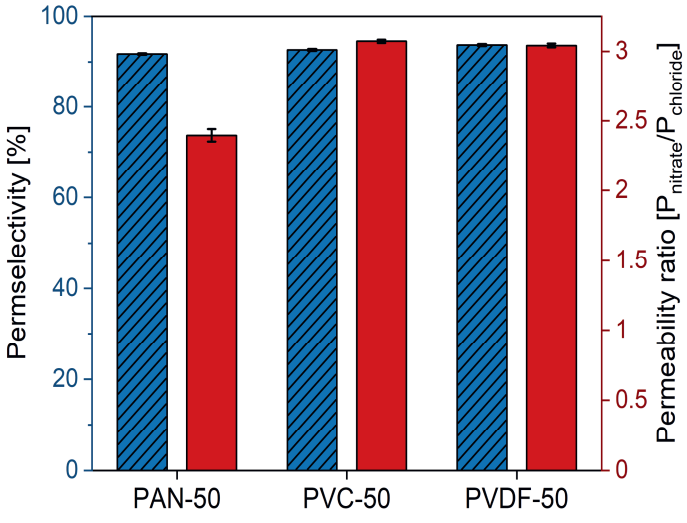

Figure 5.4: Permselectivity and permeability coefficient ratio values of the PAN-50, PVC-50, and PVDF-50 membranes. Experiments have been conducted in triplicate.

5.5.2.2. ED experiments

In this section, we present the experimental results of the transport of nitrate and chloride through the PVC-50 and PAN-50 membranes, obtained in batch-mode electrodialysis. These results are compared with those obtained in our previous work for the membrane PVDF-50 (**Chapter 4**).[52] Over time, we observed changes in the levels of nitrate and chloride in the two reservoirs for the two membranes (refer to Supporting Information **Figure S5.4**). The concentrations increased in the concentrate reservoir and declined in the diluate reservoir, with the nitrate showing a higher increasing rate than the chloride in the concentrate reservoir. The coulombic efficiency for all experiments was in the range of 93–97 %.

The nitrate over chloride selectivity was calculated over time according to **Equation 5.8**, and the values obtained are presented in **Figure 5.5** along with those of the PVDF-50 membrane. The data highlights that the PVC-50 membrane exhibits the highest selectivity, while PVDF-50 and PAN-50 show comparable selectivity, albeit with slightly lower values for PAN-50. This is further evident when analyzing the trends of the nitrate and chloride recovery ratios over time, as shown in **Figure 5.6** and obtained using **Equation 5.9**. Specifically, while the PAN-50 membrane exhibits slightly lower nitrate recovery compared to PVDF-50, the PVC-50 membrane allows for higher nitrate recovery and lower chloride recovery. Moreover, we can also observe that for all membranes, after 2 hours, corresponding to a 60% degree of desalination, the rate of nitrate increase becomes lower, while the rate of chloride increases than in the previous 2 hours, as reflected by the changes of the slopes in **Figure 5.6**. This is attributed to the faster nitrate depletion compared to chloride in the diluate, where the remaining nitrate quantity is not sufficient to sustain the fixed ionic flux of 3 mmol·h^{-1}. Indeed, the residual amounts of nitrate and chloride in the diluate at 2 hours for the PVC-50 membrane are 1.0 and 3.1 mmol, respectively. Thus, with a flux of 3 mmol·h^{-1}, it is evident that nitrate alone is not sufficient to sustain the flux. Therefore, while extending the ED for a longer duration may indeed lead to higher nitrate recovery, it should be noted that this comes at the cost of increased chloride contamination.

Compared to the selectivity values of the commercial membranes reported in one of our previous studies (selectivity values from ~1.8 to ~1.2 for AMX and ~2.8 to ~1.3 for ACS, from 0.5 to 3 h, respectively) (**Chapter 4**),[52] at any time, the selectivity values of all three membranes are higher (**Figure 5.5**). This supports the efficacy of reducing the IEC by incorporating non-charged

polymers to increase the membrane's hydrophobicity and thus achieve improved nitrate selectivity.

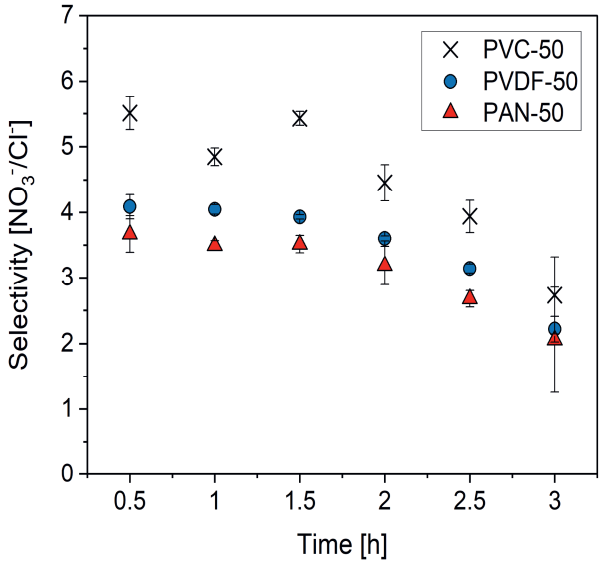

Figure 5.5: Trends of the nitrate over chloride selectivity obtained by ED for the PVC-50, and PAN-50 membranes manufactured in this study, along with that of the PVDF-50 membrane reported in our previous work. Experiments were repeated in triplicate for each membrane.

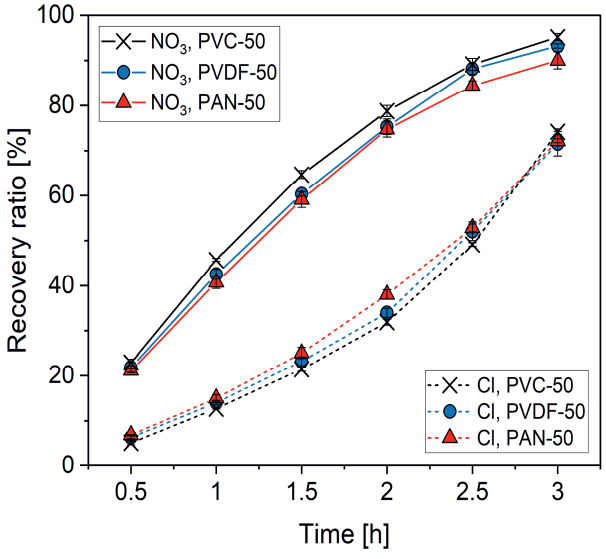

Figure 5.6: Trends of the recovery ratio of nitrate (solid lines) and chloride (dashed lines) obtained by ED for the two manufactured PVC-50 and PAN-50 membranes, along with those of the PVDF-50 membrane reported in our previous work.

As mentioned in the introduction, our initial decision to use a polymer with intrinsic hydrophobic characteristics such as PVDF was influenced by its extensive use in membrane technology and by existing literature suggesting a correlation between increased membrane hydrophobicity and enhanced nitrate selectivity. Our previous studies (**Chapters 3** and **4**),[25,52] confirmed that higher concentrations of PVDF indeed result in increased nitrate selectivity and we associated this effect to the increased membrane's hydrophobicity as reflected by the contact angle obtained compared to those of AMX and ACS. Therefore, based on these findings, we expected the PVDF-50 membrane to outperform PVC-50 and PAN-50, given its higher surface hydrophobicity, as illustrated in **Figure 5.2**. However, the results reported in the current study suggest that while an increased membrane hydrophobicity is crucial for enhancing nitrate selectivity, other factors should also be evaluated. Specifically, we recommend also considering the membrane's FCC. Previous research conducted by Epsztein *et al.*[23] highlighted the role of dehydration-induced adsorption at the water-membrane interface in ion selectivity. However, they also proposed that ions with a lower dehydration energy, such as nitrate, form stronger interactions with the membrane's charged groups, resulting in slower diffusion.

Therefore, by analyzing the fixed charge concentration of the three membranes (**Table 5.2**), we hypothesize that despite PVDF's higher surface hydrophobicity favoring nitrate adsorption over chloride, its elevated FCC hinders nitrate diffusion due to increased interaction with the membrane's charged groups. On the other hand, while the PAN-50 membrane presents the lowest surface hydrophobicity, its FCC is also the lowest observed in the series of investigated polymers, which can explain the similarity in the selectivity data of the PAN-50 and PVDF-50 membranes, though slightly lower. Therefore, we hypothesize that the PVC-50 membrane strikes a balance between surface hydrophobicity and FCC, making it – within the window of chosen polymers – the optimal choice for improved nitrate selectivity.

The higher selectivity displayed by the PVC-50 membrane presents an opportunity for further research. Based on our previous studies (**Chapters 3** and **4**),[25,52] which correlated a higher PVDF concentration with a higher nitrate selectivity, we hypothesize that by using PVC one can achieve selectivity values similar to those of the PVDF-50 membrane but with a lower percentage of polymer used.

Additionally, further membrane development is expected to benefit from obtaining a more detailed current-voltage characteristics, e.g. along the lines of a recent contribution of Zimmerman *et al*.[89] which investigated the role of the limiting current density (LCD) as a selectivity promoter in removing target ions from concentrated solutions using ED. In this study, the boundary-layer method was introduced to determine ion-specific LCD values and by operating the ED unit at the specific LCDs of target ions, the impact on the separation efficiency between counter-ions was demonstrated. This approach promoted monovalent selectivity in a multi-ionic mixture containing chloride, fluoride, and sulfate while minimizing energy consumption. These insights are valuable in exploring the performance of future membranes and optimizing their selectivity and efficiency across varying current densities.

Lastly, it is worth noting that the energy consumption values calculated using **Equation 5.12** for the three manufactured membranes (PVDF-50, PVC-50, and PAN-50) are about 20-35% higher than those obtained in our previous study (**Chapter 4**)[52] for the two commercial membranes, AMX and ACS (**Table 5.3**). However, we consider the increased energy consumption to be a reasonable trade-off given that the three manufactured membranes exhibit higher selectivity than the commercial ones.

Table 5.3: Energy consumption obtained for the batch-mode ED experiments at 20 $A \cdot m^{-2}$ for the PVDF-50, PVC-50, PAN-50, ACS, and AMX membranes.

	PVDF-50	**PVC-50**	**PAN-50**	**ACS**	**AMX**
E ($kJ \cdot g^{-1}$ NO_3)	0.57	0.61	0.60	0.48	0.45

5.6. Conclusion

To identify more environmentally sustainable polymers for AEMs with enhanced nitrate selectivity, we explored PVC and PAN as alternatives to PVDF, which previously demonstrated the best-reported nitrate selectivity. Via a casting process using PVC and PAN in combination with an ionomer solution, two AEMs were manufactured successfully.

Our findings show that all membranes have higher nitrate selectivity than the commercially available ones. This is attributed to increased hydrophobicity, which enhances membrane-nitrate

affinity. Among the polymers investigated, the PVC-based membrane outperforms both the PVDF and PAN-based ones, with the latter having slightly lower selectivity than the former.

Considering the superior hydrophobic nature of the PVDF membrane, the correlation "increased hydrophobicity = increased nitrate selectivity" alone does not explain the higher nitrate-selective performance of the PVC membrane. We, therefore, examined the difference in fixed charge concentration between the membranes, suggesting its influence on the selectivity mechanism. Specifically, membranes with higher fixed charge concentrations, like the PVDF one, provide more opportunities for mobile ions to interact with fixed charges. Consequently, the mobility of less hydrated ions like nitrate, is impeded, leading to lower diffusion rates compared to more hydrated ions like chloride.

In conclusion, our study suggests balancing hydrophobicity and fixed charge concentration in membrane manufacturing to achieve optimal nitrate selectivity.

Acknowledgments

The authors thank the Dutch Research Council – Wetsus Partnership Programme on Sustainable Water Technology for funding this project (ALWET.2019.004). This work was performed in the cooperation framework of Wetsus, European Centre of Excellence for Sustainable Water Technology (www.wetsus.nl). Wetsus is co-funded by the Dutch Ministry of Economic Affairs and Ministry of Infrastructure and Environment, the European Union Regional Development Fund, the Province of Fryslan and the Northern Netherlands Provinces. The authors like to thank the participants of the research theme "Desalination & Concentrates" for the fruitful discussions and their financial support.

Supporting information

Table S5.1: Physicochemical properties of Fumion FAS-24.

	Appearance	Matrix	Functional group	Counter-ion	IEC (meq/g)
Fumion FAS-24	Solution 24 wt% in NMP	Polyaromatic polymer	Quaternary ammonium	Bromide	1.7-1.9

Table S5.2: Chemical and physical properties of the commercial Neosepta, AMX, ACS, and CMX membranes.[52]

Membrane	Composition	Thickness (µm)	IEC ($meq \cdot g^{-1}$)	Water Uptake (%)	Electrical resistance ($\Omega\ cm^2$)
AMX	Styrene-divinyl benzene reinforced with PVC	140	2.1 ± 0.04	22 ± 0.7	3.1 ± 0.1
ACS	Styrene-divinyl benzene reinforced with PVC, with highly cross-linked layer on both of the membrane surfaces	120	1.9 ± 0.03	26 ± 0.6	3.9 ± 0.1
CMX	Cross-linked sulfonated styrene–divinylbenzene copolymer (45–65 %) and polyvinylchloride (45–55 %)	150	2.5 ± 0.05	30 ± 0.8	2.8 ± 0.1

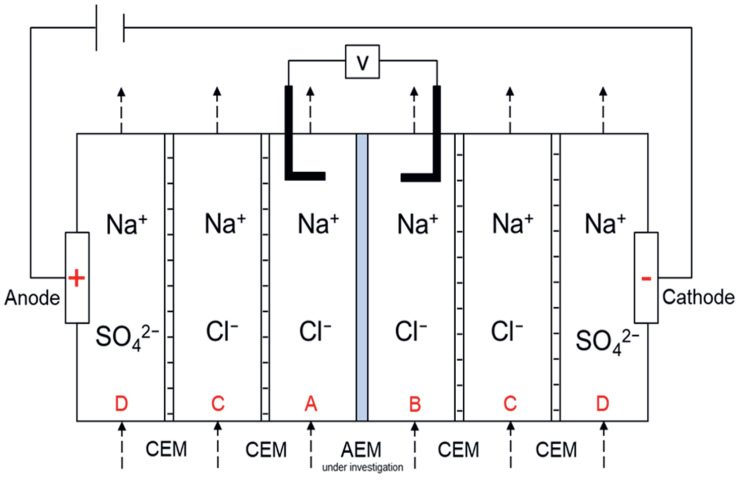

Figure S5.1: Schematic representation of the six-compartment cell used to measure the membranes electrical resistance. See text (**Section 5.3.4**) for an explanation of the compositions of solutions A, B, C, and D.

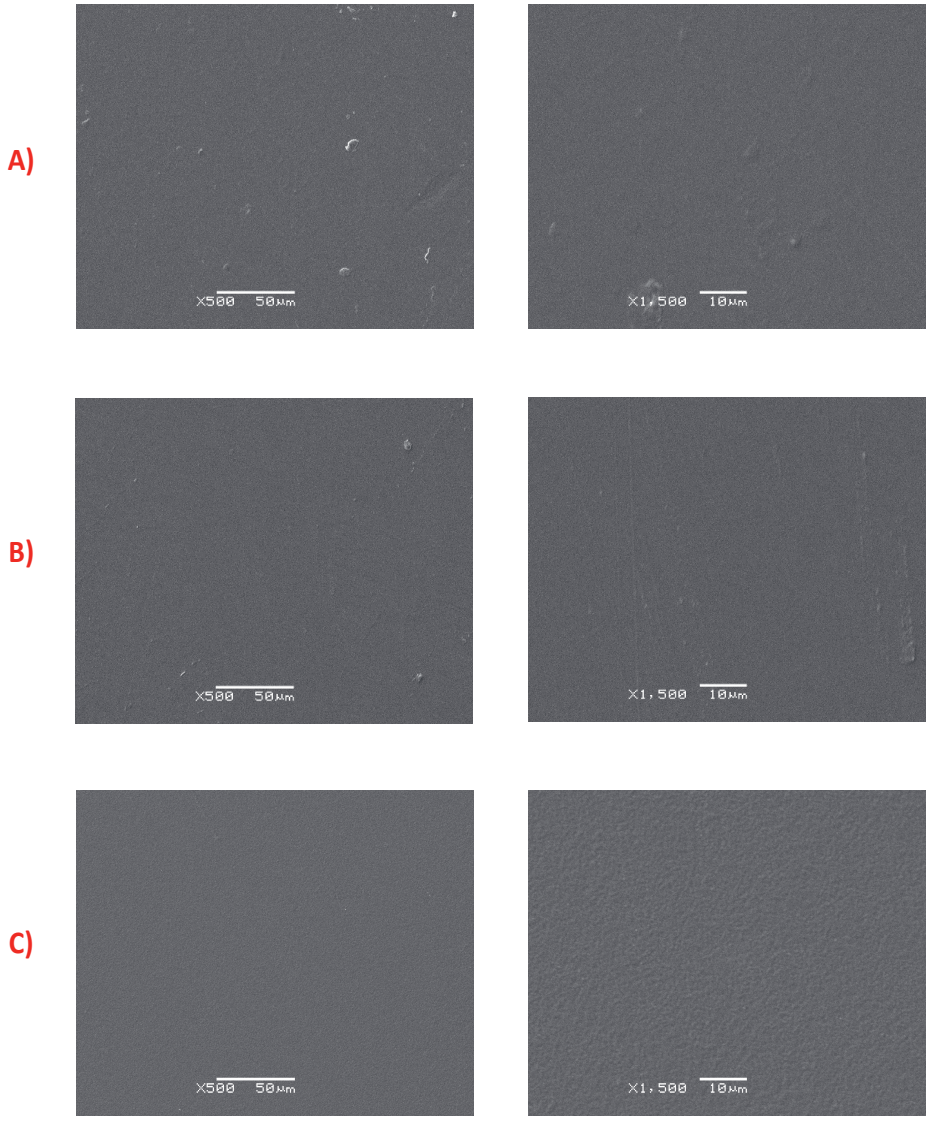

Figure S5.2: SEM images obtained with a magnification of X500 and X 1,500 for the membranes A) PVDF-50, B) PVC-50, and C) PAN-50.

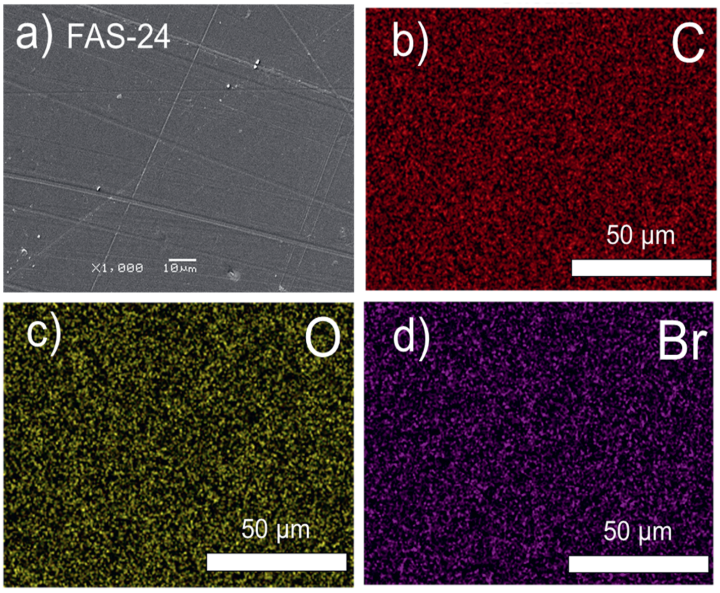

Figure S5.3: SEM images obtained with a magnification of X1,000 and relative EDX analysis for the membrane made only with the ionomer solution and labelled as FAS-24. Picture **a)** is related to the SEM image, while **b)**, **c)**, and **d)** are the EDX analysis of carbon, oxygen, and bromide.

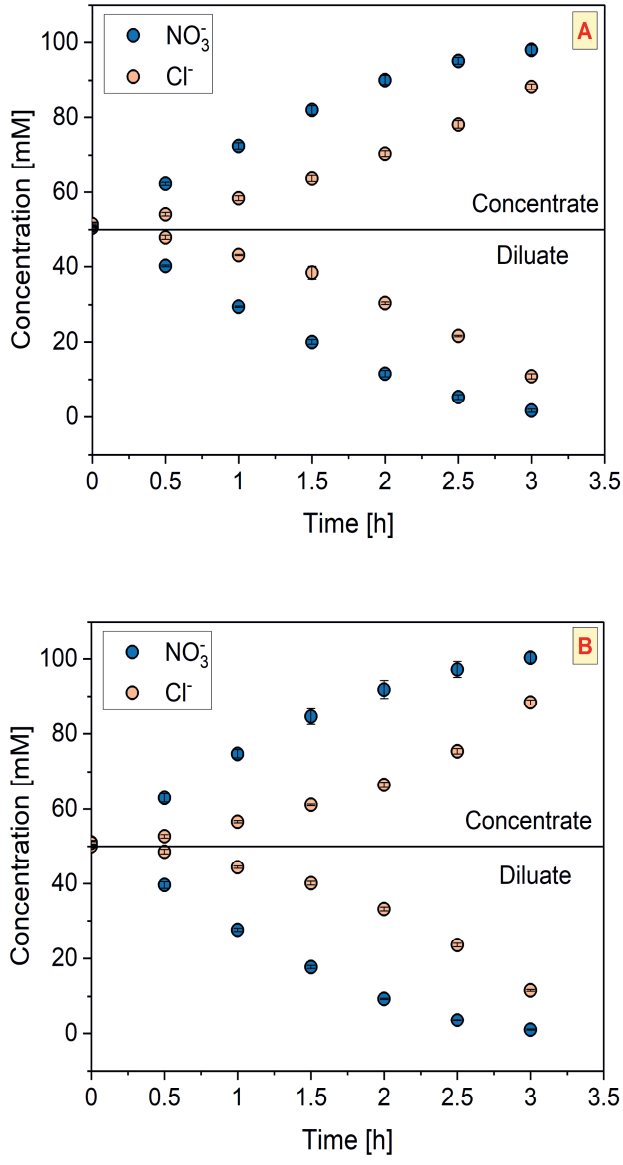

Figure S5.4: Trends of the nitrate and chloride concentration in the concentrate top) and diluate (bottom) reservoir obtained by ED for the membranes PAN-50 (**Panel A**) and PVC-50 (**Panel B**). Experiments were conducted in triplicate.

References

(1) Golubenko, D. V.; Manin, A. D.; Wang, Y.; Xu, T.; Yaroslavtsev, A. B. The Way to Increase the Monovalent Ion Selectivity of FujiFilm® Anion-Exchange Membranes by Cerium Phosphate Modification for Electrodialysis Desalination. *Desalination* **2022**, *531*, 115719. https://doi.org/10.1016/j.desal.2022.115719.

(2) Qian, Z.; Miedema, H.; de Smet, L. C. P. M.; Sudhölter, E. J. R. Permeation Selectivity in the Electro-Dialysis of Mono- and Divalent Cations Using Supported Liquid Membranes. *Desalination* **2022**, *521*. https://doi.org/10.1016/j.desal.2021.115398.

(3) Sedighi, M.; Behvand Usefi, M. M.; Ismail, A. F.; Ghasemi, M. Environmental Sustainability and Ions Removal through Electrodialysis Desalination: Operating Conditions and Process Parameters. *Desalination* **2023**, *549*, 116319. https://doi.org/10.1016/j.desal.2022.116319.

(4) Khoi, T. M.; Tran, N. A. T.; Jung, H. B.; Huynh, V. P.; Kim, Y.; Hong, J.; Yoo, C.-Y.; Kang, H. S.; Cho, Y. Selective and Continuous Ion Recovery Using Flow Electrode Capacitive Deionization with Polymer Multilayers Functionalized Ion Exchange Membrane. *Desalination* **2023**, *558*, 116626. https://doi.org/10.1016/j.desal.2023.116626.

(5) Gamaethiralalage, J. G.; de Smet, L. C. P. M. Rocking-Chair Capacitive Deionization for Phosphate Recovery *via* Rejection Mode Using Ion-Exchange Membranes. *Desalination* **2023**, *564*, 116752. https://doi.org/10.1016/j.desal.2023.116752.

(6) Zhang, H.; Li, Y.; Han, J.; Sun, Y.; He, M.; Hao, Z.; Jiang, T.; Wang, B.; Wang, W.; Liu, M. Influence of Ion Exchange Membrane Arrangement on Dual-Channel Flow Electrode Capacitive Deionization: Theoretical Analysis and Experimentations. *Desalination* **2023**, *548*, 116288. https://doi.org/10.1016/j.desal.2022.116288.

(7) Yu, Z.; Tsen, W.-C.; Qu, T.; Cheng, F.; Hu, F.; Liu, H.; Wen, S.; Gong, C. Highly Ion-Conductive Anion Exchange Membranes with Superior Mechanical Properties Based on Polymeric Ionic Liquid Filled Functionalized Bacterial Cellulose for Alkaline Fuel Cells. *Journal of Materials Research and Technology* **2023**, *23*, 6187–6199. https://doi.org/10.1016/j.jmrt.2023.02.197.

(8) Li, D.; Chu, W.; Wei, J.; Hu, Y.; He, Y.; Qin, H.; Liu, J.; He, J.; Ni, H. Effects of Hydrolysis Degree on Ion-Doped Anion Exchange Membranes in Direct Borohydride Fuel Cells. *International Journal of Hydrogen Energy* **2023**, *48* (69), 26990–27000. https://doi.org/10.1016/j.ijhydene.2023.03.235.

(9) Campione, A.; Gurreri, L.; Ciofalo, M.; Micale, G.; Tamburini, A.; Cipollina, A. Electrodialysis for Water Desalination: A Critical Assessment of Recent Developments on Process Fundamentals, Models and Applications. *Desalination* **2018**, *434* (October 2017), 121–160. https://doi.org/10.1016/j.desal.2017.12.044.

(10) Sajjad, A.-A.; Yunus, M. Y. B. M.; Azoddein, A. A. M.; Hassell, D. G.; Dakhil, I. H.; Hasan, H. A. Electrodialysis Desalination for Water and Wastewater: A Review. *Chemical Engineering Journal* **2019**, *380* (July 2019), 122231. https://doi.org/10.1016/j.cej.2019.122231.

(11) Al-Amshawee, S.; Yunus, M. Y. B. M.; Azoddein, A. A. M.; Hassell, D. G.; Dakhil, I. H.; Hasan, H. A. Electrodialysis Desalination for Water and Wastewater: A Review. *Chemical Engineering Journal* **2020**, *380*, 122231. https://doi.org/10.1016/j.cej.2019.122231.

(12) Luo, T.; Abdu, S.; Wessling, M. Selectivity of Ion Exchange Membranes: A Review. *Journal of Membrane Science* **2018**, *555* (December 2017), 429–454. https://doi.org/10.1016/j.memsci.2018.03.051.

(13) Chinello, D.; Myrstad, A.; de Smet, L. C. P. M.; Miedema, H. Modelling the Required Membrane Selectivity for $NO3^-$ Recovery from Effluent Also Containing Cl^-, While Saving Water. *Chemical Engineering Research and Design* **2023**, *193*, 409–419. https://doi.org/10.1016/j.cherd.2023.03.038.

(14) Qian, Z.; Miedema, H.; de Smet, L. C. P. M.; Sudhòlter, E. J. R. Modelling the Selective Removal of Sodium Ions from Greenhouse Irrigation Water Using Membrane Technology. *Chemical Engineering Research and Design* **2018**, *134*, 154–161. https://doi.org/10.1016/j.cherd.2018.03.040.

(15) Mubita, T.; Porada, S.; Aerts, P.; van der Wal, A. Heterogeneous Anion Exchange Membranes with Nitrate Selectivity and Low Electrical Resistance. *Journal of Membrane Science* **2020**, *607*, 118000. https://doi.org/10.1016/j.memsci.2020.118000.

(16) Mubita, T. M.; Porada, S.; Biesheuvel, P. M.; van der Wal, A.; Dykstra, J. E. Strategies to Increase Ion Selectivity in Electrodialysis. *Separation and Purification Technology* **2022**, *292*, 120944. https://doi.org/10.1016/j.seppur.2022.120944.

(17) Kikhavani, T.; Ashrafizadeh, S. N.; Van Der Bruggen, B. Nitrate Selectivity and Transport Properties of a Novel Anion Exchange Membrane in Electrodialysis. *Electrochimica Acta* **2014**, *144*, 341–351. https://doi.org/10.1016/j.electacta.2014.08.012.

(18) Oh, C.-M.; Hwang, C.-W.; Hwang, T.-S. Synthesis of a Quaternarized Poly(Vinylimidazole-Co-Trifluoroethylmethacrylate-Co-Divinylbenzene) Anion-Exchange Membrane for Nitrate Removal. *Journal of Environmental Chemical Engineering* **2014**, *2* (4), 2162–2169. https://doi.org/10.1016/j.jece.2014.09.014.

(19) Zhang, N.; Yu, H.; Zhang, J.; Jiang, X.; Yin, S.; Zhou, G.; Zhang, X.; Bao, J.; He, G. Pressure-Driven Li+/Mg2+ Selective Permeation through Size-Sieving Nanochannels: The Role of the Second Hydration Shell. *Separation and Purification Technology* **2023**, *327*, 124818. https://doi.org/10.1016/j.seppur.2023.124818.

(20) Irfan, M.; Ge, L.; Wang, Y.; Yang, Z.; Xu, T. Hydrophobic Side Chains Impart Anion Exchange Membranes with High Monovalent–Divalent Anion Selectivity in Electrodialysis. *ACS Sustainable Chem. Eng.* **2019**, *7* (4), 4429–4442. https://doi.org/10.1021/acssuschemeng.8b06426.

(21) Sata, T. Studies on Anion Exchange Membranes Having Permselectivity for Specific Anions in Electrodialysis - Effect of Hydrophilicity of Anion Exchange Membranes on Permselectivity of Anions. *Journal of Membrane Science* **2000**, *167* (1), 1–31. https://doi.org/10.1016/S0376-7388(99)00277-X.

(22) Tekinalp, Ö.; Zimmermann, P.; Burheim, O. S.; Deng, L. Designing Monovalent Selective Anion Exchange Membranes for the Simultaneous Separation of Chloride and Fluoride from Sulfate in an Equimolar Ternary Mixture. *Journal of Membrane Science* **2023**, *666*, 121148. https://doi.org/10.1016/j.memsci.2022.121148.

(23) Epsztein, R.; Shaulsky, E.; Qin, M.; Elimelech, M. Activation Behavior for Ion Permeation in Ion-Exchange Membranes: Role of Ion Dehydration in Selective Transport. *Journal of Membrane Science* **2019**, *580* (January), 316–326. https://doi.org/10.1016/j.memsci.2019.02.009.

(24) Epsztein, R.; DuChanois, R. M.; Ritt, C. L.; Noy, A.; Elimelech, M. Towards Single-Species Selectivity of Membranes with Subnanometre Pores. *Nat. Nanotechnol.* **2020**, *15* (6), 426–436. https://doi.org/10.1038/s41565-020-0713-6.

(25) Chinello, D.; Post, J.; de Smet, L. C. P. M. Selective Separation of Nitrate from Chloride Using PVDF-Based Anion-Exchange Membranes. *Desalination* **2024**, *572*, 117084. https://doi.org/10.1016/j.desal.2023.117084.
(26) Zou, D.; Xia, L.; Luo, P.; Guan, K.; Matsuyama, H.; Zhong, Z. Fabrication of Hydrophobic Bi-Layer Fiber-Aligned PVDF/PVDF-PSF Membranes Using Green Solvent for Membrane Distillation. *Desalination* **2023**, *565*, 116810. https://doi.org/10.1016/j.desal.2023.116810.
(27) Teoh, G. H.; Jawad, Z. A.; Chan, D. J. C.; Low, S. C. Surface Regeneration of Templated PVDF Membrane for Efficient Microalgae-Rich High Saline Aquaculture Wastewater Treatment in Membrane Distillation. *Desalination* **2023**, *565*, 116858. https://doi.org/10.1016/j.desal.2023.116858.
(28) Yang, H.-R.; Huang, Y.-H.; Wang, C.-F.; Chung, T.-S. Green Fabrication of PVDF Superhydrophobic Membranes Using a Green Solvent Triethyl Phosphate (TEP) for Membrane Distillation. *Desalination* **2023**, *566*, 116934. https://doi.org/10.1016/j.desal.2023.116934.
(29) Jankowski, W.; Kujawski, W.; Kujawa, J. Spicing up Membrane Distillation: Enhancing PVDF Membrane Performance with Cinnamic Acid. *Desalination* **2024**, *575*, 117304. https://doi.org/10.1016/j.desal.2024.117304.
(30) Xu, J.; Guan, K.; Luo, P.; He, S.; Matsuyama, H.; Zou, D.; Zhong, Z. Engineering PVDF Omniphobic Membranes with Flower-like Micro-Nano Structures for Robust Membrane Distillation. *Desalination* **2024**, *578*, 117442. https://doi.org/10.1016/j.desal.2024.117442.
(31) Namdari, M.; Zokaee Ashtiani, F.; Bonyadi, E. Development of a High Flux Janus PVDF Membrane for Oily Saline Water Desalination by Membrane Distillation via PDA-TEOS-APTES Surface Modification. *Desalination* **2024**, *572*, 117139. https://doi.org/10.1016/j.desal.2023.117139.
(32) Sun, B.; Wu, M.; Zhen, H.; Jia, Y.; Li, P.; Yuan, Z.; Li, X.; He, G.; Jiang, X. Tailored PVDF Membrane with Coordinated Interfacial Nano/Micro-Structure for Enhanced Membrane Distillation. *Desalination* **2024**, *573*, 117177. https://doi.org/10.1016/j.desal.2023.117177.
(33) Luo, Q.; Huang, L.; Yun, P.; Qiu, T.; Tang, B.; Huang, K.; Hu, X.; Jiang, H. Thermal-Driven Osmosis Utilizing Hollow Fiber Membranes: Sustainable Dye Water Treatment and Electricity Extraction. *Desalination* **2024**, *579*, 117485. https://doi.org/10.1016/j.desal.2024.117485.
(34) Zhang, P.; Rajabzadeh, S.; Song, Q.; Gonzales, R. R.; Jia, Y.; Xiang, S.; Li, Z.; Matsuyama, H. Development of Loose Nanofiltration PVDF Hollow Fiber Membrane for Dye/Salt Separation. *Desalination* **2023**, *549*, 116315. https://doi.org/10.1016/j.desal.2022.116315.
(35) Wang, C.; Chen, Y.; Hu, X.; Feng, X. In-Situ Synthesis of PA/PVDF Composite Hollow Fiber Membranes with an Outer Selective Structure for Efficient Fractionation of Low-Molecular-Weight Dyes-Salts. *Desalination* **2021**, *503*, 114957. https://doi.org/10.1016/j.desal.2021.114957.
(36) Zhao, Y.; Guo, J.; Li, Y.; Zhang, X.; An, A. K.; Wang, Z. Superhydrophobic and Superoleophilic PH-CNT Membrane for Emulsified Oil-Water Separation. *Desalination* **2022**, *526*, 115536. https://doi.org/10.1016/j.desal.2021.115536.
(37) Gao, J.; Cai, M.; Nie, Z.; Zhang, J.; Chen, Y. Superwetting PVDF Membrane Prepared by in Situ Extraction of Metal Ions for Highly Efficient Oil/Water Mixture and Emulsion Separation. *Separation and Purification Technology* **2021**, *275*, 119174. https://doi.org/10.1016/j.seppur.2021.119174.

(38) Lee, K. H.; Khan, I. A.; Song, L. H.; Kim, J. Y.; Kim, J.-O. Evaluation of Structural/Performance Variation between α-Al2O3 and Polyvinylidene Fluoride Membranes under Long-Term Clean-in-Place Treatment Used for Water Treatment. *Desalination* **2022**, *538*, 115921. https://doi.org/10.1016/j.desal.2022.115921.

(39) Asadi, A.; Gholami, F.; Nazari, S.; Dolatshah, M. Improved Filtration Performance of Polyvinylidene Fluoride Nanocomposite Membranes Embedded with Deep Eutectic Solvent: Application towards MBR. *Desalination* **2022**, *543*, 116088. https://doi.org/10.1016/j.desal.2022.116088.

(40) Khan, M. S.; Li, Y.; Yang, L.; Yan, Z. C.; Li, D.-S.; Qiu, J.; Xu, X.; Yang, H. Y. Improving Capacitive Deionization Performance through Tailored Iodine-Loaded ZIF-8 Composites. *Desalination* **2024**, 117486. https://doi.org/10.1016/j.desal.2024.117486.

(41) Khoi, T. M.; Kim, J.; Tran, N. A. T.; Huynh, V. P.; Lee, Y.-W.; Cho, Y. Redox Flow Deionization Using Prussian Blue and Functionalized Ion Exchange Membrane for Enhanced Selective Ion Recovery. *Desalination* **2024**, *578*, 117444. https://doi.org/10.1016/j.desal.2024.117444.

(42) Zhang, L.; Zhang, T.; Lv, S.; Song, S.; Galván, H. J. O.; Quintana, M.; Zhao, Y. Adsorbents for Lithium Extraction from Salt Lake Brine with High Magnesium/Lithium Ratio: From Structure-Performance Relationship to Industrial Applications. *Desalination* **2024**, *579*, 117480. https://doi.org/10.1016/j.desal.2024.117480.

(43) Sharma, K.; Akther, N.; Choo, Y.; Zhang, P.; Matsuyama, H.; Shon, H. K.; Naidu, G. Positively Charged Nanofiltration Membranes for Enhancing Magnesium Separation from Seawater. *Desalination* **2023**, *568*, 117026. https://doi.org/10.1016/j.desal.2023.117026.

(44) Jiang, J.; Dorji, P.; Badeti, U.; Sohn, W.; Freguia, S.; Phuntsho, S.; El Saliby, I.; Shon, H. K. Potential Nutrient Recovery from Source-Separated Urine through Hybrid Membrane Bioreactor and Membrane Capacitive Deionisation. *Desalination* **2023**, *566*, 116924. https://doi.org/10.1016/j.desal.2023.116924.

(45) Han, N.; Li, Y.; Peng, H.; Gao, R.; He, Q.; Miao, Z.; Wan, K. Adsorption of Li+ by Imprinted Capacitor Deionization — A New Method for Selective Recovery of Valuable Lithium in Acidic Solutions. *Desalination* **2023**, *565*, 116820. https://doi.org/10.1016/j.desal.2023.116820.

(46) Wang, W.; Ma, P.; Li, H. Cationic Segregation of Ca2Mn3O8 Enabling High Selectivity for Fluoride Ions through Capacitive Deionization. *Desalination* **2023**, *564*, 116798. https://doi.org/10.1016/j.desal.2023.116798.

(47) HMTShirazi, R.; Heidari, A.; Mohammadi, T. Fabrication of High-Performance MeI and HPEI Assembled PES/CPES Hollow Fiber Nanofiltration Membranes with High Positive Charges for Efficient Removal of Salt/Heavy Metal Ions. *Desalination* **2023**, *565*, 116877. https://doi.org/10.1016/j.desal.2023.116877.

(48) Mishra, S.; Singh, A. K.; Singh, J. K. Ferrous Sulfide and Carboxyl-Functionalized Ferroferric Oxide Incorporated PVDF-Based Nanocomposite Membranes for Simultaneous Removal of Highly Toxic Heavy-Metal Ions from Industrial Ground Water. *Journal of Membrane Science* **2020**, *593*, 117422. https://doi.org/10.1016/j.memsci.2019.117422.

(49) Simari, C.; Lufrano, E.; Lemes, G.; Lázaro, M. J.; Sebastián, D.; Nicotera, I. Electrochemical Performance and Alkaline Stability of Cross-Linked Quaternized Polyepichlorohydrin/PvDF Blends for Anion-Exchange Membrane Fuel Cells. *J. Phys. Chem. C* **2021**, *125* (10), 5494–5504. https://doi.org/10.1021/acs.jpcc.0c11346.

(50) Sharma, P. P.; Yadav, V.; Rajput, A.; Kulshrestha, V. PVDF-g-Poly (Styrene-Co-Vinylbenzyl Chloride) Based Anion Exchange Membrane: High Salt Removal Efficiency and Stability. *Desalination* **2018**, *444*, 35–43. https://doi.org/10.1016/j.desal.2018.07.002.

(51) Sharma, P. P.; Yadav, V.; Rajput, A.; Kulshrestha, V. Acid Resistant PVDF Based Copolymer Alkaline Anion Exchange Membrane for Acid Recovery and Electrodialytic Water Desalination. *Journal of Membrane Science* **2018**, *563*, 561–570. https://doi.org/10.1016/j.memsci.2018.06.016.

(52) Chinello, D.; de Smet, L. C. P. M.; Post, J. Selective Electrodialysis: Targeting Nitrate over Chloride Using PVDF-Based AEMs. *Separation and Purification Technology* **2024**, *342*, 126885. https://doi.org/10.1016/j.seppur.2024.126885.

(53) Ehsan, M. N.; Riza, M.; Pervez, M. N.; Li, C.-W.; Zorpas, A. A.; Naddeo, V. PFAS Contamination in Soil and Sediment: Contribution of Sources and Environmental Impacts on Soil Biota. *Case Studies in Chemical and Environmental Engineering* **2024**, *9*, 100643. https://doi.org/10.1016/j.cscee.2024.100643.

(54) Novak, P. A.; Hoeksema, S. D.; Thompson, S. N.; Trayler, K. M. Per- and Polyfluoroalkyl Substances (PFAS) Contamination in a Microtidal Urban Estuary: Sources and Sinks. *Marine Pollution Bulletin* **2023**, *193*, 115215. https://doi.org/10.1016/j.marpolbul.2023.115215.

(55) Sadia, M.; Kunz, M.; ter Laak, T.; De Jonge, M.; Schriks, M.; van Wezel, A. P. Forever Legacies? Profiling Historical PFAS Contamination and Current Influence on Groundwater Used for Drinking Water. *Science of The Total Environment* **2023**, *890*, 164420. https://doi.org/10.1016/j.scitotenv.2023.164420.

(56) Singh, K.; Kumar, N.; Kumar Yadav, A.; Singh, R.; Kumar, K. Per-and Polyfluoroalkyl Substances (PFAS) as a Health Hazard: Current State of Knowledge and Strategies in Environmental Settings across Asia and Future Perspectives. *Chemical Engineering Journal* **2023**, *475*, 145064. https://doi.org/10.1016/j.cej.2023.145064.

(57) Smalling, K. L.; Romanok, K. M.; Bradley, P. M.; Morriss, M. C.; Gray, J. L.; Kanagy, L. K.; Gordon, S. E.; Williams, B. M.; Breitmeyer, S. E.; Jones, D. K.; DeCicco, L. A.; Eagles-Smith, C. A.; Wagner, T. Per- and Polyfluoroalkyl Substances (PFAS) in United States Tapwater: Comparison of Underserved Private-Well and Public-Supply Exposures and Associated Health Implications. *Environment International* **2023**, *178*, 108033. https://doi.org/10.1016/j.envint.2023.108033.

(58) Maiti, J.; Kakati, N.; Basumatary, P.; Woo, S. P.; Yoon, Y. S. Imidazolium Functionalized Poly(Vinyl Chloride-Co-Vinyl Acetate)-Based Anion Exchange Membrane. *International Journal of Hydrogen Energy* **2016**, *41* (13), 5776–5782. https://doi.org/10.1016/j.ijhydene.2016.02.062.

(59) Khoiruddin, K.; Ariono, D.; Subagjo, S.; Wenten, Ig. Structure and Transport Properties of Polyvinyl Chloride-Based Heterogeneous Cation-Exchange Membrane Modified by Additive Blending and Sulfonation. *Journal of Electroanalytical Chemistry* **2020**, *873*, 114304. https://doi.org/10.1016/j.jelechem.2020.114304.

(60) Ahmad, T.; Guria, C. Progress in the Modification of Polyvinyl Chloride (PVC) Membranes: A Performance Review for Wastewater Treatment. *Journal of Water Process Engineering* **2022**, *45*, 102466. https://doi.org/10.1016/j.jwpe.2021.102466.

(61) Safarpour, M.; Safikhani, A.; Vatanpour, V. Polyvinyl Chloride-Based Membranes: A Review on Fabrication Techniques, Applications and Future Perspectives. *Separation and Purification Technology* **2021**, *279*, 119678. https://doi.org/10.1016/j.seppur.2021.119678.

(62) Nemati, M.; Hosseini, S. M.; Bagheripour, E.; Madaeni, S. S. Electrodialysis Heterogeneous Anion Exchange Membranes Filled with TiO2 Nanoparticles: Membranes' Fabrication and Characterization. *Journal of Membrane Science and Research* **2015**, *1* (3), 135–140.

(63) Liu, Y.; Liao, J.; Peng, G.; Dong, C.; Yang, S.; Shen, J. Poly(Vinyl Chloride)-Based Anion-Exchange Membrane with High-Antifouling Potential for Electrodialysis Application. *ACS Appl. Polym. Mater.* **2021**, *3* (5), 2529–2540. https://doi.org/10.1021/acsapm.1c00121.

(64) Zafari, M.; Kikhavani, T.; Ashrafizadeh, S. N. Hybrid Surface Modification of an Anion Exchange Membrane for Selective Separation of Monovalent Anions in the Electrodialysis Process. *Journal of Environmental Chemical Engineering* **2022**, *10* (1), 107014. https://doi.org/10.1016/j.jece.2021.107014.

(65) Kishore Chand, A. A.; Bajer, B.; Schneider, E. S.; Mantel, T.; Ernst, M.; Filiz, V.; Glass, S. Modification of Polyacrylonitrile Ultrafiltration Membranes to Enhance the Adsorption of Cations and Anions. *Membranes (Basel)* **2022**, *12* (6), 580. https://doi.org/10.3390/membranes12060580.

(66) Wang, L.; Xu, G.; Xiao, J.; Tao, M.; Zhang, W. Quaternary Ammonium-Based Functionalized Polyacrylonitrile Fibers with Polarity Tunable Inner Surface Microenvironment for C–C Bond Forming Reactions under Continuous Flow Conditions. *Ind. Eng. Chem. Res.* **2019**, *58* (27), 12401–12410. https://doi.org/10.1021/acs.iecr.9b01375.

(67) Geng, H.; Zhang, C.; Tao, M.; Ma, N.; Zhang, W. Ionic Microenvironment Constructed in Quaternary Ammonium Modified Polyacrylonitrile Fiber for Efficient CO2 Fixation. *Journal of CO2 Utilization* **2021**, *49*, 101559. https://doi.org/10.1016/j.jcou.2021.101559.

(68) Nightingale, E. R. Phenomenological Theory of Ion Solvation. Effective Radii of Hydrated Ions. *J. Phys. Chem.* **1959**, *63* (9), 1381–1387. https://doi.org/10.1021/j150579a011.

(69) Dlugolecki, P.; Nymeijer, K.; Metz, S.; Wessling, M. Current Status of Ion Exchange Membranes for Power Generation from Salinity Gradients. *Journal of Membrane Science* **2008**, *319* (1–2), 214–222. https://doi.org/10.1016/j.memsci.2008.03.037.

(70) Kitto, D.; Kamcev, J. The Need for Ion-Exchange Membranes with High Charge Densities. *Journal of Membrane Science* **2023**, *677*, 121608. https://doi.org/10.1016/j.memsci.2023.121608.

(71) Galama, A. H.; Hoog, N. A.; Yntema, D. R. Method for Determining Ion Exchange Membrane Resistance for Electrodialysis Systems. *Desalination* **2016**, *380*, 1–11. https://doi.org/10.1016/j.desal.2015.11.018.

(72) Qian, Z.; Miedema, H.; Sahin, S.; de Smet, L. C. P. M.; Sudhölter, E. J. R. Separation of Alkali Metal Cations by a Supported Liquid Membrane (SLM) Operating under Electro Dialysis (ED) Conditions. *Desalination* **2020**, *495*. https://doi.org/10.1016/j.desal.2020.114631.

(73) Luo, T.; Roghmans, F.; Wessling, M. Ion Mobility and Partition Determine the Counter-Ion Selectivity of Ion Exchange Membranes. *Journal of Membrane Science* **2020**, *597*, 117645. https://doi.org/10.1016/j.memsci.2019.117645.

(74) Nikonenko, V. V.; Pismenskaya, N. D.; Belova, E. I.; Sistat, P.; Huguet, P.; Pourcelly, G.; Larchet, C. Intensive Current Transfer in Membrane Systems: Modelling, Mechanisms and Application in Electrodialysis. *Advances in Colloid and Interface Science* **2010**, *160* (1), 101–123. https://doi.org/10.1016/j.cis.2010.08.001.

(75) Biesheuvel, P. M.; Porada, S.; Elimelech, M.; Dykstra, J. E. Tutorial Review of Reverse Osmosis and Electrodialysis. *Journal of Membrane Science* **2022**, *647*, 120221. https://doi.org/10.1016/j.memsci.2021.120221.

(76) Chen, Q.-B.; Ji, Z.-Y.; Liu, J.; Zhao, Y.-Y.; Wang, S.-Z.; Yuan, J.-S. Development of Recovering Lithium from Brines by Selective-Electrodialysis: Effect of Coexisting Cations on the Migration of Lithium. *Journal of Membrane Science* **2018**, *548*, 408–420. https://doi.org/10.1016/j.memsci.2017.11.040.

(77) Gangrade, A. S.; Cassegrain, S.; Chandra Ghosh, P.; Holdcroft, S. Permselectivity of Ionene-Based, Aemion® Anion Exchange Membranes. *Journal of Membrane Science* **2022**, *641*, 119917. https://doi.org/10.1016/j.memsci.2021.119917.

(78) Yang, A. C. C.; Narimani, R.; Zhang, Z.; Frisken, B. J.; Holdcroft, S. Controlling Crystallinity in Graft Ionomers, and Its Effect on Morphology, Water Sorption, and Proton Conductivity of Graft Ionomer Membranes. *Chem. Mater.* **2013**, *25* (9), 1935–1946. https://doi.org/10.1021/cm4005932.

(79) Wilhelm, F. G.; Pünt, I. G. M.; van der Vegt, N. F. A.; Strathmann, H.; Wessling, M. Cation Permeable Membranes from Blends of Sulfonated Poly(Ether Ether Ketone) and Poly(Ether Sulfone). *Journal of Membrane Science* **2002**, *199* (1), 167–176. https://doi.org/10.1016/S0376-7388(01)00695-0.

(80) Li, W.; Yang, F.; Lin, Z.; Sun, R.; Chen, L.; Xie, Y.; Pang, J.; Jiang, Z. Semi-Crystalline Sulfonated Poly(Ether Ketone) Proton Exchange Membranes: The Trade-off of Facile Synthesis and Performance. *Journal of Colloid and Interface Science* **2023**, *645*, 493–501. https://doi.org/10.1016/j.jcis.2023.04.116.

(81) Kamcev, J.; Paul, D. R.; Freeman, B. D. Effect of Fixed Charge Group Concentration on Equilibrium Ion Sorption in Ion Exchange Membranes. *J. Mater. Chem. A* **2017**, *5* (9), 4638–4650. https://doi.org/10.1039/C6TA07954G.

(82) Liang, S.; Kang, Y.; Tiraferri, A.; Giannelis, E. P.; Huang, X.; Elimelech, M. Highly Hydrophilic Polyvinylidene Fluoride (PVDF) Ultrafiltration Membranes via Postfabrication Grafting of Surface-Tailored Silica Nanoparticles. *ACS Appl. Mater. Interfaces* **2013**, *5* (14), 6694–6703. https://doi.org/10.1021/am401462e.

(83) Kang, G.; Cao, Y. Application and Modification of Poly(Vinylidene Fluoride) (PVDF) Membranes – A Review. *Journal of Membrane Science* **2014**, *463*, 145–165. https://doi.org/10.1016/j.memsci.2014.03.055.

(84) Wu, Q.; Tiraferri, A.; Li, T.; Xie, W.; Chang, H.; Bai, Y.; Liu, B. Superwettable PVDF/PVDF-g-PEGMA Ultrafiltration Membranes. *ACS Omega* **2020**, *5* (36), 23450–23459. https://doi.org/10.1021/acsomega.0c03429.

(85) Sheikh, F. A.; Zargar, M. A.; Tamboli, A. H.; Kim, H. A Super Hydrophilic Modification of Poly(Vinylidene Fluoride) (PVDF) Nanofibers: By in Situ Hydrothermal Approach. *Applied Surface Science* **2016**, *385*, 417–425. https://doi.org/10.1016/j.apsusc.2016.05.111.

(86) Kaufman, A. A.; Anderson, B. I. Chapter One - Coulomb's Law and Stationary Electric Field. In *Methods in Geochemistry and Geophysics*; Kaufman, A. A., Anderson, B. I., Eds.; Principles of Electric Methods in Surface and Borehole Geophysics; Elsevier, 2010; Vol. 44, pp 3–78. https://doi.org/10.1016/S0076-6895(10)44001-9.

(87) Giorno, L.; Drioli, E.; Strathmann, H. Ion-Exchange Membrane Characterization. In *Encyclopedia of Membranes*; Drioli, E., Giorno, L., Eds.; Springer: Berlin, Heidelberg, 2016; pp 1052–1056. https://doi.org/10.1007/978-3-662-44324-8_994.

(88) Kamcev, J.; Doherty, C. M.; Lopez, K. P.; Hill, A. J.; Paul, D. R.; Freeman, B. D. Effect of Fixed Charge Group Concentration on Salt Permeability and Diffusion Coefficients in Ion Exchange Membranes. *Journal of Membrane Science* **2018**, *566*, 307–316. https://doi.org/10.1016/j.memsci.2018.08.053.

(89) Zimmermann, P.; Tekinalp, Ö.; Solberg, S. B. B.; Wilhelmsen, Ø.; Deng, L.; Burheim, O. S. Limiting Current Density as a Selectivity Factor in Electrodialysis of Multi-Ionic Mixtures. *Desalination* **2023**, *558*, 116613. https://doi.org/10.1016/j.desal.2023.116613.

Chapter 6

General discussion

This chapter is dedicated to consolidating the insights gleaned from the preceding chapters and offering brief reflections on potential outlooks for further exploration.

6.1. Thesis outcomes

The aim of this thesis was to develop new anion-exchange membranes (AEMs) for the challenging selective separation of two monovalent ions, nitrate and chloride. Several AEMs were manufactured and extensively characterized in order to gain insights on the parameters involved in the selectivity mechanism such as the membrane hydrophobicity and ion dehydration. Furthermore, to identify the key parameters of a membrane-based purification process designed for the selective recovery of nitrate from a water stream that also contains chloride, we first developed a modelling tool. The findings of this study allowed us to define the required separation criteria for the membranes when applying the modelling to a real-case scenario, such as treating wastewater streams from a fertilizer plant. Following is an overview of the main findings of each chapter.

Chapter 2: **Modelling the required membrane selectivity for NO_3^- recovery from effluent also containing Cl^-, while saving water.**

In this chapter, numerical simulations based on a mass balance were carried out to describe the composition of a water stream containing nitrate and chloride being processed in a membrane-based water treatment. The membrane unit was designed to selectively allow the permeation of nitrate, while impeding chloride, thereby forming a nitrate-rich stream (permeate) and a chloride-rich stream (retentate). Depending on the selectivity of the membrane, the nitrate-rich stream may be more or less contaminated with chloride.

Initially, several simulations were performed to investigate the key process parameters affecting the membrane selectivity, such as the nitrate/chloride ratio in the stream entering the water treatment, the fraction of nitrate permeating the membrane, and the fraction of retentate recycled to reduce fresh water consumption. It was observed that a higher nitrate/chloride ratio in the incoming stream of the water treatment results in a lower required membrane selectivity to achieve a certain nitrate purity in the permeate compared to lower nitrate/chloride ratios.

The fraction of nitrate permeating the membrane influences the amount of nitrate remaining in the retentate, recycled within the system. Consequently, higher values of this fraction result in lower purity of nitrate in the permeate stream for a certain membrane selectivity value. Furthermore, the purity of nitrate in the permeate is adversely affected by the fraction of retentate recycled, as chloride accumulates in the system. Thus, higher membrane selectivity values are necessary when the recycled fraction is increased to achieve results comparable to those obtained with a lower recycled fraction.

Based on these findings, the mathematical model was applied to a real-life case involving nitrate recovery from wastewater effluents at Yara's NPK fertilizer plant production facility in Porsgrunn, Norway. The objective was to determine the minimum membrane selectivity required to maintain the chloride concentration in the permeate stream below a specified threshold. The permeate stream, enriched with nitrate, is recycled at the fertilizer plant, and the chloride thresholds are defined by Yara based on the grade of fertilizer produced. Four different scenarios were analyzed, resulting in required membrane selectivity values ranging from 3 to 30.

Chapter 3: Selective separation of nitrate from chloride using PVDF-based anion-exchange membranes.

In this chapter, the selective nitrate/chloride separation was investigated by manufacturing and characterizing PVDF-based anion-exchange membranes. Membranes with varying PVDF concentrations (ranging from 0 to 50 wt%) were fabricated by casting. Characterization results revealed a decrease in membrane water uptake with increasing PVDF concentration, attributed to heightened membrane hydrophobicity.

The permeability coefficient ratio, a measure of the affinity between the membrane and the two counter-ions, was determined by measuring the bi-ionic potential. Results showed the opposite trend compared to that of the water uptake, with the membrane containing 50 wt% of PVDF, labelled as PVDF-50, showing the highest value. This membrane, together with the membrane manufactured only using the ionomer solution, labelled as PVDF-0, and a commercial one (AMX from Neosepta) were tested under constant current conditions.

While the PVDF-0 and AMX membranes exhibited similar low nitrate over chloride selectivity in this investigation, the PVDF-50 membrane displayed a selectivity that was nearly twice as high. Selective boundary layer effects were ruled out, suggesting ion selectivity primarily stems from increased affinity between the anion and the membrane, favoring less hydrated ions for transport.

To further validate the possibility of addressing ion selectivity based on differences in hydration energy, PVDF-50 was tested with a multi-ion solution, which included bromide and fluoride ions next to nitrate and chloride. By measuring the ionic flux through the membrane under constant current conditions, we obtained a preferential permeation order of nitrate > bromide > chloride > fluoride, correlating with the hydration energy trend.

Additionally, we investigated the competitive transport of nitrate, chloride, and sulfate through PVDF-50. Results indicate preferential transport of monovalent ions, with sulfate accounting for 10 %.

Chapter 4: Selective electrodialysis: Targeting nitrate over chloride using PVDF-based AEMs.

In this chapter we examined the performance of the most effective membrane reported in **Chapter 3**, PVDF-50, in electrodialysis for the selective separation of nitrate from chloride. In particular, the membrane PVDF-50 was compared with two commercially available membranes (ACS and AMX from Neosepta), by measuring the nitrate/chloride selectivity over time. Experimental results showed the superior performance of the PVDF-50 compared with the other two membranes. The membrane hydrophobicity was assessed to determine whether the increased nitrate selectivity was related to the superior hydrophobicity of PVDF-50. The values of the contact angle, obtained via the captive bubble method, showed that the hydrophobicity increases in the order of PVDF-50 > ACS > AMX, confirming our hypothesis.

Additionally, the performance of the PVDF-50 membrane was also assessed in electrodialysis, doubling the current density. The results showed that the nitrate recovery was not affected by the variation of the current density.

Considering that with the classic configuration of an electrodialysis stack, it is not possible to prevent the transport of chloride, we also explored an alternative membrane configuration where AEMs with different nitrate selectivity were alternated. The aim of this configuration is the

contemporary depletion of chloride and nitrate concentration in one stream while the opposite changes take place in the other stream. Experiments were conducted at two different current densities, and despite proving the system's feasibility, the nitrate's increase and the chloride's decrease were found to be modest. However, with further membrane and system development, this approach has the potential to become compelling.

Chapter 5: **Effect of polymeric matrix in anion-exchange membranes on nitrate-chloride separations.**

In this chapter we investigated the impact of using different, fluorine-free polymeric matrices instead of PVDF to manufacture anion-exchange membranes for the selective separation of nitrate from chloride. Following the procedure described in previous chapters, two membranes were prepared using polyvinyl chloride (PVC) and polyacrylonitrile (PAN), in combination with the ionomer solution Fumion FAS-24 in a 50:50 ratio. The characteristics and performance of these membranes were compared with those of the PVDF-50 membrane reported in **Chapters 3** and **4**.

Results showed that while the PVDF-50 membrane exhibited the highest hydrophobic nature, the PVC-based membrane demonstrated higher nitrate selectivity, whereas the PAN-based membrane presented slightly lower selectivity. The higher selectivity of PVC-50 was unexpected given its lower hydrophobicity compared to PVDF-50. Therefore, while we still consider increasing membrane hydrophobicity as an effective method to enhance nitrate selectivity—which is corroborated by the fact that all the manufactured membranes exhibited a higher selectivity than those of the two commercial membranes AMX and ACS—we also identify the fixed charge concentration as another potentially influential parameter in the selective behavior of membranes. Indeed, considering that less hydrated ions like nitrate form stronger interactions with the fixed charge groups of the membrane compared to chloride, the diffusion of nitrate will be slowed down in membranes with higher fixed charge concentrations, such as PVDF-50. In conclusion, we believe that the higher nitrate selectivity of PVC-50 is due to a good balance between hydrophobicity and fixed charge concentration.

6.2. Integration of experimental selectivity results with theoretical modelling

The theoretical modelling study conducted in **Chapter 2** provided us with insights into the key process parameters of a membrane-based purification system designed for selectively recovering nitrate while discharging chloride. Based on these insights, we were also able to identify the required membrane selectivity once the proposed model was applied to treat the wastewater streams from Yara's fertilizer plant production in Porsgrunn, Norway. Based on the company's parameters in terms of nitrate and chloride concentration, four cases were investigated resulting in four distinct values of the minimum required membrane selectivity, respectively 3, 8, 13, and 30. While both our research and existing literature are quite far from achieving selectivity values of 13 and 30, our membranes could potentially be used in cases where the required selectivity is 3.

Indeed, as observed in **Chapters 4** and **5**, the experimental selectivity obtained for the membranes PAN-50, PVDF-50, and PVC-50 was found to be above this value. Notably, the highest selectivity demonstrated by PVC-50 indicates that this membrane is the best candidate for further improving membrane design. Indeed, as described in **Chapter 3**, increasing the concentration of a non-charged polymer in manufacturing AEMs enhances the membrane's nitrate selectivity but also its electrical resistance. This larger electrical resistance results in higher energy consumption, as reported in **Chapter 4**, where the membrane PVDF-50 was compared with two commercial membranes, AMX and ACS, which respectively possess an electrical resistance that is three and four times lower than that of PVDF-50. Therefore, one potential strategy could be reducing the concentration of PVC to lower the electrical resistance, and thus the energy consumption, while keeping the resulting selectivity above the required value of 3. Additionally, lower electrical resistance leads to a higher limiting current density, which allows for operation at higher current densities, reducing the duration of the process. While in **Chapter 4** we found that the performance of PVDF-50 was not influenced by current density, conducting a similar test to investigate the PVC-50 membrane would be interesting.

Another way to reduce the membrane's electrical resistance was reported in **Chapter 3**, where a thinner PVDF-50 membrane (45 µm in thickness) was manufactured. This thinner membrane exhibited nearly half the electrical resistance of the thicker PVDF-50 while maintaining similar

characteristics in terms of nitrate/chloride separation. However, this thin, low-resistance membrane has not been examined in ED yet, a test that would be interesting to perform. As a thinner membrane may also result in a lower mechanical strength, limiting its applicability in ED and other separation systems, it is noted that further research is warranted to assess its overall feasibility and performance.

Instead of decreasing the PVC concentration, which has been discussed previously, we can consider increasing the PVC concentration in the membrane to achieve the selectivity value of 8 obtained from the modelling. This approach is expected to enhance nitrate selectivity but will also result in higher energy consumption due to increased electrical resistance.

In this thesis, we decided not to exceed 50 wt% of the non-charged polymer to avoid a significant increase of the membrane's electrical resistance. However, further research could explore exceeding this limit to achieve higher selectivity values, accepting the trade-off of increased electrical resistance and higher energy consumption.

In conclusion, based on the discussions above, we wish to underscore the modular application of the proposed method in manufacturing nitrate-selective anion-exchange membranes. Judicious control over the nature and concentration of the non-charged polymer, along with the membrane thickness, has the potential to engineer membranes with a specific range of selectivity and tuned characteristics such as electrical resistance and mechanical strength.

Lastly, while modifying the membrane to achieve a specific selectivity is a valid strategy, the operational conditions of the membrane-based purification system can also be adjusted and optimized to reduce the required membrane selectivity. Particularly, decreasing the quantity of water recycled within the system is beneficial in this regard, as evidenced by the finding discussed in **Chapter 2**. Indeed, while recycling more water reduces fresh water consumption, it also results in a higher concentration of chloride building up in the system.

6.3. Modelling implementation

To effectively further validate the modelling outlined in **Chapter 2**, it would be helpful to consider assessing the performance of the manufactured membranes under the concentration conditions

defined in the model. Specifically, we decided to neglect water transport through the membrane, a common approach in modelling studies.[1,2]

However, it is noteworthy that the manufactured membranes exhibit some water uptake, albeit lower than commercial membranes. Moreover, while the multi-ionic experiment described in **Chapter 3** elucidated the relationship between preferential permeation and lower dehydration energy, it does not definitively indicate complete dehydration of ionic species at the membrane, as for example occurs in the case of a supported liquid membrane for the potassium/sodium selective separation as described by Qian *et al.*[3,4]

Consequently, while literature supports our assumption of partial ion dehydration,[5–7] the possibility of water transport via the hydration shells of migrated ions and via diffusion due to the concentration gradient through the membrane remains plausible. This would reduce the ion concentration in the concentrate stream due to dilution and affect the system's water balance, requiring, for example, more fresh water to be added at the mixer.

6.4. Potential applications of the manufactured AEMs

In the introduction, we briefly outlined the scope of nitrate-selective AEMs for applications related to closing water loops in greenhouses as well as treating industrial process water and contaminated water.

For greenhouses, there is an increased emphasis among researchers on selectively separating potassium, a macronutrient, from sodium.[3,4,8–10] This focus aims to eliminate sodium from water streams in closed-loop systems to prevent its detrimental effects on crops.[11,12] Conversely, nitrate, a macronutrient as well, and chloride separation has received less attention, although chloride also negatively affects crops.[13]

Recently, towards the end of the work described in the current thesis, a potential application is illustrated in a recent study by Guleria *et al.*,[13] where an efficient AEM- and CEM-supported capacitive electrodialysis (CED) process was developed to facilitate water reuse, obtained as a diluate stream with low sodium concentration, and resource recovery, obtained as a concentrate stream, for greenhouse wastewater. Their research successfully recovered nutrients but highlighted the critical need to prevent the permeation of sodium and chloride in the concentrate

stream to achieve better nutrient composition. This would also reduce nutrient discharge, which is particularly important considering the goal of zero nutrient discharge set by the Dutch greenhouse horticulture program from 2027 onwards. Therefore, combining the approach of Guleria *et al*. with the membranes described in this thesis would constitute an interesting implementation worth studying.

Another potential application is nitrate removal from contaminated groundwater.[14] As an example, **Table 6.1** reports the ion concentration in groundwater from the Israeli Coastal Aquifer, provided by the Water Authority of Israel.[15] The concurrent presence of nitrate and chloride suggests that the nitrate-selective AEMs developed in this thesis could be a potential technology worth investigating.

Table 6.1: Groundwater quality data for the Israeli Coastal Aquifer (source: Water Authority of Israel).[15]

Ion	Concentration ($mg \cdot L^{-1}$)	Concentration ($mmol\ L^{-1}$)
Nitrate (NO_3^-)	100	1.6
Chloride (Cl^-)	300	8.5
Bromide (Br^-)	0.5	6.3×10^{-3}
Fluoride (F^-)	0.6	3.2×10^{-2}
Bicarbonate (HCO_3^-)	250	3.3
Sulphate (SO_4^{2-})	30	3.2×10^{-1}
Potassium (K^+)	3	7.7×10^{-2}
Sodium (Na^+)	150	6.5
Calcium (Ca^{2+})	100	3.1×10^{-1}
Magnesium (Mg^{2+})	40	1.7

Due to the membrane's ability to differentiate between anions based on their hydration energy (**Chapter 3**, **Figure 3.7** and **Figure 3.8**), the manufactured membranes have potential applications beyond solely nitrate and chloride. As an example, they can be used to simultaneously separate chloride and fluoride from sulfate, considering the notable difference between the hydration energy values (**Table 6.2**). This topic has been recently investigated by Tekinalp *et al*.[16] They manufactured AEMs by coating poly(2,6-dimethyl-1,4-phenylene oxide), bearing quaternary ammonium groups, using alternating layers of polyelectrolytes employing layer-by-layer (LbL)

technique, a facile and modular deposition approach. The selectivity values achieved in single-stage ED using these membranes were 11.7 ± 0.2 for chloride/sulfate and 8.3 ± 0.3 for fluoride/sulfate. Based on the experiment conducted in **Chapter 3** on the monovalent versus divalent anion permeation of the PVDF-50 membrane using an equimolar mixture of nitrate, chloride, and sulfate, it would be interesting to study the chloride/sulfate selectivity performance. Indeed, by comparing the ratio of the ionic fluxes of chloride and sulfate, reported in **Figure 3.8**, the preferential chloride over sulfate permeation can be assessed. This ratio is approximately 3, and although lower than the results of Tekinalp *et al*., it is important to note that our experiments also includes nitrate, which exhibits the highest permeation. Additionally, our membranes have not been modified with such LbL coatings that are responsible for reducing sulfate transport.

Combining the different approaches now, it would be worthwhile to first evaluate the AEMs produced in this thesis through single-step ED, employing the same operational conditions reported by Tekinalp *et al*., enabling a direct comparison. Subsequently, coating the AEMs using the LbL deposition technique could be explored to enhance sulfate rejection and potentially achieve superior outcomes compared to Tekinalp's findings.

Table 6.2: hydration energy of chloride, fluoride, sulfate, potassium, and sodium.[17]

Ion	Hydration energy (kcal·mol^{-1})
Chloride (Cl^-)	81
Fluoride (F^-)	111
Sulphate (SO_4^{2-})	258
Potassium (K^+)	71
Sodium (Na^+)	87

6.5. Alternative future directions and research opportunities

In this section, we outline additional key areas that warrant further investigation, highlighting the potential for advancement and impact within nitrate selective separation.

6.5.1. Fluoroalkylation of amine

As discussed in the introduction of this thesis, previous studies focused on increasing membrane hydrophobicity to enhance nitrate selectivity.[18–22] Specifically, by varying the length of the alkyl

chains of the quaternary ammonium groups, they aimed to manipulate the hydrophobic environment surrounding the anion-exchange groups within the membrane. These studies unanimously concluded that increasing the length of the alkyl chains resulted in higher hydrophobicity of the charged groups, thereby enhancing the permeation of less hydrated ions. Therefore, based on these findings, during the course of this PhD project we have also identified the fluoroalkylation of amine[23] as a potential valuable strategy to manufacture AEMs with increased nitrate selectivity. Preliminary work has been conducted and presented in this section; however, additional investigation is required. A schematic representation of such a reaction is given in **Figure 6.1** and involves the incorporation of fluorinated functional moieties on the quaternary ammonium, thereby increasing its hydrophobicity. This approach differs from the one described in this thesis, where a ionomer and non-charged polymers were blended together, as it would result in a membrane composed solely of a homopolymer.

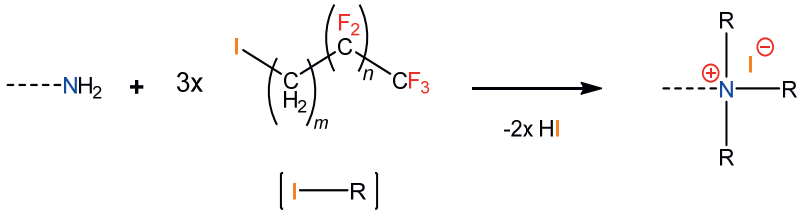

Figure 6.1: Schematic representation of the fluoroalkylation of a primary amine reaction using fluoroalkyl iodides.

Considering that several alkyl iodides (fluorinated or not) are commercially available (

Figure 6.2), this approach allows fine-tuning the hydrophobicity of the quaternary ammonium group, *e.g.* increasing or decreasing the length of the alkyl chains or the number of fluorine atoms per nitrogen.

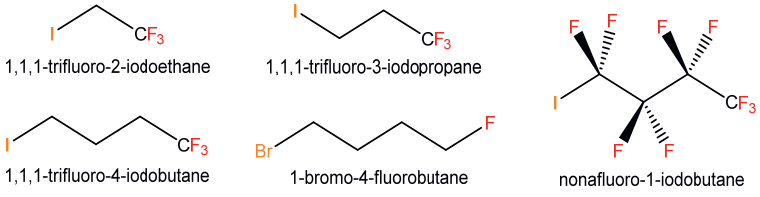

Figure 6.2: Chemical structure of commercially available alkyl iodides.

Concerning the type of amine to use, there are also several options depending on the degree of functionalization desired. For instance, using a primary amine such as *N*-(*tert*-Butoxycarbonyl)-1,2-diaminoethane (**Figure 6.3**), would theoretically allow a triple substitution on the -NH_2 group.

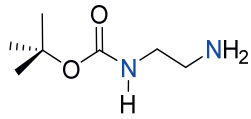

Figure 6.3: Chemical structure of the *N*-(*tert*-Butoxycarbonyl)-1,2-diaminoethane.

However, during our preliminary investigation of the reaction between this amine and 1,1,1-trifluoro-4-iodobutane (**Figure 6.4**), following a procedure adapted from Mady *et al.*,[23] we were only able to obtain the di-substituted product. Therefore, additional work is required for the implementation of this reaction, *e.g.* by extending the duration of the reaction and/or increasing the reaction temperature.

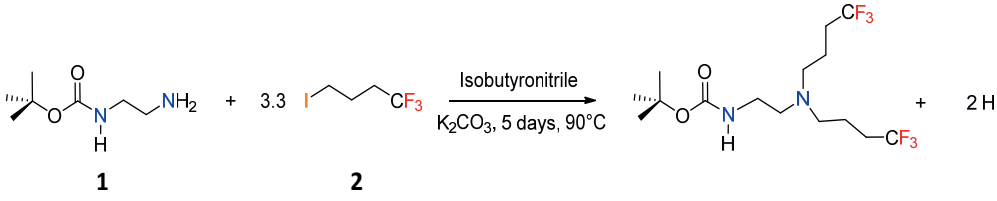

Figure 6.4: Schematic representation of the fluoroalkylation of N-(tert-Butoxycarbonyl)-1,2-diaminoethane (**1**) using 1,1,1-Trifluoro-4-iodobutane (**2**).

After obtaining the quaternary ammonium, the resulting fluorinated compound should then undergo further reactions to incorporate a double bond, enabling a polymerization reaction to produce a polymer that can be used to manufacture a membrane. The following reactions seems to be feasible to pursue this route:

- Deprotection reaction to remove the tert-ButylOxyCarbonyl (BOC) group attached to the other nitrogen atom, using for example trifluoroacetic acid.[24]
- Alkylation reaction using acryloyl chloride to introduce the double bond.[25,26]

As previously stated, using a primary amine as the *N*-(*tert*-Butoxycarbonyl)-1,2-diaminoethane would theoretically allow the incorporation of three fluorinated moieties on the quaternary ammonium. However, the entire synthetic route required to obtain a polymer could be quite long and complex, with problems such as low yield, for example. Therefore, an alternative could be seen in using commercially available methacrylate monomers, such as the 2-(diethylamino)ethyl methacrylate (**Figure 6.5**).

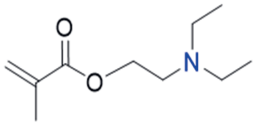

Figure 6.5: Chemical structure of the 2-(diethylamino)ethyl methacrylate.

In this context, we investigated the fluoroalkylation reaction between this amine and 1,1,1-trifluoro-4-iodobutane (**Figure 6.6**), and obtained 9 g *ca*. of the quaternized product. However, the polymerization reaction has not been performed yet due to time limitations.

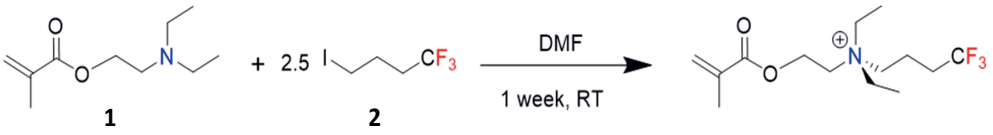

1 **2**

Figure 6.6: Schematic representation of the fluoroalkylation of 2-(diethylamino)ethyl methacrylate (**1**) using 1,1,1-trifluoro-4-iodobutane (**2**).

While using the 2-(diethylamino)ethyl methacrylate does not allow for a triple fluoroalkylation, on the other hand it requires fewer steps to obtain a fluorinated monomer that can be polymerized.

Another potential strategy, not investigated during the course of this PhD project, to obtain a polymer with functionalized quaternary ammonium groups involves modifying poly(amino-methacrylates). Various commercially available poly(amino-methacrylates) can be used for this purpose (**Figure 6.7**).

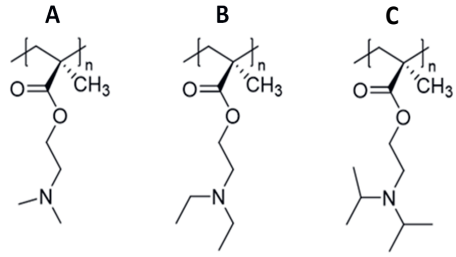

Figure 6.7: Commercially available poly(amino-methacrylates): Poly(2-(dimethylamino)ethyl methacrylate) (**A**), Poly(2-(diethylamino)ethyl methacrylate) (**B**), Poly(2-(diisopropylamino)ethyl methacrylate (**C**).

This method presents the advantage of requiring the least amount of reactions compared to the previous reported. However, due to the significant role of steric hindrance in the alkylation reaction of tertiary amine groups, and considering our goal to introduce bulky alkyl chains to increase hydrophobicity, obtaining a quaternary ammonium with this method might be more difficult than with the previous one. In fact, Sata *et al.*[21] reported that incorporating quaternary ammonium groups into a copolymer membrane composed of chloromethylstyrene and divinylbenzene becomes increasingly challenging as the molecular weight of the tertiary amine increases.

6.5.2. Poly(2,6-dimethyl-1,4-phenylene oxide) (PPO)

An additional polymer potentially worth investigating is the poly(2,6-dimethyl-1,4-phenylene oxide) (PPO), which was extensively studied by Tekinalp *et al.* for applications such as the simultaneous separation of chloride and fluoride from sulfate,[16] and palladium recovery using electrodialysis.[27] The membrane fabrication process reported in those studies involves two key steps: bromination of poly(2,6-dimethyl-1,4-phenylene oxide) and quaternization of the brominated polymer with tertiary amines. In the bromination process, PPO was brominated at different reaction temperatures to control the selectivity of bromination to the benzyl or aryl positions. N-bromosuccinimide (NBS) and a free radical initiator were used in the reaction, with the temperature adjusted to achieve the desired bromination pattern. The obtained brominated

poly(2,6-dimethyl-1,4-phenylene oxide) (BPPO) polymers were then subjected to quaternization by adding tertiary amines like trimethylamine or dimethylhexylamine. Quaternization occurred selectively with the benzyl-substitution groups, leading to the modification of the polymer backbone with quaternary ammonium groups.

6.5.3. Biopolymers

The potential importance of using biopolymers as alternatives to PVC, PAN, and especially PVDF in manufacturing the proposed AEMs in this thesis lies in their sustainability and environmental benefits. However, since the ionomer solution (Fumion FAS-24) is also a component used in the preparation of these AEMs, the biopolymers considered for further investigation must be soluble in the ionomer's solvent, which is N-methyl-2-pyrrolidone (NMP).

For instance, cellulose acetate (CA), **Figure 6.8**, which has been widely used in membrane fabrication already[28] and is soluble in NMP[29–31] is a potential interesting candidate. However, its intrinsic hydrophilicity[32] can result in less hydrophobic membranes compared to those based on PVC, PVDF, and PAN presented in this thesis, potentially leading to less selective membranes. Interestingly, recent studies have demonstrated that the hydrophilicity of CA can be significantly reduced by processing the polymer via electrospinning techniques,[33–36] routes that may be worth to explore within this context. The hydrophobic properties of the electrospun CA mats were attributed to several factors, such as increased surface roughness, reduced availability of hydrophilic functional groups, and tight packing of nanofibers.

Another biopolymer soluble in NMP and thus potentially attractive for further research is poly(lactic acid) (PLA), **Figure 6.8**. Domingues *et al*.,[37] used PLA to manufacture hollow-fiber membranes by wet spinning with a phase-inversion technique using NMP as the solvent and water as the nonsolvent in the precipitation bath. Moreover, they also developed flat sheet membranes[38] using the liquid-induced phase separation technique for biomedical and packaging applications.

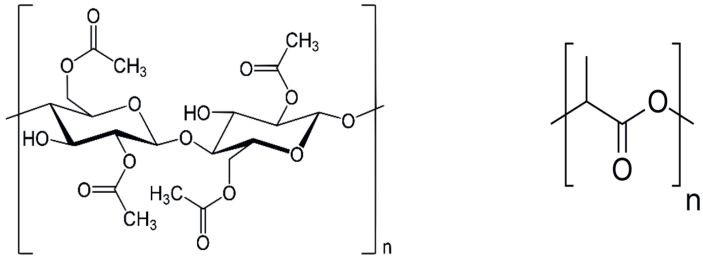

1 **2**

Figure 6.8: Chemical structure of (**1**) cellulose acetate, and (**2**) poly(lactic acid).

Instead of blending a non-charged biopolymer with an ionomer, an alternative approach is directly incorporating anion-exchange groups, such as quaternary ammonium, onto the (bio)polymer backbone. For example, Schmitt *et al*.[39] synthesized AEMs from cellulose within the framework of polymer electrolyte fuel cells that operate in alkaline media. Cellulose was first tosylated, that is the conversion of some hydroxyl groups into p-toluenesulfonate (tosylate) groups, increasing the cellulose's reactivity towards amines. Next, the tosylated cellulose is reacted with 1,4-diazabicyclo[2.2.2]octane (DABCO) in dimethylformamide, replacing the tosylate groups with DABCO to form quaternary ammonium groups attached to the cellulose backbone. Finally, the membrane was crosslinked with diiodobutane to improve its mechanical stability and casted onto a petri dish, allowing the solvent to evaporate to obtain a membrane. Although the membranes manufactured by Schmitt *et al*. exhibit high ion-exchange capacity (IEC) and high water uptake (WU), indicating low membrane hydrophobicity, decreasing the degree of substitution of the quaternary ammonium groups could adjust the IEC and WU, potentially increasing the membrane's hydrophobicity and thus leading to a nitrate-selective behavior.

6.5.4. Supported liquid membranes (SLMs)

Qian *et al*.[3,4] developed supported liquid membranes (SLMs) using ACCUREL polypropylene membrane as the porous support (thickness: 100 µm, pore size: 0.1 µm), impregnated with 2-nitrophenyl-n-octyl ether (NPOE) as the lipophilic organic phase. The borate salt tetrakis[3,5-bis(trifluoromethyl)phenyl]borate (NaBArF) is dissolved in the organic phase, providing

preferential permeation for cations over anions, similar to the effect of fixed charges in conventional ion-exchange membranes.

These SLMs demonstrated preferential transport of potassium over sodium, which was attributed to the lower dehydration energy of the former (**Table 6.2**). Theoretically, this approach can also be pursued to achieve nitrate/chloride selective separations by substituting the borate salt, which presents a negative charge, with a positively charged salt soluble in the lipophilic organic phase (NPOE). Güell *et al.*,[40] developed SLMs for the separation of arsenate [As(V)] and arsenite [As(III)] salts, using tricaprylylmethylammonium chloride (Aliquat 336, **Figure 6.9**) as the mobile carrier within the membrane. Another potentially interesting candidate to achieve SLM-based nitrate/chloride selectivity could be tetraphenylphosphonium bromide (**Figure 6.9**), presenting a similar structure to the borate salt NaBArF.

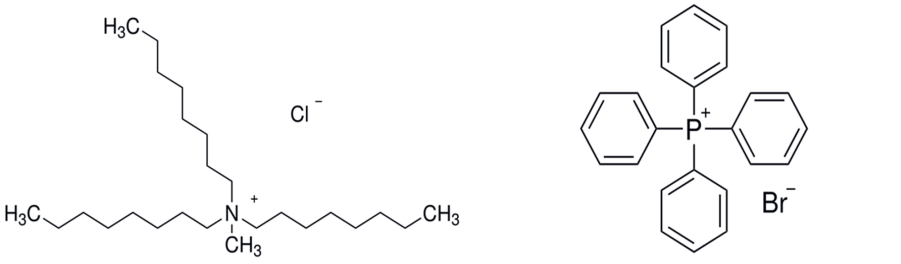

Figure 6.9: Chemical structures of the Aliquat® 336 and tetraphenylphosphonium bromide, which are considered for potential use in SLM-based nitrate/chloride separation.

While this approach shows promise, its unresolved issues are primarily linked to the potential leaching of the organic phase and dissolved salt, which are constrained within the porous support solely by capillary forces. Moreover, the SLMs of Qian *et al*. showed high electrical resistance values (440 $\Omega \cdot cm^2$) due to the lower solubility of the borate salt, resulting in a low ion-exchange capacity of the membrane. Hence, the strategic selection of both the organic solvent and salt is crucial in the development of SLMs for selective nitrate/chloride separation.

6.5.5. Potassium/sodium selective separation

In **Section 6.5.1**, we addressed the challenges related to the synthetic, more elaborate approach aiming to yield a homogeneous anion-exchange membrane structure where all functionalities are covalently attached. This strategy can potentially be extrapolated also for manufacturing cation-exchange membranes to achieve potassium/sodium selective separation, by synthesizing monomers with bulkier and/or fluorine moieties nearby the sulfonic acid groups. However, the complexness of the approach remains. On the other hand, while the development of SLMs for selectively separating potassium from sodium offers an easier manufacturing process with also the potential to move away from the use of fluoride, it still presents other challenges in terms of stability and very high electrical resistance (**Section 6.5.4**). Consequently, the strategy proposed in this thesis, involving increasing the concentration of a non-charged polymer in manufacturing membrane to enhance selectivity toward less hydrated ions, holds promise also for addressing the demanding potassium/sodium separation task. While non-charged polymers such as PVC, and PAN remain viable options, alternative choices are needed for the ionomer solution beyond Fumion FAS-24 due to its anion-exchange nature. For this reason, an attractive alternative is the Fumion E-600 (Fumatech BWT GmbH), a cation-exchange ionomer composed of sulfonated Poly(Ether Ether Ketone) (sPEEK).

Based on the findings of this thesis, we recommend initiating future membrane manufacturing along these lines with a 50:50 ratio of non-charged polymer to ionomer solution. The results regarding selectivity in electrodialysis (ED), along with characterization parameters such as water uptake and water contact angles, can be used for comparison with the anion-exchange membranes discussed in this thesis. This comparative analysis will help to highlight potential similarities or differences, providing insights into the selectivity mechanism.

References

(1) Tedesco, M.; Hamelers, H. V. M.; Biesheuvel, P. M. Nernst-Planck Transport Theory for (Reverse) Electrodialysis: I. Effect of Co-Ion Transport through the Membranes. *Journal of Membrane Science* **2016**, *510* (March), 370–381. https://doi.org/10.1016/j.memsci.2016.03.012.

(2) Fan, H.; Yip, N. Y. Elucidating Conductivity-Permselectivity Tradeoffs in Electrodialysis and Reverse Electrodialysis by Structure-Property Analysis of Ion-Exchange Membranes. *Journal of Membrane Science* **2019**, *573*, 668–681. https://doi.org/10.1016/j.memsci.2018.11.045.

(3) Qian, Z.; Miedema, H.; Sahin, S.; de Smet, L. C. P. M.; Sudhölter, E. J. R. Separation of Alkali Metal Cations by a Supported Liquid Membrane (SLM) Operating under Electro Dialysis (ED) Conditions. *Desalination* **2020**, *495*. https://doi.org/10.1016/j.desal.2020.114631.

(4) Qian, Z.; Miedema, H.; de Smet, L. C. P. M.; Sudhölter, E. J. R. Permeation Selectivity in the Electro-Dialysis of Mono- and Divalent Cations Using Supported Liquid Membranes. *Desalination* **2022**, *521*. https://doi.org/10.1016/j.desal.2021.115398.

(5) Epsztein, R.; Shaulsky, E.; Dizge, N.; Warsinger, D. M.; Elimelech, M. Role of Ionic Charge Density in Donnan Exclusion of Monovalent Anions by Nanofiltration. *Environmental Science and Technology* **2018**, *52* (7), 4108–4116. https://doi.org/10.1021/acs.est.7b06400.

(6) Epsztein, R.; Shaulsky, E.; Qin, M.; Elimelech, M. Activation Behavior for Ion Permeation in Ion-Exchange Membranes: Role of Ion Dehydration in Selective Transport. *Journal of Membrane Science* **2019**, *580* (January), 316–326. https://doi.org/10.1016/j.memsci.2019.02.009.

(7) Epsztein, R.; DuChanois, R. M.; Ritt, C. L.; Noy, A.; Elimelech, M. Towards Single-Species Selectivity of Membranes with Subnanometre Pores. *Nat. Nanotechnol.* **2020**, *15* (6), 426–436. https://doi.org/10.1038/s41565-020-0713-6.

(8) Krishna B, A.; Lindhoud, S.; de Vos, W. M. Hot-Pressed Polyelectrolyte Complexes as Novel Alkaline Stable Monovalent-Ion Selective Anion Exchange Membranes. *Journal of Colloid and Interface Science* **2021**, *593*, 11–20. https://doi.org/10.1016/j.jcis.2021.02.077.

(9) Ahdab, Y. D.; Schücking, G.; Rehman, D.; Lienhard, J. H. Treatment of Greenhouse Wastewater for Reuse or Disposal Using Monovalent Selective Electrodialysis. *Desalination* **2021**, *507*, 115037. https://doi.org/10.1016/j.desal.2021.115037.

(10) Krishna B, A.; Zwijnenberg, H. J.; Lindhoud, S.; de Vos, W. M. Sustainable K+/Na+ Monovalent-Selective Membranes with Hot-Pressed PSS-PVA Saloplastics. *Journal of Membrane Science* **2022**, *652*, 120463. https://doi.org/10.1016/j.memsci.2022.120463.

(11) Läuchli, A.; Grattan, S. R. Plant Growth And Development Under Salinity Stress. In *Advances in Molecular Breeding Toward Drought and Salt Tolerant Crops*; Jenks, M. A., Hasegawa, P. M., Jain, S. M., Eds.; Springer Netherlands: Dordrecht, 2007; pp 1–32. https://doi.org/10.1007/978-1-4020-5578-2_1.

(12) Zhang, J.-L.; Flowers, T. J.; Wang, S.-M. Mechanisms of Sodium Uptake by Roots of Higher Plants. *Plant Soil* **2010**, *326* (1), 45–60. https://doi.org/10.1007/s11104-009-0076-0.

(13) Guleria, T.; van den Broeke, J.; Platteau, I.; Rijnaarts, T.; Alhadidi, A.; Gutierrez, L.; Cornelissen, E. Water Reuse and Resource Recovery from Greenhouse Wastewater by Capacitive Electrodialysis at Pilot Scale. *Desalination* **2024**, *583*, 117669. https://doi.org/10.1016/j.desal.2024.117669.
(14) Abascal, E.; Gómez-Coma, L.; Ortiz, I.; Ortiz, A. Global Diagnosis of Nitrate Pollution in Groundwater and Review of Removal Technologies. *Science of The Total Environment* **2022**, *810*, 152233. https://doi.org/10.1016/j.scitotenv.2021.152233.
(15) Modi, A.; Kasher, R. Nitrate Removal from Contaminated Groundwater by Micellar-Enhanced Ultrafiltration Using a Polyacrylonitrile Membrane with a Hydrogel-Stabilized ZIF-L Layer. *Water Research* **2024**, *254*, 121384. https://doi.org/10.1016/j.watres.2024.121384.
(16) Tekinalp, Ö.; Zimmermann, P.; Burheim, O. S.; Deng, L. Designing Monovalent Selective Anion Exchange Membranes for the Simultaneous Separation of Chloride and Fluoride from Sulfate in an Equimolar Ternary Mixture. *Journal of Membrane Science* **2023**, *666*, 121148. https://doi.org/10.1016/j.memsci.2022.121148.
(17) Marcus, Y. Thermodynamics of Solvation of Ions. *J. CHEM. SOC. FARADAY TRANS.* **1991**, *87*.
(18) Liao, J.; Yu, X.; Chen, Q.; Gao, X.; Ruan, H.; Shen, J.; Gao, C. Monovalent Anion Selective Anion-Exchange Membranes with Imidazolium Salt-Terminated Side-Chains: Investigating the Effect of Hydrophobic Alkyl Spacer Length. *Journal of Membrane Science* **2020**, *599*, 117818. https://doi.org/10.1016/j.memsci.2020.117818.
(19) Mubita, T. M.; Porada, S.; Biesheuvel, P. M.; van der Wal, A.; Dykstra, J. E. Strategies to Increase Ion Selectivity in Electrodialysis. *Separation and Purification Technology* **2022**, *292*, 120944. https://doi.org/10.1016/j.seppur.2022.120944.
(20) Mubita, T.; Porada, S.; Aerts, P.; van der Wal, A. Heterogeneous Anion Exchange Membranes with Nitrate Selectivity and Low Electrical Resistance. *Journal of Membrane Science* **2020**, *607*, 118000. https://doi.org/10.1016/j.memsci.2020.118000.
(21) Sata, T. Studies on Anion Exchange Membranes Having Permselectivity for Specific Anions in Electrodialysis - Effect of Hydrophilicity of Anion Exchange Membranes on Permselectivity of Anions. *Journal of Membrane Science* **2000**, *167* (1), 1–31. https://doi.org/10.1016/S0376-7388(99)00277-X.
(22) Irfan, M.; Ge, L.; Wang, Y.; Yang, Z.; Xu, T. Hydrophobic Side Chains Impart Anion Exchange Membranes with High Monovalent–Divalent Anion Selectivity in Electrodialysis. *ACS Sustainable Chem. Eng.* **2019**, *7* (4), 4429–4442. https://doi.org/10.1021/acssuschemeng.8b06426.
(23) Mady, M. F.; Kelland, M. A. Fluorinated Quaternary Ammonium Bromides: Studies on Their Tetrahydrofuran Hydrate Crystal Growth Inhibition and as Synergists with Polyvinylcaprolactam Kinetic Gas Hydrate Inhibitor. *Energy and Fuels* **2013**, *27* (9), 5175–5181. https://doi.org/10.1021/ef401292m.
(24) Shiau, S.-F.; Juang, T.-Y.; Chou, H.-W.; Liang, M. Synthesis and Properties of New Water-Soluble Aliphatic Hyperbranched Poly(Amido Acids) with High pH-Dependent Photoluminescence. *Polymer* **2013**, *54* (2), 623–630. https://doi.org/10.1016/j.polymer.2012.12.013.
(25) Ali, S.; Cuchiara, M. L.; West, J. L. Chapter 8 - Micropatterning of Poly(Ethylene Glycol) Diacrylate Hydrogels. In *Methods in Cell Biology*; Piel, M., Théry, M., Eds.; Micropatterning in Cell Biology Part C; Academic Press, 2014; Vol. 121, pp 105–119. https://doi.org/10.1016/B978-0-12-800281-0.00008-7.

(26) Mohan Kulkarni, B. S. Process for the Preparation of N-Substituted Acrylamides. US 6,369,249 B1. https://patentimages.storage.googleapis.com/0f/a5/52/5cc68898d815f6/US6369249.pdf.
(27) Tekinalp, Ö.; Wang, X.; Zimmermann, P.; Stokke Burheim, O.; Deng, L. Tailoring Anion Exchange Membranes for Palladium Recovery from Industrial Solutions Using Electrodialysis. *Chemical Engineering Journal* **2024**, *488*, 151037. https://doi.org/10.1016/j.cej.2024.151037.
(28) Vatanpour, V.; Pasaoglu, M. E.; Barzegar, H.; Teber, O. O.; Kaya, R.; Bastug, M.; Khataee, A.; Koyuncu, I. Cellulose Acetate in Fabrication of Polymeric Membranes: A Review. *Chemosphere* **2022**, *295*, 133914. https://doi.org/10.1016/j.chemosphere.2022.133914.
(29) Li, G.; Wang, J.; Hou, D.; Bai, Y.; Liu, H. Fabrication and Performance of PET Mesh Enhanced Cellulose Acetate Membranes for Forward Osmosis. *Journal of Environmental Sciences* **2016**, *45*, 7–17. https://doi.org/10.1016/j.jes.2015.11.025.
(30) Jami'an, W. N. R.; Hasbullah, H.; Mohamed, F.; Yusof, N.; Ibrahim, N.; Ali, R. R. Effect of Evaporation Time on Cellulose Acetate Membrane for Gas Separation. *IOP Conf. Ser.: Earth Environ. Sci.* **2016**, *36* (1), 012008. https://doi.org/10.1088/1755-1315/36/1/012008.
(31) Mubashir, M.; Dumée, L. F.; Fong, Y. Y.; Jusoh, N.; Lukose, J.; Chai, W. S.; Show, P. L. Cellulose Acetate-Based Membranes by Interfacial Engineering and Integration of ZIF-62 Glass Nanoparticles for CO2 Separation. *Journal of Hazardous Materials* **2021**, *415*, 125639. https://doi.org/10.1016/j.jhazmat.2021.125639.
(32) Sun, Z.; Chen, F. Hydrophilicity and Antifouling Property of Membrane Materials from Cellulose Acetate/Polyethersulfone in DMAc. *International Journal of Biological Macromolecules* **2016**, *91*, 143–150. https://doi.org/10.1016/j.ijbiomac.2016.05.072.
(33) Ding, B.; Li, C.; Hotta, Y.; Kim, J.; Kuwaki, O.; Shiratori, S. Conversion of an Electrospun Nanofibrous Cellulose Acetate Mat from a Super-Hydrophilic to Super-Hydrophobic Surface. *Nanotechnology* **2006**, *17* (17), 4332. https://doi.org/10.1088/0957-4484/17/17/009.
(34) Adepu, S.; Gaydhane, M. K.; Kakunuri, M.; Sharma, C. S.; Khandelwal, M.; Eichhorn, S. J. Effect of Micropatterning Induced Surface Hydrophobicity on Drug Release from Electrospun Cellulose Acetate Nanofibers. *Applied Surface Science* **2017**, *426*, 755–762. https://doi.org/10.1016/j.apsusc.2017.07.197.
(35) Mikaeili, F.; Gouma, P. I. Super Water-Repellent Cellulose Acetate Mats. *Sci Rep* **2018**, *8* (1), 12472. https://doi.org/10.1038/s41598-018-30693-2.
(36) Ruhela, A.; Kasinathan, G. N.; Rath, S. N.; Sasikala, M.; Sharma, C. S. Electrospun Freestanding Hydrophobic Fabric as a Potential Polymer Semi-Permeable Membrane for Islet Encapsulation. *Materials Science and Engineering: C* **2021**, *118*, 111409. https://doi.org/10.1016/j.msec.2020.111409.
(37) Domingues, R. C. C.; Pereira, C. C.; Borges, C. P. Morphological Control and Properties of Poly(Lactic Acid) Hollow Fibers for Biomedical Applications. *Journal of Applied Polymer Science* **2017**, *134* (47), 45494. https://doi.org/10.1002/app.45494.
(38) Domingues, R. C. C.; Pereira, C. C.; Borges, C. P. Preparation of Poly(Lactic Acid) Flat Sheet Membranes by Liquid Induced Phase Separation. *Macromolecular Symposia* **2016**, *368* (1), 128–135. https://doi.org/10.1002/masy.201600008.

(39) Schmitt, F.; Granet, R.; Sarrazin, C.; Mackenzie, G.; Krausz, P. Synthesis of Anion Exchange Membranes from Cellulose: Crosslinking with Diiodobutane. *Carbohydrate Polymers* **2011**, *86* (1), 362–366. https://doi.org/10.1016/j.carbpol.2011.04.055.

(40) Güell, R.; Fontàs, C.; Anticó, E.; Salvadó, V.; Crespo, J. G.; Velizarov, S. Transport and Separation of Arsenate and Arsenite from Aqueous Media by Supported Liquid and Anion-Exchange Membranes. *Separation and Purification Technology* **2011**, *80* (3), 428–434. https://doi.org/10.1016/j.seppur.2011.05.015.

Summary

Nitrogen fertilizers are critical in agriculture due to their role in plant growth and reproduction. However, the extensive use of nitrogen fertilizers has impacted agricultural sustainability and led to environmental concerns. A significant portion of the applied fertilizer is not absorbed by crops, leading to issues like water pollution and health risks from nitrate contamination in drinking water.

To tackle these challenges, technologies such as electrodialysis (ED) can be employed. Ion-exchange membranes (IEMs) are integral components of ED, selectively allowing the passage of specific ions while blocking others, thereby facilitating the separation of ionic species. State-of-the-art membrane technology enables the separation of cations from anions and divalent from monovalent ions. However, separating ions with the same valence remains challenging. In particular, the separation of nitrate from chloride, given their similar physicochemical properties, is difficult. Achieving this separation would enable the recovery and recycling of valuable resources like nitrate from waste/process water streams in fertilizer plants and agricultural and horticultural practices, contributing to a circular economy.

Driven by the possibility of employing the small difference in the dehydration energies of nitrate and chloride for ion separation, this thesis aims to develop new anion-exchange membranes (AEMs) with improved nitrate selectivity. Previous studies have shown that increasing membrane hydrophobicity enhances the transport of less hydrated ions, such as nitrate. Therefore, this thesis explores the effect of increasing membrane hydrophobicity on the nitrate/chloride selective separation.

Chapter 1 provides a comprehensive introduction to above-mentioned issues, detailing the environmental impact of nitrogen fertilizers, the principles and challenges of ion-exchange membranes in electrodialysis, and the specific focus of this thesis on enhancing nitrate selectivity through increased membrane hydrophobicity.

Chapter 2 presents a mass balance-based modelling tool for the selective recovery of nitrate from a wastewater stream containing chloride, aiming to improve ion-separation efficiency and reduce water consumption in a water purification system. The key element of the process is a membrane unit with a nitrate over chloride permeation selectivity. Initially, the study outlines the interplay between several key process parameters for a generic water purification system, such as the nitrate/chloride feed ratio and the fraction of nitrate and water recovered, influencing the

required membrane selectivity. These findings have then been applied to four scenarios of a real-life application involving nitrate recovery from a fertilizer plant's effluent, resulting in required membrane selectivity values ranging from 3 to 30.

Chapter 3 focuses on the development and characterization of new polyvinylidene fluoride (PVDF)-based anion-exchange membranes (AEMs) for the selective separation of nitrate from chloride. PVDF was chosen for its inherent hydrophobic nature. The membranes have been manufactured via casting using a commercially available ionomer solution in combination with PVDF, offering a straightforward membrane fabrication method. The impact of varying the PVDF content (0 to 50 wt%) within the membrane was investigated, with the PVDF-50 membrane containing 50 wt% PVDF showing the highest nitrate selectivity under constant current conditions. This selectivity was found to be almost twice as high as that of a widely used commercial membrane (AMX from Neosepta). To gain insights into the relationship between hydration energy and preferential ion transport, and thus the selectivity mechanism, the ionic fluxes of multiple monovalent anions through this best-performing PVDF-based anion-exchange membranes were evaluated.

Chapter 4 investigates the application of the best-performing membrane from Chapter 3 (*i.e.* PVDF-50) for nitrate over chloride selective separation in electrodialysis. The selectivity results obtained and membrane properties such as ion-exchange capacity, permselectivity, and hydrophobicity have been compared with those of two commercial membranes (AMX and ACS from Neosepta). The PVDF-50 membrane showed the highest reported nitrate over chloride selectivity and its performance in ED was found to be independent of applied current density. Additionally, this chapter describes the potential of a proposed approach called nitrate-selectrodialysis (NO_3-SED), leveraging the differences in nitrate over chloride selectivity of various AEMs to achieve concurrent nitrate concentration and chloride depletion in an aqueous stream.

Chapter 5 explores the impact of using different polymeric matrices than PVDF on the fabrication of nitrate-selective anion-exchange membranes (AEMs) as well as their properties and performance. In particular, two fluorine-free alternative polymers, polyvinyl chloride (PVC) and polyacrylonitrile (PAN), were used in combination with the ionomer solution used in previous chapters to successfully manufacture the polymer-based membranes. The PVC and PAN-based

membranes were tested in ED and the nitrate over chloride selectivity followed the trend of PVC > PVDF > PAN > commercial membranes. Furthermore, membrane properties such as electrical resistance, ion-exchange capacity, water uptake, fixed charge concentration, surface morphology, and hydrophobicity have been analyzed, culminating in the conclusion that selectivity for this type of membranes is governed by hydrophobicity and fixed charge concentration.

Chapter 6 provides an overview of the findings synthesized from the research chapters, a discussion of some implications in relation to the model and potential applications of the studied AEMs. Moreover, it also presents potential directions for future research.

Sommario

I fertilizzanti azotati sono fondamentali in agricoltura per il loro ruolo nella crescita e nella riproduzione delle piante. Tuttavia, l'uso estensivo di questi fertilizzanti ha determinato un forte impatto sulla sostenibilità agricola e sollevato preoccupazioni ambientali. Infatti, una parte significativa del fertilizzante applicato non viene assorbita dalle colture, portando a problemi come l'inquinamento delle acque e quindi a rischi per la salute dovuti alla contaminazione da nitrati.

Per affrontare queste sfide, tecnologie come l'elettrodialisi (ED) possono essere impiegate. In questo contesto, le membrane a scambio ionico (in inglese ion-exchange membranes, IEMs) sono componenti integrali e fondamentali dell'ED, consentendo il passaggio selettivo di specifici ioni e facilitando così la separazione di differenti specie ioniche.

Le membrane attualmente disponibili permettono la separazione selettiva di cationi da anioni (e viceversa) e di ioni monovalenti da bivalenti (e viceversa). Tuttavia, la separazione di specie ioniche con la stessa valenza rimane una sfida. In particolare, data la simile natura fisico-chimica, la separazione del nitrato dal cloruro risulta difficile. Conseguire questa separazione permetterebbe, ad esempio, il recupero e il riciclaggio di una risorsa preziosa come il nitrato dalle acque di processo delle fabbriche di fertilizzanti e serre, contribuendo così a creare un'economia circolare.

Guidati dalla possibilità di sfruttare la piccola differenza nelle energie di disidratazione del nitrato e del cloruro per ottenerne una separazione selettiva, questa tesi mira a sviluppare nuove membrane a scambio anionico (in inglese anion-exchange membranes, AEMs) con più elevata selettività per il nitrato. In particolare, considerando che studi precedenti hanno dimostrato che l'aumento dell'idrofobicità della membrana migliora il trasporto di ioni meno idratati, come il nitrato, in questa tesi esploreremo l'effetto dell'aumento dell'idrofobicità delle membrane sulla separazione selettiva nitrato/cloruro.

Il **Capitolo 1** fornisce un'introduzione completa riguardo ai problemi ambientali e sulla salute umana associati all'eccessivo uso dei fertilizzanti azotati, e ai principi e le sfide relative allo sviluppo delle membrane a scambio ionico, focalizzandosi sullo scopo di questa tesi: migliorare la selettività delle membrane per il nitrato attraverso l'aumento della loro idrofobicità.

Il **Capitolo 2** presenta uno strumento interattivo di calcolo basato sui bilanci di massa in un sistema di purificazione dell'acqua, progettato per il recupero selettivo del nitrato da acque di processo contenenti anche cloruro, con l'obiettivo di migliorare l'efficienza della separazione ionica e ridurre il consumo d'acqua. L'elemento chiave del processo è un'unità a membrana con selettività per il nitrato rispetto al cloruro. Lo studio descrive l'interazione tra i principali parametri del processo in un sistema di purificazione generico e la loro influenza sul valore della selettività della membrana richiesta. Questi parametri includono il rapporto nitrato/cloruro nel flusso di alimentazione e la frazione di nitrato e acqua recuperati. I risultati di questa prima parte dello studio sono stati poi applicati a quattro scenari relativi al recupero del nitrato dalle acque di processo di un impianto di produzione di fertilizzanti, al fine di determinare i valori minimi di selettività della membrana necessari per mantenere la concentrazione del cloruro al di sotto di livelli prestabiliti. I valori minimi di selettività ottenuti variano da 3 a 30.

Il **Capitolo 3** si concentra sullo sviluppo e la caratterizzazione di nuove membrane a scambio anionico (AEM) a base di polivinilidenfluoruro (PVDF) per la separazione selettiva del nitrato dal cloruro. Il PVDF è stato scelto per la sua natura intrinsecamente idrofobica. Le membrane sono state fabbricate tramite un processo di casting utilizzando una soluzione ionomerica in combinazione con il PVDF, risultando in un metodo di fabbricazione semplice. L'impatto della variazione del contenuto di PVDF (dallo 0 al 50 % in peso) all'interno delle membrane è stato investigato, con la membrana PVDF-50, contenente il 50 % in peso di PVDF, che ha mostrato la massima selettività per il nitrato in condizioni di corrente costante. Questa selettività è risultata essere quasi doppia rispetto a quella di una membrana commerciale quale AMX di Neosepta. Per ottenere informazioni sulla relazione tra energia di idratazione e preferenziale trasporto ionico, e quindi sul meccanismo di selettività, sono stati valutati i flussi ionici di vari anioni monovalenti attraverso la membrana PVDF-50.

Il **Capitolo 4** esamina l'applicazione della membrana PVDF-50 nella separazione selettiva nitrato/cloruro in elettrodialisi. I risultati ottenuti in termini di selettività e le proprietà della membrana, come la capacità di scambio ionico, la permselettività e l'idrofobicità, sono stati confrontati con quelli di due membrane commerciali quali AMX e ACS di Neosepta. La membrana PVDF-50 ha mostrato la massima selettività riportata per il nitrato rispetto al cloruro, con

prestazioni in elettrodialisi indipendenti dalla densità di corrente applicata. Inoltre, questo capitolo descrive le potenzialità di un approccio innovativo chiamato nitrato-selectrodialisi (NO_3-SED), che sfrutta la differente selettività nitrato/cloruro di diverse AEMs per ottenere la simultanea concentrazione di nitrato e deplezione di cloruro in una soluzione.

Il **Capitolo 5** esplora l'effetto dell'utilizzo di matrici polimeriche diverse dal PVDF sulla fabbricazione di membrane a scambio anionico (AEM) selettive per il nitrato, e quindi sulle loro proprietà e prestazioni in elettrodialisi. In particolare, sono stati utilizzati due polimeri alternativi privi di fluoro, polivinilcloruro (PVC) e poliacrilonitrile (PAN), in combinazione con la soluzione ionomerica, per fabbricare con successo le membrane. Le membrane a base di PVC e PAN sono state testate in elettrodialisi (ED) e la selettività nitrato/cloruro ottenuta è stata confrontata con quella precedentemente ottenuta per la membrana a base di PVDF. In particolare, la selettività verso il nitrato diminuisce nell'ordine PVC > PVDF > PAN > membrane commerciali. Inoltre, sono state analizzate le proprietà delle membrane, come resistenza elettrica, capacità di scambio ionico, assorbimento d'acqua, concentrazione di carica fissa, morfologia superficiale e idrofobicità, concludendo che la selettività di queste membrane è governata dall'idrofobicità e dalla concentrazione di carica fissa.

Il **Capitolo 6** fornisce una panoramica dei risultati ottenuti nei capitoli precedenti, confrontando i risultati teorici del Capitolo 2 con quelli sperimentali dei capitoli successivi. Inoltre, in questo capitolo conclusivo vengono discusse le potenziali applicazioni delle AEM presentate in questa tesi e le future direzioni per lo sviluppo di membrane selettive per il nitrato.

Acknowledgements

Completing this PhD thesis has been a challenging yet incredibly rewarding journey, and it would not have been possible without the support and guidance of many individuals to whom I am profoundly grateful.

First of all, I would like to express my deepest gratitude to my supervisors, Louis de Smet, Henk Miedema, and Jan Post, for their support, guidance, and encouragement throughout my research. Your expertise and dedication have been invaluable in shaping this work.

I am also deeply thankful to my thesis committee members for their valuable time spent evaluating my thesis.

A special thanks goes to my office mates Joao, Xiao, Lester, Dhyana, Shih-Hsuan, Santiago, Salman, and Berke for their support and for creating an enjoyable office environment full of laughter and relevant research questions. Thank you, Rita and Jolanda, for spending time together during lunch and watching Emily in Paris. Many thanks to the Italian community I have found at Wetsus: Carlo, Laura, Simona, Cristina, Michele, Giulia, Francesca, Maddalena, Concetta, Giordana, and many others I cannot recall now. To my students, whom I had the privilege to supervise: Jean, you were my first student, and I truly appreciated your calm presence. Idoia, I will always remember the time spent in the lab with you, working hard but always laughing and teasing each other. Katerina, your calm presence and organizational skills have been pivotal for me. Idoia and I tried to hide our crazy side from you, but I think we lasted only two hours. Tesse, last but not least, your energy, motivation, and endless curiosity gave me the boost to conclude my work.

To all my Wetsus colleagues, each of you has been fundamental during this journey with our chats in the lab, laughter, and time spent together. Thank you, Cees, Bert, and Johannes, for making Wetsus an amazing workplace.

Thanks to the Desalination & Concentrates research theme for the fruitful discussions and support. A special thanks go to Yara, the industrial partner of this project, in the person of Amund Myrstad.

I would also like to extend my gratitude to the technician staff, especially Harm van der Kooi for his precious help, to the canteen staff, the secretaries, HR, and the analytical team. Thanks to the ORC group from Wageningen University for their support and help in the organic synthesis.

Thanks to all my friends in Italy. Unfortunately, distance has kept us apart, but your constant friendship and support, even from afar, have meant the world to me.

I also extend my deepest gratitude to my family, who has always encouraged me to pursue my dreams, whether that meant moving abroad or taking on new challenges. Your support has been my foundation, and I am forever grateful for the love and confidence you've given me throughout this journey.

Finally, I am deeply indebted to my partner, Terezija Jovanovski, for her endless support, love, and patience during this journey. Your unwavering belief in me has been a constant source of strength and motivation.

To all those who have contributed to this work, whether mentioned here or not, your support has been invaluable, and I am truly grateful.

Thank you!

Bedankt!

Grazie!

Hvala!

About the Author

Daniele was born on the 1st of October 1990, in Livorno, Italy. After completing high school, he worked as a salesman at Leroy Merlin store in Livorno, before opting to pursue further education. He embarked on the BSc in Chemistry for the Industry and Environment at the University of Pisa, where he graduated with distinction, achieving a top grade of 110/110 *cum laude*. His thesis focused on the research of new tanning agents with reduced environmental impact, conducted in collaboration with Po.Te.Co. in Santa Croce sull'Arno, Pisa.

Continuing his academic journey, Daniele obtained his MSc in Industrial Chemistry from the same university in November 2018, achieving the highest grade of 110/110. His master's thesis, conducted at the University of Groningen, delved into the utilization of polyisobutylene succinic anhydride (PIBSA) for the preparation of mechanochromic materials and electroconductive nanocomposite materials using carbon nanotubes.

Following his master's degree, Daniele worked as a product development technologist at Laviosa Chimica Mineraria Spa in Livorno, Italy. There, he explored the applications of clay minerals across various industrial sectors, including household and personal care, beverages, paper production, animal feed, agriculture, and coatings, identifying new potential application areas.

In 2019, he commenced his doctoral research at Wetsus, the European centre of excellence for sustainable water technology in Leeuwarden, The Netherlands. The findings of this research project are presented in this thesis.

List of publications

Chinello, D.; Myrstad, A.; de Smet, L. C. P. M.; Miedema, H. Modelling the required membrane selectivity for NO_3^- recovery from effluent also containing Cl^-, while saving water. *Chemical Engineering Research and Design* **2023**, *193*, 409-419.

Chinello, D.; Post, J.; de Smet, L. C. P. M. Selective separation of nitrate from chloride using PVDF-based anion-exchange membranes. *Desalination* **2024**, *572*, 117084.

Chinello, D.; de Smet, L. C. P. M.; Post, J. Selective Electrodialysis: targeting nitrate over chloride using PVDF-based AEMs. *Separation and Purification Technology* **2024**, *342*, 126885.

Chinello, D.; Post, J.; de Smet, L. C. P. M. Effect of polymeric matrix in anion-exchange membranes on nitrate-chloride separations. *Separation and Purification Technology* **2025**, *355*, 129440

Overview of Completed Training Activities

Discipline-specific activities	Organizing institute (s)	Year
Environmental Technology for Impact (ETEi)	ETE	2020
Advanced Organic Chemistry course	ORC	2020 - 2021
Chemistry As INovating Science (Chains)	NWO	2020
VLAG online lecture	VLAG	2020
12th European Symposium on Electrochemical Engineering (ESEE)	Wetsus	2021
Wetsus Congress*	Wetsus	2021-2023
Chemistry For the Future (CFF)**	DCCI, University of Pisa	2022
European Water Technology Week	Wetsus	2022
EuroMembrane*	IMT, University of Bologna	2022

*oral presentation **poster presentation

General courses	Organizing institute (s)	Year
Searching and organize literature	WGS	2020
MATLAB Onramp	MathWorks	2020
Social media Workshop	Wetsus	2020
VLAG PhD week	VLAG	2021
Starting day	Wetsus	2021
Communication styles	Wetsus	2021
Presentation course	Wetsus	2021
Supervision course	Wetsus	2021
Talents course	Wetsus	2021
How to present online	VLAG	2021
Facilitator training	Wetsus	2022
PhD Workshop Carousel	WGS	2022
Career perspective	Wetsus	2023

Other activities	Organizing institute (s)	Year
Preparation of research proposal	ORC	2019
Desalination & Concentrates theme meetings	Wetsus	2019-2024
Lunch presentations	Wetsus	2020-2024
Introduction to water and climate	Edx - TU Delft	2020
Urban Sewage Treatment	Edx - TU Delft	2020
Drinking Water Treatment	Edx - TU Delft	2020

Teaching activities	Organizing institute (s)	Year
ORC12803 Organic Chemistry 1	ORC	2020-2022
ORC12903 Organic Chemistry 2	ORC	2020-2022
ORC13803 Bio-organic chemistry for life sciences	ORC	2020-2022
Supervision BSc and MSc students		2022-2024

The research presented in this thesis was funded by the Dutch Research Council – Wetsus Partnership Programme on Sustainable Water Technology (ALWET.2019.004), and performed in the cooperation framework of Wetsus, European Centre of Excellence for Sustainable Water Technology (www.wetsus.nl). Wetsus is co-funded by the Dutch Ministry of Economic Affairs and Ministry of Infrastructure and Environment, the European Union Regional Development Fund, the Province of Fryslan and the Northern Netherlands Provinces.

Financial support from Wageningen University and Wetsus for printing this thesis is gratefully acknowledged.

Cover design by Celine Kugler

Printed by ProefschriftMaken